UNIVERSIDAD DE CASTILLA-LA MANCHA

FACULTAD DE CIENCIAS Y TECNOLOGÍAS QUÍMICAS

DEPARTAMENTO DE INGENIERÍA QUÍMICA

DEFINICIÓN Y OPTIMIZACIÓN DE LA SÍNTESIS DE NANOMATERIALES BASADOS EN GRAFENO

Memoria que para optar al grado de Doctor en Ingeniería Química presenta:

MARÍA DEL PRADO LAVÍN LÓPEZ

Directores:

Dra. Amaya Romero Izquierdo

Dr. José Luis Valverde Palomino

Composición del tribunal:

Dr. Fernando Dorado Fernández

Dr. Antonio Nieto-Márquez Ballesteros

Dr. Agustín Garrido Fernández

Profesores que han emitido informes favorables de la tesis:

Dra. María Martín Aranda

Dr. Ángel Caravaca Huertas

Ciudad Real, 3 de febrero de 2017

D. José Luis Valverde, catedrático de Ingeniería Química de la Universidad de Castilla-La Mancha y **Dª. Amaya Romero Izquierdo**, Profesora Titular de Ingeniería Química de la Universidad de Castilla-La Mancha,

CERTIFICAN: Que el presente trabajo de investigación titulado "Definición y optimización de la síntesis de nanomateriales basados en grafeno", constituye la memoria que presenta **Dª. María del Prado Lavín López** para aspirar al grado de Doctor en Ingeniería Química y que ha sido realizada en los laboratorios del Departamento de Ingeniería Química bajo su supervisión.

Y para que conste a efectos oportunos, firman el presente certificado

En Ciudad Real, a 3 de febrero de 2017

D. José Luis Valverde Palomino Dª. Amaya Romero Izquierdo

Agradecimientos

En estas líneas quiero expresar mi agradecimiento a todas y cada una de las personas que han colaborado en la realización de la presente Tesis Doctoral.

En primer lugar a mis directores de tesis. A Jose Luis, por darme la oportunidad de comenzar esta etapa de mi vida, enseñarme lo que es la investigación y transmitirme sus ganas de enfrentarme a nuevos retos y aprender a resolverlos. A Amaya por su confianza e interés, por enseñarme a luchar por sacar las cosas adelante y darme su cariño y apoyo durante los buenos y malos momentos. También me gustaría agradecer a Graphenano, en especial a Mario, Martín y Jose Antonio, no solo por la financiación de esta tesis, sino el por apoyo e interés mostrado y la confianza depositada en mí durante todos estos años.

A mis compañeros del Departamento de Ingeniería Química, en especial a los del Laboratorio de Catálisis y Materiales, por los buenos ratos que hemos pasado. A Conchi y Arcadio, porque sin vuestra ayuda este trabajo no hubiera sido posible.

A Ester, Magda, Ana y Silvia, porque más que compañeras de trabajo sois amigas. A mi "Umpa-Lumpa" favorito, por tu constancia, tus ganas de trabajar y tu alegría, porque sin ti la mitad de esta tesis no hubiera sido posible. A mis riquillas, Mery y Carolina, porque siempre nos hemos apoyado y nos lo hemos pasado muy bien, porque todos estos años en el laboratorio no habrían sido lo mismo sin vosotras.

No puedo acabar estas líneas sin agradecer a mis amigas y amigos todo su apoyo y sus palabras de ánimo, por saber sacarme una sonrisa y animarme en todo momento.

Pero sobre todo a mis padres y mi hermano, porque desde pequeña me habéis apoyado en todo y habéis hecho posible que todas y cada una de mis metas en la vida se fueran cumpliendo. Gracias de corazón. Por último me gustaría a agradecer todo su apoyo y fortaleza a Pablin, porque siempre consigues sacarme una sonrisa por muy mal que estén las cosas.

A todos los que de una manera u otra han aportado su granito de arena para la realización de esta tesis doctoral.

Tabla de contenidos

Nomenclatura

C: Carbono

0D, 1D, 2D, 3D: Dimensión 0, 1, 2 y 3

GICs: Compuestos Intercalados del Grafito

SiC: Carburo de Silicio

IUPAC: International Union of Pure and Applied Chemistry

SiO_2: Óxido de silicio

CVD: Deposición Química en fase Vapor (Chemical Vapor Deposition)

FET: Transistores de Efecto de Campo

Ni: Níquel

Fe: Hierro

Pd: Paladio

Ru: Rutenio

Ir: Iridio

Cu: Cobre

Co: Cobalto

Pt: Platino

G: Grafito

GrO: Óxido de grafito

GO: Óxido de grafeno

TEM: Transmisión Electrónica de alta Resolución

C/O: Relación carbono/oxígeno

NO_2: Dióxido de nitrógeno

N_2O_4: Tetraóxido de nitrógeno

ClO_2: Dióxido de cloro

$NaNO_3$: Nitrato sódico

ADN: Ácido desoxirribonucleico

VIH: Virus de la inmunodeficiencia humana

HNO_3: Ácido nítrico

$KClO_3$: Clorato de potasio

H_2SO_4: Ácido sulfúrico

$KMnO_4$: Permanganato potásico

P_2O_5: Anhídrido fosfórico

$K_2S_2O_3$: Persulfato potásico

H_3PO_4: Ácido fosfórico

RGrO: Óxido de grafito reducido

RGO: Óxido de grafeno reducido

PVP: Polivinilpirrolidona

CH_4: Metano

$FeCl_3$: Tricloruro de hierro

HF: Ácido fluorhídrico

Na_2CO_3: Carbonato sódico

H_2O_2: Agua oxigenada

HCl: Ácido clorhídrico

CH_3CH_2OH: Etanol

C_2H_6O: Éter dietílico seco

N_2H_6O: Hidracina monohidratada

$C_6H_8O_6$: Ácido ascórbico

h: hora

min: minuto

s: segundo

H_2: Hidrógeno

N_2: Nitrógeno

v/v: volumen/volumen

ºC: Grado centígrado

Nml/min: Normal mililitro minuto

Nl/min: Normal litro minuto

PET: Tereftalato de polietileno

g: gramos

ml: mililitros

Mn_2O_7: Óxido de manganeso (VII)

rpm: Revoluciones por minuto

H-RGO: Óxido de grafeno reducido químicamente con hidracina

A-RGO: Óxido de grafeno reducido químicamente con ácido ascórbico

T-RGrO: Óxido de grafito reducido térmicamente

T-RGO: Óxido de grafeno reducido térmicamente

HMP-RGO: Óxido de grafeno reducido por el método múltiples fases con hidracina

AMP-RGO: Óxido de grafeno reducido por el método múltiples fases con ácido ascórbico

SEM: Microscopía Electronica de Barrido

FWHM: Full Width at Half Maximum

L_D: Distancia entre defectos

$C(\lambda)$: Constante, 102 nm^2

TGA: Análisis termigravimétrico

DTG: Derivada termigravimétrica

XRD: Difracción de Rayos X

d_{002}: Espaciado interlaminar

L_c: Tamaño medio cristalino en la dirección perpendicular a las láminas de grafeno

L_a: Tamaño medio cristalino en la dirección paralela a las láminas de grafeno

λ: longitud de onda de la radiación (λ=1,5404 Å).

θ: ángulo de difracción correspondiente al pico [002] del grafito y [001] y [100] de los materiales derivados del grafeno.

K_a: constante de Scherrer (1,84 para compuestos carbonosos).

K_c: constante de Scherrer (0,90 para compuestos carbonosos).

B: FWHM (Full Width at Half Maximum)

Ar: Argón

CO_2: Dióxido de carbono

FTIR: Espectroscopia Infrarroja de la Transformada de Fourier

UATR: Reflectante atenuado universal total

H: Hidrogeno

N: Nitrógeno

O: Oxigeno

S: Azufre

BET: Brunauer, Emmett y Teller

P: Presión

P_0: Presión atmósferica

VBA: Visual Basic

sccm: standard cubic centimeters per minute

Resumen

La presente tesis doctoral, desarrollada en el Departamento de Ingeniería Química de la Universidad de Castilla-La Mancha y financiada por Graphenano S.L. a través de los contratos UCTR120087 y UCTR160177, forma parte de un amplio programa de investigación orientado a la preparación de nanomateriales carbonosos. Precisamente, el grupo de Catálisis y Materiales de dicho departamento posee una amplia experiencia en este ámbito del conocimiento. En el año 2002 se inició la primera tesis doctoral relacionada con la preparación de nanofibras de carbono. En posteriores investigaciones, se continuó con la preparación de nanotubos y nanoesferas de carbono y carbono-nitrógeno, así como el posterior uso de todos estos nanomateriales en diferentes aplicaciones. Hasta el momento, se han completado cinco tesis doctorales, excluyendo la presente, de las que se han derivado más de 30 artículos en revistas indexadas.

Con la presente tesis doctoral se inició el estudio de los procesos de síntesis de grafeno y de otros nanomateriales relacionados con éste (especialmente óxido de grafito y óxido de grafeno reducido). Este material, ha recibido una considerable atención en los últimos años tras la concesión, en 2010, del Premio Nobel de Física a Andre Geim y Konstantin Novovselov por su descubrimiento.

Desde que Richard Feynmman, en el año 1959, introdujera el concepto de nanotecnología (ciencia que se dedica al diseño y manipulación de la materia a nivel atómico o molecular), este ámbito del conocimiento se ha desarrollado de forma exponencial, principalmente en los últimos años, llegando a su cúspide con el descubrimiento de los nanotubos de carbono y el grafeno.

El grafeno se define como un material carbonoso con un solo átomo de espesor, cuyos átomos están unidos mediante enlaces sp^2 y empaquetados en una estructura hexagonal. El carbono es un elemento fascinante pues aun siendo uno de los materiales más comunes de la naturaleza, la forma en que se conecta con otros átomos da lugar a muy

diversos materiales. Así, empaquetado densamente en una estructura tridimensional forma **diamante,** mientras que cuando se organiza en capas bidimensionales débilmente unidas forma **grafito**.

Hasta hace apenas 12 años se pensaba que, si se conseguía aislar una lámina individual de grafito, ésta tendría tal cantidad defectos que sería inestable a temperatura ambiente. Este hecho fue rebatido en el año 2004 por los físicos Andre Geim y Konstantin Novoselov al conseguir aislar una lámina individual de grafito utilizando el método de la cinta Scoth®, que consiste en adherir una porción de dicha cinta sobre una muestra de grafito separando de esta manera las láminas más superficiales del mismo. Repitiendo de forma indefinida el proceso sobre las láminas liberadas, se puede llegar a aislar láminas individuales de un átomo de espesor, conocidas como grafeno.

El grafeno presenta unas propiedades excepcionales como son su elevada conductividad térmica y eléctrica, elasticidad, resistencia y ligereza. Estas extraordinarias propiedades permiten que el grafeno pueda usarse en la manufactura de elementos esenciales, de uso cotidiano como ordenadores, coches, teléfonos móviles, elementos constructivos y pinturas.

Dentro de la familia de los nanomateriales relacionados con el grafeno destaca el óxido de grafeno, que puede definirse como una lámina de grafeno funcionalizada con distintos grupos oxigenados. Este nanomaterial puede emplearse como precursor en la producción de grafeno o como un nanomaterial individual, presentando propiedades como su elevada conductividad eléctrica y flexibilidad, alta resistencia a la fractura y carácter antibacteriano. Estas propiedades hacen del óxido de grafeno un material excelente con múltiples aplicaciones que van desde el campo de la construcción hasta el de biomedicina, pasando por el tratamiento de aguas o la industria alimentaria. La reducción o eliminación parcial de los grupos oxigenados presentes en la estructura del óxido de grafeno da lugar a un nuevo nanomaterial, el óxido de

grafeno reducido que, debido a sus propiedades, intermedias entre las del óxido de grafeno y el grafeno, permite su aplicación en campos tan diferentes como la fabricación de ánodos o de aptasensores.

Teniendo en cuenta lo expuesto anteriormente, se planteó una investigación centrada en la síntesis y caracterización de nanomateriales basados en grafeno. Con tal fin, la investigación desarrollada se centró en los siguientes objetivos:

- Revisión bibliográfica para conocer los antecedentes más relevantes de la síntesis de grafeno.
- Diseño y puesta a punto de una instalación experimental con la que sintetizar grafeno mediante el método CVD a escala de laboratorio.
- Diseño y puesta a punto de una instalación experimental a escala de laboratorio para sintetizar óxido de grafito y óxido de grafeno.
- Diseño y puesta a punto de una instalación experimental para sintetizar, a escala de laboratorio, óxido de grafeno reducido.
- Optimización de las técnicas de caracterización, ya existentes en el laboratorio, y puesta a punto de otras nuevas para el estudio de las propiedades de los nanomateriales basados en grafeno.
- Estudio de la influencia de las variables de operación que repercuten en la síntesis de grafeno mediante el método de Deposición Química en fase Vapor.
- Estudio de distintos sustratos catalíticos en la síntesis de grafeno (cobre, níquel y hierro).
- Transferencia del grafeno sintetizado por el método de Deposición en fase Vapor sobre cobre a substratos arbitrarios usando nuevos agentes químicos.

- Estudio de la optimización de las variables de operación que repercuten en la síntesis de óxido de grafeno.
- Estudio de diferentes métodos de reducción de óxido de grafeno (química, térmica y múltiples fases).

La presente tesis doctoral, abarca el estudio de la síntesis y caracterización de grafeno siguiendo dos estrategias diferentes: la estrategia *Bottom-Up*, en la que se parte de moléculas gaseosas de hidrocarburo para sintetizar láminas de grafeno sobre un metal, y la estrategia *Top Down* en la que se usa grafito como materia prima para sintetizar materiales derivados del grafeno (en polvo o en suspensión).

En primer lugar, se optimizaron las principales variables de operación que influyen sobre la síntesis de grafeno mediante el método de Deposición Química en fase Vapor (CVD) a presión atmosférica. Para ello se usaron diferentes metales de transición (Ni, Cu, Fe) policristalinos como catalizadores, metano (CH_4) como fuente carbonosa, hidrógeno (H_2) como gas reductor, y nitrógeno (N_2) como gas inerte. Las variables de operación estudiadas fueron: temperatura, tiempo, relación entre los caudales de metano e hidrógeno y caudal total de gases (CH_4+H_2), todas ellas durante la etapa de reacción. Para una exhaustiva caracterización de las muestras de grafeno obtenidas se utilizaron tanto la espectroscopía Raman como la microscopía óptica. Además, se diseñó una aplicación Excel-VBA para analizar la calidad del grafeno depositado sobre las láminas metálicas que, basándose en las imágenes obtenidas por microscopía óptica, permitía calcular el porcentaje de cada uno de los tipos de grafeno (monocapa, bicapa, pocas capas o multicapa) depositados sobre el catalizador metálico, determinando un "parámetro de calidad" en función de dichos porcentajes.

La síntesis de grafeno por el método CVD se llevó a cabo, en primer lugar, usando cobre policristalino como catalizador. El cobre es un metal

con una baja solubilidad al carbón, lo cual repercute en el mecanismo de crecimiento que experimenta el grafeno sobre dicho metal. En la síntesis de grafeno en metales con baja solubilidad al carbón, el mecanismo de crecimiento ocurre de manera superficial, en lo que se conoce como "*self-limited surface deposition growth*". La superficie metálica caliente actúa como catalizador, consiguiendo la descomposición térmica de los hidrocarburos en la superficie del mismo. Tras la síntesis de grafeno sobre cobre, se pudo comprobar que la lámina de grafeno obtenida no era homogénea, estando aproximadamente el 81% de la superficie del metal cubierta por grafeno multicapa. Sin embargo, a medida que se optimizaban las variables de operación se obtuvo un grafeno de mayor calidad, reduciendo el porcentaje de grafeno multicapa sobre la lámina hasta alrededor de un 11% y recubriendo aproximadamente la mitad de la lámina (56%) por grafeno bicapa. Las condiciones de operación óptimas usando cobre policristalino como catalizador fueron: 1050ºC, 10 minutos de reacción, relación CH_4/H_2 de 0.07 v/v y caudal total de gases (CH_4+H_2) durante la etapa de reacción de 60 Nml/min.

Determinadas aplicaciones como las relacionadas con la telefonía móvil o *tablets*, requieren transferir el grafeno desde la lámina metálica a determinados substratos, como plástico o cristal. Por esta razón, una vez optimizadas las variables de operación, se llevó a cabo la transferencia del grafeno depositado sobre cobre a una oblea PET y, posteriormente, a un substrato arbitrario, en este caso, una placa de microscopio óptico. Para ello, además del agente químico más usado en bibliografía ($FeCl_3$), se estudiaron dos nuevos agentes químicos, que no contaminan ni ensucian la lámina de grafeno: HF: $2Na_2CO_3{\cdot}3H_2O_2$ (4:1) y H_2O_2 (30%p./v.):agua regia ($1HNO_3$:3HCl):H_2O (1:1:2). De los tres agentes químicos estudiados, el que presentó mejor resultado fue el H_2O_2 (30%p./v.): agua Regia ($1HNO_3$:3HCl): H_2O (1:1:2) consiguiéndose una transferencia rápida (apenas unos segundos) y limpia del grafeno que, a su vez, puede ser usado en diferentes aplicaciones.

A continuación, y con el objetivo de sintetizar grafeno monocapa, se llevó a cabo la optimización de las principales variables de operación que influyen sobre la síntesis de grafeno mediante el método CVD utilizando níquel policristalino como catalizador. En el caso de los metales con alta solubilidad al carbón, como el níquel, tiene lugar un mecanismo de crecimiento de segregación superficial, conocido como "*surface segregation growth mechanism"*. En este caso, los átomos de carbono se disuelven en el interior del catalizador y, cuando éste comienza a enfriarse, estos átomos segregan desde el interior a la superficie del metal formando las láminas de grafeno. Se estudió en detalle la influencia de la temperatura, la relación de los caudales CH_4/H_2, el caudal total de gases (CH_4+H_2) y el tiempo durante la etapa de reacción. De nuevo, las principales técnicas empleadas para la caracterización del grafeno obtenido fueron la microscopía óptica y la espectroscopía Raman. A medida que se optimizaban las diferentes variables de operación y teniendo en cuenta los valores del "parámetro de calidad" obtenidos con la aplicación Excel-VBA, aumentaba el porcentaje de grafeno monocapa sobre la lámina, disminuyendo el porcentaje de grafeno multicapa. La muestra óptima, en la cual el 80 % de la lámina estaba recubierta por grafeno monocapa, se obtuvo a 980ºC, una relación entre caudales CH_4/H_2 de 0,07 v/v y un caudal total de gases de 80 Nml/min para un tiempo reacción de 60 segundos.

El estudio anterior demostró la viabilidad de sintetizar grafeno monocapa sobre metales con elevada solubilidad al carbón. Por ello, y con el objetivo de disminuir los costes de producción, se llevó a cabo un estudio similar a los anteriores pero utilizando hierro policristalino como metal catalítico. El hierro, al igual que el níquel, es un metal de elevada solubilidad al carbón, pero mucho más barato. Los resultados obtenidos demostraron que las condiciones óptimas de operación, es decir, aquellas en las que se maximiza el porcentaje de grafeno monocapa sobre la lámina de hierro policristalina, fueron: 1025ºC, una relación CH_4/H_2de 0.25 v/v y caudal total de gases (CH_4+H_2) de 80

Nml/min para un tiempo de reacción de 7 min. En estas condiciones, el 62,4 % de la lámina quedó recubierta por grafeno monocapa.

A continuación, se llevó a cabo la síntesis y caracterización de materiales derivados del grafeno siguiendo la estrategia *Top Down*. En primer lugar se sintetizó óxido de grafito mediante el *método de Hummers Mejorado*, el cual se intentó optimizar introduciendo determinados cambios que no afectaran significativamente al producto final. Se seleccionó dicho método por ser el que mayor rendimiento presenta y con el que se obtiene un producto final menos defectuoso. La optimización del proceso de síntesis de óxido de grafito por el *método de Hummers Mejorado* logró disminuir el tiempo de oxidación de 12 a 3 horas, eliminar la etapa de coagulación y reducir a la mitad las etapas de lavado. Además, se suprimió el uso de H_3PO_4 durante la etapa de oxidación y se logró incrementar hasta cinco veces la producción de óxido de grafito por tanda. El material final obtenido presentó unas características y propiedades muy similares al obtenido mediante el *método de Hummers Mejorado* sin optimizar, es decir, el descrito en bibliografía, pero con la ventaja de que se redujeron considerablemente los costes de producción.

Por último, se llevó a cabo un estudio en el que se compararon tres estrategias de reducción de óxido de grafeno diferentes. En primer lugar se estudió la *reducción química* de los grupos oxigenados presentes en la estructura del óxido de grafeno utilizando hidracina o ácido ascórbico como agentes reductores. La hidracina es el agente reductor más utilizado debido a su elevada eficacia pero posee el inconveniente de ser tóxico y dañino para el medio ambiente. El ácido ascórbico, más conocido como vitamina C, es completamente inocuo y respetuoso con el medioambiente, pero presenta una efectividad menor que la hidracina. Como era de esperar, los resultados obtenidos pusieron de manifiesto el elevado poder reductor de la hidracina, con la que se consiguió eliminar un mayor porcentaje de grupos oxigenados de la

estructura del óxido de grafeno. A continuación, se llevó a cabo la reducción o eliminación parcial de los grupos funcionales oxigenados presentes en el óxido de grafito mediante un tratamiento térmico suave (T < 300ºC), conocido como *reducción térmica*. Los resultados obtenidos pusieron de manifiesto la eficacia y sencillez del método térmico, con tasas de reducción de grupos oxigenados similares a las obtenidas con el método de reducción químico.

Por último, y con la finalidad de incrementar el grado de reducción de grupos oxigenados, se siguió una estrategia de reducción basada en la combinación de las dos anteriores, conocida como *reducción múltiples fases*, que se basa en la reducción térmica del óxido de grafito seguida de una reducción química con hidracina o ácido ascórbico.

De las tres estrategias de reducción estudiadas, la reducción basada en múltiples fases usando ácido ascórbico como agente reductor mostró la mayor efectividad, reduciendo hasta en un 27% los grupos oxigenados presentes en el óxido de grafito y obteniendo un material con una estructura y unas características similares a las obtenidas usando una única estrategia de reducción.

Capítulo 1: Introducción.

1.1. Carbono

El Carbono es un elemento químico, sólido a temperatura ambiente, de número atómico 6 y símbolo C. Dependiendo de las condiciones de síntesis durante su crecimiento, este elemento puede encontrarse en la naturaleza en diferentes formas alotrópicas [1].

Entre las diferentes formas alotrópicas del carbono se encuentran el material más blando y el más duro conocido en la naturaleza: grafito y diamante, respectivamente. Ambos materiales están formados por enlaces C-C, aunque son muy diferentes entre sí. El **grafito** (Figura 1.1.a.) es un material opaco y extremadamente blando, con brillo metálico. Es un excelente conductor de la electricidad. Sus átomos están empaquetados en una estructura hexagonal; poseen hibridación sp^2 y están unidos mediante fuerzas de Van de Waals. Por otro lado, el **diamante** (Figura 1.1.b.) es un material semitransparente, de elevada dureza y aislante. La estructura de éste material presenta una disposición de átomos con hibridación sp^3, unidos en una red tetraédrica.

Recientemente, se han conocido nuevos alótropos del carbono, como los **fullerenos** (Figura 1.1.c.), descubiertos en 1985 por Curl, Kroto y Smalley. Los fullerenos presentan una estructura esférica cerrada compuesta por átomos de carbono que, a su vez, están conectados a otros tres átomos de carbono. Esta estructura, por lo tanto, está configurada por 20 hexágonos y 12 pentágonos coincidentes en 60 puntos.

Otros alótropos del carbono, descubiertos recientemente, son las nanoestructuras de carbono, como los **nanotubos de carbono** (Figura 1.1.d.), las **nanofibras de carbono** (Figura 1.1.e.) y las **nanoesferas de carbono**. Las similitudes entre los nanotubos y las nanofibras de carbono hacen difícil diferenciarlos a priori. Estos materiales tienen en común su naturaleza grafítica, estando ambos formados por una red

hexagonal de átomos de carbono unidos mediante hibridaciones sp^2. Por esta razón, las nanofibras y los nanotubos de carbono comparten numerosas propiedades físicas y químicas. Probablemente, la principal diferencia entre ambos radique en su estructura tridimensional ya que las nanofibras de carbono presentan planos discontinuos que se originan en los bordes de grano de las fibras. Este hecho no se observa en los nanotubos de carbono. En estos últimos se pueden diferenciar láminas concéntricas de grafeno a lo largo de un eje, configurando una estructura continua [2]. Las nanoesferas de carbono también presentan estructura grafítica, con una porosidad muy baja y un área superficial moderada, consecuencia de su geometría esférica [3]. Las nanoesferas de carbono presentan una alta actividad química superficial, directamente relacionada con su estructura. En este alótropo del carbono, las hojas de grafeno que componen la estructura están normalmente abiertas, dejando muchos huecos abiertos en los extremos [4].

El ultimo alótropo del carbono descubierto hasta el momento es el **grafeno** (Figura 1.1.f.), el cual está formado por una red bidimensional de átomos de carbono que presentan hibridación sp^2 que están empaquetados en una red cristalina con forma de panal de abejas [5].

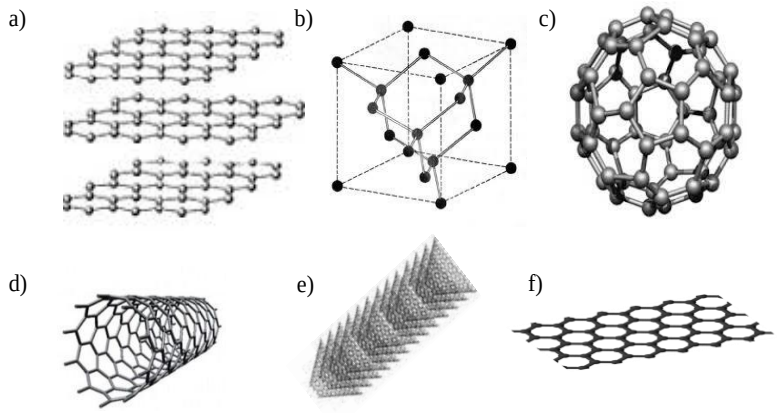

Figura 1.1. Alótropos del carbono: a) Grafito, b) Diamante, c) Fullereno, d) Nanotubo de Carbono, e) Nanofibra de Carbono f) Grafeno.

1.2. Grafeno

1.2.1. Definición del grafeno

El grafeno es un alótropo del carbono de un sólo átomo de espesor [6], cuya estructura está compuesta por una única lámina plana en la cual los átomos de carbono presentan hibridación sp^2 y donde cada átomo está unido mediante un enlace covalente a otros tres átomos de carbono (Figura 1.2.). Éstos, se encuentran densamente empaquetados en una red cristalina en forma de estructura hexagonal de dos dimensiones (2D) compuesta, a su vez, de 2 subredes triangulares superpuestas [7].

Al ser un cristal bidimensional, cada átomo de carbono es accesible por ambos lados, lo que supone una mayor interacción con las moléculas que le rodean [8].

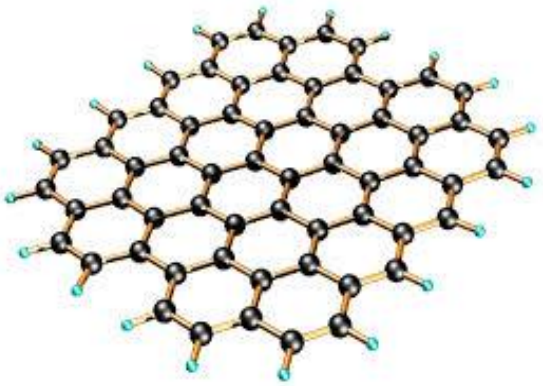

Figura 1.2. Estructura del grafeno.

En el grafeno, cada átomo de carbono se une a otros tres mediante fuertes enlaces covalentes tipo σ, los cuales dan lugar a su estructura hexagonal [9]. El enlace tipo π, perpendicular al plano, proporciona una interacción débil entre las diferentes capas de grafeno y es el causante de sus peculiares propiedades electrónicas.

El término grafeno se utiliza para hacer referencia a un material formado por pocas láminas, desde una hasta diez láminas superpuestas.

Las propiedades del mismo variarán en función de su dimensión [6]. Tomando como base diferenciadora el número de láminas, el grafeno puede ser clasificado en cuatro tipos: monocapa, bicapa, pocas capas (cuando se presentan de 3 a 4 capas) y multicapa (cuando éste está constituido por 5 o más capas, hasta 10).

Esta estructura monoatómica, compuesta de anillos de benceno desprovistos de sus átomos de hidrógeno, se considera la base para el entendimiento de las propiedades de otros alótropos de carbono [10], y se puede considerar como el constituyente básico de otras sustancias grafíticas. Así, si se envolviera en forma de bola proporcionaría fullerenos; si lo hiciera cilíndricamente originaría nanotubos; si se superpusiera tridimensionalmente daría lugar a grafito como se muestra en la Figura 1.3. [6].

El nombre grafeno, *graphene* en inglés, es una combinación de la palabra *grafito* y el sufijo *–ene*. Este término apareció por primera vez en el año 1987 [11] para describir láminas individuales de grafito como constituyente fundamental de los compuestos intercalados del grafito (GICs). Este término también se usó en las primeras descripciones de los nanotubos de carbono [12] así como en las del grafeno epitaxial [13] y en las de los hidrocarbonos policíclicos aromáticos [14].

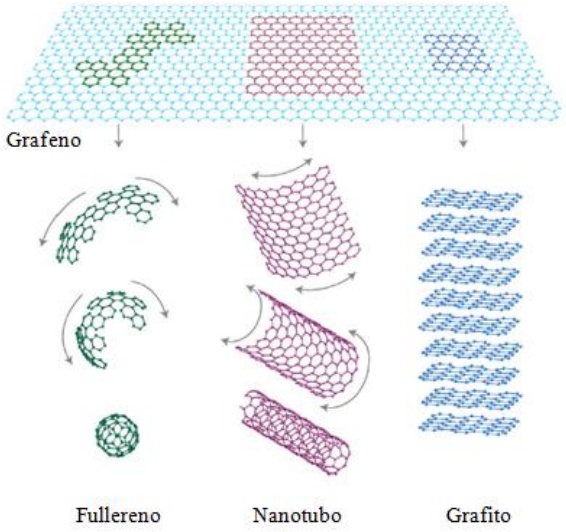

Figura 1.3. Estructuras derivadas del grafeno: fullereno (0D), nanotubo de carbono (1D) y grafito (3D) [6].

1.2.2. Historia del grafeno

El grafeno es uno de los materiales más ampliamente investigados actualmente y está considerado, por las peculiares propiedades que presenta, como un material fascinante [6].

Diversos investigadores han trabajado durante años en el estudio del grafeno y sus derivados. Las investigaciones más pioneras las llevó a cabo Brodie en el año 1860, quién sintetizó óxido de grafito [15]. Más tarde, Staudenmaier, en el año 1898, propuso una mejora del método de Brodie mediante la adición de un nuevo oxidante (clorato potásico) y la acidificación de la mezcla con ácidos concentrados [16]. Décadas después (1958), Hummers y sus colaboradores desarrollaron un método completamente diferente para la síntesis de óxido de grafeno, más respetuoso con el medio ambiente y en el que se conseguía un mayor grado de oxidación del producto. Años después se han desarrollado diversas modificaciones de éste método, con la finalidad de obtener una mayor oxidación [17].

Tanto el enlace químico como la estructura del grafeno se describieron durante la década de 1930, aunque el primer estudio de la estructura electrónica de bandas lo realizó el teórico canadiense P. R. Wallace, en 1947, como punto de partida para entender las propiedades electrónicas del grafito 3D. Sin embargo, no se indagó en su estudio durante las décadas posteriores ya que se pensaba que se trataba de un material termodinámicamente inestable, debido a las fluctuaciones térmicas que podían destruir el orden del cristal, provocando la fusión del mismo.

En el año 1962 Boehm y sus colaboradores utilizaron por primera vez el término "grafeno", en la revista alemana Z. Naturforsch, para referirse al grafito exfoliado químicamente, proceso por el cual se separan las láminas de grafito en presencia de ácidos fuertes, generando así "el material más delgado que existe". Ese mismo año, este equipo de investigación, logró la síntesis de óxido de grafeno reducido mediante la reducción térmica y química de óxido de grafeno [18].

El primer tratamiento térmico usado para sintetizar grafeno se realizó en el año 1975, sublimando carburo de silicio (SiC) a 800ºC [19]. Este método es conocido como crecimiento epitaxial de grafeno sobre SiC. En esa misma década se investigó el crecimiento epitaxial de grafeno sobre la superficie de otros materiales [20]. A raíz de estas investigaciones, se han realizado numerosos esfuerzos para crear láminas finas de grafito por exfoliación mecánica, (empezando en 1990 y hasta 2004) aunque no se consiguió nada más fino que un material con un grosor de 50-100 láminas [21].

En los años 80 se descubrieron los nanotubos de carbono (grafeno enrollado), material que comparte numerosas propiedades con el grafeno, que resulta ser de gran interés en diversas aplicaciones [22].

En años posteriores, se observaron láminas individuales de grafeno directamente a través del microscopio electrónico [23]. El término grafeno fue usado por primera vez en el año 1987 por Boehm y sus

colaboradores [11] para describir láminas individuales de grafito, como constituyentes de los compuestos de intercalación del grafito (GICs). Oficialmente, la IUPAC formalizó la definición de grafeno en el año 1997 [24].

En el año 1999, Ruoff y sus colaboradores lograron la exfoliación micromecánica del grafito obteniendo láminas finas del mismo [25]. Este hecho fue la base de las investigaciones realizadas en la Universidad de Manchester por Andre Geim y Kostya Novoselov quienes en el año 2004 lograron extraer grafeno de un átomo de espesor a partir de grafito a granel. Los investigadores consiguieron separar las diferentes capas de grafeno mediante el proceso de escisión micromecánica o técnica de la cinta Scotch® y las transfirieron sobre una superficie SiO_2, [8]. Este método permitió observar directamente y por primera vez (año 2005) el comportamiento del efecto Hall cuántico anómalo del grafeno además de otras propiedades electrónicas [26, 27]. Este comportamiento anómalo fue confirmado el mismo año por la pareja de investigadores constituida por Philip Kim y Yuanbo Zhang [27].

Durante los años posteriores se investigaron nuevas técnicas para sintetizar grafeno. Por ejemplo, en el año 2006 se iniciaron las primeras investigaciones para sintetizar grafeno por el método de Deposición Química en fase Vapor (CVD) [28].

Debido a la importancia que ha adquirido este material, en el año 2010, la Real Academia de las Ciencias de Suecia decidió galardonar a Andre Geim y Kostya Novoselov con el premio Nobel de física por sus investigaciones [29].

En 2013, la industria y la academia unieron sus fuerzas para concentrarse en la investigación del grafeno en lo que se conoce como la iniciativa *Graphene Flagship*, que se concedió aprovechando una

convocatoria de la Comisión Europea para hacer frente a los grandes retos de la ciencia y la tecnología [30].

La Figura 1.4. muestra una línea del tiempo que resume los descubrimientos y avances más relevantes del grafeno citados anteriormente:

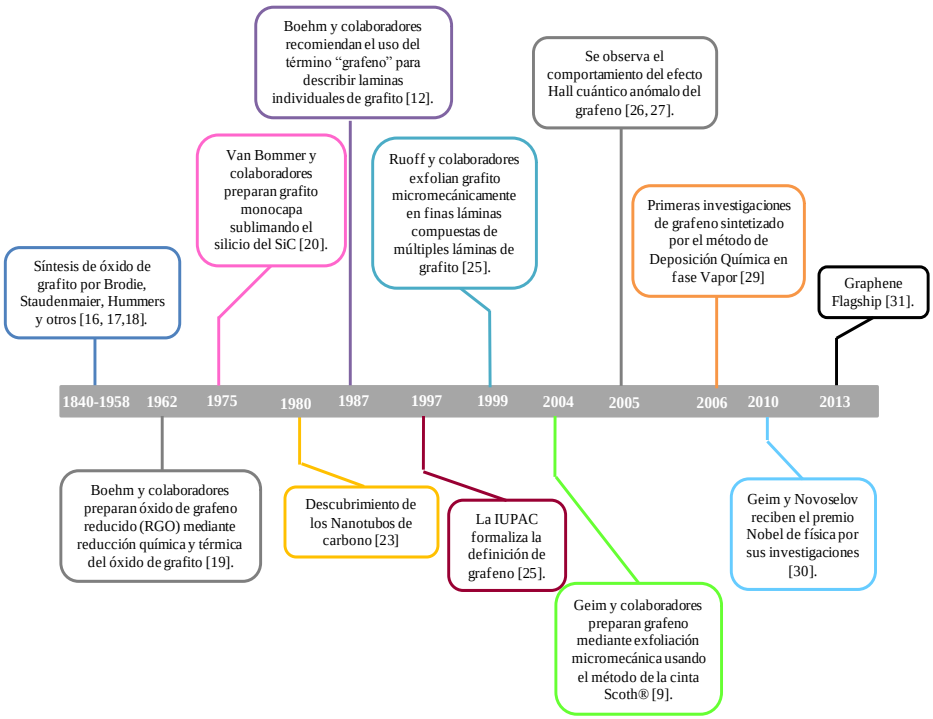

Figura 1.4. Breve historia del grafeno**.**

1.2.3. Propiedades del grafeno

El grafeno es un material con propiedades únicas, que le hacen especialmente atractivo, tanto desde el punto de vista de la investigación básica como por sus posibles aplicaciones.

1.2.3.1. Propiedades electrónicas

El grafeno es un semiconductor de banda prohibida (gap) cero. Comparte con los metales que el gap electrónico es nulo [10] y, sin

embargo, tiene una densidad de estados en el nivel de Fermi nula, característica propia de los semiconductores.

Los portadores de carga del grafeno cuentan con una elevada movilidad intrínseca de electrones que, a temperatura ambiente, puede alcanzar los 200000 $cm^2V^{-1}s^{-1}$ [31] siendo además, dicha movilidad, poco dependiente de la temperatura [6]. Esta movilidad tan elevada de los portadores de carga del grafeno, superando la de los actuales transistores de Si, asegura el transporte balístico a distancias sub-micrométricas incluso a temperatura ambiente.

Por otro lado, la calidad del grafeno se advierte en un acentuado efecto de campo eléctrico ambipolar, tal que los portadores de carga pueden moverse continuamente entre electrones y huecos en concentraciones tan altas como 10^{13} cm^{-2} [6].

Otras de las inusuales propiedades electrónicas de grafeno son el efecto Hall cuántico (QHE) que presenta, que puede observarse a temperatura ambiente [6], y la resistividad intrínseca que muestra a temperatura ambiente de tan solo 10^{-8} Ω (valor incluso menor que el de la plata, que es el material conocido con menor resistividad) [32].

1.2.3.2. Propiedades físico-químicas

El grafeno es el material más fino descubierto hasta el momento, con sólo una lámina de átomos de carbono, un espesor de 0,34 nm y una baja densidad de 2,22 g/cm^3 [33].

El grafeno presenta una elevada área superficial específica de aproximadamente 2600 m^2 g^{-1} [34]. Además, es de 100 a 1000 veces más grande que las moléculas orgánicas típicas por lo que estas redes cristalinas sirven de base para la síntesis de nuevas moléculas híbridas.

1.2.3.3. Propiedades térmicas

La conductividad térmica del grafeno, capacidad de un material para transferir calor, es mayor que la de cualquier material conocido. En 2008, Balandin y sus colaboradores llevaron a cabo una serie de experimentos utilizando una técnica óptica de no contacto que permitía medir la conductividad térmica de una lámina monoatómica de grafeno suspendida sobre un sustrato de Si/SiO_2. El valor obtenido fue de 5000 W/mK [35].

1.2.3.4. Propiedades mecánicas

Se ha demostrado, mediante experimentos mecánicos, que el grafeno es el material más duro medido hasta el momento [9]. Presenta un elevado módulo de Young de aproximadamente 1TPa, lo que le permite soportar tensiones elevadas antes de romperse. Simultáneamente, presenta una elevada flexibilidad que se evidencia en la formación de pliegues en sus hojas [36].

Además, el grafeno posee una fuerza de ruptura de 42 N/m [9] y presenta deformaciones elásticas reversibles de hasta un 20%, valor superior a cualquier otro material conocido en la naturaleza [37].

Estas excepcionales propiedades mecánicas son de suma importancia para aprovechar el grafeno como material estructuralmente fuerte así como para comprender y controlar la durabilidad del grafeno utilizado en electrónica y almacenamiento de energía [38].

1.2.3.5. Propiedades ópticas

El grafeno es un material muy atractivo debido a su elevada transparencia óptica ya que, al tratarse de un material con un ínfimo espesor, los fotones lo atraviesan fácilmente. Posee una tasa de absorción sorprendentemente alta para tratarse de un material con una sola capa atómica de espesor. Una lámina de grafeno absorbe casi el 2,3% de la intensidad de la luz blanca que llega a su superficie [39],

aumentando dicha absorción linealmente con la adición de sucesivas capas [40].

Presenta además, una transmitancia óptica muy elevada de, aproximadamente un 97,4% [41].

En la Figura 1.5. se comparan las extraordinarias propiedades del grafeno con las de otros materiales, poniendo de manifiesto el gran interés que ha despertado este material en los últimos años [42].

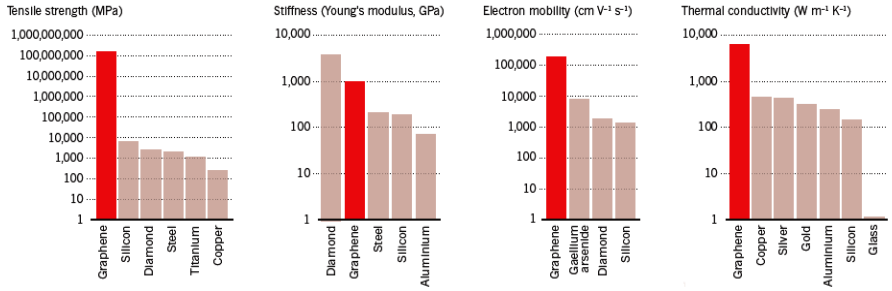

Figura 1.5. Propiedades eléctricas, mecánicas y térmicas del grafeno comparadas con las de otros materiales [42].

1.2.4. Aplicaciones del grafeno

Debido a sus excelentes propiedades, el grafeno es considerado un material muy prometedor para numerosas aplicaciones (Figura 1.6.).

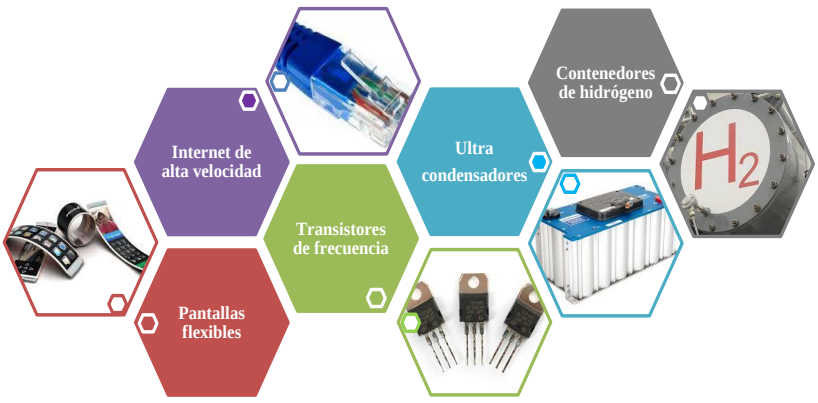

Figura 1.6. Aplicaciones del grafeno.

Como se ha comentado anteriormente, el grafeno posee una conductividad térmica muy elevada, propiedad que hace que sea un material más conductor que el silicio. Esta característica permite su utilización en aplicaciones tales como transistores o circuitos, haciendo que éstos trabajen de manera más rápida [43]. Además, debido a la elevada movilidad de electrones que permite, se está estudiando su uso en la fabricación de transistores de efecto de campo (FET) [8], con velocidades de conmutación muy elevada (algunos prototipos ya han alcanzado los 100 GHz).

Debido a su elevada movilidad electrónica a temperatura ambiente y a la baja densidad de defectos en su estructura cristalina, el grafeno ha sido integrado en sensores de gases y biosensores [44].

Investigadores de la Universidad de Cambridge lograron que el grafeno fuera capaz de captar una gran cantidad de luz, lo que podría emplearse en la producción de un nuevo tipo de cables de fibra óptica de mayor capacidad. Estos cables de grafeno podrían transmitir información cientos de veces más rápido que los actuales [45], lo que implica que, en un futuro, puedan usarse para aumentar la capacidad y rapidez de Internet, la telefonía móvil y todas las comunicaciones que se puedan llevar a cabo.

La baja transmitancia óptica, de tan sólo un 2,3% en el rango del visible, y la elevada conductividad eléctrica, hacen del grafeno un material único para la creación de películas ultrafinas o pantallas conductoras transparentes [46].

El grafeno puede utilizarse para el almacenamiento de hidrógeno debido a su gran capacidad de absorber grandes cantidades de este gas [6]. Esta singular capacidad del grafeno se debe a su gran superficie específica, baja densidad y una química superficial favorable.

Otra aplicación atractiva es la de su uso en forma de polvo en la construcción de baterías eléctricas, que son ya uno de las principales aplicaciones comerciales de este material. La elevada conductividad del polvo de grafeno podría introducir mejoras en la eficiencia de las baterías, relevando así a las nanofibras de carbono, utilizadas en las baterías modernas [45].

Debido a su transparencia y flexibilidad, el grafeno puede utilizarse en la fabricación de células solares que podrían ser instaladas en los exteriores de edificios y otros entornos.

Además, la aparición del grafeno ha supuesto un gran avance en el desarrollo de los supercapacitadores. Se han desarrollado dispositivos que almacenen tanta energía como las baterías, con la ventaja añadida de que pueden recargarse en segundos. Desde hace algunos años, se está estudiando la incorporación de grafeno en los electrodos de los supercapacitadores, observándose claros beneficios en lo que a densidad energética y potencia se refiere.

La Tabla 1.1. muestra la relación existente entre las propiedades del grafeno y las principales aplicaciones derivadas de cada una de ellas.

Tabla 1.1. Características y aplicaciones del grafeno.

PROPIEDADES	APLICACIONES	REF.
Elevada movilidad de electrones	Transistores Láseres Foto detectores	[5, 47]
Elevada área superficial **Conductancia**	Sensores	[6, 48]
Estructura de banda lineal (espectro de Dirac para fermiones sin masa)	Transistores de efecto de campo	[8]
Elevada conductividad electrónica **Elevada movilidad de electrones** **Elevada tansmitancia óptica**	Películas transparentes conductoras	[48]
Elevada área superficial **Transferencia de electrones a lo largo de la superficie 2D**	Dispositivos de energía limpios	[48]
Efecto Hall cuántico anómalo	Transistores balísticos	[49]
Elevada conductividad	Materiales conductores, Baterías eléctricas	[6]
Fácil absorción de gases	Control de la contaminación	[47]
Transparencia (>99%) **Elevada conductividad electrónica**	Pantallas táctiles	[50]
Impermeabilidad	Recubrimientos	[51]
Elevada Resistencia mecánica (dureza)	Construcción	[5]

Por otro lado, es necesario tener en cuenta la morfología del grafeno con objeto de poder relacionar sus propiedades y aplicaciones, puesto que éstas resultan ser distintas, según la naturaleza en la que se encuentra, ya sea en polvo o lámina. En la Tabla 1.2 se muestra un pequeño resumen.

Tabla 1.2. Relación entre la morfología del grafeno, sus propiedades y aplicaciones.

	LÁMINA	**POLVO**
Propiedades	Elevada movilidad electrónica Elevada conductividad electrónica Elevada conductividad térmica Elevada transparencia	Baja movilidad electrónica Conductividad electrónica media Conductividad térmica media
Aplicaciones	Electrónica Fotónica Pantallas Iluminación Paneles solares	Composites Recubrimientos conductores Baterías Supercondensadores Biotecnología

1.2.5. Métodos de síntesis del grafeno

El grafeno se obtuvo por primera vez en el año 2004, siguiendo el procedimiento de exfoliación micromecánica de grafito [8]. Tras este descubrimiento, se han desarrollado otros procedimientos alternativos, consiguiendo obtener grafeno tanto multicapa [52, 53] como monocapa [54, 55]. Dependiendo de su morfología (lámina o polvo) el grafeno puede sintetizarse mediante numerosos métodos. Basándose en la naturaleza del material de partida se pueden diferenciar dos estrategias diferentes para sintetizar grafeno: *Bottom-Up* y *Top-Down* (Figura 1.7.). La estrategia *Bottom-Up* comprende aquellos métodos que utilizan una fuente carbonosa gaseosa para sintetizar grafeno depositado sobre una

lámina. La estrategia *Top-Down* engloba aquellos métodos en los que se ataca el grafito para separar las láminas que lo conforman y formar láminas aisladas de grafeno [56].

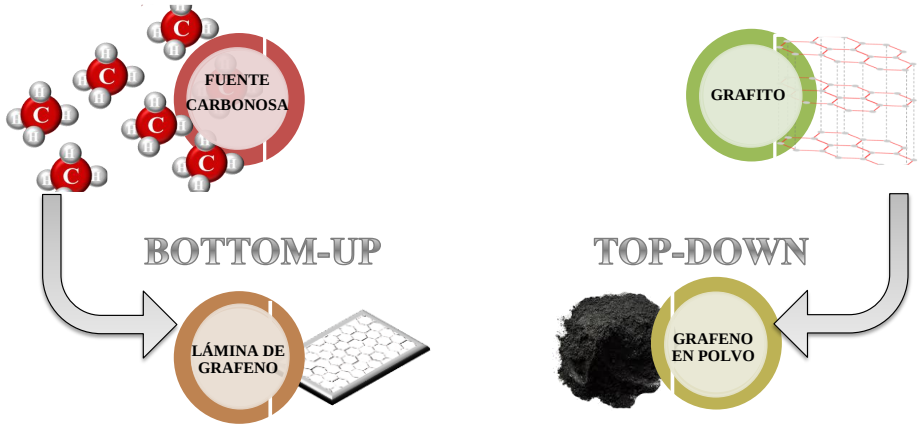

Figura 1.7. Estrategias *Bottom-Up* y *Top-Down* para sintetizar grafeno.

1.2.5.1. Estrategia Bottom-Up

Dentro de la estrategia *Bottom-Up*, cabe destacar los siguientes métodos:

a) Crecimiento epitaxial sobre carburo de silicio (SiC)

El crecimiento epitaxial es un método por el cual se consigue crecer monocapas aisladas de grafeno sobre un cristal monocristalino de carburo de silicio (SiC), el cual es usado como substrato.

Este método consiste en calentar obleas de SiC a elevadas temperaturas (>1100ºC) y alto vacío. En las condiciones mencionadas se consigue que los átomos de Si se sublimen (paso de sólido a gas) consiguiendo el crecimiento epitaxial de grafeno sobre su superficie (los átomos de carbono se reordenan formando grafeno) [57].

A pesar de obtener grafeno de gran calidad estructural, elevada movilidad electrónica y ser un método fácilmente escalable, la descomposición térmica de SiC posee el inconveniente de ser altamente

costosa, debido a las condiciones de operación y al coste del substrato [58, 59].

b) Descomposición química en fase vapor (CVD)

En el método de descomposición química en fase vapor una fuente carbonos se descompone catalíticamente sobre un substrato metálico [60]. La superficie metálica, que actúa como catalizador, provoca, tras la descomposición térmica de los hidrocarburos presentes, la disolución de los átomos de carbono generados en el interior del metal. El grafeno se forma sobre la superficie del metal una vez se alcanza la saturación de estos y el conjunto se enfría.

La solubilidad del carbono en el metal y las condiciones de crecimiento son los factores determinantes que afectan a la deposición superficial del mismo y a la morfología, calidad y espesor de las láminas de grafeno formadas [61].

Se pueden usar diferentes metales de transición como catalizadores en este método: Ni [62, 63], Fe [64], Pd [65], Ru [66], Ir [67] y Cu [5, 59]. De todos ellos, los más usados son el níquel, metal sobre el que se sintetizó por primera vez grafeno usando éste método de síntesis, y el cobre [54, 55, 68].

Como fuente carbonosa se usan normalmente hidrocarburos gaseosos. Aunque también se usan otras fuentes de carbono, especialmente en los estudios más recientes, como residuos orgánicos, plásticos o alimentos. Así, alimentos de bajo valor y desechos sólidos, se pueden transformar con éxito en grafeno de alta calidad, lo que supone una nueva forma de reciclar carbono a partir de fuentes impuras, resultando muy interesante económica y medioambientalmente [58].

1.2.5.2. Estrategia Top-Down

Dentro de la estrategia *Top-Down*, cabe destacar los siguientes métodos:

a) Exfoliación micromecánica de grafito o método de la cinta Scotch®

La exfoliación micromecánica de grafito consiste en la separación de la capa más externa de dicho sólido en "laminillas" u "hojuelas" mediante raspado fino, utilizando para ello un objeto de superficie solida o cinta adhesiva [6]. El grafeno se obtuvo en estado libre por primera vez mediante esta última técnica por la pareja Geim-Novoselov, hecho, entre otros, que les llevó a ganar el premio Nobel de Física en el año 2010. Los investigadores anteriormente mencionados, obtuvieron capas de grafeno que, tras suspenderlas en acetona, se transfirieron sobre SiO_2 [8]. Al tratarse de una técnica manual, el grafeno obtenido es de elevada calidad aunque el rendimiento del proceso es bajo. Este hecho hace que se comenzaran a estudiar nuevas técnicas que definieran procesos de más fácil escalado industrial.

b) Exfoliación de grafito en fase líquida

La exfoliación de grafito en fase líquida puede ser química o mecánica. La **exfoliación química** o método conocido como de Hummers implica la oxidación química del grafito, empleando oxidantes fuertes en medio ácido. En este método, los agentes oxidantes separan las láminas de grafito mediante la incorporación covalente de grupos funcionales oxigenados, como hidroxilos o carboxilos, obteniéndose *óxido de grafito*. Posteriormente, el óxido de grafito se exfolia a *óxido de grafeno* para conseguir la separación de sus láminas. El óxido de grafeno se reduce utilizando agentes reductores tales como H_2, hidroquinona, hidracina o ácido ascórbico, obteniendo "grafeno químicamente modificado" u óxido de grafeno reducido. Con la reducción se consigue obtener, hasta cierto punto, un producto con propiedades similares a las del grafeno [69]. Este método permite producir grandes cantidades de producto de baja calidad estructural con un bajo coste [58].

La **exfoliación mecánica** permite separar las láminas que conforman el grafito suspendido en disolventes orgánicos u acuosos mediante ondas de ultrasonido. El material obtenido es de alta calidad; no obstante, no resulta de gran interés industrial dado su bajo rendimiento y su alto coste de producción [70, 71].

1.3. Óxido de grafito

1.3.1. Definición de óxido de grafito

El **óxido de grafito (GrO)** es un conjunto de láminas de grafeno funcionalizadas, compuestas principalmente por átomos de carbono, oxígeno e hidrógeno que se puede emplear como precursor del grafeno o como material grafítico en sí mismo.

El óxido de grafito posee una estructura similar a la del grafito, diferenciándose ambas en que los grupos oxigenados presentes en el óxido de grafito le confieren mayor distancia entre las capas que lo conforman (Figura 1.8.) [72].

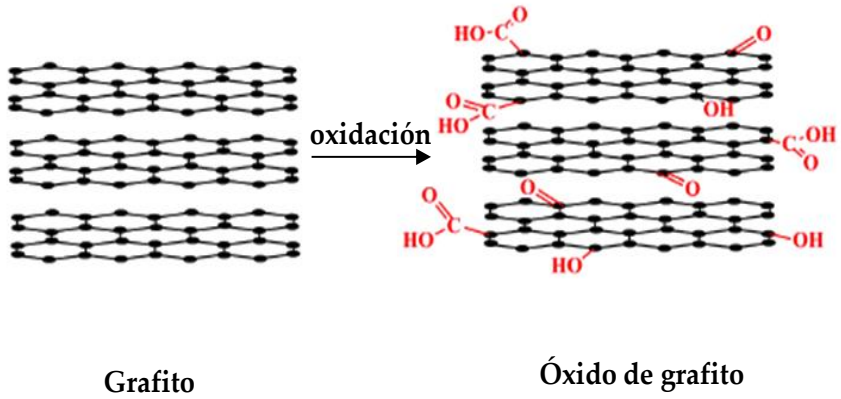

Figura 1.8. Evolución de grafito a oxido de grafito [73].

1.3.2. Estructura química del óxido de grafito

Aunque los métodos de síntesis de óxido de grafito se conocen desde hace 150 años, el conocimiento de su compleja estructura aún no está del todo claro, lo que ha llevado a proponer numerosos modelos [74] .

En el año 1939, **Hofmann y Holst** propusieron un modelo sencillo de estructura que contenía unidades repetidas de 1,2-epóxidos en todo el plano basal (Figura 1.9.) [75].

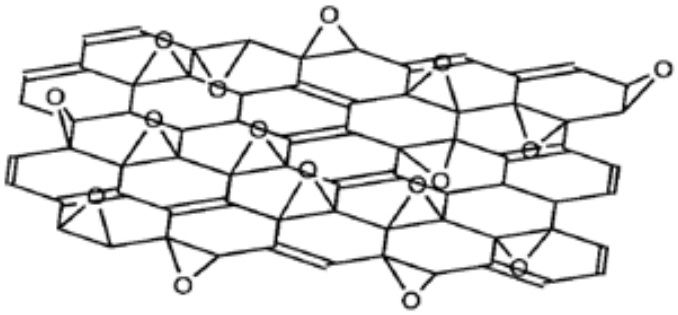

Figura 1.9. Estructura del óxido de grafito propuesta por Hofmann [74].

Más tarde, en 1946, **Ruess** sugirió un nuevo modelo en el que, además de grupos epoxi, existían también grupos hidroxilo y grupos éter que establecían puentes de hidrógeno entre los átomos de carbono, por lo que la estructura de las láminas de carbono era tridimensional y estaba fuertemente distorsionada (Figura 1.10.) [75].

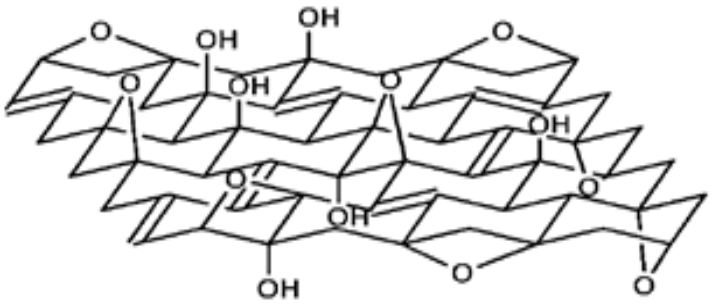

Figura 1.10. Estructura del óxido de grafito propuesta por Ruess [74].

En 1969, **Scholz y Boehm** propusieron un nuevo modelo que estaba compuesto únicamente de grupos hidroxilo y cetonas, en lugar de grupos epoxi y éter (Figura 1.11.)[74].

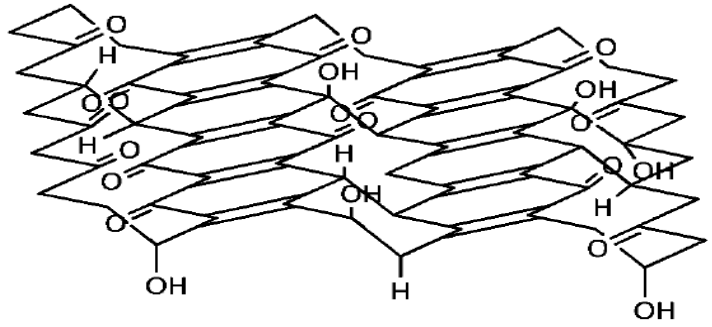

Figura 1.11. Estructura del óxido de grafito propuesta por Scholz y Boehm [74].

Posteriormente, **Nakajima y Matsuo** propusieron un nuevo modelo que consistía en una estructura similar a la del grafito, pero en la que los átomos de oxígeno de los grupos epoxi, unían capas adyacentes (Figura 1.12.) [75].

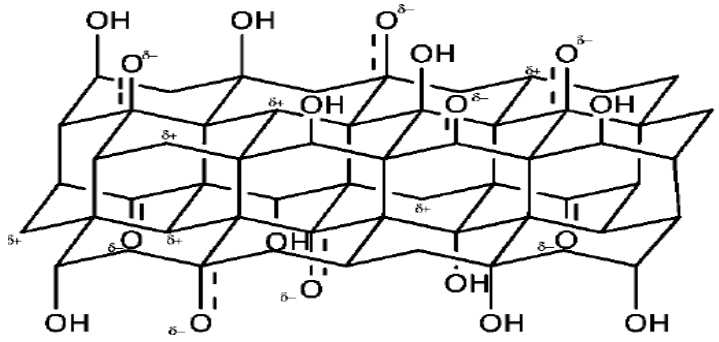

Figura 1.12. Estructura del óxido de grafito propuesta por Nakajima y Matsuo [74].

Al comprobar que los modelos anteriores arrojaban resultados similares mediante resonancia magnética nuclear, **Lerf y Klinowski** propusieron otro modelo en el cual los grupos oxigenados, como 1,2 epóxidos (-O-), y grupos hidroxilo (-OH) formaban el plano basal, mientras que el borde plano contenía además grupos carboxilos (-COOH) (Figura 1.13.) [74-76].

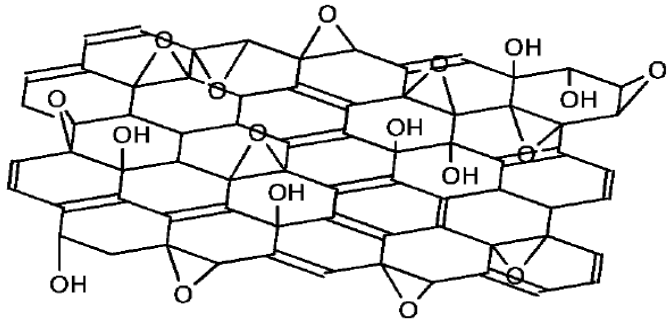

Figura 1.13. Estructura del óxido de grafito propuesta por Lerf y Klinowski [74].

La validez del modelo de Left-Klinowski fue posteriormente demostrada mediante microscopía de transmisión electrónica de alta resolución (TEM), [74].

Por último, **Dekany** introdujo un nuevo modelo que presenta características comunes a los modelos anteriores de Ruess y Scholz-Boehm [75]. La descripción de Dekany propone que el óxido de grafito está formado por sillas de ciclohexano y cintas hexagonales. Las sillas de ciclohexano contienen 1,3-epóxido y grupos hidroxilos terciarios, mientras que las cintas de hexágonos están conformadas con cetonas cíclicas y quinonas. También se han introducido grupos fenólicos en el modelo, con objeto de explicar la acidificación del óxido de grafito (Figura 1.14.) [74].

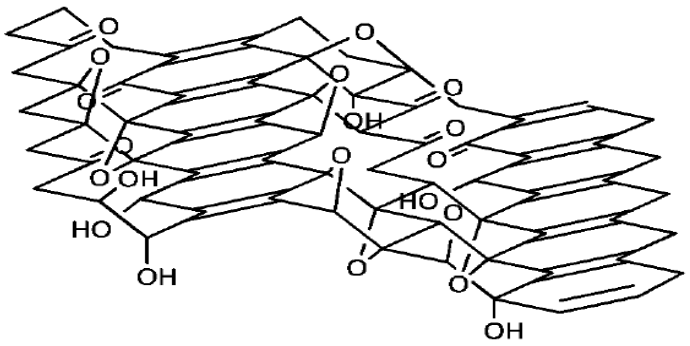

Figura 1.14. Estructura del óxido de grafito propuesta por Dekany [74].

Actualmente, las teorías más aceptadas sugieren que el óxido de grafito no presenta unos grupos funcionales concretos sino que ha de ser descrito a través de un modelo estructural dinámico [74]. Así, la estructura del óxido de grafito varía en función del grado de oxidación, los materiales de partida y evoluciona constantemente en presencia de agua.

1.3.3. Historia del óxido de grafito

El óxido de grafito se descubrió en 1859 coincidiendo con la importación por parte de Inglaterra de una cantidad muy abundante de grafito de Ceylon (ahora conocido como Sri Lanka) [74]. El profesor Brodie, de la Universidad de Oxford, trató de medir el peso molecular de dicho grafito oxidándolo con ácido nítrico fumante en presencia de clorato de potasio. Tras repetir cuatro veces el procedimiento de oxidación en las mismas condiciones, y dejar secar a 100ºC, se obtuvo un sólido que se dispersaba en agua pura o alcalina, pero no en medio ácido. Por esta razón, Brodie denomino el material "ácido grafítico" [74].

En 1898, Staudenmaier mejoró el método de oxidación añadiendo clorato de potasio en pequeñas porciones y acidificando la mezcla con ácido sulfúrico concentrado. El material obtenido por Staudenmaier poseía una relación C/O similar a la preparada por Brodie. Sin embargo, este método era más simple puesto que no requería las cuatro repeticiones del proceso de oxidación [74].

Unas décadas después, en 1937, Hofmann remplazó el uso de ácido nítrico fumante por ácido nítrico no fumante en la etapa de oxidación. De esta forma, el método era más seguro y menos contaminante [74].

En 1958, Hummers y Offeman usaron permanganato potásico como agente oxidante en presencia de una mezcla concentrada de ácido sulfúrico y nitrato sódico. Este método era más seguro, ya que producía ácido nítrico in situ evitando el uso directo de ácido nítrico fumante, con

un carácter altamente corrosivo. La combinación de permanganato potásico y nitrato sódico dio lugar a una forma más oxidada de grafito. Como tal, el método de Hummers fue muy bien recibido y acogido por muchos investigadores. Sin embargo, el procedimiento tenía el inconveniente principal de producir gases tóxicos, principalmente NO_2, N_2O_4 y ClO_2 haciendo el método medioambientalmente desfavorable e inseguro [74].

En un esfuerzo por mejorar el método de oxidación, Tour, en 2010, reemplazó el uso de $NaNO_3$ por ácido fosfórico, con un carácter menos corrosivo [77]. Este método proporcionó una forma más oxidada y con un plano basal grafítico menos defectuoso. La posibilidad de producción de óxido de grafito a gran escala mediante este método era más viable, ya que no implicaba reacciones altamente exotérmicas ni la liberación de gases tóxicos [74].

1.3.4. Propiedades del óxido de grafito

A continuación se detallan las propiedades más interesantes del óxido de grafito:

- Los grupos carbonilo, hidroxilo y epoxi presentes en su estructura hacen que sea muy hidrófilo; es decir, presenta gran afinidad por el agua. Cuando las moléculas de agua son adsorbidas, se acumulan entre las láminas del GrO, dando lugar a enlaces por puente de hidrógeno entre los grupos oxigenados y las moléculas de agua, influyendo en sus propiedades electrónicas, mecánicas y estructurales [78].
- Tiene la capacidad de adsorber algunos tipos de compuestos como pueden ser: lantánidos, actínidos y otros productos de fisión de grandes volúmenes de soluciones acuosas [79-81].
- Posee propiedades de inhibición bacteriana [48].

- La resistencia eléctrica del GrO es independiente de la temperatura y, por lo general, constante [19].
- Es un material fácilmente funcionalizable [82].
- El equipo de Andre Geim, Rahul Nair e Irina Grigoriva demostró que las membranas de GO son impermeables a todos los gases y líquidos excepto al agua [83].

1.3.5. Aplicaciones del óxido de grafito

Las aplicaciones más interesantes de este material se listan a continuación:

- Una de las principales ventajas del óxido de grafito es su fácil dispersabilidad en agua y disolventes orgánicos debido a la presencia de grupos oxigenados. Ésta propiedad hace que el GrO pueda mezclarse fácilmente con cerámicas o polímeros, con la finalidad de mejorar sus propiedades eléctricas [84].
- El óxido de grafito se puede usar para la desalinización de agua usando ósmosis inversa, así como para la fabricación de membranas para la purificación de agua [85].
- Es posible usarlo en el diseño de supercondensadores, mejorando la conductividad eléctrica y la capacitancia específica [86].
- Por sus propiedades antibacterianas puede usarse en la manufactura de vendas, envases alimentarios y productos médicos [87].
- El GrO se puede utilizar como inmunosensor electroquímico y sensor de glucosa [88]. También puede usarse en la detección del ADN y de proteínas, lo que abre esperanzas a la hora de mejorar el diagnóstico del VIH [89].

- El óxido de grafito se ha considerado como un precursor prominente y un material de partida para la síntesis de grafeno [90].

1.3.6. Métodos de síntesis del óxido de grafito

Los diferentes métodos de síntesis de óxido de grafito usan como materia prima grafito. En todos ellos se procede a la oxidación de grafito en medio ácido.

1.3.6.1. Método de Brodie

Como se ha comentado anteriormente, en 1859, Brodie preparó el primer lote de óxido de grafito mientras investigaba la estructura del grafito a través de su reactividad. Durante su investigación, Brodie añadió $KClO_3$ a una suspensión de grafito y ácido nítrico (HNO_3) fumante. Lavó el producto y lo secó a 100ºC antes de volverlo a tratar en atmósfera oxidante. El resultado obtenido fue un sólido con una relación C:H:O de 61,04:1,85:31.11 [74]. Brodie decidió llamar a este material ácido grafitico tras comprobar que era posible su dispersión en agua neutra o básica pero no en medio ácido [91].

El producto obtenido mediante éste método presentaba una serie de ventajas como eran su débil acidez o la suave dispersabilidad en disolución básica. Las principales desventajas observadas estaban asociadas al pequeño tamaño de partícula del óxido de grafito obtenido y a las imperfecciones estructurales presentes en dicho material.

1.3.6.2. Método de Staudenmaier

En 1898 Staudenmaier mejoró el método de oxidación desarrollado por Brodie mediante la adición de clorato potásico ($KClO_3$) en pequeñas porciones y la acidificación de la mezcla con ácido sulfúrico (H_2SO_4) concentrado. Esta mejora modificó la estequiometria del óxido de grafito obteniendo una relación C: O de 2:1 [88].

Este método tiene una serie de desventajas ya que, para su ejecución, es necesario un tiempo de síntesis elevado (la adición de $KClO_3$ dura más de una semana). Además, es un método peligroso ya que pueden generarse explosiones.

1.3.6.3. Método de Hummers y sus modificaciones y mejoras

Seis décadas después de que Staudenmaier desarrollara su método, Hummers y Offeman, en la Institución de Investigación Industrial National Lead Company, desarrollaron otro método alternativo para producir óxido de grafito.

El método consistía en oxidar grafito con permanganato potásico ($KMnO_4$), en presencia de ácido sulfúrico (H_2SO_4) y nitrato sódico ($NaNO_3$).

La principal ventaja del método de Hummers radica en el alto grado de oxidación del producto final comparado con los métodos descritos anteriormente. Sin embargo, a pesar de ello, se sigue considerando que el grado de oxidación es incompleto [17].

Con el propósito de mejorar el método de Hummers, Kovtyujhova y sus colaboradores, propusieron en 1999 un nuevo método denominado método de Hummers Modificado [92], muy similar al método de Hummers. La principal diferencia radica en la introducción de una etapa de preoxidación usando ácido sulfúrico (H_2SO_4), persulfato potásico ($K_2S_2O_8$) y anhídrido fosfórico (P_2O_5) [93, 94].

La principal ventaja que aporta el método de Hummers modificado es la mejora del grado de oxidación del óxido de grafito que queda reflejado en el aumento de la relación C: O hasta un valor de 4:3,1. Sin embargo, el proceso de separación y purificación del producto es demasiado tedioso [77].

En el año 2010, Marcano, Tour y sus colaboradores [77] propusieron un método alternativo al de Hummers, conocido como método de Hummers mejorado o método de Tour. Actualmente es uno de los métodos más utilizados para la preparación de óxido de grafito. Dicho método, además de excluir la utilización de $NaNO_3$ e incluir como agente oxidante el $KMnO_4$, requiere una relación 9:1 de ácido sulfúrico (H_2SO_4)/ ácido fosfórico (H_3PO_4), lo que mejora la eficacia del proceso de oxidación. De los tres métodos de Hummers comentados (Hummers, Hummers modificado y Hummers mejorado), éste es el que permite obtener mayor cantidad de producto. Además, no genera gases tóxicos y permite un fácil control de la temperatura de reacción, lo que supone un gran avance en la producción de óxido de grafito a gran escala [77].

Las principales ventajas del método de Hummers mejorado o método de Tour son la disminución de la cantidad de defectos en el plano basal del óxido de grafito obtenido, y la posibilidad de producir una gran cantidad de producto. Este es un método medioambientalmente favorable, ya que no se generan gases tóxicos durante su síntesis.

En la Figura 1.15. se muestra una comparativa entre el método de Hummers, el método de Hummers mejorado y el método de Hummers modificado, detallando las diferencias existentes entre cada uno de ellos.

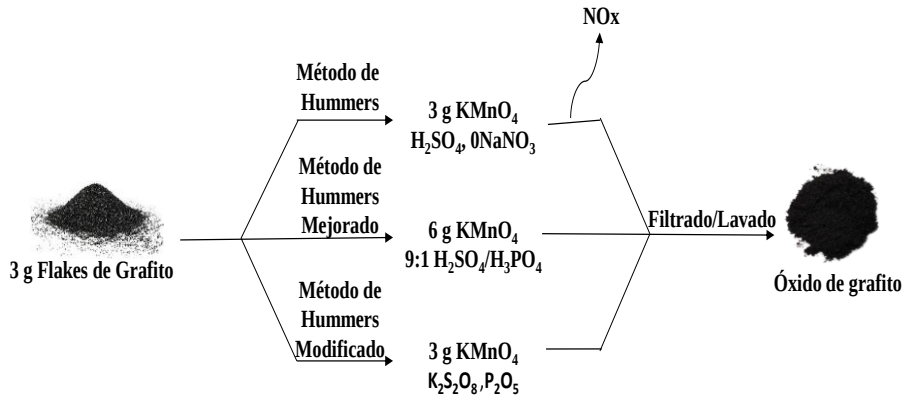

Figura 1.15. Comparación de los tres métodos de síntesis Hummers.

1.4. Óxido de grafeno

1.4.1. Definición de óxido de grafeno

El óxido de grafeno (GO) se define como una monocapa de óxido de grafito (GrO) funcionalizada que puede obtenerse por exfoliación de dicho óxido mediante diversos métodos, como pueden ser sonicación o agitación mecánica (Figura 1.16). El óxido de grafeno se puede utilizar como precursor de grafeno o como material en sí mismo debido a sus propiedades únicas adquiridas gracias a la existencia de numerosos grupos oxigenados en su estructura, principalmente, hidroxilos y epoxi [75].

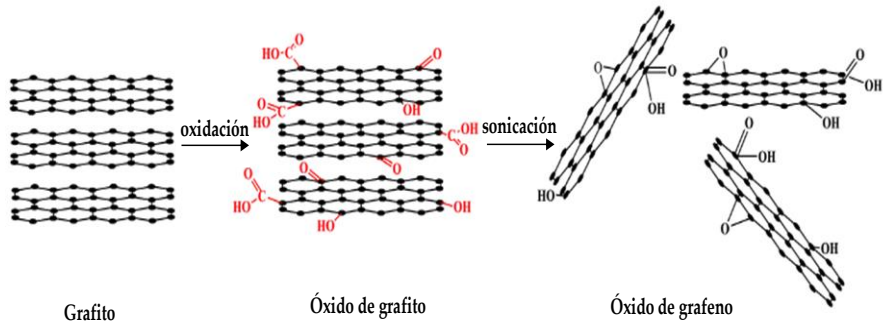

Figura 1.16. Evolución de grafito a oxido de grafeno [73].

1.4.2. Propiedades del óxido de grafeno

Las propiedades del óxido de grafito (aparatado 1.3.4.) y del óxido de grafeno no difieren ya que en el paso de uno a otro no se realiza ninguna reacción química que pueda alterar sus propiedades, si no que se realiza un proceso físico (separación de las láminas de óxido de grafito).

1.4.3. Aplicaciones del óxido de grafeno

Debido a que óxido de grafeno se obtiene tras la separación de las láminas de óxido de grafito las aplicaciones de ambos materiales son prácticamente las mismas (apartado 1.3.5.).

1.4.4. Síntesis de óxido de grafeno

De forma general, la síntesis de GO se basa en la separación de cada una de las láminas de grafeno oxidadas que constituyen el GrO. El óxido de grafito presenta moléculas hidrofílicas, lo cual permite que el agua penetre entre sus capas y éstas se separen gracias a su presencia. Al introducir grupos funcionales oxigenados entre las capas, las fuerzas de Van der Waals, que mantienen dichas capas unidas, se debilitan, lo que ayuda a su separación. Además, los grupos funcionales del GrO acentúan la hidrofilia de las láminas de grafeno, generando nuevas fuerzas de repulsión, haciendo aún más sencilla la separación laminar del óxido de grafito.

Para conseguir la separación de las láminas de grafeno oxidadas que constituyen el GrO se utiliza principalmente la técnica de sonicación.

Se conoce como sonicación al proceso que utiliza la energía del sonido para agitar las partículas de un sistema. Una corriente eléctrica transmite su energía a un sistema mecánico que la convertirá en vibraciones de alta intensidad que generan ondas de ultrasonido. Los ultrasonidos generan a su vez, vibraciones en el material objetivo. Si contiene líquidos se generarán millones de burbujas microscópicas, las cuales sufren rápidos procesos de expansión y colapsos que pueden transmitir su energía a otros materiales [95]. De esta manera, se consiguen separar o exfoliar las láminas presentes en el óxido de grafito para obtener óxido de grafeno.

1.5. Óxido de grafeno reducido

1.5.1. Definición de óxido de grafeno reducido

El óxido de grafeno reducido (RGO) es el espécimen intermedio existente entre el óxido de grafeno (GO) y el grafeno en sí mismo. Se obtiene mediante la reducción del óxido de grafito u óxido de grafeno (en función del método de reducción) a través de diferentes vías [75].

1.5.2. Estructura del óxido de grafeno reducido

La principal diferencia que existe entre la estructura del GO y del RGO es que este último presenta notables defectos estructurales y un menor número de grupos oxigenados.

La estructura del óxido de grafito reducido (RGO) presenta deformaciones alrededor del plano basal debido a que las láminas del material han sido muy atacadas durante el proceso de reducción. Además de presentar defectos estructurales y diversas dislocaciones, pueden aparecer inclusiones que provocan un mayor desorden laminar [96] .

1.5.3. Propiedades del óxido de grafeno reducido

Las propiedades del óxido de grafeno reducido son similares a las del GO y el grafeno, debido a que su estructura es una mezcla de ambas, ya que nunca se ha conseguido reducir lo suficientemente el GO como para obtener grafeno propiamente dicho [74].

- El grafeno presenta una elevada resistencia a la tracción (100 GPa) y un elevado módulo de Young (1TPa) [9]. Sin embargo, para aprovechar sus propiedades mecánicas es necesario conseguir una dispersión de las láminas de manera homogénea dentro de una matriz y este hecho es difícil de conseguir con grafeno. Sin embargo, el óxido de grafeno reducido, aunque presenta defectos cristalinos, estos no afectan al módulo de Young; además, se dispersa mejor en disolventes de una forma homogénea [97].
- Al contrario que el GO, la resistencia eléctrica del RGO si presenta dependencia con la temperatura [98].

- Debido a la interacción de los enlaces π-π* de la estructura del RGO, la superficie específica y la conductividad eléctrica son bajas [99].

1.5.4. Aplicaciones del óxido de grafeno reducido

Las principales aplicaciones del óxido de grafeno reducido son:

- Fabricación de ánodos compuestos por nanopartículas de silicio y RGO para mejorar el rendimiento de la dispersión de los iones del material, con la posibilidad de crear baterías con elevado rendimiento, superando a las constituidas con litio (aumentan la vida útil del material en comparación con las de litio) [100].
- Fabricación de aptasensores (sensores que funcionan a través de las hebras de ADN como elemento de reconocimiento para capturar células cancerígenas en la superficie del sensor) [101, 102].

1.5.5. Métodos de reducción del óxido de grafeno

Se pueden diferenciar tres estrategias diferentes para reducir o eliminar parcialmente los grupos funcionales oxigenados del óxido de grafeno con el fin de obtener óxido de grafeno reducido.

1.5.5.1. Reducción térmica

a) Recocido térmico

El óxido de grafito se puede reducir mediante el proceso denominado "reducción por recocido térmico". Este método consiste en un calentamiento rápido para exfoliar el óxido de grafito hasta obtener óxido de grafeno reducido [103-106]. El mecanismo de exfoliación se basa en la eliminación de los grupos oxigenados presentes en la estructura mediante la formación de especies carbonosas (CO, CO_2) [107].

Las láminas exfoliadas se pueden llamar directamente óxido de grafeno reducido (o grafeno químicamente derivado), lo cual significa que el calentamiento rápido no solo ha exfoliado el óxido de grafito si no que, además, ha eliminado parcialmente los grupos funcionales oxigenados presentes en las láminas del mismo. Este efecto dual, hace de la expansión térmica del óxido de grafito una buena estrategia para producir RGO a gran escala [72].

El gran inconveniente asociado a este método de reducción radica en el daño estructural que se produce en el material resultante [108]. Como consecuencia, el RGO obtenido posee una superficie rugosa y está formado por cristales de pequeño tamaño [104] ya que, durante la brusca descomposición de los grupos funcionales oxigenados, también se eliminan átomos de carbono del plano basal, quedando distorsionadas las láminas de grafeno resultantes.

b) Reducción por radiación microondas y foto reducción

Como alternativa al recocido térmico, se han probado otras fuentes de calentamiento poco convencionales para reducir o eliminar los grupos funcionales del óxido de grafeno, destacando entre ellas, la radiación microondas [109, 110] y la foto-radiación [111, 112].

La principal ventaja de la radiación microondas sobre los métodos convencionales de calentamiento es que las sustancias se calientan rápida y uniformemente. La reducción de óxido de grafeno a óxido de grafeno reducido en un microondas convencional se puede obtener en 1 minuto en condiciones ambientales (presión atmosférica y 25ºC) [109]. Por otro lado, la foto-reducción de las láminas de óxido de grafeno se puede llevar a cabo con una lámpara de Xenón a cortas distancias, la cual proporciona 9 veces la energía necesaria para calentar el óxido de grafeno a 100ºC. Esta temperatura debe ser más que suficiente para inducir la reacción de desoxigenación, obteniendo un grado de reducción del óxido de grafeno mucho mayor [72].

1.5.5.2. Reducción química

a) Reducción química por agentes reductores

La reducción o eliminación de los grupos funcionales oxigenados utilizando agentes reductores se basa en la reacción química de éstos con el óxido de grafeno. Normalmente, la reducción se puede llevar a cabo a temperatura ambiente o bien mediante un calentamiento moderado. Como resultado, el requerimiento de equipos no es tan crítico como en la reducción térmica, lo que hace que la reducción química sea un método más barato y sencillo para la producción en masa de RGO.

En la Figura 1.17. se resumen las ventajas y los inconvenientes de los principales agentes químicos utilizados en la reducción de óxido de grafeno [113-115].

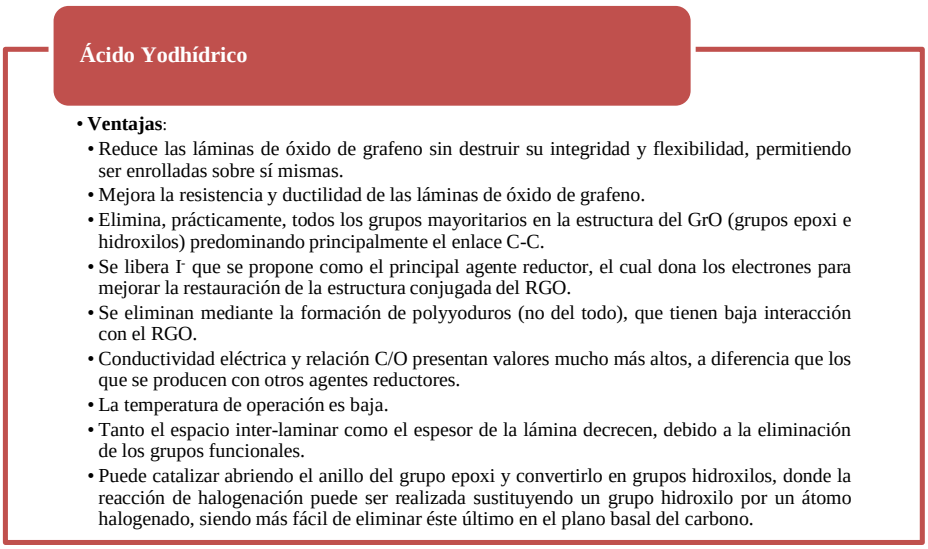

Figura 1.17. Ventajas e inconvenientes de los agentes reductores más usados en la reducción de óxido de grafeno.

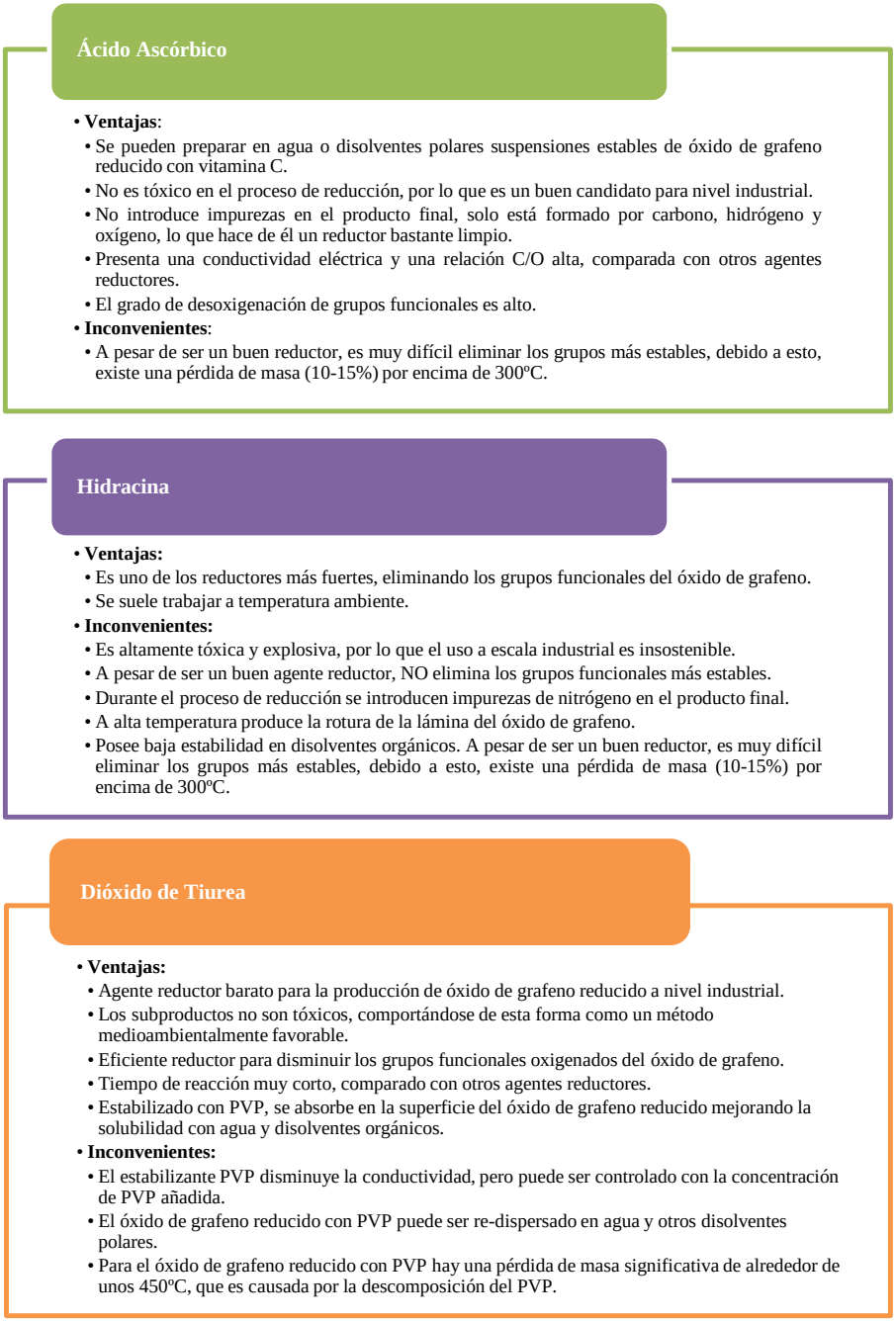

Figura 1.17. Continuación. Ventajas e inconvenientes de los agentes reductores más usados en la reducción de óxido de grafeno.

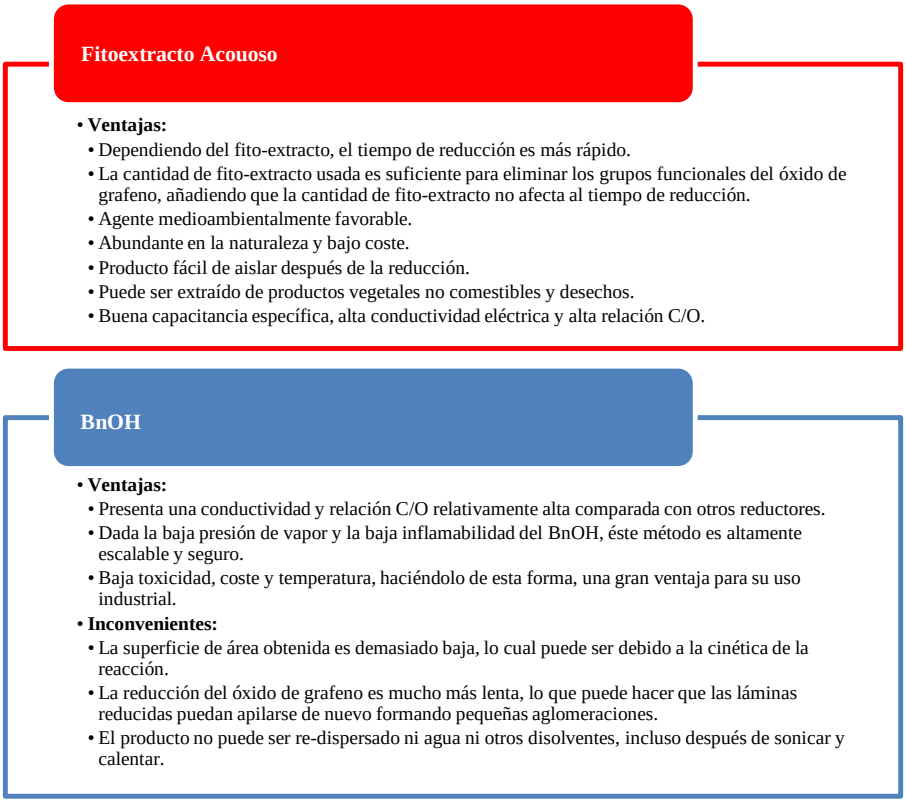

Figura 1.17. Continuación. Ventajas e inconvenientes de los agentes reductores más usados en la reducción de óxido de grafeno.

b) Reducción solvotérmica

La reducción solvotérmica es una técnica emergente dentro de la reducción química del óxido de grafeno [116, 117]. En un proceso solvotérmico se realizan una serie de reacciones químicas en un disolvente determinado en condiciones supercriticas. Las propiedades físico-químicas de un disolvente sometido a estas condiciones puede mejorar la difusión química de las especies [118].

La reducción solvotérmica de GO a RGO es un proceso simple y respetuoso con el medioambiente, ya que no requiere de agentes reductores tóxicos [119]. Sin embargo, requiere un elevado tiempo de proceso para producir un producto de alta calidad y, además, es difícil

conseguir un producto con un bajo contenido en grupos oxigenados [120].

1.5.5.3. Reducción múltiples fases

Las estrategias de reducción explicadas anteriormente se realizan en una sola etapa. Para mejorar dichas estrategias, diferentes grupos de investigación han propuesto llevar a cabo la reducción de los grupos funcionales oxigenados en múltiples etapas [121, 122].

En la mayoría de las reacciones químicas, el efecto de los reactivos es selectivo. Como consecuencia, el uso de un agente reductor no elimina normalmente todo el oxígeno contenido en los grupos funcionales. Para conseguir este objetivo de reducción completa, diversos autores han propuesto llevar a cabo la reducción en múltiples etapas. Así, Eda y colaboradores [122] demostraron que una pre-reducción con hidracina en fase vapor puede disminuir efectivamente la temperatura de recocido necesaria para obtener una buena reducción de las láminas de óxido de grafeno. Por otro lado, Gao y colaboradores [121] propusieron un proceso de reducción en tres etapas: desoxigenación con $NaBH_4$, deshidratación con ácido sulfúrico controlado y recocido térmico.

1.6. Referencias

1. Adler, J. y Pine, P., *Visualization techniques for modelling carbon allotropes.* Computer Physics Communications, 2009, **180** (4): p. 580-582.
2. Jiménez, V., Sánchez, P., Sánchez, M. L., Nieto-Márquez, A., Valverde, J. L. y Romero, A., *Carbon nanofibers: Synthesis, types, properties and chemical activation*, in *Activated Carbon: Classifications, Properties and Applications*. 2011, Nova Science Publishers, Inc. p. 267-296.

3. Nieto-Márquez, A., Valverde, J. L. y Keane, M. A., *Catalytic growth of structured carbon from chloro-hydrocarbons.* Applied Catalysis A: General, 2007, **332** (2): p. 237-246.
4. Nieto-Márquez, A., Romero, R., Romero, A. y Valverde, J. L., *Carbon nanospheres: Synthesis, physicochemical properties and applications.* Journal of Materials Chemistry, 2011, **21** (6): p. 1664-1672.
5. Lavin-Lopez, M. P., Valverde, J. L., Cuevas, M. C., Garrido, A., Sanchez-Silva, L., Martinez, P. y Romero-Izquierdo, A., *Synthesis and characterization of graphene: Influence of synthesis variables.* Physical Chemistry Chemical Physics, 2014, **16** (7): p. 2962-2970.
6. Geim, A. K. y Novoselov, K. S., *The rise of graphene.* Nature Materials, 2007, **6** (3): p. 183-191.
7. Horing, N. J. M., *Aspects of the theory of graphene.* Philosophical Transactions of the Royal Society A: Mathematical, Physical and Engineering Sciences, 2010, **368** (1932): p. 5525-5556.
8. Novoselov, K. S., Geim, A. K., Morozov, S. V., Jiang, D., Zhang, Y., Dubonos, S. V., Grigorieva, I. V. y Firsov, A. A., *Electric field in atomically thin carbon films.* Science, 2004, **306** (5696): p. 666-669.
9. Lee, C., Wei, X., Kysar, J. W. y Hone, J., *Measurement of the elastic properties and intrinsic strength of monolayer graphene.* Science, 2008, **321** (5887): p. 385-388.
10. Castro Neto, A. H., Guinea, F., Peres, N. M. R., Novoselov, K. S. y Geim, A. K., *The electronic properties of graphene.* Reviews of Modern Physics, 2009, **81** (1): p. 109-162.
11. Hamwi, A., Mouras, S., Djurado, D. y Cousseins, J. C., *New synthesis of first stage graphite intercalation compounds with fluorides.* Journal of Fluorine Chemistry, 1987, **35** (1): p. 151.
12. Saito, R., Fujita, M., Dresselhaus, G. y Dresselhaus, M. S., *Electronic structure of graphene tubules based on C60.* Physical Review B, 1992, **46** (3): p. 1804-1811.

13. Forbeaux, I., Themlin, J. M. y Debever, J. M., *Heteroepitaxial graphite on 6H-SiC(0001): Interface formation through conduction-band electronic structure.* Physical Review B - Condensed Matter and Materials Physics, 1998, **58** (24): p. 16396-16406.
14. Simpson, C. D., Brand, J. D., Berresheim, A. J., Przybilla, L., Räder, H. J. y Müllen, K., *Synthesis of a giant 222 carbon graphite sheet.* Chemistry - A European Journal, 2002, **8** (6): p. 1424-1429.
15. Brodie, B. C., *XXIII. - Researches on the atomic weight of graphite.* Quarterly Journal of the Chemical Society of London, 1860, **12** (1): p. 261-268.
16. Staudenmaier, L. y Chikashige, M., *Das Atomgewicht des Tellurs.* Zeitschrift für Analytische Chemie, 1897, **36** (1): p. 281-284.
17. Hummers Jr, W. S. y Offeman, R. E., *Preparation of graphitic oxide.* Journal of the American Chemical Society, 1958, **80** (6): p. 1339.
18. Boehm, H. P., Clauss, A., Fischer, G. O. y Hofmann, U., *Dünnste kohlenstoff-folien.* Zeitschrift fur Naturforschung - Section B Journal of Chemical Sciences, 1962, **17** (3): p. 150-153.
19. Van Bommel, A. J., Crombeen, J. E. y Van Tooren, A., *LEED and Auger electron observations of the SiC(0001) surface.* Surface Science, 1975, **48** (2): p. 463-472.
20. Oshima, C. y Nagashima, A., *Ultra-thin epitaxial films of graphite and hexagonal boron nitride on solid surfaces.* Journal of Physics Condensed Matter, 1997, **9** (1): p. 1-20.
21. Geim, A. K. y Kim, P., *Carbon wonderland.* Scientific American, 2008, **298** (4): p. 90-97.
22. Kroto, H. W., Heath, J. R., O'Brien, S. C., Curl, R. F. y Smalley, R. E., *C60: Buckminsterfullerene.* Nature, 1985, **318** (6042): p. 162-163.
23. Meyer, J. C., Geim, A. K., Katsnelson, M. I., Novoselov, K. S., Booth, T. J. y Roth, S., *The structure of suspended graphene sheets.* Nature, 2007, **446** (7131): p. 60-63.

24. *IUPAC - International Union of Pure and Applied Chemistry: Home [Internet]*. 1997 [cited 2016 01-23]; Available from: http://goldbook.iupac.org/G02683.html.
25. Ruoff, R. S., Nat. Nanotechnol., 2008, **3**: p. 10.
26. Novoselov, K. S., Jiang, D., Schedin, F., Booth, T. J., Khotkevich, V. V., Morozov, S. V. y Geim, A. K., *Two-dimensional atomic crystals.* Proceedings of the National Academy of Sciences of the United States of America, 2005, **102** (30): p. 10451-10453.
27. Zhang, Y., Tan, Y. W., Stormer, H. L. y Kim, P., *Experimental observation of the quantum Hall effect and Berry's phase in graphene.* Nature, 2005, **438** (7065): p. 201-204.
28. N'Diaye, A. T., Bleikamp, S., Feibelman, P. J. y Michely, T., *Two-dimensional Ir cluster lattice on a graphene moiré on Ir(111).* Physical Review Letters, 2006, **97** (21).
29. *Kungliga Vetenskapsakademien - Hem [Internet]*. 2010 [cited 2016-01-23]; Available from: http://www.kva.se/en/.
30. *Graphene Flagship [Internet]*. 2013 [cited 2016 01-24]; Available from: http://graphene-flagship.eu/.
31. Morozov, S. V., Novoselov, K. S., Katsnelson, M. I., Schedin, F., Elias, D. C., Jaszczak, J. A. y Geim, A. K., *Giant Intrinsic Carrier Mobilities in Graphene and Its Bilayer.* Physical Review Letters, 2008, **100** (1): p. 016602.
32. Solis, P. *Modificación superficial de materiales de carbón: grafito y grafeno*. 2011; Available from: http://digital.csic.es/handle/10261/34323.
33. Dong, L. X. y Chen, Q., *Properties, synthesis, and characterization of graphene.* Signal, Image and Video Processing, 2010, **4** (1): p. 45-51.
34. Peigney, A., Laurent, C., Flahaut, E., Bacsa, R. R. y Rousset, A., *Specific surface area of carbon nanotubes and bundles of carbon nanotubes.* Carbon, 2001, **39** (4): p. 507-514.

35. Balandin, A. A., Ghosh, S., Bao, W., Calizo, I., Teweldebrhan, D., Miao, F. y Lau, C. N., *Superior thermal conductivity of single-layer graphene.* Nano Letters, 2008, **8** (3): p. 902-907.
36. Geim, A. K., *Graphene: Status and prospects.* Science, 2009, **324** (5934): p. 1530-1534.
37. Pereira, V. M., Castro Neto, A. H. y Peres, N. M. R., *Tight-binding approach to uniaxial strain in graphene.* Physical Review B, 2009, **80** (4): p. 045401.
38. Ovid'ko, I. A., *Metal-graphene nanocomposites with enhanced mechanical properties: A review.* Reviews on Advanced Materials Science, 2014, **38** (2): p. 190-200.
39. Bae, S., Kim, H., Lee, Y., Xu, X., Park, J. S., Zheng, Y., Balakrishnan, J., Lei, T., Ri Kim, H., Song, Y. I., Kim, Y. J., Kim, K. S., Özyilmaz, B., Ahn, J. H., Hong, B. H. y Iijima, S., *Roll-to-roll production of 30-inch graphene films for transparent electrodes.* Nature nanotechnology, 2010, **5** (8): p. 574-578.
40. Singh, V., Joung, D., Zhai, L., Das, S., Khondaker, S. I. y Seal, S., *Graphene based materials: Past, present and future.* Progress in Materials Science, 2011, **56** (8): p. 1178-1271.
41. Zhu, S. E., Yuan, S. y Janssen, G. C. A. M., *Optical transmittance of multilayer graphene.* EPL, 2014, **108** (1).
42. Savage, N., *Materials science: Super carbon.* Nature, 2012, **483** (7389 SUPPL.): p. S30-S31.
43. Prasher, R., *Graphene spreads the heat.* Science, 2010, **328** (5975): p. 185-186.
44. Yoon, H. J., Jun, D. H., Yang, J. H., Zhou, Z., Yang, S. S. y Cheng, M. M. C., *Carbon dioxide gas sensor using a graphene sheet.* Sensors and Actuators, B: Chemical, 2011, **157** (1): p. 310-313.
45. Oyanedel, J. P. *Siete aplicaciones revolucionarias del grafeno para la tecnología moderna*. 2013 [cited 2016 01-12]; Available from: https://www.fayerwayer.com/2013/06/siete-aplicaciones-revolucionarias-del-grafeno-para-la-tecnologia-moderna/.

46. Li, X., Zhu, Y., Cai, W., Borysiak, M., Han, B., Chen, D., Piner, R. D., Colomba, L. y Ruoff, R. S., *Transfer of large-area graphene films for high-performance transparent conductive electrodes.* Nano Letters, 2009, **9** (12): p. 4359-4363.
47. Katsnelson, M. I., *Graphene: carbon in two dimensions.* Materials Today, 2007, **10** (1-2): p. 20-27.
48. Zhu, Y., Murali, S., Cai, W., Li, X., Suk, J. W., Potts, J. R. y Ruoff, R. S., *Graphene and graphene oxide: Synthesis, properties, and applications.* Advanced Materials, 2010, **22** (35): p. 3906-3924.
49. Geim, A. K., Dubonos, S. V., Lok, J. G. S., Grigorieva, I. V., Maan, J. C., Theil Hansen, L. y Lindelof, P. E., *Ballistic hall micromagnetometry.* Applied Physics Letters, 1997, **71** (16): p. 2379-2381.
50. Nair, R. R., Wu, H. A., Jayaram, P. N., Grigorieva, I. V. y Geim, A. K., *Unimpeded permeation of water through helium-leak-tight graphene-based membranes.* Science, 2012, **335** (6067): p. 442-444.
51. Boukhvalov, D. W. y Katsnelson, M. I., *Chemical functionalization of graphene.* Journal of Physics Condensed Matter, 2009, **21** (34).
52. Zhang, Y., Gong, T., Liu, W., Zhang, X., Chang, J., Wang, K. y Wu, D., *Strong visible light emission from well-aligned multiwalled carbon nanotube films under infrared laser irradiation.* Applied Physics Letters, 2005, **87** (17): p. 173114.
53. Berger, C., Song, Z., Li, T., Li, X., Ogbazghi, A. Y., Feng, R., Dai, Z., Marchenkov, A. N., Conrad, E. H., First, P. N. y de Heer, W. A., *Ultrathin Epitaxial Graphite: 2D Electron Gas Properties and a Route toward Graphene-based Nanoelectronics.* The Journal of Physical Chemistry B, 2004, **108** (52): p. 19912-19916.
54. Yu, Q., Lian, J., Siriponglert, S., Li, H., Chen, Y. P. y Pei, S. S., *Graphene segregated on Ni surfaces and transferred to insulators.* Applied Physics Letters, 2008, **93** (11).
55. Li, X., Magnuson, C. W., Venugopal, A., Tromp, R. M., Hannon, J. B., Vogel, E. M., Colombo, L. y Ruoff, R. S., *Large-area graphene*

single crystals grown by low-pressure chemical vapor deposition of methane on copper. Journal of the American Chemical Society, 2011, **133** (9): p. 2816-2819.

56. Edwards, R. S. y Coleman, K. S., *Graphene synthesis: Relationship to applications.* Nanoscale, 2013, **5** (1): p. 38-51.
57. Sutter, P., *Epitaxial graphene: How silicon leaves the scene.* Nature Materials, 2009, **8** (3): p. 171-172.
58. Ruan, G., Sun, Z., Peng, Z. y Tour, J. M., *Growth of graphene from food, insects, and waste.* ACS Nano, 2011, **5** (9): p. 7601-7607.
59. Reina, A., Jia, X., Ho, J., Nezich, D., Son, H., Bulovic, V., Dresselhaus, M. S. y Jing, K., *Large area, few-layer graphene films on arbitrary substrates by chemical vapor deposition.* Nano Letters, 2009, **9** (1): p. 30-35.
60. Jacobberger, R. M., Machhi, R., Wroblewski, J., Taylor, B., Gillian-Daniel, A. L. y Arnold, M. S., *Simple Graphene Synthesis via Chemical Vapor Deposition.* Journal of Chemical Education, 2015, **92** (11): p. 1903-1907.
61. Avouris, P. y Dimitrakopoulos, C., *Graphene: Synthesis and applications.* Materials Today, 2012, **15** (3): p. 86-97.
62. Kim, K. S., Zhao, Y., Jang, H., Lee, S. Y., Kim, J. M., Ahn, J. H., Kim, P., Choi, J. Y. y Hong, B. H., *Large-scale pattern growth of graphene films for stretchable transparent electrodes.* Nature, 2009, **457** (7230): p. 706-710.
63. Lavin-Lopez, M. P., Valverde, J. L., Ruiz-Enrique, M. I., Sanchez-Silva, L. y Romero, A., *Thickness control of graphene deposited over polycrystalline nickel.* New Journal of Chemistry, 2015, **39** (6): p. 4414-4423.
64. An, H., Lee, W. J. y Jung, J., *Graphene synthesis on Fe foil using thermal CVD.* Current Applied Physics, 2011, **11** (4 SUPPL.): p. S81-S85.

65. Choucair, M., Thordarson, P. y Stride, J. A., *Gram-scale production of graphene based on solvothermal synthesis and sonication.* Nature nanotechnology, 2009, **4** (1): p. 30-33.
66. Vázquez de Parga, A. L., Calleja, F., Borca, B., Passeggi, M. C. G., Hinarejos, J. J., Guinea, F. y Miranda, R., *Periodically Rippled Graphene: Growth and Spatially Resolved Electronic Structure.* Physical Review Letters, 2008, **100** (5): p. 056807.
67. Coraux, J., N'Diaye, A. T., Engler, M., Busse, C., Wall, D., Buckanie, N., Meyer Zu Heringdorf, F. J., Van Gastel, R., Poelsema, B. y Michely, T., *Growth of graphene on Ir(111).* New Journal of Physics, 2009, **11**.
68. Hamilton, J. C. y Blakely, J. M., *Carbon segregation to single crystal surfaces of Pt, Pd and Co.* Surface Science, 1980, **91** (1): p. 199-217.
69. Kim, H., Abdala, A. A. y Macosko, C. W., *Graphene/Polymer Nanocomposites.* Macromolecules, 2010, **43** (16): p. 6515-6530.
70. Hernandez, Y., Nicolosi, V., Lotya, M., Blighe, F. M., Sun, Z. Y., De, S., McGovern, I. T., Holland, B., Byrne, M. y Gun'ko, Y. K., Nat. Nanotechnol., 2008, **3**: p. 563.
71. Lotya, M., Hernandez, Y., King, P. J., Smith, R. J., Nicolosi, V., Karlsson, L. S., Blighe, F. M., De, S., Wang, Z., McGovern, I. T., Duesberg, G. S. y Coleman, J. N., *Liquid Phase Production of Graphene by Exfoliation of Graphite in Surfactant/Water Solutions.* Journal of the American Chemical Society, 2009, **131** (10): p. 3611-3620.
72. Pei, S. y Cheng, H. M., *The reduction of graphene oxide.* Carbon, 2012, **50** (9): p. 3210-3228.
73. Li, J., Zeng, X., Ren, T. y van der Heide, E., *The Preparation of Graphene Oxide and Its Derivatives and Their Application in Bio-Tribological Systems.* Lubricants, 2014, **2** (3): p. 137.
74. Chua, C. K. y Pumera, M., *Chemical reduction of graphene oxide: A synthetic chemistry viewpoint.* Chemical Society Reviews, 2014, **43** (1): p. 291-312.

75. Dreyer, D. R., Park, S., Bielawski, C. W. y Ruoff, R. S., Chemical Society Reviews, 2010, **39**: p. 228.
76. Lee, D. W., De Los Santos V, L., Seo, J. W., Felix, L. L., Bustamante D, A., Cole, J. M. y Barnes, C. H. W., *The structure of graphite oxide: Investigation of its surface chemical groups.* Journal of Physical Chemistry B, 2010, **114** (17): p. 5723-5728.
77. Marcano, D. C., Kosynkin, D. V., Berlin, J. M., Sinitskii, A., Sun, Z., Slesarev, A., Alemany, L. B., Lu, W. y Tour, J. M., *Improved synthesis of graphene oxide.* ACS Nano, 2010, **4** (8): p. 4806-4814.
78. Lerf, A., Buchsteiner, A., Pieper, J., Schöttl, S., Dekany, I., Szabo, T. y Boehm, H. P., *Hydration behavior and dynamics of water molecules in graphite oxide.* Journal of Physics and Chemistry of Solids, 2006, **67** (5–6): p. 1106-1110.
79. Zhao, G., Wen, T., Yang, X., Yang, S., Liao, J., Hu, J., Shao, D. y Wang, X., *Preconcentration of U(vi) ions on few-layered graphene oxide nanosheets from aqueous solutions.* Dalton Transactions, 2012, **41** (20): p. 6182-6188.
80. Li, Z., Chen, F., Yuan, L., Liu, Y., Zhao, Y., Chai, Z. y Shi, W., *Uranium(VI) adsorption on graphene oxide nanosheets from aqueous solutions.* Chemical Engineering Journal, 2012, **210**: p. 539-546.
81. Romanchuk, A. Y., Slesarev, A. S., Kalmykov, S. N., Kosynkin, D. V. y Tour, J. M., *Graphene oxide for effective radionuclide removal.* Physical Chemistry Chemical Physics, 2013, **15** (7): p. 2321-2327.
82. Min, Y., Zhang, K., Zhao, W., Zheng, F., Chen, Y. y Zhang, Y., *Enhanced chemical interaction between TiO2 and graphene oxide for photocatalytic decolorization of methylene blue.* Chemical Engineering Journal, 2012, **193–194**: p. 203-210.
83. Martínez, V. G., *Estudio de la estabilidad del Óxido de grafeno con el tiempo.* 2013.
84. Domingues, S. H., Kholmanov, I. N., Kim, T., Kim, J., Tan, C., Chou, H., Alieva, Z. A., Piner, R., Zarbin, A. J. G. y Ruoff, R. S.,

Reduction of graphene oxide films on Al foil for hybrid transparent conductive film applications. Carbon, 2013, **63**: p. 454-459.

85. Gao, W., Majumder, M., Alemany, L. B., Narayanan, T. N., Ibarra, M. A., Pradhan, B. K. y Ajayan, P. M., *Engineered Graphite Oxide Materials for Application in Water Purification.* ACS Applied Materials & Interfaces, 2011, **3** (6): p. 1821-1826.
86. Wang, H., Hao, Q., Yang, X., Lu, L. y Wang, X., *Graphene oxide doped polyaniline for supercapacitors.* Electrochemistry Communications, 2009, **11** (6): p. 1158-1161.
87. Hu, W., Peng, C., Luo, W., Lv, M., Li, X., Li, D., Huang, Q. y Fan, C., *Graphene-based antibacterial paper.* ACS Nano, 2010, **4** (7): p. 4317-4323.
88. Chua, C. K., Sofer, Z. y Pumera, M., *Graphite oxides: Effects of permanganate and chlorate oxidants on the oxygen composition.* Chemistry - A European Journal, 2012, **18** (42): p. 13453-13459.
89. Zhao, X.-H., Ma, Q.-J., Wu, X.-X. y Zhu, X., *Graphene oxide-based biosensor for sensitive fluorescence detection of DNA based on exonuclease III-aided signal amplification.* Analytica Chimica Acta, 2012, **727**: p. 67-70.
90. Sheka, E. F. y Popova, N. A., *Molecular theory of graphene oxide.* Physical Chemistry Chemical Physics, 2013, **15** (32): p. 13304-13322.
91. Dreyer, D. R., Park, S., Bielawski, C. W. y Ruoff, R. S., *The chemistry of graphene oxide.* Chemical Society Reviews, 2010, **39** (1): p. 228-240.
92. Kovtyukhova, N. I., *Layer-by-layer assembly of ultrathin composite films from micron-sized graphite oxide sheets and polycations.* Chemistry of Materials, 1999, **11** (3): p. 771-778.
93. Ma, C., Liu, W., Shi, M., Lang, X., Chu, Y., Chen, Z., Zhao, D., Lin, W. y Hardacre, C., *Low loading platinum nanoparticles on reduced graphene oxide-supported tungsten carbide crystallites as a*

highly active electrocatalyst for methanol oxidation. Electrochimica Acta, 2013, **114**: p. 133-141.

94. Nikolakopoulou, A., Tasis, D., Sygellou, L., Dracopoulos, V., Galiotis, C. y Lianos, P., *Study of the thermal reduction of graphene oxide and of its application as electrocatalyst in quasi-solid state dye-sensitized solarcells in combination with PEDOT.* Electrochimica Acta, 2013, **111**: p. 698-706.
95. Choucair, M., Thordarson, P. y Stride, J. A., *Gram-scale production of graphene based on solvothermal synthesis and sonication.* Nat Nano, 2009, **4** (1): p. 30-33.
96. Meyer, J. C., Kisielowski, C., Erni, R., Rossell, M. D., Crommie, M. F. y Zettl, A., *Direct imaging of lattice atoms and topological defects in graphene membranes.* Nano Letters, 2008, **8** (11): p. 3582-3586.
97. Zandiatashbar, A., Lee, G. H., An, S. J., Lee, S., Mathew, N., Terrones, M., Hayashi, T., Picu, C. R., Hone, J. y Koratkar, N., *Effect of defects on the intrinsic strength and stiffness of graphene.* Nature Communications, 2014, **5**.
98. Goldsmith, B. R., Lu, Y., Zhengtang, L. y Johnson, A. T., *Temperature dependence of the noise amplitude in graphene and graphene oxide.* Physica Status Solidi - Rapid Research Letters, 2009, **3** (6): p. 178-180.
99. Li, H., Liang, S., Li, J. y He, L., *The capacitive deionization behaviour of a carbon nanotube and reduced graphene oxide composite.* Journal of Materials Chemistry A, 2013, **1** (21): p. 6335-6341.
100. De Guzman, R. C., Yang, J., Cheng, M. M. C., Salley, S. O. y Simon Ng, K. Y., *A silicon nanoparticle/reduced graphene oxide composite anode with excellent nanoparticle dispersion to improve lithium ion battery performance.* Journal of Materials Science, 2013, **48** (14): p. 4823-4833.

101. Kochmann, S., Hirsch, T. y Wolfbeis, O. S., *Graphenes in chemical sensors and biosensors.* TrAC - Trends in Analytical Chemistry, 2012, **39**: p. 87-113.
102. Robinson, J. T., Perkins, F. K., Snow, E. S., Wei, Z. y Sheehan, P. E., *Reduced graphene oxide molecular sensors.* Nano Letters, 2008, **8** (10): p. 3137-3140.
103. Wu, Z. S., Ren, W., Gao, L., Liu, B., Jiang, C. y Cheng, H. M., *Synthesis of high-quality graphene with a pre-determined number of layers.* Carbon, 2009, **47** (2): p. 493-499.
104. Schniepp, H. C., Li, J. L., McAllister, M. J., Sai, H., Herrera-Alonson, M., Adamson, D. H., Prud'homme, R. K., Car, R., Seville, D. A. y Aksay, I. A., *Functionalized single graphene sheets derived from splitting graphite oxide.* Journal of Physical Chemistry B, 2006, **110** (17): p. 8535-8539.
105. McAllister, M. J., Li, J. L., Adamson, D. H., Schniepp, H. C., Abdala, A. A., Liu, J., Herrera-Alonso, M., Milius, D. L., Car, R., Prud'homme, R. K. y Aksay, I. A., *Single sheet functionalized graphene by oxidation and thermal expansion of graphite.* Chemistry of Materials, 2007, **19** (18): p. 4396-4404.
106. Wu, Z. S., Ren, W., Gao, L., Zhao, J., Chen, Z., Liu, B., Tang, D., Yu, B., Jiang, C. y Cheng, H. M., *Synthesis of graphene sheets with high electrical conductivity and good thermal stability by hydrogen arc discharge exfoliation.* ACS Nano, 2009, **3** (2): p. 411-417.
107. Mattevi, C., Eda, G., Agnoli, S., Miller, S., Mkhoyan, K. A., Celik, O., Mostrogiovanni, D., Granozzi, G., Garfunkel, E. y Chhowalla, M., Advanced Functional Materials, 2009, **19**: p. 2577.
108. Kudin, K. N., Ozbas, B., Schniepp, H. C., Prud'homme, R. K., Aksay, I. A. y Car, R., *Raman spectra of graphite oxide and functionalized graphene sheets.* Nano Letters, 2008, **8** (1): p. 36-41.

109. Zhu, Y., Murali, S., Stoller, M. D., Velamakanni, A., Piner, R. D. y Ruoff, R. S., *Microwave assisted exfoliation and reduction of graphite oxide for ultracapacitors.* Carbon, 2010, **48** (7): p. 2118-2122.
110. Hassan, H. M. A., Abdelsayed, V., Khder, A. E. R. S., Abouzeid, K. M., Terner, J., El-Shall, M. S., Al-Resayes, S. I. y El-Azhary, A. A., *Microwave synthesis of graphene sheets supporting metal nanocrystals in aqueous and organic media.* Journal of Materials Chemistry, 2009, **19** (23): p. 3832-3837.
111. Zhang, Y., Guo, L., Wei, S., He, Y., Xia, H., Chen, Q., Sun, H. B. y Xiao, F. S., *Direct imprinting of microcircuits on graphene oxides film by femtosecond laser reduction.* Nano Today, 2010, **5** (1): p. 15-20.
112. Cote, L. J., Cruz-Silva, R. y Huang, J., *Flash reduction and patterning of graphite oxide and its polymer composite.* Journal of the American Chemical Society, 2009, **131** (31): p. 11027-11032.
113. Dreyer, D. R., Murali, S., Zhu, Y., Ruoff, R. S. y Bielawski, C. W., *Reduction of graphite oxide using alcohols.* Journal of Materials Chemistry, 2011, **21** (10): p. 3443-3447.
114. Wang, J., Zhou, T., Deng, H., Chen, F., Wang, K., Zhang, Q. y Fu, Q., *An environmentally friendly and fast approach to prepare reduced graphite oxide with water and organic solvents solubility.* Colloids and Surfaces B: Biointerfaces, 2013, **101**: p. 171-176.
115. Thakur, S. y Karak, N., *Green reduction of graphene oxide by aqueous phytoextracts.* Carbon, 2012, **50** (14): p. 5331-5339.
116. Zhou, Y., Bao, Q., Tang, L. A. L., Zhong, Y. y Loh, K. P., *Hydrothermal dehydration for the "green" reduction of exfoliated graphene oxide to graphene and demonstration of tunable optical limiting properties.* Chemistry of Materials, 2009, **21** (13): p. 2950-2956.
117. Wang, H., Robinson, J. T., Li, X. y Dai, H., *Solvothermal reduction of chemically exfoliated graphene sheets.* Journal of the American Chemical Society, 2009, **131** (29): p. 9910-9911.

118. Demazeau, G., *Solvothermal processes: A route to the stabilization of new material.* Journal of Materials Chemistry, 1999, **9** (1): p. 15-18.
119. Tien, H. N., Luan, V. H., Lee, T. K., Kong, B. S., Chung, J. S., Kim, E. J. y Hur, S. H., *Enhanced solvothermal reduction of graphene oxide in a mixed solution of sulfuric acid and organic solvent.* Chemical Engineering Journal, 2012, **211-212**: p. 97-103.
120. Compton, O. C., Jain, B., Dikin, D. A., Abouimrane, A., Amine, K. y Nguyen, S. T., *Chemically active reduced graphene oxide with tunable C/O ratios.* ACS Nano, 2011, **5** (6): p. 4380-4391.
121. Gao, W., Alemany, L. B., Ci, L. y Ajayan, P. M., *New insights into the structure and reduction of graphite oxide.* Nature Chemistry, 2009, **1** (5): p. 403-408.
122. Eda, G., Fanchini, G. y Chhowalla, M., *Large-area ultrathin films of reduced graphene oxide as a transparent and flexible electronic material.* Nature nanotechnology, 2008, **3** (5): p. 270-274.

Capítulo 2: Metodología y materiales.

2.1. Reactivos y gases empleados

A continuación se detallan los reactivos utilizados, indicando su concentración o pureza y la empresa suministradora.

2.1.1. Síntesis de grafeno por el método CVD

- Nitrógeno, envasado en botellas de acero a 200 bares con una pureza superior al 99,999%, PRAXAIR.
- Hidrógeno, envasado en botellas de acero a 200 bares con una pureza superior al 99,999%, PRAXAIR.
- Metano, envasado en botellas de acero a 300 bares con una pureza superior al 99,5%, PRAXAIR.
- Lámina de cobre policristalino, espesor de 0,025mm, pureza del 99,99% y dimensiones 150x150mm, GOODFELLOW.
- Lámina de níquel policristalino, espesor de 0,025mm, pureza del 99,99% y dimensiones 150x150mm, GOODFELLOW.
- Lámina de hierro policristalino, espesor de 0,025mm, pureza del 99,99% y dimensiones 150x150mm, GOODFELLOW.

2.1.2. Transferencia de grafeno a substratos arbitrarios

- Lámina de grafeno depositado sobre cobre por el método CVD.
- Nitto Denko thermal released tapes (PET).
- $FeCl_3$, pureza 97%, PANREAC.
- Ácido Fluorhídrico (HF), pureza del 48%, SIGMA ALDRICH.
- Carbonato sódico (Na_2CO_3), concentración 99,999%, SIGMA ALDRICH.
- Peróxido de hidrógeno (H_2O_2), concentración de 110 volúmenes, PANREAC.
- Ácido nítrico (HNO_3), pureza del 70%, SIGMA ALDRICH.
- Ácido clorhídrico, concentración 5 N, PANREAC.
- Agua desionizada.

2.1.3. Síntesis de óxido de grafito y óxido de grafeno

- Grafito en polvo sintético (< 20 μm), ALDRICH CHEMISTRY.
- Permanganato potásico, pureza superior al 99 %, PANREAC.
- Ácido sulfúrico (H_2SO_4), pureza del 96 %, PANREAC.
- Ácido fosfórico (HPO_3), pureza del 50 %, PANREAC.
- Peróxido de hidrógeno (H_2O_2), concentración de 110 volúmenes, PANREAC.
- Ácido clorhídrico (HCl), concentración 5 N, PANREAC.
- Etanol (CH_3CH_2OH), pureza superior al 99,5%, PANREAC.
- Agua desionizada.
- Éter dietílico seco (C_2H_6O) (máximo 0,01% de agua), pureza superior al 99,7%, PANREAC.
- Hielo en escamas.

2.1.4. Síntesis de óxido de grafeno reducido

- Óxido de grafito
- Óxido de grafeno
- Hidracina monohidratada (N_2H_6O), pureza del 98%. SIGMA-ALDRICH.
- Ácido ascórbico L(+), pureza del 99%, ($C_6H_8O_6$). NORMAPUR.

2.2. Metodología

2.2.1. Síntesis de grafeno por el método CVD

La Deposición Química en fase Vapor (Chemical Vapour Deposition) se basa en una reacción superficial catalítica en la que se expone un substrato metálico, que actúa como catalizador, a una fuente carbonosa, generalmente hidrocarburos, produciéndose la nucleación y posterior crecimiento de una lámina de grafeno al descomponerse los hidrocarburos sobre la superficie metálica [1-3].

El diagrama de la instalación experimental empleada para sintetizar láminas de grafeno por el método de Deposición Química en fase Vapor (CVD) se observa en la Figura 2.1.

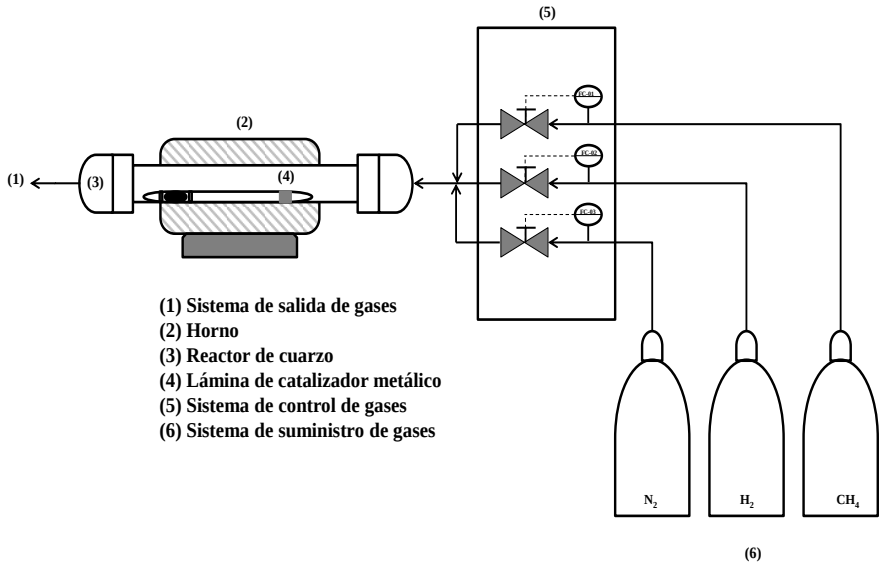

Figura 2.1. Diagrama de la instalación experimental para la síntesis de grafeno por el método CVD.

La síntesis de grafeno por el método CVD se desarrolla de la siguiente manera: se deposita la lámina metálica o catalizador sobre una góndola de cuarzo (diámetro de 0,03 m y longitud de 0,4 m) que se introduce en un reactor tubular (Figura 2.2.a.), con unas dimensiones de 0,04 m de diámetro y 1 m de longitud, del mismo material. Dicha góndola (Figura 2.2.b.) está diseñada para que sea posible localizar un imán que permita el arrastre de la misma a través del reactor. Una vez que ha concluido el proceso de síntesis, se procede a la extracción del reactor de la lámina de metal sobre la que se ha depositado el grafeno para su posterior caracterización.

a)

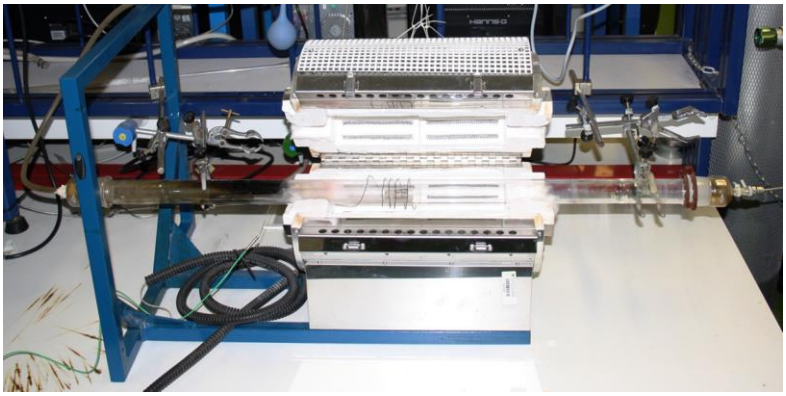

b)

Figura 2.2. Instalación experimental para la síntesis de grafeno mediante el método CVD: a) Sistema de reacción, b) Góndola de cuarzo.

La síntesis de grafeno por el método de Deposición Química en fase Vapor puede dividirse en cuatro etapas.

- **Etapa de calentamiento**

  Esta etapa se basa en calentar el sistema de reacción desde temperatura ambiente (20ºC) hasta la temperatura de reducción (900ºC) usando para ello una rampa de calentamiento de 10ºC/min. Los gases usados durante esta etapa son N_2, que actúa como gas inerte, e H_2 que actúa como gas reductor para prevenir la oxidación de la lámina metálica.

- **Etapa de reducción**

  Esta etapa se realiza a 900ºC y tiene una duración de 45 minutos. Se usan los mismos gases que en la etapa de calentamiento (N_2 e H_2). En esta etapa, el gas reductor interviene como agente activador de la superficie del metal sobre la que se deposita el carbono,

aumentando su tamaño de grano y eliminando posibles defectos estructurales existentes sobre la superficie del mismo.

- **Etapa de reacción**

En esta etapa comienza el crecimiento propiamente dicho del grafeno sobre la lámina metálica. La etapa de reacción se lleva a cabo a diferentes temperaturas y tiempos. Durante esta etapa se cierra el gas inerte y se mantiene constante el flujo de hidrógeno, puesto que se ha demostrado que la contribución del hidrógeno en el crecimiento de grafeno implica varios beneficios, ya que aparte de ser usado como gas reductor, actúa como reactivo en la etapa de reacción, controlando el tamaño y la morfología del grafeno a lo largo de toda la lámina. Para que comience el crecimiento de la lámina de grafeno sobre el metal es necesario introducir en el sistema la fuente de carbono (CH_4).

- **Etapa de enfriamiento**

En esta última etapa se enfría el sistema desde la temperatura de reacción hasta temperatura ambiente (20ºC) usando una rampa de enfriamiento de 10ºC/min. Durante esta etapa se inyecta gas inerte (N_2) que barre la lámina de metal conteniendo grafeno.

Es importante tener en cuenta que los caudales de gases que se introducirán en cada una de las etapas explicadas, así como la temperatura y el tiempo de reacción, dependerán de las condiciones de síntesis estudiadas. Así, la temperatura de reacción podrá variar entre 900ºC y 1050ºC, la relación entre la fuente de carbono y el hidrógeno (CH_4/H_2) lo hará entre 0.07 v/v y 0.4 v/v, el tiempo de reacción entre 30 segundo y 40 minutos y, finalmente, el caudal total de gases lo hará entre 60 Nml/min y 130 Nml/min.

La Figura 2.3. muestra el diagrama de las diferentes etapas de la síntesis de grafeno por el método CVD teniendo en cuenta las temperaturas, tiempos y gases empleados en cada una de ellas.

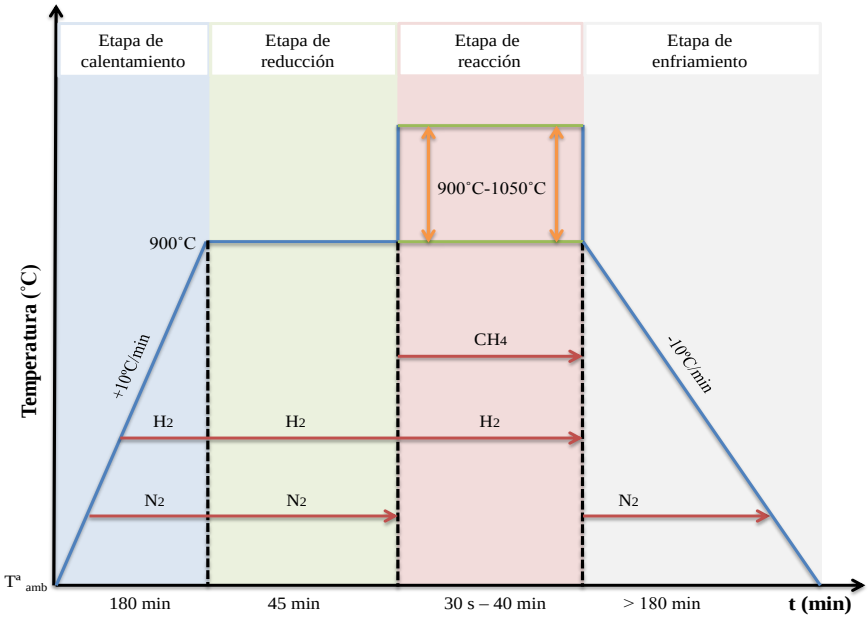

Figura 2.3. Diagrama de etapas de la síntesis de grafeno por el método CVD

2.2.2. Transferencia de grafeno depositado sobre cobre sintetizado por el método CVD a substratos arbitrarios

Para transferir grafeno depositado sobre cobre a un substrato arbitrario, se pega una oblea de PET del pack Nitto Denko en la parte superior de la lámina de grafeno depositado sobre cobre. A continuación, con la finalidad de obtener una superficie lisa y sin arrugas, se aplica presión sobre la lámina de PET con un rodillo de caucho.

A continuación, la oblea de PET con la lámina de grafeno depositado sobre cobre unida, se introduce en uno de los métodos de ataque químico (*etchings*) estudiados con la finalidad de que el grafeno depositado sobre la lámina de cobre quede transferido a la oblea de PET.

De esta manera se pueden diferenciar tres procedimientos diferentes, en función del método *etching* utilizado:

- Uso de la disolución 1M de $FeCl_3$ como agente de ataque químico. La disolución debe calentarse hasta aproximadamente 55ºC antes de comenzar con el procedimiento de transferencia. A continuación, la oblea de PET con grafeno se introduce en la disolución durante 20 minutos, tiempo necesario para alcanzar el completo consumo de la lámina metálica.
- Uso de la disolución formada por HF:$2Na_2CO_3 \cdot 3H_2O_2$ (4:1). En este caso se trabaja a temperatura ambiente. La oblea de PET con la lámina de grafeno adherida se introduce en la disolución durante aproximadamente 1 hora.
- Uso de la disolución formada por H_2O_2: Agua Regia: H2O (1:1:2). Se trabaja a temperatura ambiente y, una vez introducida la oblea de PET con la lámina metálica adherida, solo son necesarios unos pocos segundos para que la lámina metálica se consuma totalmente.

  Una vez consumida la lámina metálica, la oblea de PET con el grafeno adherido se lava con agua desionizada lo que permite eliminar las trazas de agente químico que puedan quedar sobre la misma, y se deja secar. A continuación, se procede a transferir la oblea de PET con el grafeno depositado sobre un substrato arbitrario (lámina de microscopio). Para ello, se pega la oblea de PET (por el lado en el que tiene el grafeno transferido) sobre una placa de microscopio aplicando presión para conseguir una superficie lisa y sin arrugas. Finalmente, la placa de microscopio se calienta a aproximadamente a 100ºC. A esta temperatura, la oblea de PET pierde su capacidad de adhesión. Como consecuencia, la lámina de grafeno se separa de la oblea de PET y queda transferida a la placa de microscopio.

2.2.3. Síntesis de óxido de grafito

El procedimiento experimental seguido para la síntesis de óxido de grafito está basado en el método de Hummers mejorado o método de Tour en el que, a partir de grafito, se obtiene óxido de grafito (GrO). De entre todos los métodos existentes para sintetizar óxido de grafito, se seleccionó el método de Hummers mejorado debido a su alto rendimiento. Además, es el más respetuoso con el medio ambiente y permite obtener un producto con menos defectos estructurales[4].

A continuación se describen las etapas del proceso de síntesis de óxido de grafito mediante el método de Hummers mejorado:

- **Oxidación del grafito**

Esta primera etapa consiste en la oxidación del grafito usando como agente oxidante permanganato potásico ($KMnO_4$) en presencia de un medio ácido. Para ello se utilizó la instalación experimental mostrada esquemáticamente en la Figura 2.4.

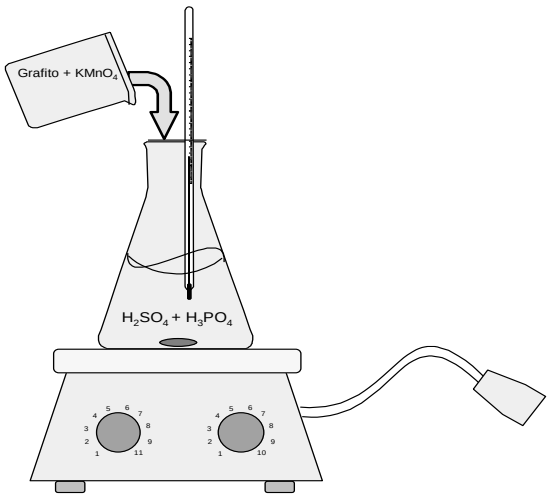

Figura 2.4. Instalación experimental usada para llevar a cabo la etapa de reacción.

El procedimiento experimental seguido fue el siguiente. Se introducen en un matraz Erlenmeyer 360 ml de ácido sulfúrico (H_2SO_4) concentrado y 40 ml de ácido fosfórico (H_3PO_4). Posteriormente, se añade lentamente una mezcla de grafito (3 g) y permanganato potásico ($KMnO_4$) (9 g). Esta adición debe realizarse con agitación mecánica con el objeto de evitar puntos calientes que puedan conducir a explosiones localizadas. La reacción se mantiene a 50ºC durante 12 horas. Aunque el $KMnO_4$ es un oxidante fuerte, el causante de la oxidación del grafito es el óxido de manganeso (VII) (Mn_2O_7) que se produce al mezclar el primero con H_2SO_4, responsable último de oxidar al grafito. El Mn_2O_7 es una sustancia explosiva a temperaturas superiores a 55ºC o en contacto con compuestos orgánicos. Por este motivo, la adición de la mezcla de permanganato potásico y grafito a la mezcla de ácidos se realiza lentamente [5].

La reactividad del permanganato, que sólo puede activarse en disolución ácida, se puede describir a través las siguientes reacciones [5, 6].

$$KMnO_4 + 3H_2SO_4 \rightarrow K^+ + MnO_3^+ + H_3O^+ + 3HSO_4^- \quad \text{(Reacción 1)}$$

$$MnO_3^+ + MnO_4^- \rightarrow Mn_2O_7 \quad \text{(Reacción 2)}$$

Con el tratamiento de oxidación descrito, se pretende aumentar la distancia entre las láminas de grafito mediante la incorporación de grupos oxigenados tales como grupos hidroxilo, grupos epóxidos o grupos carbonilos [7]. De esta forma, se debilitan las fuerzas de Van der Waals que mantienen unidas dichas láminas.

- **Adición de H_2O_2**

Tras el proceso de oxidación, se procede a la adición de peróxido de hidrógeno (H_2O_2). Para ello, se mezclan 400 g de hielo en escamas con 3 ml de H_2O_2. Posteriormente, sobre la mezcla formada por el hielo y el

H_2O_2, se añade la mezcla de ácidos, grafito y permanganato potásico. Este proceso transcurre con liberación de una gran cantidad de calor que se compensa con la adición de hielo.

La mezcla obtenida se filtra a vacío, obteniéndose una torta compacta (Figura 2.5.).

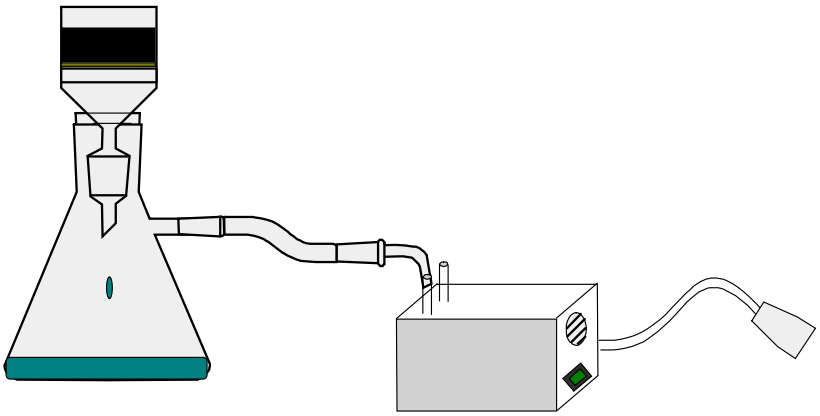

Figura 2.5. Equipo para la filtración a vacío.

El papel del H_2O_2 en el proceso es el de eliminar el exceso de oxidante es decir, el $KMnO_4$ residual [8], a través de la siguiente reacción:

$$2KMnO_4 + H_2SO_4 + H_2O_2 \rightarrow 2MnO_2 + K_2SO_4 + 2H_2O + O_2 \qquad \text{(Reacción 3)}$$

- **Etapa de lavado o purificación**

Esta etapa tiene como finalidad purificar el óxido de grafito. Para ello, la torta obtenida en los pasos anteriores, se somete a dos procesos de lavado mediante filtración a vacío. Cada lavado se realiza con 200 ml de agua desionizada (para neutralizar el pH), 200 ml de ácido clorhídrico (para eliminar los restos de metales) y 200 ml de etanol (para disminuir la temperatura de secado).

La purificación, a pesar de ser una etapa extremadamente lenta, es de vital importancia debido a que el óxido de grafito contaminado con sales de potasio es altamente inflamable y plantea riesgo de incendio [9].

- **Coagulación**

Tras el lavado se procede a la coagulación del óxido de grafito con 200 ml de éter dietético seco, cuyo exceso se elimina por filtración a vacío.

2.2.4. Síntesis de óxido de grafeno

El óxido de grafeno (GO) se obtiene mediante la exfoliación del óxido de grafito. Para ello, se mezclan 800 g de GrO y 800 ml de agua desionizada y se introducen en un reactor con camisa refrigerada para mantener la disolución a temperatura ambiente durante el proceso (Figura 2.6.). El óxido de grafito se sonica con el equipo UP200S Hielscher Ultrasonic Homogenizers para una amplitud del 50% y un ciclo completo, durante 2 horas. El óxido de grafito se dispersa muy bien en agua debido a la repulsión electrostática entre los grupos oxigenados ionizables de su estructura, es decir, aquellos que se encuentran desprotonados [10].

Figura 2.6. Equipo utilizado para la sonicación del óxido de grafito.

Tras el proceso de sonicación, el sólido obtenido se separa del solvente acuoso por centrifugación o gradiente gravimétrico (10000 rpm durante 30 min).

El producto obtenido se seca a 100ºC durante 8 horas obteniendo óxido de grafeno.

2.2.5. Síntesis de óxido de grafeno reducido

La síntesis de óxido de grafeno reducido se realiza mediante tres métodos: reducción química, reducción térmica y reducción múltiples fases.

- **Reducción Química**

Consiste en reducir o eliminar parcialmente los grupos funcionales oxigenados presentes en el óxido de grafeno utilizando oxidantes químicos fuertes. Para ello, se utilizaron dos agentes oxidantes químicos diferentes: hidracina y ácido ascórbico. El primero de ellos es un líquido inflamable e incoloro con olor a amoniaco. Es un compuesto con un potencial de reducción muy elevado pero sin embargo, es altamente tóxico y peligroso. Por otro lado, el ácido ascórbico, aunque tiene un potencial de reducción menor, es un compuesto inocuo y respetuoso con el medioambiente.

- Hidracina

La reducción química del óxido de grafeno usando hidracina monohidratada se lleva a cabo añadiendo 800 mg dicho agente reductor a 800 ml de disolución de óxido de grafeno. A continuación, la disolución se calienta a 90ºC durante 3 horas manteniendo una agitación constante [11].

Tras el proceso de reducción, la mezcla se somete a centrifugación (1000 rpm, 30 min) para conseguir la precipitación del óxido de grafeno reducido por diferencial gravimétrico. Posteriormente, el sólido

obtenido se lava repetidamente con 200 ml de agua desionizada para eliminar cualquier traza existente de hidracina. El óxido de grafeno reducido químicamente con hidracina (H-RGO) se seca en una estufa a 100ºC durante 8 horas [12].

- Ácido Ascórbico

La reducción química del óxido de grafeno usando ácido ascórbico se lleva a cabo mezclando 800 ml de disolución de óxido de grafeno con 800 mg ácido ascórbico. La disolución se mantiene a temperatura ambiente con agitación durante 48 horas [13].

Tras el proceso de reducción, la disolución obtenida se centrifuga (1000 rpm, 30 min) para conseguir la precipitación del óxido de grafeno reducido por diferencia gravimétrica. Posteriormente, se filtra el sólido obtenido y se lava repetidamente con 200 ml agua desionizada con objeto de eliminar cualquier traza existente de ácido ascórbico. El producto obtenido (A-RGO) se seca a 100ºC durante 8 horas [12, 14].

- **Reducción Térmica**

Esta reducción consiste en eliminar parcialmente los grupos oxigenados presentes en el óxido de grafito mediante una expansión violenta del material, a temperaturas moderadas.

El método de reducción térmica se realiza en una estufa de secado (Figura 2.7.) a bajas temperaturas (<300ºC) produciéndose una brusca expansión de las láminas de grafeno que conforman el óxido de grafito. Mediante dicha expansión, se logran separar las láminas de grafeno reduciéndose, al mismo tiempo, la cantidad de grupos oxigenados presentes en el mismo [15], obteniendo óxido de grafeno reducido térmicamente (T-RGrO). .

Figura 2.7. Estufa de secado utilizada en la síntesis de óxido de grafeno reducido térmicamente.

- **Reducción Múltiples fases**

Este método es básicamente una combinación de los métodos de reducción anteriores que busca maximizar la cantidad de grupos oxigenados funcionales reducidos o eliminados.

El procedimiento experimental seguido consiste en llevar a cabo una primera reducción térmica a baja temperatura (<300ºC), en la que se produce la expansión del material obteniendo óxido de grafito reducido térmicamente (T-RGrO). A continuación, con la finalidad de separar aún más las láminas de grafeno y obtener óxido de grafeno reducido térmicamente (T-RGO), el material se sonica durante 1h (amplitud 50%, ciclo completo). Finalmente, para conseguir una mayor eliminación de los grupos funcionales oxigenados de la estructura, se realiza una segunda etapa de reducción química usando hidracina o ácido ascórbico como agentes reductores. Como resultado, se obtiene óxido de grafeno reducido mediante el método múltiples fases usando hidracina (HMP-RGO) o ácido ascórbico (AMP-RGO).

2.3. Técnicas de caracterización

Caracterizar un material consiste en determinar sus propiedades de acuerdo a parámetros físico-químicos. En el caso del grafeno y sus derivados, existen múltiples métodos de caracterización, entre los que destacan los mencionados a continuación.

2.3.1. Microscopía electrónica de barrido (SEM)

Del inglés 'Scanning Electron Microscopy' es una técnica de caracterización utilizada para el análisis de superficies obteniendo información del relieve, textura, tamaño, forma de grano y composición química. En esta técnica, los electrones secundarios de baja energía (<50 eV) emitidos desde la superficie de la muestra se utilizan para dar una imagen. Para facilitar la emisión de electrones resulta necesario metalizar la muestra previamente (recubrir con una pequeña capa de metal conductor) [16].

En esta investigación se utilizó un equipo SEM de la marca Phenom ProX (Figura 2.8.). La preparación de la muestra requiere que una pequeña cantidad de muestra se adhiera al soporte portamuestras. Tanto la preparación de la muestra, como su posterior caracterización, se realizan en condiciones controladas de humedad y temperatura.

Figura 2.8. Equipo Microscopía Electrónica de Barrido (SEM).

2.3.2. Espectroscopia Raman

La espectroscopia Raman es una poderosa técnica de caracterización de todos los alótropos del carbono, por lo que resulta muy útil en el estudio del grafeno. Resulta ser rápida, no destructiva, de alta resolución y capaz de suministrar gran cantidad de información estructural y electrónica [17, 18]. Se basa en el estudio de la luz que dispersa un material cuando se le hace incidir un haz de luz monocromático sobre él (radiación láser). Una porción de la luz es dispersada inelásticamente, sufriendo ligeros cambios de frecuencia que resultan ser característicos del material analizado, e independientes de la frecuencia de la luz incidente [19].

El equipo Raman utilizado en esta investigación es de la marca SENTERRA (Figura 2.9.). Posee un enrejado de difracción de 600 líneas por milímetro y un láser de 532 nm de longitud de onda. Además, posee una potencia muy baja para evitar cualquier tipo de calentamiento.

Figura 2.9. Equipo espectroscopía Raman.

Gracias a la información proporcionada por el espectro Raman, se puede diferenciar sin ambigüedad entre grafito, grafeno, óxido de grafito, óxido de grafeno u óxido de grafeno reducido [20]. El primer

espectro Raman del grafeno fue medido por Ferrari y col. [20] en 2006, sólo dos años después de haber sido aislado por primera vez.

La Figura 2.10. muestra, a modo de ejemplo, el espectro Raman característico del grafeno monocapa. En él pueden observarse tres bandas características: la banda D, G y 2D.

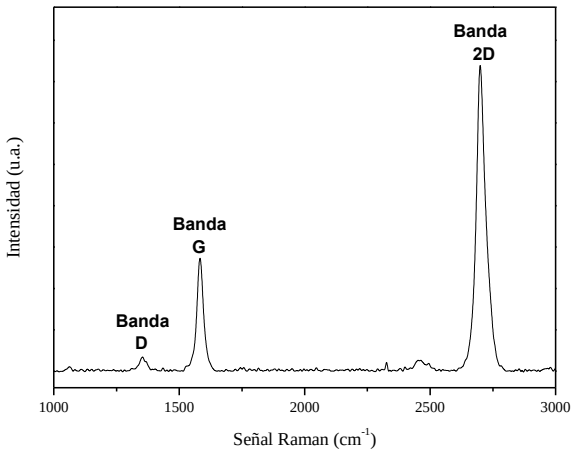

Figura 2.10. Espectro Raman de una lámina de grafeno monocapa.

La banda D aparece en el espectro Raman correspondiente al grafeno entre los valores de 1200-1350 cm^{-1} y se atribuye a los defectos presentes en la lámina, por lo que también es llamada banda defecto. Esta banda es débil en el grafeno y grafito de alta calidad, resultando significativa en materiales defectuosos [21].

La banda G, que aparece a longitudes de onda comprendidas entre 1580 y 1620 cm^{-1}, se debe al movimiento de dos átomos de carbono vecinos unidos por enlaces sp^2. La posición de la banda puede variar en función de la presión ejercida sobre la muestra y el dopaje de la misma, mientras que su intensidad es menos susceptible a estos factores [22].

La banda 2D, que aparece en torno a 2700 cm^{-1}, es sensible al número de capas de grafeno y muestra una estructura más compleja con el aumento

de las mismas, debido al acoplamiento de diversos picos [22, 23]. La Figura 2.11. muestra las diferencias existentes en la banda 2D, así como su deconvolución, según el número de capas de grafeno presentes en la muestra [20, 24]. Se puede observar que la diferencia más significativa entre el grafeno monocapa y el grafito es que la banda 2D correspondiente al grafeno cuenta con una única contribución mientras que la del grafito, presenta un perfil asimétrico con la presencia de dos contribuciones. Este hecho se ha estudiado en muestras con diferente número de capas [20, 25] y tiene su explicación en la evolución de la estructura electrónica del grafito a medida que se van añadiendo capas [26].

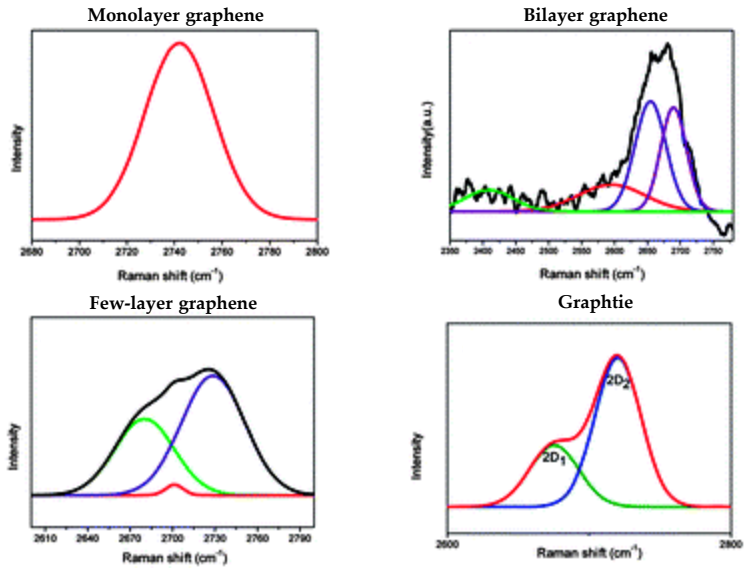

Figura 2.11. Deconvolución de la banda 2D del grafito y del grafeno en función del número de capas [18].

Para llevar a cabo una caracterización exhaustiva de la muestra de grafeno, hay que tener en cuenta ciertas relaciones entre las intensidades de las bandas obtenidas por espectroscopía Raman. Así, la relación de intensidades entre la banda D y la banda G (I_D/I_G) sirve para cuantificar la cantidad de defectos presentes en la muestra [20, 27].

Por su parte, la relación entre las bandas 2D y G (I_{2D}/I_G) permite identificar si la muestra obtenida es grafeno monocapa, bicapa, pocas capas o multicapa [21].

Otro parámetro a tener en cuenta es el Full Width at Half Maximum (FWHM, cm^{-1}) que está relacionado con el tiempo de vida de los estados excitados [25]. Este parámetro se calcula como la diferencia de la Señal Raman a la altura media de la banda 2D (anchura de la banda 2D).

Finalmente, la posición de la banda 2D del espectro Raman del grafeno debe desplazarse a menores valores de Señal Raman (cm^{-1}) en comparación con la posición de dicha banda en el grafito, situada en torno a 2710 cm^{-1} [28].

Por su parte, en el espectro Raman característico del óxido de grafito, y debido a su naturaleza, aparecen únicamente dos bandas: la banda D y la banda G (Figura 2.12.). La ausencia del pico 2D en este material se debe al desorden que presenta la muestra después del proceso de oxidación [29]. Las posiciones e intensidades relativas a dichas bandas permiten analizar diferentes características del óxido de grafito. Uno de los parámetros más empleados en muestras que se alejan relativamente poco del orden grafítico es la intensidad de la banda D respecto a la G, expresada como el cociente entre sus intensidades (I_D/I_G). Como ya se ha comentado, esta relación de intensidades crece con el desorden estructural de la red grafítica, sirviendo así como indicador del grado de desorden de la muestra. Valores característicos de esta relación para el óxido de grafito oscilan entre 0,7 y 1 [30]. La relación entre las intensidades de dichas bandas experimenta cambios a medida que se va tratando el material, aumentando su valor cuando el óxido de grafito es reducido mediante los diferentes métodos. Así, por ejemplo, para el óxido de grafeno, el valor de la relación I_D/I_G presenta valores próximos a la unidad, mientras que para el óxido de grafito reducido químicamente, dicha relación puede oscilar entre 1,14 y 1,28 [31].

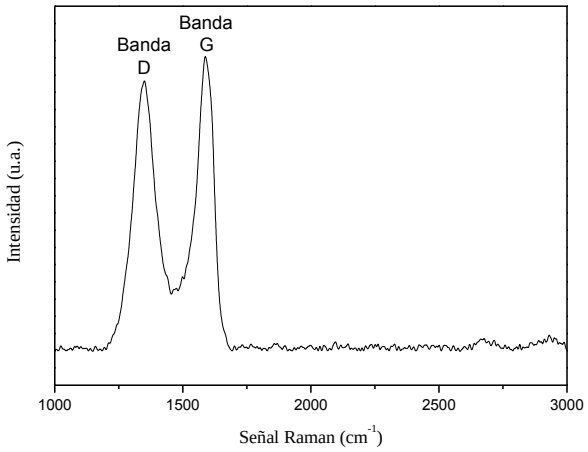

Figura 2.12. Espectro Raman del óxido de grafito.

La evolución del desorden experimentado en los materiales basados en grafeno puede ser cuantificada mediante el parámetro "distancia entre defectos (L_D)" que se calcula como $L_D=\sqrt{C\ (\lambda)/(ID/IG)}$, donde el valor de C ($\lambda$) es 102 nm^2.

2.3.3. Microscopía Óptica

Aun siendo un material bidimensional de tan sólo un átomo de espesor, el grafeno es visible con ayuda de un microscopio óptico cuando se deposita sobre un sustrato dieléctrico.

Para observar la muestra de grafeno microscópicamente, se utilizó el microscopio óptico insertado en el espectrómetro Raman, utilizando un aumento de 50X.

2.3.4. Difracción de Rayos X (XRD)

Se trata de una técnica de caracterización no destructiva en la que se obtiene información sobre la estructura cristalina y la distancia entre los átomos de la muestra. Consiste en la interacción de un haz de Rayos X, de una determinada longitud de onda, con una sustancia cristalina

consiguiendo su difracción. Los haces difractados forman un conjunto de conos denominados Debye-Scherrer, cada uno de los cuales es consecuencia de diferentes conjuntos de planos [32].

La realización de los ensayos de difracción de Rayos-X se llevó a cabo en un difractómetro (PHILIPS, modelo PW-1711) con radiación CuKα (λ = 1.5404 Å).

Los materiales derivados del grafeno presentan dos picos característicos en su espectro de difracción de Rayos X, el pico [001] y el pico [100], mientras que espectro de difracción de Rayos X del grafito queda representado por un solo pico [002] (Figura 2.13.) .

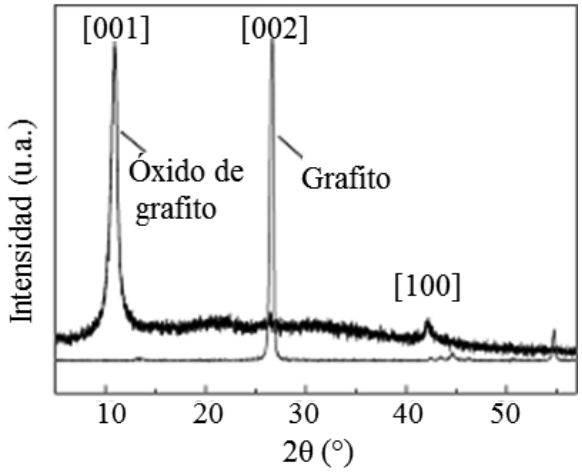

Figura 2.13. Espectro de difracción de Rayos X del grafito y del óxido de grafito.

La posición y anchura de ambos picos permiten determinar diferentes parámetros cristalinos característicos del material, tales como el espaciado interlaminar (d_{002}) y el tamaño medio cristalino en la dirección perpendicular (L_c) y paralela (L_a) a las láminas de grafeno (Figura 2.14.).

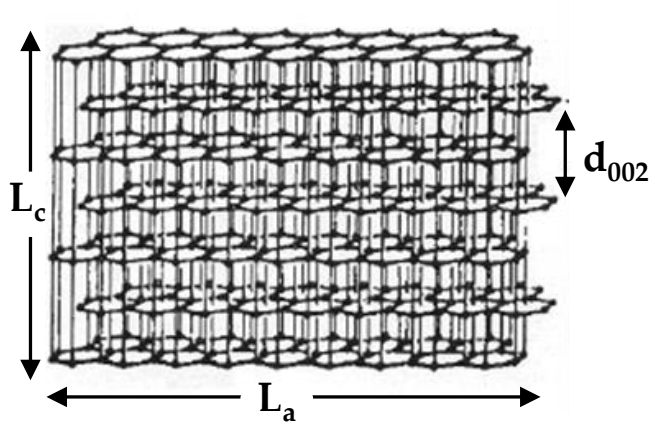

Figura 2.14. Representación gráfica de los parámetros d_{002}, L_a y L_c.

El espaciado interlaminar (d_{002}), se calcula a partir del pico [001] de los materiales derivados del grafeno y del pico [002] del grafito, utilizando la ecuación de Braggs:

$$d_{002} = \frac{\lambda}{2 \cdot sen\,(\theta)}$$

donde λ y θ son:

λ: longitud de onda de la radiación (λ=1,5404 Å).

θ: ángulo de difracción correspondiente al pico [002] del grafito y [001] de los materiales derivados del grafeno.

El tamaño medio cristalino en la dirección perpendicular (L_c) de las láminas de grafeno, obtenido del pico [002] del grafito y [001] de los materiales derivados del grafeno y, el tamaño medio cristalino en la dirección paralela (L_a) de las láminas de grafeno, obtenido a partir del pico [100] de los materiales derivados del grafeno, se determinan mediante la ecuación de Scherrer:

$$L_a = \frac{K_a \cdot \lambda}{B \cdot \cos(\theta)}\,,\; L_c = \frac{K_c \cdot \lambda}{B \cdot cos\,(\theta)}$$

donde K_a, K_c, λ, B y θ son:

K_a: constante de Scherrer (1,84 para compuestos carbonosos) [33].

K_c: constante de Scherrer (0,90 para compuestos carbonosos) [33].

λ: longitud de onda de la radiación (λ=1,5404 Å).

B: FWHM. Este parámetro se calcula como la anchura del pico a la mitad del mismo.

θ: ángulo de difracción correspondiente al pico [002] en el grafito y [001] y [100] en los materiales derivados del grafeno.

2.3.5. Análisis termogravimétrico

Mediante el análisis termogravimétrico se registra, de manera continua, la variación de peso de una muestra con el tiempo y la temperatura en una atmósfera específica que puede ser estática o dinámica. Durante el análisis se usa un caudal determinado utilizando como gases más habituales el N_2, aire, Ar y CO_2.

En esta investigación se utilizó un equipo de análisis termogravimétrico METTLER TOLEDO, modelo TGA/DSC 1 STARe (Figura 2.15.). Las muestras (aproximadamente 8 mg) se ubican en un crisol de cerámica de alúmina y se introducen en el equipo mediante un brazo robótico. Una vez dentro, se calientan a una velocidad de 10°C/min desde 30 hasta 1000ºC. Los datos experimentales se recogen y controlan mediante un software proporcionado por METTLER TOLEDO STAR.

Figura 2.15. Termobalanza (TGA).

2.3.6. Espectroscopía Infrarroja de la Transformada de Fourier (FTIR)

El FTIR es una técnica de caracterización en la que, mediante un haz de luz de diferentes frecuencias, se mide la cantidad de luz absorbida de una muestra para estudiar la vibración y la rotación de las moléculas en la región infrarroja del espectro electromagnético.

En esta investigación se utilizó un espectrómetro "SpectrumTwo" (Perkin Elmer, Inc.) (Figura 2.16.) con un reflectante atenuado universal total (UATR), que consiste en un accesorio de reflexión interna, usado para simplificar el análisis de sólidos, polvos, pastas, geles y líquidos. Además, el equipo posee un cristal de diamante el cual, debido a su dureza, puede soportar altas presiones de trabajo y permite trabajar con bases y ácidos fuertes.

Figura 2.16. Equipo Espectroscopía Infrarroja por Transformada de Fourier (FTIR).

2.3.7. Análisis elemental

Mediante este análisis se determina el contenido de los principales elementos químicos, tales como carbono (C), hidrógeno (H), nitrógeno (N), oxígeno (O) y azufre (S), de una muestra en polvo.

Este análisis se realizó en un analizador elemental LECO CHNS-932 capaz de detectar todos los elementos y mostrar el porcentaje másico de cada uno de ellos. La separación de elementos de la muestra se produce por combustión a alta temperatura (950ºC) mediante la inyección de una dosis elevada de oxígeno puro.

El porcentaje de C, H, N y S será una media de los valores obtenidos en los diez ensayos realizados a cada muestra. El analizador elemental separa los gases producidos y los detecta con un detector de conductividad térmica (TCD).

El porcentaje de oxígeno (O) de la muestra se calcula por diferencia según la siguiente ecuación:

$$O = 100 - C + H + N + S \quad (Ecuación\ 4)$$

siendo O, C, H, N y S los porcentajes másicos de oxígeno, carbono, hidrógeno, nitrógeno y azufre, respectivamente.

2.3.8. Análisis del área superficial y volumen total de poros

La base para medir el área superficial total de un sólido por fisisorción de un gas consiste en detectar el número de moléculas de gas necesarias para cubrir la superficie del sólido. Una vez que el área que ocupa la molécula es conocida, el área superficial del sólido se puede estimar a partir del número de moléculas de gas absorbidas, medidas volumétricas o gravimétricamente (Brunauer, Emmett y Teller).

Los análisis de área superficial, volumen de poros y área de poros se realizaron mediante adsorción-desorción de N_2 a -196ºC, empleando un equipo de la marca QUANTACHROM modelo QUADRASORB SI, con seis puertos de desgasificación y tres de análisis, controlado por un software (QUADRAWIN) que recoge los valores de presión relativa para cada volumen de N_2 dosificado.

Previamente al análisis es necesario realizar una desgasificación de las muestras a 80ºC aplicando vacío durante 6 horas. Una vez desgasificadas, se lleva a cabo la adsorción añadiendo cantidades crecientes de nitrógeno, para abarcar todo el intervalo de presiones relativas hasta aproximarse a la saturación (P/P_0 = 0,995). Alcanzada la saturación, la desorción se realiza a vacío, reduciendo la presión relativa escalonadamente. El tiempo de estabilización de cada medida se fija en 5 s.

La superficie específica se calcula utilizando el modelo Brunauer Emmett-Teller (BET) aplicado a la rama de adsorción de nitrógeno en el intervalo de presiones parciales seleccionado para cada material, de forma que se evitara en todo momento la condensación capilar en los mesoporos.

2.4. Análisis de la calidad del grafeno obtenido por el método CVD

Con objeto de poder medir cuantitativamente la calidad de las láminas de grafeno sintetizadas por el método CVD, se diseñó una aplicación Excel-VBA basada en el análisis de las imágenes de microscopía óptica de las láminas de grafeno. En las imágenes de microscopía óptica, es posible observar cuatro colores diferentes. Mediante espectroscopía Raman se demuestra que, cada uno de los colores presentes en las imágenes está relacionado con un tipo de grafeno diferente. Así, el color naranja oscuro se corresponde con grafeno multicapa, el naranja claro con grafeno pocas capas, el amarillo con grafeno bicapa y, por último, el color blanco con grafeno monocapa (Figura 2.17).

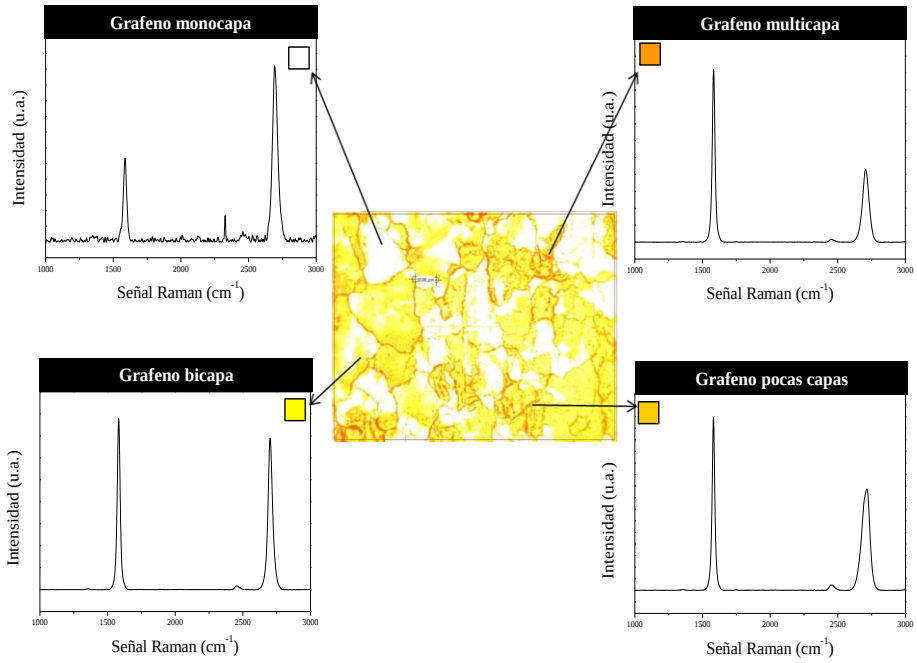

Figura 2.17. Espectros Raman correspondiente a cada uno de las zonas de color obtenidas en las imágenes de microscopía ópticas de las láminas de grafeno sintetizadas por el método CVD.

Así, una vez analizadas las imágenes de microscopía óptica, la aplicación Excel-VBA determina el porcentaje de cada uno de los tipos de grafeno (multicapa, pocas capas, bicapa y monocapa) presentes en la lámina de grafeno depositada sobre el sustrato metálico.

Por último, en función de los porcentajes de cada tipo de grafeno, la aplicación Excel-VBA determina el parámetro de "Calidad de la lámina de grafeno" que está relacionado con la calidad de la misma. Para ello, la aplicación asigna los valores de 1, 10, 100 y 1000 (escala logarítmica) al 100% de la muestra recubierta con grafeno multicapa, pocas capas, bicapa y monocapa, respectivamente. El parámetro de "Calidad de la lámina de grafeno" se calcula como un promedio del porcentaje obtenido para cada tipo de grafeno [27, 34, 35].

2.5. Referencias

1. Kim, K. S., Zhao, Y., Jang, H., Lee, S. Y., Kim, J. M., Ahn, J. H., Kim, P., Choi, J. Y. y Hong, B. H., *Large-scale pattern growth of graphene films for stretchable transparent electrodes.* Nature, 2009, **457** (7230): p. 706-710.
2. Reina, A., Jia, X., Ho, J., Nezich, D., Son, H., Bulovic, V., Dresselhaus, M. S. y Jing, K., *Large area, few-layer graphene films on arbitrary substrates by chemical vapor deposition.* Nano Letters, 2009, **9** (1): p. 30-35.
3. Sutter, P. W., Flege, J. I. y Sutter, E. A., *Epitaxial graphene on ruthenium.* Nature Materials, 2008, **7** (5): p. 406-411.
4. Marcano, D. C., Kosynkin, D. V., Berlin, J. M., Sinitskii, A., Sun, Z., Slesarev, A., Alemany, L. B., Lu, W. y Tour, J. M., *Improved synthesis of graphene oxide.* ACS Nano, 2010, **4** (8): p. 4806-4814.
5. Koch, K. R., *Oxidation by Mn207: An impressive demonstration of the powerful oxidizing property of dimanganeseheptoxide.* Journal of Chemical Education, 1982, **59** (11): p. 973.

6. Dreyer, D. R., Park, S., Bielawski, C. W. y Ruoff, R. S., *The chemistry of graphene oxide.* Chemical Society Reviews, 2010, **39** (1): p. 228-240.
7. Chua, C. K. y Pumera, M., *Chemical reduction of graphene oxide: A synthetic chemistry viewpoint.* Chemical Society Reviews, 2014, **43** (1): p. 291-312.
8. Xu, H., Wang, D., He, S., Li, J., Feng, B., Ma, P., Xu, P., Gao, S., Zhang, S., Liu, Q., Lu, J., Song, S. y Fan, C., *Graphene-based nanoprobes and a prototype optical biosensing platform.* Biosensors and Bioelectronics, 2013, **50**: p. 251-255.
9. Kim, F., Luo, J., Cruz-Silva, R., Cote, L. J., Sohn, K. y Huang, J., *Self-Propagating Domino-like Reactions in Oxidized Graphite.* Advanced Functional Materials, 2010, **20** (17): p. 2867-2873.
10. Li, D., Müller, M. B., Gilje, S., Kaner, R. B. y Wallace, G. G., *Processable aqueous dispersions of graphene nanosheets.* Nature nanotechnology, 2008, **3** (2): p. 101-105.
11. Martinez, G., Salavagione, H., *Nanocompuestos poliméricos de grafeno: preparación y propiedades.* Revista Iberoamericana de Polímeros, 2011, **12** (1): p. 53-63.
12. Li, S., Zhu, F., Meng, F., Li, H., Wang, L., Zhao, J., Yue, Q., Liu, J. y Jia, J., *Separation of graphene oxide by density gradient centrifugation and study on their morphology-dependent electrochemical properties.* Journal of Electroanalytical Chemistry, 2013, **703**: p. 135-145.
13. Zhang, J., Yang, H., Shen, G., Cheng, P., Zhang, J. y Guo, S., *Reduction of graphene oxide vial-ascorbic acid.* Chemical Communications, 2010, **46** (7): p. 1112-1114.
14. Zhu, Y., Murali, S., Cai, W., Li, X., Suk, J. W., Potts, J. R. y Ruoff, R. S., *Graphene and graphene oxide: Synthesis, properties, and applications.* Advanced Materials, 2010, **22** (35): p. 3906-3924.

15. Huh, S. H., *Thermal Reduction of Graphene Oxide, Physics and Applications of Graphene - Experiments*,, Mikhailov, D. S., Editor. 2011, InTech.
16. Lin, P.-C., Lin, S., Wang, P. C. y Sridhar, R., *Techniques for physicochemical characterization of nanomaterials.* Biotechnology Advances, 2014, **32** (4): p. 711-726.
17. Ferrari, A. C. y Robertson, J., *Raman spectroscopy of amorphous, nanostructured, diamond-like carbon, and nanodiamond.* Philosophical Transactions of the Royal Society A: Mathematical, Physical and Engineering Sciences, 2004, **362** (1824): p. 2477-2512.
18. Malard, L. M., Pimenta, M. A., Dresselhaus, G. y Dresselhaus, M. S., *Raman spectroscopy in graphene.* Physics Reports, 2009, **473** (5-6): p. 51-87.
19. Lavin-Lopez, M. P., Valverde, J. L., Ruiz-Enrique, M. I., Sanchez-Silva, L. y Romero, A., *Thickness control of graphene deposited over polycrystalline nickel.* New Journal of Chemistry, 2015, **39** (6): p. 4414-4423.
20. Ferrari, A. C., Meyer, J. C., Scardaci, V., Casiraghi, C., Lazzeri, M., Mauri, F., Piscanec, S., Jiang, D., Novoselov, K. S., Roth, S. y Geim, A. K., *Raman spectrum of graphene and graphene layers.* Physical Review Letters, 2006, **97** (18).
21. Mattevi, C., Kim, H. y Chhowalla, M., *A review of chemical vapour deposition of graphene on copper.* Journal of Materials Chemistry, 2011, **21** (10): p. 3324-3334.
22. Ferrari, A. C., *Raman spectroscopy of graphene and graphite: Disorder, electron-phonon coupling, doping and nonadiabatic effects.* Solid State Communications, 2007, **143** (1-2): p. 47-57.
23. Mohanty, N., Nagaraja, A., Armesto, J. y Berry, V., *High-throughput, ultrafast synthesis of solutiondispersed graphene via a facile hydride chemistry.* Small, 2010, **6** (2): p. 226-231.

24. Marquina, J., Power, Ch. y González, J., *Espectroscopía Raman del grafeno monocapa y el grafi to:*

acoplamiento electrón fonón y efectos no adiabáticos. Tumbaga, 2010, **5**: p. 183-194.

25. Wang, Y. Y., Ni, Z. H., Yu, T., Shen, Z. X., Wang, H. M., Wu, Y. H., Chen, W. y Wee, A. T. S., *Raman studies of monolayer graphene: The substrate effect.* Journal of Physical Chemistry C, 2008, **112** (29): p. 10637-10640.

26. Cançado, L. G., Reina, A., Kong, J. y Dresselhaus, M. S., *Geometrical approach for the study of ${G}^{\ensuremath{'}}$ band in the Raman spectrum of monolayer graphene, bilayer graphene, and bulk graphite.* Physical Review B, 2008, **77** (24): p. 245408.

27. Lavin-Lopez, M. P., Valverde, J. L., Cuevas, M. C., Garrido, A., Sanchez-Silva, L., Martinez, P. y Romero-Izquierdo, A., *Synthesis and characterization of graphene: Influence of synthesis variables.* Physical Chemistry Chemical Physics, 2014, **16** (7): p. 2962-2970.

28. Calizo, I., Teweldebrhan, D., Bao, W., Miao, F., Lau, C. N. y Balandin, A. A., *Spectroscopic Raman nanometrology of graphene and graphene multilayers on arbitrary substrates.* Journal of Physics: Conference Series, 2008, **109** (1): p. 5.

29. Krishnamoorthy, K., Veerapandian, M., Yun, K. y Kim, S. J., *The chemical and structural analysis of graphene oxide with different degrees of oxidation.* Carbon, 2013, **53**: p. 38-49.

30. Gao, J., Liu, F., Liu, Y., Ma, N., Wang, Z. y Zhang, X., *Environment-friendly method to produce graphene that employs vitamin C and amino acid.* Chemistry of Materials, 2010, **22** (7): p. 2213-2218.

31. Eigler, S., Dotzer, C. y Hirsch, A., *Visualization of defect densities in reduced graphene oxide.* Carbon, 2012, **50** (10): p. 3666-3673.

32. Jimenez-Cotillas, V., *Sintesis, activación quimica y aplicaciones de nanoestructuras de carbono*, in *Chemical Engineerin*. 2011, University of Castilla-La Mancha: Ciudad Real.
33. Blanton, T. N. y Majumdar, D., *Characterization of X-ray irradiated graphene oxide coatings using X-ray diffraction, X-ray photoelectron spectroscopy, and atomic force microscopy.* 61st Annual Conference on Applications of X-ray Analysis: Denver X-ray Conference, DXC 2012, 2013, **28** (2): p. 68-71.
34. Lavin-Lopez, M. P., Valverde, J. L., Garrido, A., Sanchez-Silva, L., Martinez, P. y Romero-Izquierdo, A., *Novel etchings to transfer CVD-grown graphene from copper to arbitrary substrates.* Chemical Physics Letters, 2014, **614** (0): p. 89-94.
35. Lavin-Lopez, M. P., Valverde, J. L., Sanchez-Silva, L. y Romero, A., *Influence of the Total Gas Flow at Different Reaction Times for CVD-Graphene Synthesis on Polycrystalline Nickel.* Journal of Nanomaterials, 2016, **2016**: p. 9.

Chapter 3: Synthesis and characterization of graphene deposited over polycrystalline copper: Influence of the synthesis variables.

Resumen

El presente capítulo resume los resultados obtenidos en el estudio de optimización del crecimiento de grafeno sobre láminas de cobre policristalinas usando el método de Deposición Química en fase Vapor a presión atmosférica. En este estudio se han usado CH_4 and H_2 como gases precursores. La espectroscopía Raman ha sido la técnica de caracterización en la que se ha centrado el estudio de optimización. Se analizaron en detalle diferentes parámetros de crecimiento que afectan a la síntesis de grafeno, tales como la temperatura y el tiempo de reacción, la relación entre los caudales de CH_4 e H_2 durante la etapa de reacción y el caudal total de gases (CH_4+H_2) durante la etapa de reacción. Se pudo comprobar que, el crecimiento de grafeno no era homogéneo en toda la muestra, estando ésta recubierta en su mayoría por grafeno multicapa. Sin embargo, a medida que se realizaban los experimentos y se modificaban los parámetros de reacción, el grafeno sintetizado iba ganando calidad llegando a obtener una muestra recubierta en su mayoría por grafeno bicapa.

Se diseñó una aplicación Excel-VBA para analizar la calidad del grafeno depositado sobre las láminas de cobre. La muestra óptima de grafeno se obtuvo para el menor tiempo de reacción estudiado (10 minutos), la mayor temperatura de síntesis (1050ºC), una relación CH_4/H_2 de 0.07 v/v y un caudal total de gases durante la etapa de reacción (CH_4+H_2) de 60 Nml/min.

Abstract

The optimization of graphene growth over polycrystalline copper foils using an atmospheric pressure Chemical Vapor Deposition setup is reported. CH_4 and H_2 were used as precursor gases. Raman spectroscopy was selected as the main graphene characterization technique during graphene synthesis optimization. Different growth parameters, including temperature and reaction time, CH_4/H_2 flow rate ratio in the feed and total flow of gases during the reaction step, were studied in detail. It was shown that graphene growth was not homogeneous in the entire sample obtaining multilayer graphene deposited over most of the copper foil. However, as the synthesis parameters were optimized, graphene was gained better quality, obtaining bilayer graphene over most of the sheet for the optimized conditions.

A homemade software was used to analyse the quality value of graphene sheet, which is related to the quality of the synthesised graphene. Higher quality graphene was obtained with the optimization of the synthesis parameters. An optimal bilayer graphene sample was prepared at the lowest growth time (10 min) and the highest synthesis temperature (1050 ºC), using a CH_4/H_2 flow rate ratio and a total flow rate ratio of precursors of 0.07 v/v and 60 Nml (CH_4+H_4), respectively.

3.1. Introduction

Graphene, a two dimensional sheet of carbon atoms, has recently gained attention due to its promising properties, mainly those related to electronics applications [1-5]. It was firstly obtained in the form of small flakes of the order of several microns through mechanical exfoliation of graphite using Scotch® Tape method [6]. Although with this procedure is possible to obtain graphene with the highest quality, the most efficient procedures should be developed for manufacturing graphene at industrial scale.

Graphene can be synthesized by a variety of method such as *arc discharge* [6, 7], *epitaxial growth on SiC* [8-13], *unzipping carbon nanotubes* [14-16], *chemical conversion* [17], *self-assembly of surfactants* [18] and *Chemical Vapor Deposition (CVD)* [19-23].

Chemical vapor deposition (CVD) is a technique that has the ability to synthesize wafer scale graphene and the advantage of produced large size of graphene [24, 25]. Also, it is a low cost method, leading to a high the yield if compared to the other growth methods. However, the graphene growth from CVD tends to wrinkle due to the difference in thermal expansion between graphene and metal layer. This could be decreased via proper annealing, but is still an ongoing research challenge [26]. In CVD, a metal substrate is put into a furnace and heated to high temperatures.

Copper is usually used as the substrate material for graphene synthesis using the CVD method due to its small carbon solubility at elevated temperatures [27], which allows to better control the number of graphene layers. Other transition metals, such as Co and Pt are alternative used although less frequently [28, 29].

In order to obtained uniformity and high quality graphene, it is crucial to understand the details of the growth kinetics and nucleation.

Graphene growth by CVD is a catalytic process involving the surface diffusion and hydrocarbon decomposition, which involves different steps in the graphene growth such as, the adsorption and de-absorption of hydralarbon molecules on copper, which are followed by the decomposition of hydrocarbon to form carbon atoms, the aggregation of carbon atoms on the copper surface to form the graphene nucleation centres and finally, the diffusion and attachment of carbon atoms to nucleation centres to form graphene[30, 31].

Several studies have demonstrated a close correlation between the CVD growth parameters and the number of graphene layers and the quality of synthesized graphene, which enables the formation of bilayer and few-layers graphene on Cu substrates.

Ma *et al.* found that the growth temperature influence, significantly, the graphene quality. Increasing the temperature, increases the quality of graphene, while at low temperatures, the samples contained a large number of defects [32, 33]. Also, Rybin, *et al.* discovered that an increase in the temperature induced an increment in the carbon atoms dissolved in the metal layer, producing more graphene layers [34]. Recent studies showed that the concentration of hydrogen plays an important role in providing the quality of the graphene grown by CVD, which is related with the CH_4/H_2 ratio and the total flow rate of CH_4 and H_2 during the reaction step.

Gao, *et al.* found that a high hydrogen concentration worsened the graphene quality using an atmospheric pressure CVD system, as a result of the increased defects and wrinkles [35]. In a similar way, Vlassiouk, *et al.* demonstrated the presence of a critical value of hydrogen concentration for graphene growth. No graphene nucleation was observed below this value, while high hydrogen concentration caused a worsening in the quality of graphene [36]. Finally, several groups found that that the key to growing bilayer and few-layers graphene is the concentration of active carbon species [37] which is

related with the CH_4/H_2 ratio and the total flow rate of CH_4 and H_2 during the reaction step.

The aim of this work is to optimize the graphene growth on copper foils using a homemade atmospheric pressure chemical vapor deposition setup. CH_4 was used as the precursor gas whereas H_2 and N_2 were used as carrier gases. Thus, different growth parameters, presumably affecting the CVD-grown graphene characteristics: temperature and reaction time, molar ratio CH_4/H_2 in the feed and total flow of gases entering the reactor, have been studied in detail. The resulting materials were characterized by Raman spectroscopy since it allowed to evaluate both the number of graphene layers and the defects present in them [38].

3.2. Experimental

3.2.1. Materials

25 μm thick cooper sheets with a high purity grade (99.99%) were purchased from GOODFELLOW. Hydrogen and nitrogen with a high purity grade (99.999%) packaged in steel cylinders (Praxair) and methane (99.5% of grade purity) packaged in a steel cylinder (Praxair) were purchased from Sigma Aldrich Chemical Co.

3.2.2. Method

Graphene samples were grown on 25 μm thick copper foil in a 40-inch quartz tube heated by a furnace (Figure 3.1.) using the CVD method [22].

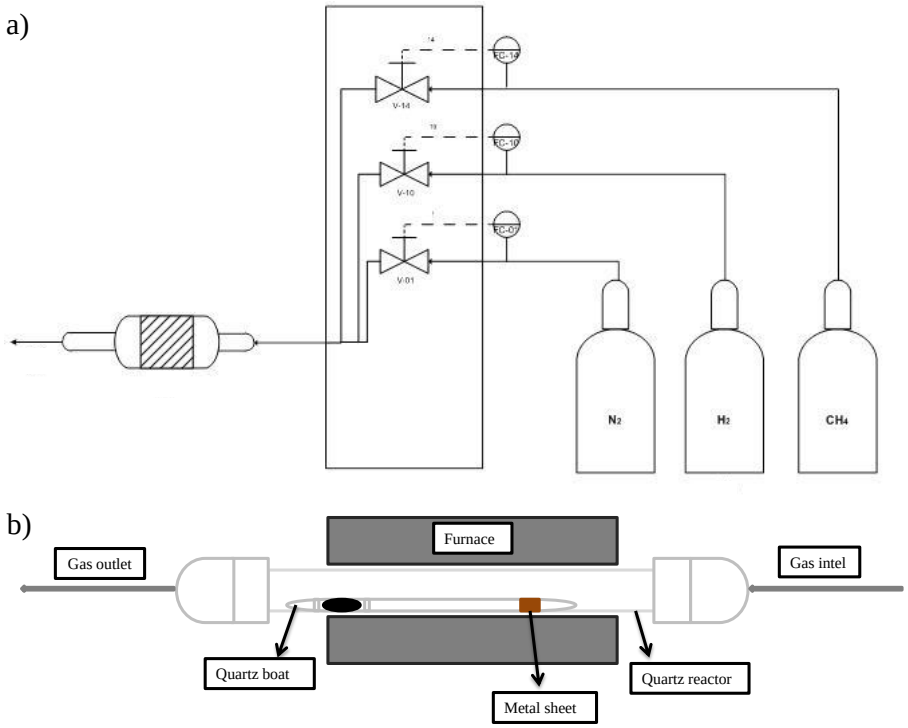

Figure 3.1. a) Set-up used for CVD synthesis of graphene on copper. b) Experimental quartz reactor used in graphene synthesis.

Under atmospheric pressure, the furnace was heated to 900ºC with a 400 sccm flow of N_2 and 100 sccm flow of H_2 to prevent copper oxidation. After that, the furnace was maintained at 900ºC during 45 minutes to allow the annealing of the copper foil. Then, a 30 sccm flow of methane was introduced while nitrogen was tuned-off during a growth time ranging from 5 to 40 minutes at the different temperatures used for the graphene synthesis (900 ºC-1050 ºC). Finally, the system was cooled (~10 ºC/min) by flowing 400 sccm of nitrogen. The synthesis process is summarized in Figure 3.2.

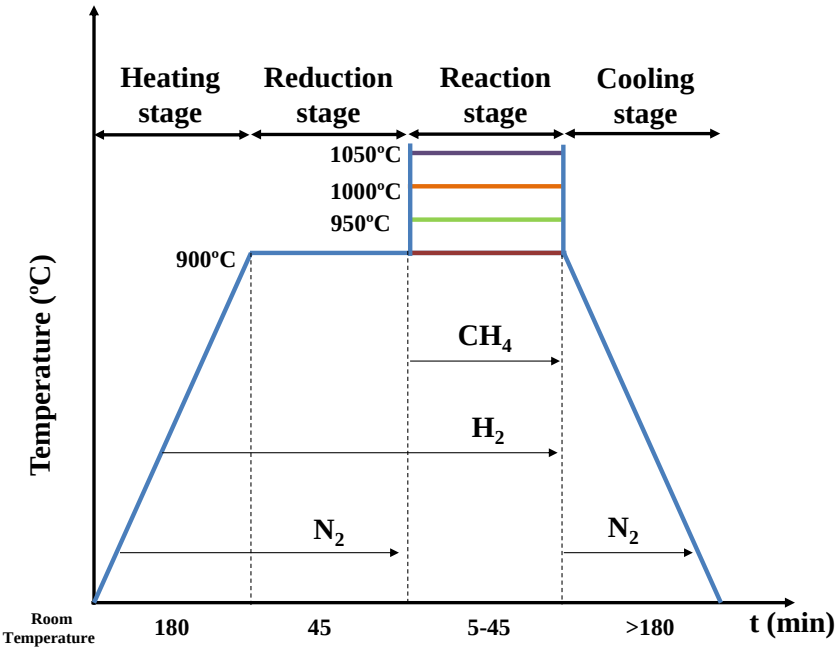

Figure 3.2. Summary of the stages, times, temperatures and gases used during graphene synthesis.

3.2.3. Characterization

Raman spectroscopy and optical microscopy were used to analyse the synthesized graphene samples. For these purposes, a SENTERRA spectrometer with 600 lines/mm grating, 532 nm laser wavelengths at a very low laser power level (< 1 mW) to avoid any heating effect and X20 SENTERRA microscope were used.

Raman spectroscopy is considered as a reliable and quick method to characterize graphene [39-41]. D peak, visible at ~1350 cm^{-1} is related with the presence of defects (edges, dislocations, cracks or vacancies) in graphitic materials [40]. Two peaks more named to as G and 2D are visible at ~1560 cm^{-1} and 2690 cm^{-1}, respectively. G peak denotes the symmetry-allowed graphite band and is a way of checking the vibration on the same plane of sp^2 hybridized carbon atoms, which compose

graphene sheets [40]. 2D peak originates from second order double resonant Raman scattering from zone boundary and is the hall-marks of different numbers of graphene layers [42, 43].

The amount of defects present in graphene samples can be quantified by measuring the intensity ratio of the D and G bands (I_D/I_G). On the other hand, the number of graphene layers is directly related to the ratio (I_{2D}/I_G). These parameters were characteristics of CVD-grown of graphene on Cu [43-46]. Typical values of the ratios I_D/I_G and for I_{2D}/I_G for bilayer graphene have been reported, being in the range 0.1-0.3 [45] and 0.4-1 respectively [22, 30, 46, 47].

Other remarkable parameters in the characterization of graphene are the following ones: ***FWHM*** (Full Width at Half Maximum) and ***2D peak position or 2D Raman Shift*** (Raman Shift, cm^{-1}). FWHM is related to the life-time of the excited states (life-time for the Raman scattering process), which is the time delay between the absorption of the incident photon and the emission of the outgoing one [5], which is calculated as the Raman Shift difference to the half average height of the 2D band. Characteristic values of FWHM in bilayer graphene are in the range 45-65 cm^{-1} [44-46]. On the other hand, *2D Raman Shift* (Raman Shift, cm^{-1}) in graphene Raman spectrum (around 2690 cm^{-1}) should be displaced to lower Raman shift values if compared to that in graphite Raman spectrum (ranging from 2710 to 2720 cm^{-1}) [39]. It is important to note that 2D Raman band shape and position are good fingerprints that indicate the presence of single and bilayer graphene samples and. Thus, the 2D mode in bulk graphite can be decomposed in two components ($2D_1$ and $2D_2$). Single layer graphene has a single component. Nevertheless, the 2D Raman band in bilayer graphene is fitted to four components. Moreover, in bulk graphite, $2D_1$ component is less intense than $2D_2$ one, whereas in bilayer graphene both of them have almost the same intensity. An increase in the number of layers leads to an increment of intensity of the $2D_2$ component if compared to the $2D_1$ one

[41]. Finally, although Raman spectrum of graphene grown on copper showed fluorescence **[48]**, the peaks in the Raman spectrum could be clearly identified. Anyway, 2D band deconvolution of the best sample obtained at each reaction time were conducted in order to determinate the number of graphitic layers present in the synthesized graphene.

3.2.4. Graphene quality analysis

It was designed a homemade Excel-VBA application in order to analyse the graphene quality focusing in the image of the sample obtaining using optical microscopy. This software allows know the percentage of each type of graphene presents the graphene sheet. Depending of the obtained percentage, the software assigned a number between 1 and 1000 which allow quantify the quality of the sample, obtaining a number between 0 and 10 if the most of the sample is multilayer graphene or few-layer graphene, between 10 and 1000 if the most of the sample is bilayer graphene and between 100 and 1000 if the most of the sample is monolayer graphene.

3.3. Results and discussion

Four main parameters which affect the process, including reaction temperature and reaction time, the relation between CH_4 and H_2 and the total flow involving during the reaction step were selected to be studies in detail due to their influence on the structure of deposited graphene layers. The reaction temperature was the main key parameter of this experiment, varying the reaction time at each temperature. These parameters in combination with two others (CH_4/H_2 rate and total flow rate), allow controlling the process more carefully. Thereby, the relation between methane and hydrogen were varied from 0.03 to 0.45 v/v have been selected and the total flow involving during reaction step were varied between 40 and 140 Nml/min.

3.3.1. Influence of the synthesis temperature at different reaction times

Table 3.1. lists the Raman parameters obtained at different reaction times (5, 10, 20, 30 and 40 minutes) varying the synthesis temperature between 900ºC and 1050ºC, and keeping the rest of operational parameters constant: CH_4/H_2 molar flow rate ratio of 0.3 v/v, and total flow of gases (CH_4+H_2) =130 Nml/min.

Table 3.1. Influence of the synthesis temperature at different reaction times.
RAMAN characterization parameters.

Experiment set	$T_{reaction}$ (ºC)	$t_{reaction}$ (min)	I_D/I_G	I_{2D}/I_G	FWHM (cm^{-1})	2D Raman Shift (cm^{-1})
1	900	5	0.48	0.26	73	2709
	950	5	0.28	0.29	67	2709
	1000	5	0.19	0.31	67	2709
	1050	5	0.08	0.38	67	2709
2	900	10	0.54	0.27	73	2704
	950	10	0.28	0.28	67	2709
	1000	10	0.25	0.32	67	2709
	1050	10	0.16	0.43	67	2709
3	900	20	0.36	0.25	78	2709
	950	20	0.33	0.28	67	2709
	1000	20	0.29	0.31	67	2710
	1050	20	0.24	0.35	67	2709
4	900	30	0.48	0.23	73	2709
	950	30	0.32	0.37	61	2706
	1000	30	0.27	0.33	70	2711
	1050	30	0.25	0.35	65	2709
5	900	40	0.38	0.23	67	2704
	950	40	0.32	0.37	67	2704
	1000	40	0.31	0.26	67	2709
	1050	40	0.24	0.35	67	2709

Figure 3.3. shows the corresponding Raman spectra. These spectrums were focused in the multilayer graphene area since most of the sample was covered by this graphene type.

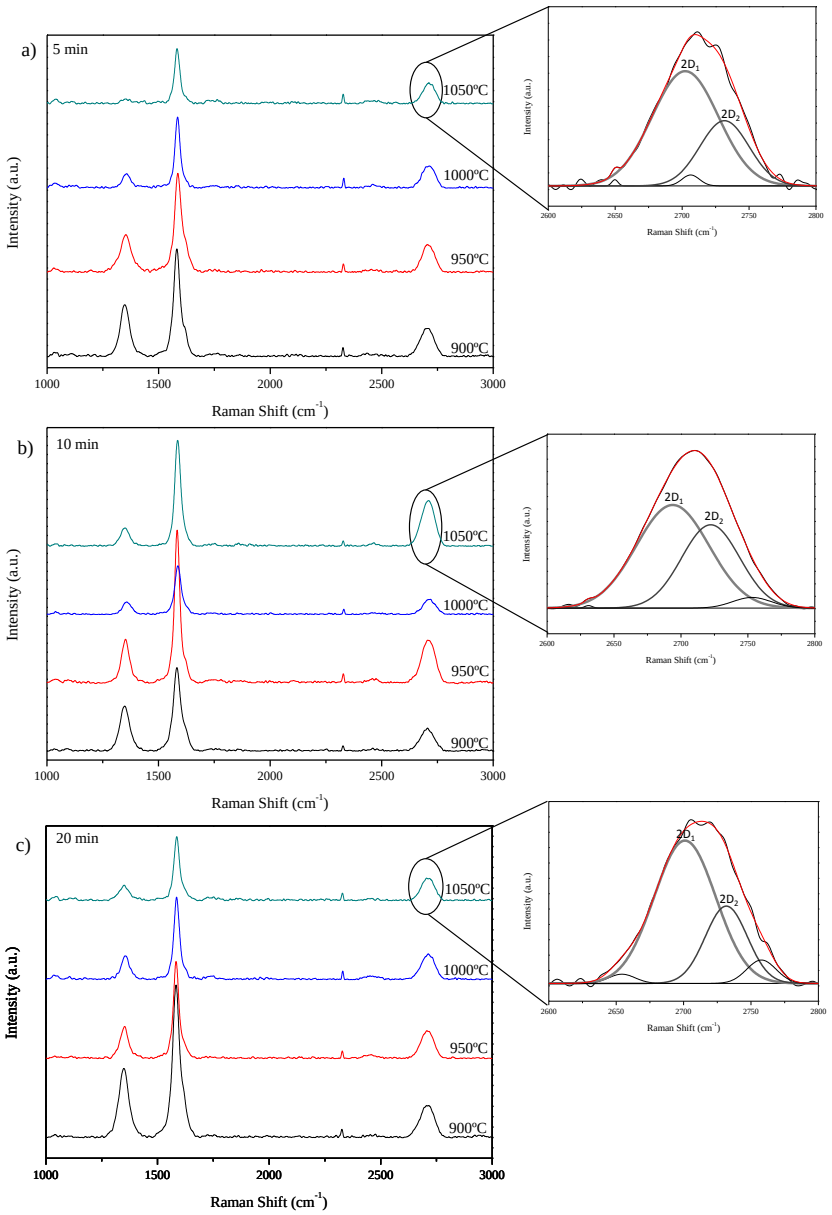

Figure 3.3. Influence of the synthesis temperature at different reaction times. Raman spectrum and 2D peak deconvolution. a) 5 min reaction time, b) 10 min reaction time, c) 20 min reaction time.

(Synthesis conditions: 900-1050ºC, CH_4/H_2=0.3 v/v, 130 Nml (CH_4+H_2)/min).

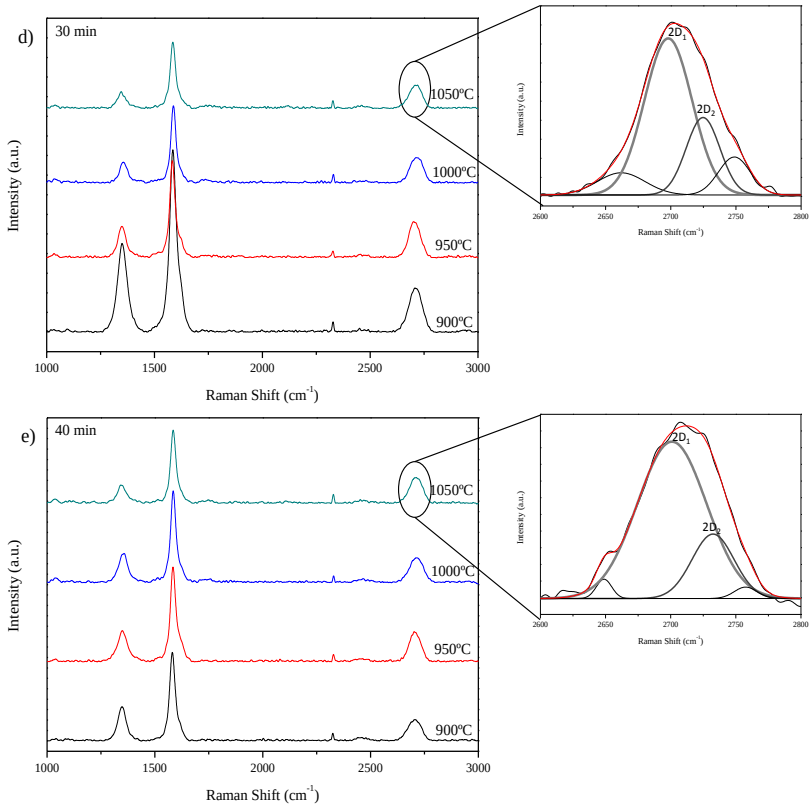

Figure 3.3. Continuation. Influence of the synthesis temperature at different reaction times. Raman spectrum and 2D peak deconvolution. d) 30 min reaction, e) 40 min reaction time.

(Synthesis conditions: 900-1050ºC, CH_4/H_2=0.3 v/v, 130 Nml (CH_4+H_2)/min).

In all cases, I_D/I_G ratio decreased when the synthesis temperature was increased, indicating a decrease in the amount of defects present in the carbon structure [49]. On the other hand, the I_{2D}/I_G ratio increased with the synthesis temperature, indicating a decrease in the number of graphene layers present in the samples. In other words, it is possible to assert that the graphene quality improved with increasing synthesis temperatures [49]. This trend is not clear for samples obtained after 30

and 40 minutes on stream. On the other hand, the position of 2D peaks and the values of FWHM were similar for all the products obtained, indicating that these parameters were not affected by both the synthesis temperature and the reaction time.

The growth of graphene on copper is a surface catalysis process, which occurs by a nucleation step because of the small solubility of carbon in this metal [22, 27, 50-52]. At low temperatures, the mobility of the carbon atoms leading to thin film growth is reduced [53, 54]. This means that before they can be attached to growing atoms sites on the substrate, additional atoms (ad-atoms) are being deposited onto them, due to the continuous decomposition of the precursor (CH_4 in this case). As the growth temperature increase, the mobility of these ad-atoms also increases. Consequently, they are attached to more favourable sites before being covered by additional ad-atoms. The overall result is that at elevated temperatures the growth of the carbon structure is more ordered. Regarding the influence of the reaction time, it appears that positively influences on the quality in terms of defects and the decreasing of the number of layers in the resulting materials during the growth step. Optimum samples were selected in each set of experiments attending to the I_D/I_G ratio, I_{2D}/I_G ratio, FWHM and 2D Raman Shift values. Thus, the samples with the best properties (in this case, with the lowest I_D/I_G ratio and the highest I_{2D}/I_G ratio) were generally obtained at the highest synthesis temperature (1050ºC) and at relatively low reaction times (10 minutes). A deconvolution of 2D peak for all these selected samples was performed (Figure 3, inset). Four contributions, characteristics of bilayer graphene, were obtained [41]. At the lowest reaction time (5 minutes), it could be observed that the intensity of $2D_1$ intensity was much higher than that of $2D_2$, indicating that few layer graphene was formed. At 10 minutes, intensities of $2D_1$ and $2D_2$ were similar being a characteristic of bilayer graphene [41]. At higher reaction

times (> 20 minutes), the difference between the intensities of $2D_1$ and $2D_2$ progressively increased, indicating that few layers graphene was grown. In the light of the obtained results, it is clear that the graphene with the best properties was obtained at 1050 ºC and 10 minutes of reaction time.

For these conditions, the values of I_D/I_G and I_{2D}/I_G ratios were the lowest and the highest ones, respectively. Note that at this reaction time, D peak was practically negligible. Similar results were obtained by other investigation groups [32-34, 55]. Although most of the sample was covered by multilayer graphene, it was considered desirable analysed the different kinds of graphene presented in the sample. Figure 1.4. a shows an optical microscopy image of the optimum sample obtaining in the present study.

It could be visually observed the presence of three different kinds of graphene (bright orange correspond with multilayer graphene, light orange correspond with few-layer graphene and yellow colour correspond with bilayer graphene). In Figure 3.4. b it could be observed the RAMAN spectrums corresponding to each type of graphene, observing that the main important RAMAN parameters improved and so, the graphene quality, obtaining the best RAMAN parameters for bilayer graphene and the worst ones for multilayer graphene.

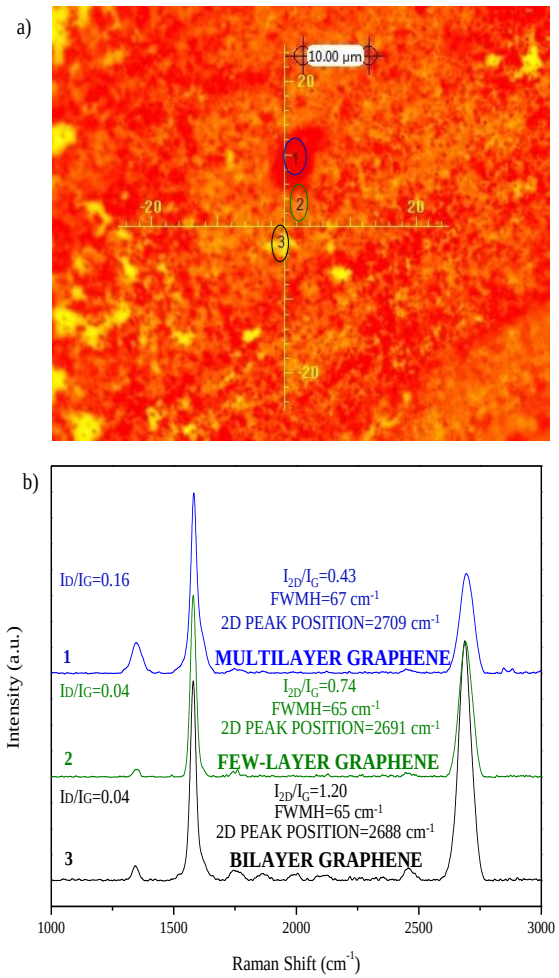

Figure 3.4. Influence of the synthesis temperature at different reaction times. a) Optical Microscopy of the optimum sample analysing different types of graphene. b) Raman spectrum of the three different types of graphene presented in the optimum sample.

(Synthesis conditions: 1050 ºC, 10 min reaction, CH_4/H_2=0.3 v/v, 130 Nml (CH_4+H_2)/min).

Table 3.2. shows the percentages of the different types of graphene presented in the optimum sample obtaining in the present study using the designed homemade software. A quality value, of 4.2 indicated that the most of the graphene sheet was recovered by multilayer graphene.

Table 3.2. Influence of the synthesis temperature at different reaction times. Percentages of each type of graphene presented in the optimum sample and graphene quality value.

% Multilayer graphene	81.34%
% Few-layer graphene	17.00%
% Bilayer graphene	1.66%
Quality value of graphene	4.2

Figure 3.5. shows the RAMAN spectra of both parent graphite and the selected bilayer graphene and the corresponding 2D band deconvolutions. As observed, position of 2D peak in graphene was around 2709 cm^{-1} whereas the same peak in graphite was encountered at around 2718 cm^{-1}. On the other hand, I_{2D}/I_G ratio in graphene (0.43) was as expected higher than that in graphite (0.29). The opposite trend was observed if the I_D/I_G ratio is taken into consideration. In addition, remarkable changes in the shape and position of 2D peak were observed as a function of the material. Thus, 2D band in graphite was deconvoluted into two components, D_1 and D_2 [41], being the former less intense than latter. Nevertheless, in the bilayer graphene sample 2D band was fitted to four components, being the difference in the intensities of $2D_1$ and $2D_2$ much lower. As above mentioned, an increase of the $2D_1$ intensity would indicate that the number of layers tends to decrease [41].

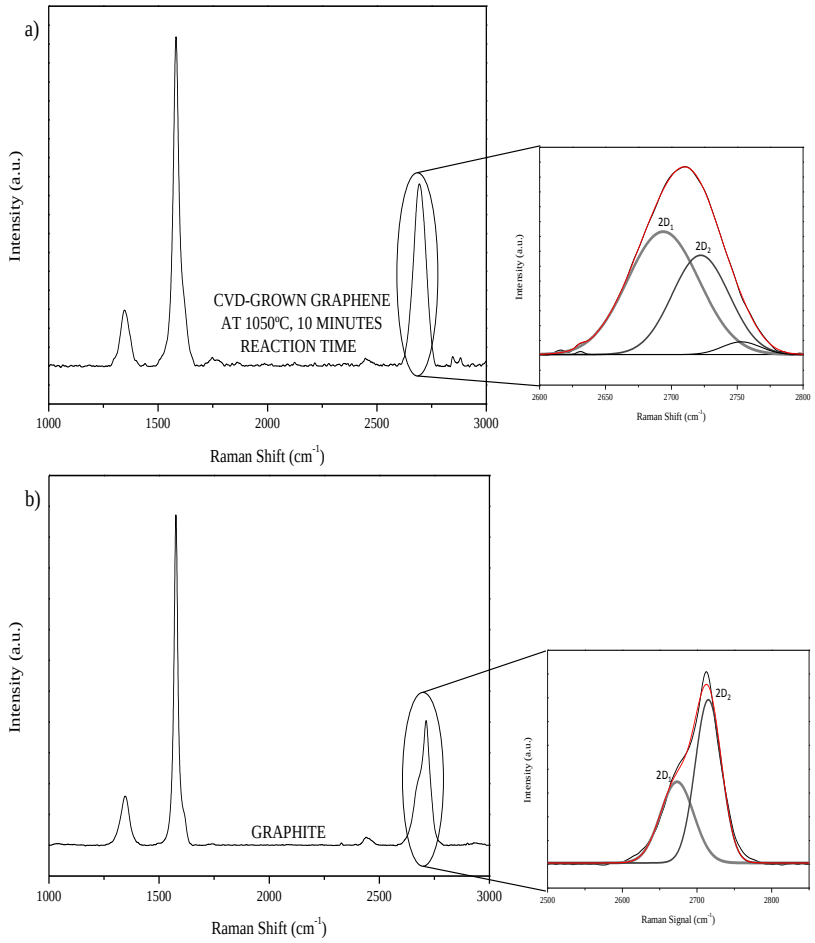

Figure 3.5. Influence of the synthesis temperature at different reaction times. a) Raman spectrum and 2D peak deconvulation for the optimum sample. b) Raman spectrum and 2D peak deconvolution of graphite.
(Synthesis conditions: 1050 ºC, 10 min reaction time, CH_4/H_2=0.3, 130 Nml (CH_4+H_2)/min).

3.3.2. Influence of the relation between CH_4 and H_2 molar flow rates (CH_4/H_2 ratio)

Several synthesis experiments were performed varying the CH_4/H_2 molar flow rate ratio in the range 0.03-0.45 v/v, keeping the rest of synthesis variables (reaction temperature: 1050 ºC, reaction time: 10

minutes, total flow: 130 Nml (CH_4 + H_2)/ min) constant. Figure 3.6. shows the variation of the different Raman parameters, I_D/I_G and I_{2D}/I_G (Figure 3.6. a) and, FWHM and 2D Raman Shift (Figure 3.6. b) with CH_4/H_2 molar flow rate ratio.

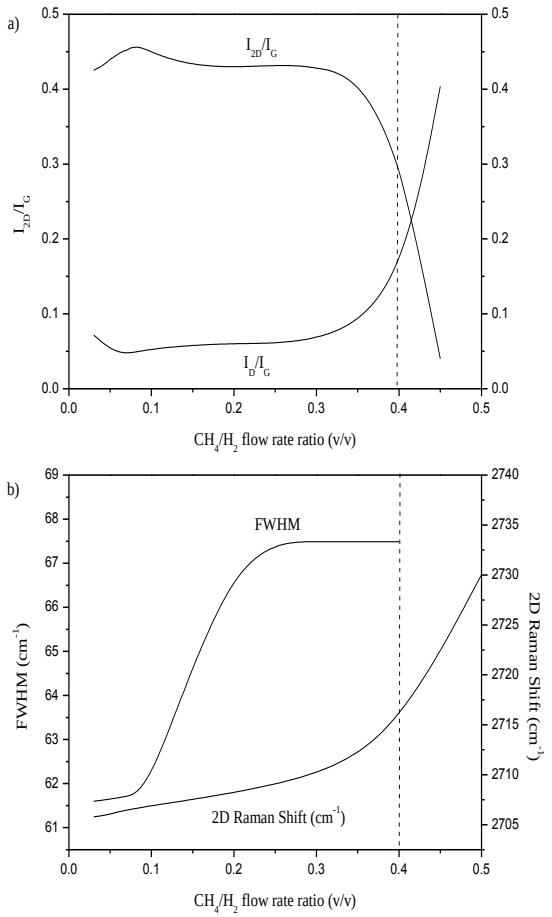

Figure 3.6. Influence of the CH_4/H_2 molar flow rate ratio. a) I_{2D}/I_G and I_D/I_G. b) FWHM and 2D Raman Shift.

(Synthesis conditions: 1050 ºC, 10 min reaction, CH_4/H_2=0.03-0.45 v/v, 130 Nml (CH_4+H_2)/min).

The following conclusions could be established:

- High CH_4/H_2 molar flow rate ratios (≥0.4 v/v) gave rise to graphene samples with a large structural disorder (high I_D/I_G ratio values) and a

large number of layers (low I_{2D}/I_G ratio values and 2D Raman Shift shifted to higher values in the spectrum).

- By increasing the CH_4/H_2 molar flow rate ratio to values not exceeding 0.4 v/v, the value of the I_{2D}/I_G ratio tended to slightly decrease, remaining the value of I_D/I_G ratio practically constant. Furthermore, the values of FWHM and 2D Raman Shift in the spectrum tended to slightly increase indicating that low CH_4/H_2 molar flow rate ratio values (≤0.1 v/v) were required to obtain high quality graphene samples with a small number of layers.

Similar results were obtained by other investigation groups [37, 55]. According to the obtained results, graphene sample synthesized using a CH_4/H_2 molar flow rate ratio of 0.07 v/v was selected as the reference to carry out the following set of experiments. Raman spectrum for this sample and the corresponding 2D band deconvolution are shown in Figure 3.7.

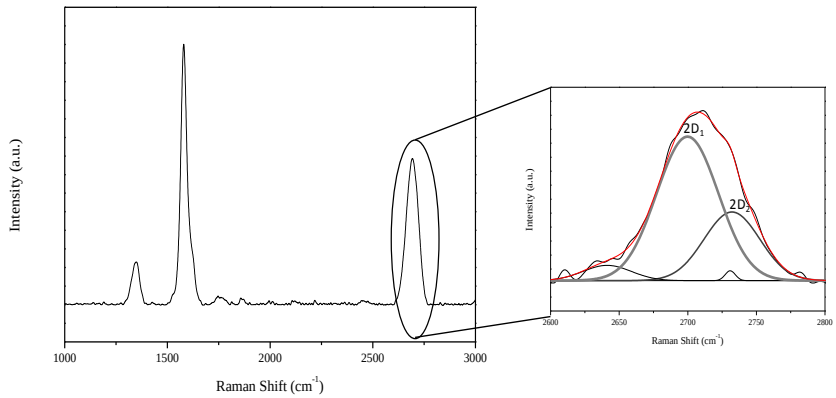

Figure 3.7. Influence of the CH_4/H_2 molar flow rate ratio. Optimum sample. Raman spectrum and 2D peak deconvolution.
(Synthesis conditions: 1050 ºC, 10 min reaction, CH_4/H_2=0.07 v/v, 130 Nml (CH_4+H_2)/min).

Figure 3.8. a shows an optical microscopy picture of the optimum sample obtained in this study. It could be visually observed that the proportion of multilayer graphene decreased thus obtaining a graphene with best quality. In Figure 3.8. b it could be observed the RAMAN

spectrum and the main RAMAN parameters of each type of graphene above commented.

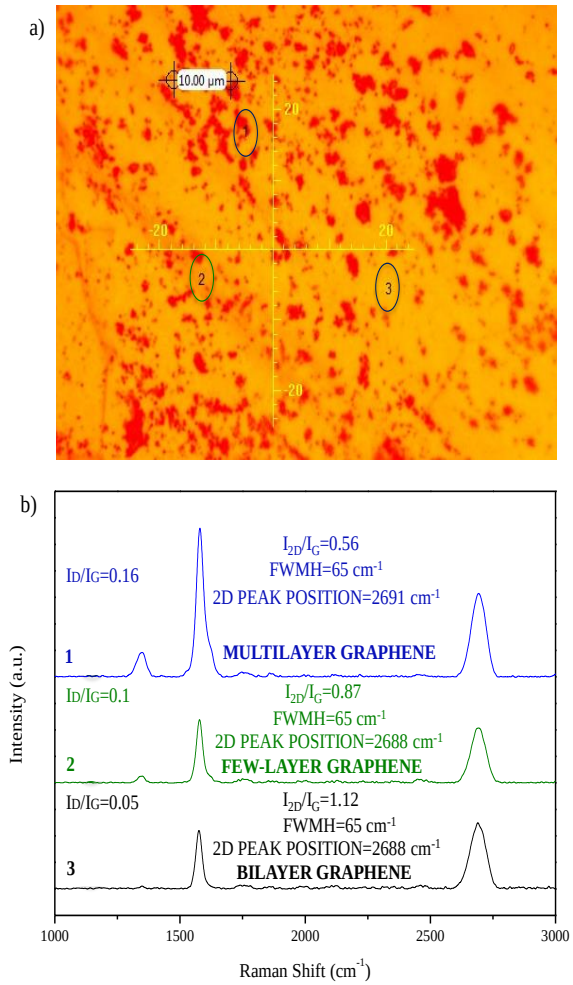

Figure 3.8. Influence of the CH_4/H_2 molar flow rate ratio. a) Optical Microscopy of the optimum sample analyzing different types of graphene. b) Raman spectrum of the three different types of graphene presented in the optimum sample.
(Synthesis conditions: 1050 ºC, 10 min reaction, CH_4/H_2=0.07 V/V, 130 Nml (CH_4+H_2)/min).

Table 3.3. shows the percentages of the different types of graphene presented in the optimum sample. A quality value of 34.7 indicated that approximately the half of the sample was covered by few-layer graphene and around 30% was covered by bilayer graphene (high quality).

Table 1.3. Influence of the CH_4/H_2 molar flow rate ratio. Percentages of each type of graphene presented in the optimum sample and graphene quality value.

% Multilayer graphene	19.67%
% Few-layer graphene	50.92%
% Bilayer graphene	29.41%
Quality value of graphene	34.7

3.3.3. Influence of the total flow of gases (CH_4+H_2) during the reaction step

Several synthesis experiments were performed varying the total flow of gases (CH_4+H_2) in the range 40-140 Nml/min, keeping the rest of conditions (reaction temperature: 1050 ºC, reaction time: 10 minutes, CH_4/H_2 molar flow rate ratio: 0.07 v/v) constant.

Table 3.4. lists the main Raman characterization parameters measured to the resulting products whereas Figure 3.9. shows their RAMAN spectra. As a general trend, the smaller the total flow, the better the characteristics of synthesized graphene were obtained, specifically, the value I_D/I_G ratio increased with the total flow. Similar results were obtained for other investigation groups [35, 36].

Table 3.4. Influence of the total flow of gases (CH_4+H_2) during the reaction step. Raman characterization parameters and value assigned depending of the quality of graphene.

Q_{total} (Nml/min)	I_D/I_G	I_{2D}/I_G	FWHM (cm^{-1})	2D Raman Shift (cm^{-1})
40	0.09	0.45	62	2707
60	0.08	0.44	61	2706
100	0.10	0.45	61	2706
130	0.15	0.46	61	2706
140	0.14	0.40	61	2711

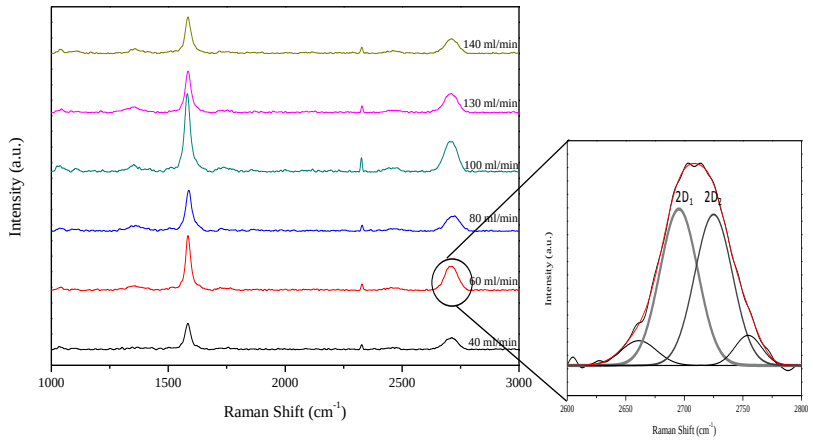

Figure 3.9. Influence of the total flow (CH_4+H_2) during the reaction step. Raman spectrum and 2D peak deconvolution.
(Synthesis conditions: 1050ºC, 10 min reaction, CH_4/H_2=0.07 v/v, 40-140 Nml (CH_4+H_2)/min).

This phenomenon was related to the slowdown of carbon deposition on the metal sheet [56]. For all the tested samples, the rest of parameters in the Raman characterization were kept almost constant, indicating that total flow rate does not seem to be an important factor in controlling the number of layers in the final products.

Optimum sample was synthesized using a total flow of 60 Nml/min was selected as the best material prepared in this work. 2D peak deconvolution in this sample (Figure 3.9. inset) showed the four contributions characteristic of high quality bilayer graphene, presenting both $2D_1$ and $2D_2$ contributions similar intensities.

Figure 3.10.a shows an optical microscopy picture of the optimum sample. It was observed that the proportion of multilayer graphene decreased (bright orange colour area), obtaining bilayer graphene (yellow colour area) for the most part of the sample. In Figure 3.10.b it could be observed the RAMAN spectrum and the main RAMAN parameters which are characteristics of each type of graphene presented in the optimum sample.

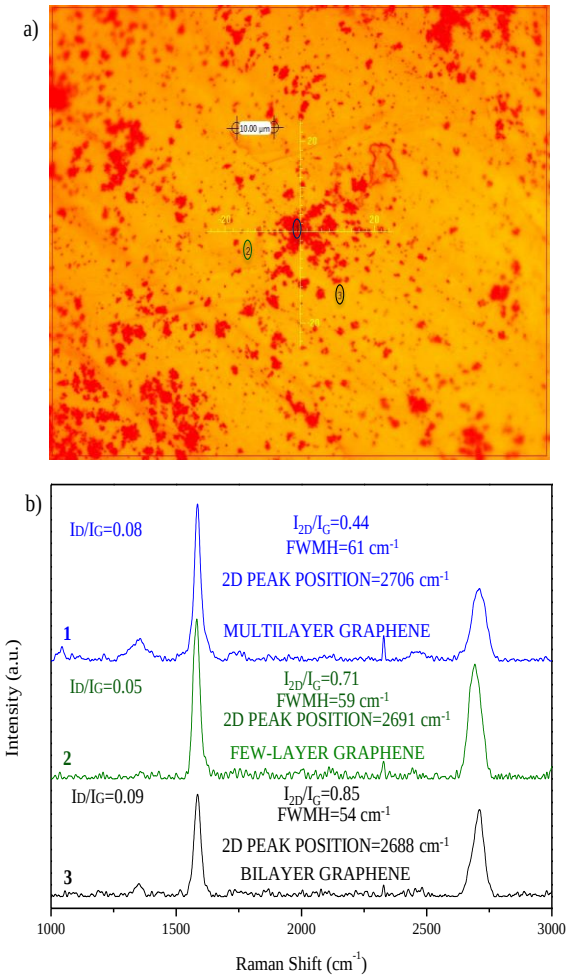

Figure 3.10. Influence of the total flow of gases (CH_4+H_2) during the reaction step. a) Optical Microscopy of the optimum sample analyzing different types of graphene. b) Raman spectrum of the three different types of graphene presented in the optimum sample.

(Synthesis conditions: 1050 ºC, 10 min reaction, CH_4/H_2=0.07 v/v, 60 Nml (CH_4+H_2)/min).

Finally, Table 3.5. shows the percentages of the different types of graphene presented in the optimum sample obtained in this last study. A quality value of 59.3 indicated that more than half of all deposited graphene was of bilayer type with a high quality.

Table 3.5. Influence of the total flow of gases (CH_4+H_2) during the reaction step. Percentages of each type of graphene presented in the optimum sample and graphene quality value.

% Multilayer graphene	10.87%
% Few-layer graphene	33.27%
% Bilayer graphene	55.86%
Quality value of graphene	59.3

It was observed that the quality value and thus, the quality of the sample was improved while the synthesis conditions were optimized, obtaining the best quality graphene for the influence of the total flow (CH_4+H_2) in which the most of the sample was covering by bilayer graphene.

3.4. Conclusions

The aim of the paper was to optimize the graphene synthesis using an atmospheric pressure chemical vapour deposition (CVD) system. Copper foils were used as the substrate material due to its small carbon solubility at elevated temperatures [13] which allows the better control of the graphene layers. CH_4 was used as precursor gas while H_2 was used to remove native oxide as well as to grow copper grains. N_2 acted as carrier gas during synthesis to dilute the precursor gas. Raman spectroscopy was used as characterization technique due to graphene has a characteristic Raman spectrum which can be used to distinguish the number of graphene layers and defects of the sample. Different growth parameters including temperature and reaction time, molar ratio CH_4/H_2 in the feed and total flow of gases flowing during the reaction step were studied in detail. It was shown that graphene growth was not homogeneous in the entire sample. Thus, multilayer graphene was present in most of the samples; however as the synthesis parameters were optimized, graphene was gained better quality, obtaining in the best optimized sample, bilayer graphene for the most

part of the sample (56%). The conditions for the optimum sample were as follows: growth time (10 min), synthesis temperature (1050 ºC), CH_4/H_2 flow ratio (0.07 v/v) and total flow rate ratio of precursors (60 Nml ($CH_4 + H_2$)/ min).

3.5. References

1. Novoselov, K. S., Geim, A. K., Morozov, S. V., Jiang, D., Zhang, Y., Dubonos, S. V., Grigorieva, I. V. and Firsov, A. A., *Electric field in atomically thin carbon films.* Science, 2004, **306** (5696): p. 666-669.
2. Novoselov, K. S., Geim, A. K., Morozov, S. V., Jiang, D., Katsnelson, M. I., Grigorieva, I. V., Dubonos, S. V. and Firsov, A. A., *Two-dimensional gas of massless Dirac fermions in graphene.* Nature, 2005, **438** (7065): p. 197-200.
3. Geim, A. K. and Novoselov, K. S., *The rise of graphene.* Nature Materials, 2007, **6** (3): p. 183-191.
4. Geim, A. K., *Graphene: Status and prospects.* Science, 2009, **324** (5934): p. 1530-1534.
5. Wang, Y. Y., Ni, Z. H., Yu, T., Shen, Z. X., Wang, H. M., Wu, Y. H., Chen, W. and Wee, A. T. S., *Raman studies of monolayer graphene: The substrate effect.* Journal of Physical Chemistry C, 2008, **112** (29): p. 10637-10640.
6. Li, N., Wang, Z., Zhao, K., Shi, Z., Gu, Z. and Xu, S., *Synthesis of single-wall carbon nanohorns by arc-discharge in air and their formation mechanism.* Carbon, 2010, **48** (5): p. 1580-1585.
7. Karmakar, S., Kulkarni, N. V., Nawale, A. B., Lalla, N. P., Mishra, R., Sathe, V. G., Bhoraskar, S. V. and Das, A. K., *A novel approach towards selective bulk synthesis of few-layer graphenes in an electric arc.* Journal of Physics D: Applied Physics, 2009, **42** (11).
8. Rollings, E., Gweon, G. H., Zhou, S. Y., Mun, B. S., McChesney, J. L., Hussain, B. S., Fedorov, A. V., First, P. N., de Heer, W. A.

and Lanzara, A., *Synthesis and characterization of atomically thin graphite films on a silicon carbide substrate.* Journal of Physics and Chemistry of Solids, 2006, **67** (9-10): p. 2172-2177.

9. de Heer, W. A., Berger, C., Wu, X., First, P. N., Conrad, E. H., Li, X., Li, T., Sprinkle, M., Hass, J., Sadowski, M. L., Potemski, M. and Martinez, G., *Epitaxial graphene.* Solid State Communications, 2007, **143** (1-2): p. 92-100.
10. Ni, Z. H., Chen, W., Fan, X. F., Kuo, J. L., Yu, T., Wee, A. T. S. and Shen, Z. X., *Raman spectroscopy of epitaxial graphene on a SiC substrate.* Physical Review B - Condensed Matter and Materials Physics, 2008, **77** (11).
11. Sutter, P. W., Flege, J. I. and Sutter, E. A., *Epitaxial graphene on ruthenium.* Nature Materials, 2008, **7** (5): p. 406-411.
12. Seyller, T., Bostwick, A., Emtsev, K. V., Horn, K., Ley, L., McChesney, J. L., Ohta, T., Riley, J. D., Rotenberg, E. and Speck, F., *Epitaxial graphene: a new material.* physica status solidi (b), 2008, **245** (7): p. 1436-1446.
13. Sprinkle, M., Soukiassian, P., De Heer, W. A., Berger, C. and Conrad, E. H., *Epitaxial graphene: The material for graphene electronics.* Physica Status Solidi - Rapid Research Letters, 2009, **3** (6): p. A91-A94.
14. Kosynkin, D. V., Higginbotham, A. L., Sinitskii, A., Lomeda, J. R., Dimiev, A., Price, B. K. and Tour, J. M., *Longitudinal unzipping of carbon nanotubes to form graphene nanoribbons.* Nature, 2009, **458** (7240): p. 872-876.
15. Hirsch, A., *Unzipping carbon nanotubes: A peeling method for the formation of graphene nanoribbons.* Angewandte Chemie - International Edition, 2009, **48** (36): p. 6594-6596.
16. Jiao, L., Zhang, L., Wang, X., Diankov, G. and Dai, H., *Narrow graphene nanoribbons from carbon nanotubes.* Nature, 2009, **458** (7240): p. 877-880.

17. Yang, X., Dou, X., Rouhanipour, A., Zhi, L., Räder, H. J. and Müllen, K., *Two-dimensional graphene nanoribbons.* Journal of the American Chemical Society, 2008, **130** (13): p. 4216-4217.
18. Zhang, W., Cui, J., Tao, C. A., Wu, Y., Li, Z., Ma, L., Wen, Y. and Li, G., *A strategy for producing pure single-layer graphene sheets based on a confined self-assembly approach.* Angewandte Chemie - International Edition, 2009, **48** (32): p. 5864-5868.
19. Wang, X., You, H., Liu, F., Li, M., Wan, L., Li, S., Li, Q., Xu, Y., Tian, R., Yu, Z., Xiang, D. and Cheng, J., *Large-scale synthesis of few-layered graphene using CVD.* Chemical Vapor Deposition, 2009, **15** (1-3): p. 53-56.
20. Wang, Y., Chen, X., Zhong, Y., Zhu, F. and Loh, K. P., *Large area, continuous, few-layered graphene as anodes in organic photovoltaic devices.* Applied Physics Letters, 2009, **95** (6).
21. Dervishi, E., Li, Z., Watanabe, F., Biswas, A., Xu, Y., Biris, A. R., Saini, V. and Biris, A. S., *Large-scale graphene production by RF-cCVD method.* Chemical Communications, 2009 (27): p. 4061-4063.
22. Li, X., Cai, W., An, J., Kim, S., Nah, J., Yang, D., Piner, R., Velamakanni, A., Jung, I., Tutuc, E., Banerjee, S. K., Colombo, L. and Ruoff, R. S., *Large-area synthesis of high-quality and uniform graphene films on copper foils.* Science, 2009, **324** (5932): p. 1312-1314.
23. Chae, S. J., Günes, F., Kim, K. K., Kim, E. S., Han, G. H., Kim, S. M., Shin, H. J., Yoon, S. M., Choi, J. Y., Park, M. H., Yang, C. W., Pribat, D. and Lee, Y. H. *Synthesis of large-area graphene layers on nickel film by chemical vapor deposition: Wrinkle formation*. in *Carbon Nanotubes, Graphene, and Associated Devices II*. 2009. San Diego, CA.
24. Obraztsov, A. N., *Chemical vapour deposition: Making graphene on a large scale.* Nature nanotechnology, 2009, **4** (4): p. 212-213.

25. Emtsev, K. V., Bostwick, A., Horn, K., Jobst, J., Kellogg, G. L., Ley, L., McChesney, J. L., Ohta, T., Reshanov, S. A., Röhrl, J., Rotenberg, E., Schmid, A. K., Waldmann, D., Weber, H. B. and Seyller, T., *Towards wafer-size graphene layers by atmospheric pressure graphitization of silicon carbide.* Nature Materials, 2009, **8** (3): p. 203-207.
26. Bae, S., Kim, H., Lee, Y., Xu, X., Park, J. S., Zheng, Y., Balakrishnan, J., Lei, T., Ri Kim, H., Song, Y. I., Kim, Y. J., Kim, K. S., Özyilmaz, B., Ahn, J. H., Hong, B. H. and Iijima, S., *Roll-to-roll production of 30-inch graphene films for transparent electrodes.* Nature nanotechnology, 2010, **5** (8): p. 574-578.
27. López, G. A. and Mittemeijer, E. J., *The solubility of C in solid Cu.* Scripta Materialia, 2004, **51** (1): p. 1-5.
28. Ruan, G., Sun, Z., Peng, Z. and Tour, J. M., *Growth of graphene from food, insects, and waste.* ACS Nano, 2011, **5** (9): p. 7601-7607.
29. Sun, Z., Yan, Z., Yao, J., Beitler, E., Zhu, Y. and Tour, J. M., *Growth of graphene from solid carbon sources.* Nature, 2010, **468** (7323): p. 549-552.
30. Liu, W., Li, H., Xu, C., Khatami, Y. and Banerjee, K., *Synthesis of high-quality monolayer and bilayer graphene on copper using chemical vapor deposition.* Carbon, 2011, **49** (13): p. 4122-4130.
31. Li, X., Cai, W., Colombo, L. and Ruoff, R. S., *Evolution of graphene growth on Ni and Cu by carbon isotope labeling.* Nano Letters, 2009, **9** (12): p. 4268-4272.
32. Zhang, Y., Gao, T., Gao, Y., Xie, S., Ji, Q., Yan, K., Peng, H. and Liu, Z., *Defect-like structures of graphene on copper foils for strain relief investigated by high-resolution scanning tunneling microscopy.* ACS Nano, 2011, **5** (5): p. 4014-4022.
33. Nie, S., Wofford, J. M., Bartelt, N. C., Dubon, O. D. and McCarty, K. F., *Origin of the mosaicity in graphene grown on Cu(111).* Physical Review B - Condensed Matter and Materials Physics, 2011, **84** (15).

34. Rybin, M. G., Pozharov, A. S. and Obraztsova, E. D., *Control of number of graphene layers grown by chemical vapor deposition.* Physica Status Solidi (C) Current Topics in Solid State Physics, 2010, **7** (11-12): p. 2785-2788.
35. Gao, L., Ren, W., Zhao, J., Ma, L. P., Chen, Z. and Cheng, H. M., *Efficient growth of high-quality graphene films on Cu foils by ambient pressure chemical vapor deposition.* Applied Physics Letters, 2010, **97** (18).
36. Vlassiouk, I., Regmi, M., Fulvio, P., Dai, S., Datskos, P., Eres, G. and Smirnov, S., *Role of hydrogen in chemical vapor deposition growth of large single-crystal graphene.* ACS Nano, 2011, **5** (7): p. 6069-6076.
37. Ma, L., Ren, W., Dong, Z., Liu, L. and Cheng, H., *Progress of graphene growth on copper by chemical vapor deposition: Growth behavior and controlled synthesis.* Chinese Science Bulletin, 2012, **57** (23): p. 2995-2999.
38. Ferrari, A. C., Meyer, J. C., Scardaci, V., Casiraghi, C., Lazzeri, M., Mauri, F., Piscanec, S., Jiang, D., Novoselov, K. S., Roth, S. and Geim, A. K., *Raman spectrum of graphene and graphene layers.* Physical Review Letters, 2006, **97** (18).
39. Calizo, I., Teweldebrhan, D., Bao, W., Miao, F., Lau, C. N. and Balandin, A. A., *Spectroscopic Raman nanometrology of graphene and graphene multilayers on arbitrary substrates.* Journal of Physics: Conference Series, 2008, **109** (1): p. 5.
40. Wall, M., *Raman spectroscopy optimizes graphene characterization.* Advanced Materials and Processes, 2012, **170** (4): p. 35-38.
41. Das, A., Chakraborty, B. and Sood, A. K., *Raman spectroscopy of graphene on different substrates and influence of defects.* Bulletin of Materials Science, 2008, **31** (3): p. 579-584.
42. Suk, J. W., Kitt, A., Magnuson, C. W., Hao, Y., Ahmed, S., An, J., Swan, A. K., Goldberg, B. B. and Ruoff, R. S., *Transfer of CVD-*

grown monolayer graphene onto arbitrary substrates. ACS Nano, 2011, **5** (9): p. 6916-6924.

43. Reina, A., Jia, X., Ho, J., Nezich, D., Son, H., Bulovic, V., Dresselhaus, M. S. and Jing, K., *Large area, few-layer graphene films on arbitrary substrates by chemical vapor deposition.* Nano Letters, 2009, **9** (1): p. 30-35.
44. Chen, S., Cai, W., Piner, R. D., Suk, J. W., Wu, Y., Ren, Y., Kang, J. and Ruoff, R. S., *Synthesis and characterization of large-area graphene and graphite films on commercial Cu-Ni alloy foils.* Nano Letters, 2011, **11** (9): p. 3519-3525.
45. Lee, S., Lee, K. and Zhong, Z., *Wafer scale homogeneous bilayer graphene films by chemical vapor deposition.* Nano Letters, 2010, **10** (11): p. 4702-4707.
46. Lee, D., Lee, K., Jeong, S., Lee, J., Choi, B. and Kim, O., *Process optimization for synthesis of high-quality graphene films by low-pressure chemical vapor deposition.* Japanese Journal of Applied Physics, 2012, **51** (6 PART 2).
47. Lenski, D. R. and Fuhrer, M. S., *Raman and optical characterization of multilayer turbostratic graphene grown via chemical vapor deposition.* Journal of Applied Physics, 2011, **110** (1).
48. Costa, S. D., Righi, A., Fantini, C., Hao, Y., Magnuson, C., Colombo, L., Ruoff, R. S. and Pimenta, M. A., *Resonant Raman spectroscopy of graphene grown on copper substrates.* Solid State Communications, 2012, **152** (15): p. 1317-1320.
49. Nemanich, R. J. and Solin, S. A., *First- and second-order Raman scattering from finite-size crystals of graphite.* Physical Review B, 1979, **20** (2): p. 392-401.
50. Mattevi, C., Kim, H. and Chhowalla, M., *A review of chemical vapour deposition of graphene on copper.* Journal of Materials Chemistry, 2011, **21** (10): p. 3324-3334.
51. Wu, W., Jauregui, L. A., Su, Z., Liu, Z., Bao, J., Chen, Y. P. and Yu, Q., *Growth of single crystal graphene arrays by locally controlling*

nucleation on polycrystalline Cu using chemical vapor deposition. Advanced Materials, 2011, **23** (42): p. 4898-4903.

52. Yu, Q., Jauregui, L. A., Wu, W., Colby, R., Tian, J., Su, Z., Cao, H., Liu, Z., Pandey, D., Wei, D., Chung, T. F., Peng, P., Guisinger, N. P., Stach, E. A., Bao, J., Pei, S. S. and Chen, Y. P., *Control and characterization of individual grains and grain boundaries in graphene grown by chemical vapour deposition.* Nature Materials, 2011, **10** (6): p. 443-449.
53. Venables, J. A., Spiller, G. D. T. and Hanbucken, M., *Nucleation and growth of thin films.* Reports on Progress in Physics, 1984, **47** (4): p. 399-459.
54. Ratsch, C. and Venables, J. A., *Nucleation theory and the early stages of thin film growth.* Journal of Vacuum Science and Technology A: Vacuum, Surfaces and Films, 2003, **21** (5): p. S96-S109.
55. Liang, C., Wang, W., Li, T. and Wang, Y. *Optimization on the synthesis of large-area single-crystal graphene domains by chemical vapor deposition on copper foils*. in *2012 2nd International Conference on Manipulation, Manufacturing and Measurement on the Nanoscale, 3M-NANO 2012*. 2012. Xi'an.
56. Avouris, P. and Dimitrakopoulos, C., *Graphene: Synthesis and applications.* Materials Today, 2012, **15** (3): p. 86-97.

Chapter 4: Novel etchings to transfer CVD-grown graphene from copper to arbitrary substrates.

Resumen

En este capítulo se ha estudiado la síntesis de nuevos procedimientos (*etchings*) para la transferencia de grafeno, sintetizado por el método CVD a substratos arbitrarios. Además de la disolución de $FeCl_3$ que normalmente se usa para transferir grafeno a otros substratos, se han probado dos nuevas disoluciones para la transferencia de grafeno basadas en las mezclas: $HF:2Na_2CO_3{\cdot}3H_2O_2$ (4:1) y H_2O_2 (30%p./v.):agua regia ($1HNO_3$:3HCl):H_2O (1:1:2). Con dichas disoluciones es posible transferir grafeno a obleas de PET y desde éstas a substratos arbitrarios (por ejemplo, portaobjetos de microscopio). El grafeno transferido se analizó en detalle usando la técnica de Espectroscopia Raman.

Abstract

Novel and simple etchings for direct transfer of CVD-grown graphene synthesized over Cu to arbitrary substrates are reported in this chapter. Besides the classical transfer method using $FeCl_3$, two novel etching solutions have been used for transfer graphene over different substrates: $HF{:}2Na_2CO_3{\cdot}3H_2O_2$ (4:1) and H_2O_2 (30% p./v.): aqua Regis ($1HNO_3{:}3HCl$): H_2O (1:1:2). By using these etching solutions, graphene was firstly transferred to PET wafers and then to arbitrary substrates (microscope slides). The resulting materials were analyzed and discussed in detail using Raman Spectroscopy.

4.1. Introduction

As was commented in previous chapters, graphene can be synthesized by a variety of methods. Among them, Chemical Vapor Deposition stands out due to its large-area and high quality of the resulting graphene [1]. Regarding practical application of graphene, reliable methods for transferring graphene from metallic substrates to other arbitrary substrates are needed [2].

Different methods to transfer CVD-growth graphene from metals to arbitrary substrates [3] have been studied. One of them is based on using poly-(methyl-methacrylate) as a supporting material to transfer mechanical exfoliated graphene flakes [4] and carbon nanotubes [5]. Recent studies have reported a novel PMMA transfer technique in which a second liquid PMMA coating stage is included [6]. However, this technique can be only used to transfer graphene onto flat substrates [3].

On the other hand, novel dry methods to transfer CVD-grown graphene onto arbitrary substrates have been reported as cleaner and gentler simple transfer techniques than polymer-based methods [2, 3, 7]. These dry methods are an ideal alternative for the manufacture of a great variety of chemical, optical and electronic devices that use large and uniform graphene sheets [2].

According to recent researches, the most used technique to transfer CVD-grown graphene to arbitrary substrates is based on using $FeCl_3$ as an etching solution [8]. Related to this method, a thermal release adhesive has to be tapped on the top of the graphene layer and then soak in a $FeCl_3$ solution to remove metal layer ($FeCl_3$ etching attacks chemically to the metal substrate). The resulting graphene film deposited on the polymer support could be ready to transfer onto different substrates.

In the present study, CVD-grown graphene on Cu has been transferred to different substrates using the $FeCl_3$ solution-based method. In this work, two novel etching solutions have been used during the transfer method: $HF:2Na_2CO_3{\cdot}3H_2O_2$ (4:1) and, H_2O_2 (30% p. /v.): aqua Regis ($1HNO_3$:3HCl): H_2O (1:1:2). Firstly, graphene was transferred to a PET wafer using the three different etching solutions. After that, graphene was again transferred to other arbitrary substrates such as microscope slides. The most important characteristics of the resulting materials were analyzed and discussed in detail using Raman Spectroscopy.

4.2. Experimental

4.2.1. Materials

Graphene sheets, with dimensions of 2.5x4 cm^2, were supplied by *Graphenano Nanotechnology*. Thermal release tapes, manufactured from PET (poly-ethylene terephthalate), were supplied by *Nitto Denko*.

4.2.2. Method

Two graphene transfer methods from metallic layers to arbitrary substrates, which instantly etch metal layers, have been developed.

The procedure to accomplish the transfer method is the following: Firstly, thermal release tapes were attached to the CVD-grown graphene on copper. Thus, a thermal adhesive tape should be placed on the top of the graphene layer and then, in order to obtain a smooth and unwrinkled surface, a firm pressure must be applied to the tape using a rubber roll. In this way, a suitable sheet that facilitates graphene transference was obtained. Until now, the above-mentioned experimental procedure was commonly used in the majority of transfer methods. In this point, three different etchings were chosen to check the effectiveness of the graphene transfer. Besides the most normally used etching solution ($FeCl_3$, 1M), there were considered two new ones;

HF:$2Na_2CO_3 \cdot 3H_2O_2$ (4:1) and, H_2O_2 (30% p. /v.): aqua Regis ($1HNO_3$:3HCl): H_2O (1:1:2). These two solutions have been compared with the most common one used in scientific literature, which is a 1 M solution of $FeCl_3$. Consequently three different procedures were performed:

1. One of the graphene sheet adhered to the PET wafer was soaked in a 1 M $FeCl_3$ solution in order to remove the metal layer. This etching should be warmed up from 55-65ºC to improve the attack of the metallic layer, which took about 20 minutes to disappear.
2. Another graphene sheet adhered to the PET wafer was soaked in a HF:2Na2CO3·$3H_2O_2$ (4:1) solution to remove the metal layer. This etching took about 1 hour to totally remove the metal layer.
3. Finally, a third PET wafer was soaked in a H_2O_2 (30% p. /v.): aqua Regis ($1HNO_3$:3HCl): H_2O (1:1:2) etching. Few seconds were needed to completely remove the metal layer.

Until this point, the procedure is the same for the three PET wafer obtained. Once the metal layer was removed, each PET wafer was cleaned with deionized water (D.I.) and allowed to dry. As a result of this, three PET wafer covers with graphene were obtained by using these three different etching solutions.

Nevertheless, the resulting graphene filmed onto the polymer (PET) support has to be transferred onto other arbitrary substrates. In the present study, the selected arbitrary substrate was a microscope slide. The suitable method to do it involves placing the dry PET wafer with the graphene on the cleaned substrate surface. Then, a firm pressure was applied in order to obtain a smooth and unwrinkled surface. The PET wafer with graphene was adhered to the surface substrate. By heating the substrate with the attached PET taped up to about 100ºC, the tape lost its adhesion capacity. Consequently, the graphene film was detached from the PET wafer and transferred to the substrate.

Figure 4.1. illustrates the procedure followed to transfer CVD-grown graphene from Cu layers to arbitrary substrates.

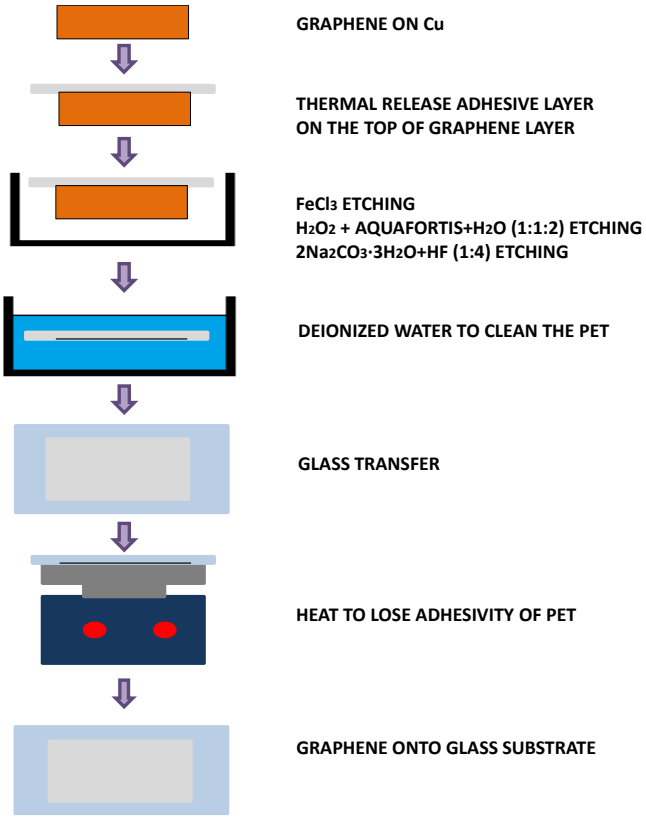

Figure 4.1. Schematic illustration of the direct method to transfer CVD-grown graphene from Cu layers to arbitrary substrates.

4.2.3. Characterization

Raman spectroscopy

Raman Spectroscopy (SENTERRA confocal (X50 objective) spectrometer with 600 lines/mm grating, 532 nm laser wavelength at a very low laser power level (< 1 mW) to avoid any heating effect) was used to evaluate the quality of the transferred graphene onto PET wafers and arbitrary substrates. Raman analyses were performed on the

substrate, PET wafer and microscope slide, in order to check if the transference had successfully occurred.

Raman spectroscopy is considered as a reliable and quick method to characterize graphene [9-12]. Figure 4.2. shows the Raman spectra of graphite and CVD-grown graphene on Cu.

D peak, visible at ~ 1350 cm^{-1}, is related to the presence of defects (edges, dislocations, cracks or vacancies) in graphitic materials [12]. Two more peaks named G and 2D bands are visible at around 1580-1620 cm^{-1} and ~ 2700 cm^{-1}, respectively. G peak denotes the symmetry-allowed graphite band and, is a way of checking the vibration on the same plane of sp^2 hybridized carbon atoms, which compose graphene sheets [12]. 2D peak, originated from second order double resonant Raman scattering from zone boundary, is the hallmarks of different numbers of graphene layers [3, 13].

The amount of defects present in graphene samples can be quantified by measuring the intensity ratio of D and G bands (I_D/I_G). On the other hand, the number of graphene layers is directly related to the ratio of G and 2D bands (I_{2D}/I_G). These parameters are characteristics of CVD-grown of graphene [14]. Other remarkable parameters in the characterization of graphene are the following ones: ***FWHM*** (Full Width at Half Maximum) and ***2D and G peak position*** (Raman Shift, cm^{-1}). FWHM is related to the life-time of the excited states (life-time for the Raman scattering process), which is the time delay between the absorption of the incident photon and the emission of the outgoing one [15], which is calculated as the Raman Shift difference to the half average height of 2D band. On the other hand, *G peak position* in graphene Raman spectrum is located around 1560 cm^{-1}. A variation in the position of this peak may be attributed to electronic doping between the graphene and the substrate [16]. Finally *2D peak position or 2D Raman Shift* in graphene Raman spectrum (around 2700 cm^{-1}) should be displaced to lower Raman shift values if compared to that in graphite Raman spectrum (ranging from 2710 to 2720 cm^{-1}) [9].

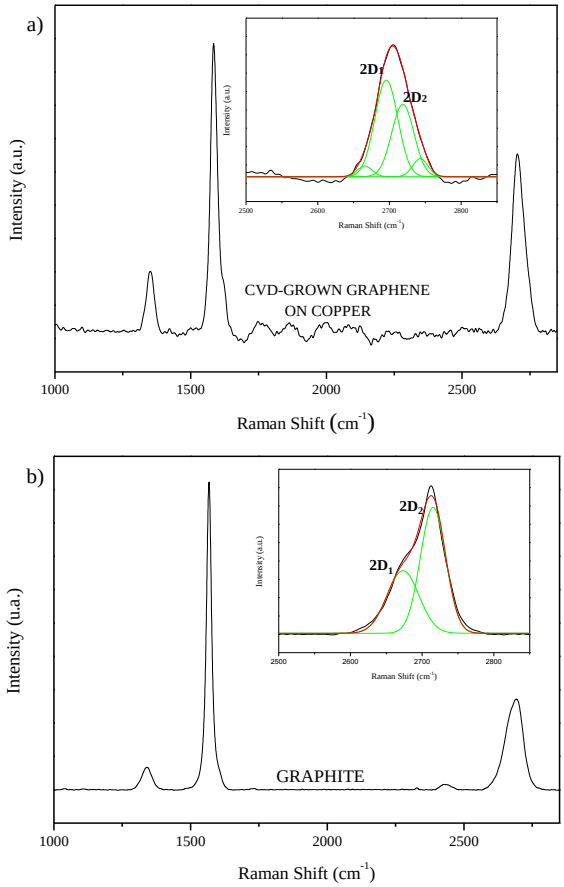

Figure 4.2. a) Raman spectra and the 2D peak deconvolution of graphene on copper b) Raman spectrum and the 2D peak deconvolution of graphite.

It is important to note that 2D Raman band shape and position are good fingerprints that indicate the presence of monolayer, bilayer, few-layer and multilayer graphene samples. Thus, the 2D mode in bulk graphite, few-layer and multilayer graphene has been reported to be decomposed in two components [17]. Monolayer graphene has a single component. Nevertheless, the 2D Raman band in bilayer graphene is fitted to four components. Finally, although the Raman spectrum of graphene grown on metals shows fluorescence [18], this one has been treated using the SENTERRA Raman spectrometer software, thus allowing to clearly

identify the different peaks appearing in the Raman spectrum.

4.3. Results and discussion

Table 4.1. lists the different experiments performed.

Table 4.1. Samples studied in this research.

Sample	Substrate	Etching
1	PET	(1 M) $FeCl_3$
2	PET	HF:$2Na_2CO_3 \cdot 3H_2O_2$ (4:1)
3	PET	H_2O_2 (30% p. /v.): aqua Regis (1HNO_3:3HCl): H_2O (1:1:2)
4	Microscope slide	1
5	Microscope slide	2
6	Microscope slide	3

Figure 4.3. illustrates the obtained polymer substrates (PET) after treat them with the different etchings solutions and further cleaning with D.I. water.

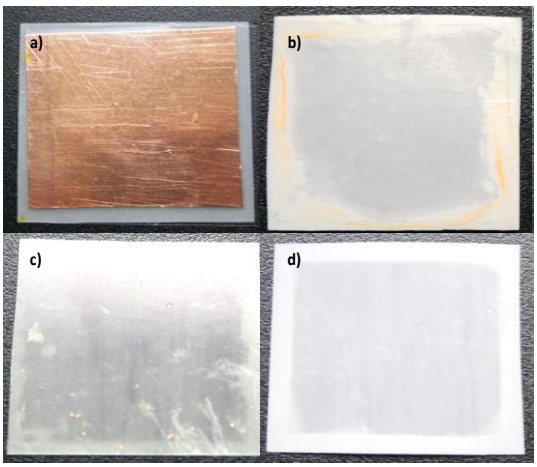

Figure 4.3. a) PET wafer over a Cu grown graphene sheet; b) PET wafer after etching with $FeCl_3$ (1M) and cleaning with D.I. water; c) PET wafer after etching with HF:$2Na_2CO_3 \bullet 3H_2O_2$ (4:1) and cleaning with D.I. water; d) PET wafer after etching with H_2O_2(110 volumes): aqua Regis (1 HNO_3:3HCl):H_2O (1:1:2) and cleaning with D.I. water.

In all PET wafers, the region where graphene is placed could be clearly distinguished. As observed, PET wafer before the transfer process was totally white, being bilayer graphene grown on copper coated over it (Figure 4.3.a.). When $FeCl_3$ (1M) was used as the etching solution, a dirty yellow area in the plastic appeared due to the Fe action (Figure 4.3.b.).

In order to obtain a clean wafer, it was necessary a cleaning stage. Firstly, acetone was used as a cleaning agent but a loss of adhesiveness of the PET was observed. As a result of this, graphene transfer from the PET wafer to other substrates was not feasible. This is the reason why acetone was ruled out as a PET wafer cleaning solution. Consequently, D.I. water was selected for this purpose.

Using HF: 2Na2CO3·3H_2O_2 (4:1) as an etching solution (Figure 4.3.c.), a clean white surface was obtained due to the action of the 2Na_2CO_3·3H_2O_2. However, part of the adhesiveness of the PET wafer was lost after the cleaning stage with D.I water. Finally, when (H_2O_2 (30% p. /v.): aqua Regis (1HNO_3:3HCl): H_2O (1:1:2) was used as an etching solution (Figure 4.3.d.), a clean white surface was also obtained. In this case, the PET wafer adhesiveness was maintained without alterations, which is essential for ensuring future transfers of the bilayer graphene from PET to other substrates.

Figure 4.4. shows the Raman spectra of the CVD-grown bilayer graphene transferred onto PET wafers using the three different etching solutions. If the Raman spectra of bilayer graphene transferred to PET wafer is compared to that the one of bilayer graphene on copper (Figure 2a), it can be concluded that the different transfer steps affected the quality of the resulting material. In all cases, it was noted that D peak intensity increased.

The best Raman spectrum was obtained for the transferred graphene using H_2O_2 (30% p. /v.): aqua Regis (1HNO_3:3HCl): H_2O (1:1:2) as an

etching solution. Note that D and 2D peaks intensities were the lowest and the highest respectively. This Raman spectrum was similar to that the one obtained for bilayer graphene on copper, being the level of noise pretty lower than the one observed on the other two samples.

Figure 4.4. also shows Raman spectra of the CVD-grown bilayer graphene transferred from different PET wafers to microscope slides. The spectrums obtained were characteristic of bilayer graphene but the spectrum noise was dependent on the etching solution used. In good agreement with the previous discussion, the best Raman spectrum of all the microscope slides was the one obtained from the transferred graphene using H_2O_2 (30% p. /v.): aqua Regis (1HNO_3:3HCl): H_2O (1:1:2) as an etching solution.

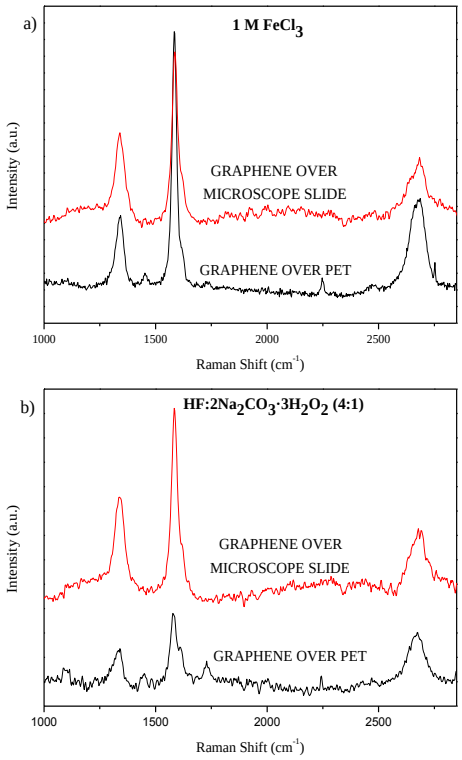

Figure 4.4. Raman spectrum of graphene over both PET and microscope slides using the following etchings media: a) $FeCl_3$ (1M); b) HF:2Na_2CO_3·3H_2O_2 (4:1); c) H_2O_2(110 volumes): aqua Regis (1HNO_3:3HCl):H_2O (1:1:2).

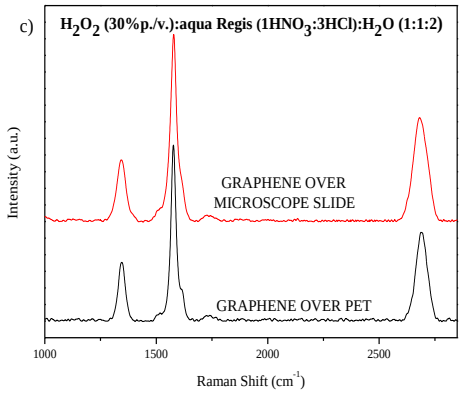

Figure 4.4. Continuation. Raman spectrum of graphene over both PET and microscope slides using the following etchings media: a) $FeCl_3$ (1M); b) HF:$2Na_2CO_3{\cdot}3H_2O_2$ (4:1); c) H_2O_2(110 volumes): aqua Regis (1HNO_3:3HCl):H_2O (1:1:2).

Table 4.2. summarizes the main Raman parameters of the different samples containing graphene. The intensity between D and G bands (I_D/I_G ratio), related to the presence of structural defects in the graphene sample [19], varied between 0.12 and 0.48 for graphene coated over PET wafers, and between 0.14-0.53 for graphene coated over microscope slides, being always higher when $FeCl_3$ (1M) and HF: 2Na2CO3·$3H_2O_2$ (4:1) were used as etching solutions (samples 1, 2, 4, 5). This fact could be due to the possible changes in the nature and the density of the defects [9]. On the other hand, the intensity between 2D and G bands (I_{2D}/I_G ratio), related to the quality and number of graphene layers [19], varied between 0.36 and 0.72 in PET wafers, and between 0.32 and 0.43 for graphene coated over microscope slides. In all samples, 2D Raman shifts in the spectrums were maintained on the range of 2676-2686 cm^{-1}, characteristic of graphene materials. Nevertheless, values of FWHM were considerably higher when $FeCl_3$ (1M) and HF: 2Na2CO3·$3H_2O_2$ (4:1) were used as etching solutions (samples 1, 2, 4, 5).

Table 4.2. Characteristic Raman parameters of graphene on copper and graphene transferred over PET and microscope slide.

Sample	I_D/I_G	I_{2D}/I_G	2D Raman Shift (cm^{-1})	FWHM (cm^{-1})
Graphite	0.13	0.38	2713	81
Graphene on Cu	0.25	0.69	2690	55
1	0.28	0.36	2686	80
2	0.48	0.72	2676	80
3	0.12	0.51	2681	73
4	0.53	0.39	2683	90
5	0.50	0.32	2683	65
6	0.14	0.43	2683	59

According to the results obtained in this work, the best etching for transferring graphene is based on the use of aqua Regis ($1HNO_3$:3HCl): H_2O (1:1:2). To verify the homogeneity of the best transfer process (H_2O_2 (30% p. /v.): aqua Regis ($1HNO_3$:3HCl): H_2O (1:1:2)), different spots in a specific area of the sample were measured using Raman Spectroscopy (Figure 5). In Figure 2.5. it could be observed the Raman spectrum and an image performed using optical microscopy in which graphene was transferred properly and it is uniform through the microscope slide.

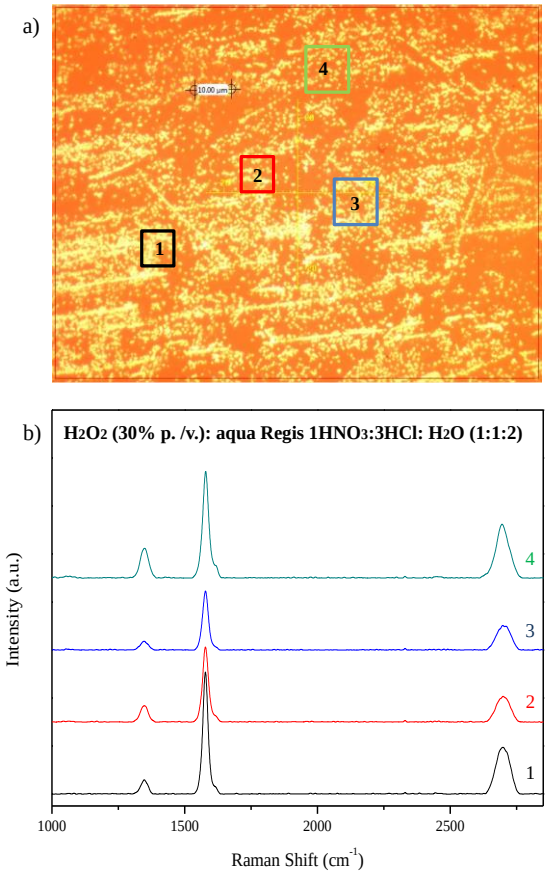

Figure 4.5. a) Optical Microscopy image of the graphene transferred over microscope slide. b) Raman mapping performed to the microscope slide using H_2O_2 (110 volumes): aqua Regis ($1HNO_3$:3HCl):H_2O (1:1:2) as etching.

4.4. Conclusions

Novel transfer etchings to transfer CVD-Cu grown graphene to arbitrary substrates have been developed. These etchings could be useful to transfer large-area graphene to arbitrary substrates (such as composites, plastics or glass) and manufacture a great variety of practical devices. It has been demonstrated that it is possible to transfer bilayer graphene over clean and white plastics. The best transfer etching

here was based on the use of H_2O_2 (110 volumes): aqua Regis ($1HNO_3$:3HCl): H_2O (1:1:2) as the etching solution. Thank to this, it was possible to avoid the PET wafer adhesiveness loss during the transfer process, which is crucial if a successful graphene transfer to arbitrary substrates is required.

4.5. References

1. Yao, Y. and Wong, C. P., *Monolayer graphene growth using additional etching process in atmospheric pressure chemical vapor deposition.* Carbon, 2012, **50** (14): p. 5203-5209.
2. Regan, W., Alem, N., Alemán, B., Geng, B., Girit, Ç., Maserati, L., Wang, F., Crommie, M. and Zettl, A., *A direct transfer of layer-area graphene.* Applied Physics Letters, 2010, **96** (11).
3. Suk, J. W., Kitt, A., Magnuson, C. W., Hao, Y., Ahmed, S., An, J., Swan, A. K., Goldberg, B. B. and Ruoff, R. S., *Transfer of CVD-grown monolayer graphene onto arbitrary substrates.* ACS Nano, 2011, **5** (9): p. 6916-6924.
4. Reina, A., Son, H., Jiao, L., Fan, B., Dresselhaus, M. S., Liu, Z. and Kong, J., *Transferring and identification of single- and few-layer graphene on arbitrary substrates.* Journal of Physical Chemistry C, 2008, **112** (46): p. 17741-17744.
5. Jiao, L., Fan, B., Xian, X., Wu, Z., Zhang, J. and Liu, Z., *Creation of nanostructures with poly(methyl methacrylate)-mediated nanotransfer printing.* Journal of the American Chemical Society, 2008, **130** (38): p. 12612-12613.
6. Li, X., Zhu, Y., Cai, W., Borysiak, M., Han, B., Chen, D., Piner, R. D., Colomba, L. and Ruoff, R. S., *Transfer of large-area graphene films for high-performance transparent conductive electrodes.* Nano Letters, 2009, **9** (12): p. 4359-4363.
7. Kang, J., Hwang, S., Kim, J. H., Kim, M. H., Ryu, J., Seo, S. J., Hong, B. H., Kim, M. K. and Choi, J. B., *Efficient transfer of large-*

area graphene films onto rigid substrates by hot pressing. ACS Nano, 2012, **6** (6): p. 5360-5365.

8. Lee, Y., Bae, S., Jang, H., Jang, S., Zhu, S. E., Sim, S. H., Song, Y. I., Hong, B. H. and Ahn, J. H., *Wafer-scale synthesis and transfer of graphene films.* Nano Letters, 2010, **10** (2): p. 490-493.
9. Calizo, I., Teweldebrhan, D., Bao, W., Miao, F., Lau, C. N. and Balandin, A. A., *Spectroscopic Raman nanometrology of graphene and graphene multilayers on arbitrary substrates.* Journal of Physics: Conference Series, 2008, **109** (1): p. 5.
10. Das, A., Chakraborty, B. and Sood, A. K., *Raman spectroscopy of graphene on different substrates and influence of defects.* Bulletin of Materials Science, 2008, **31** (3): p. 579-584.
11. Rao, C. N. R., Maitra, U. and Matte, H. S. S. R., *Synthesis, Characterization, and Selected Properties of Graphene*. 2012, Wiley-VCH. p. 1-47.
12. Wall, M., *Raman spectroscopy optimizes graphene characterization.* Advanced Materials and Processes, 2012, **170** (4): p. 35-38.
13. Reina, A., Jia, X., Ho, J., Nezich, D., Son, H., Bulovic, V., Dresselhaus, M. S. and Jing, K., *Large area, few-layer graphene films on arbitrary substrates by chemical vapor deposition.* Nano Letters, 2009, **9** (1): p. 30-35.
14. Gong, Y., Zhang, X., Liu, G., Wu, L., Geng, X., Long, M., Cao, X., Guo, Y., Li, W., Xu, J., Sun, M., Lu, L. and Liu, L., *Layer-controlled and wafer-scale synthesis of uniform and high-quality graphene films on a polycrystalline nickel catalyst.* Advanced Functional Materials, 2012, **22** (15): p. 3153-3159.
15. Wang, Y. Y., Ni, Z. H., Yu, T., Shen, Z. X., Wang, H. M., Wu, Y. H., Chen, W. and Wee, A. T. S., *Raman studies of monolayer graphene: The substrate effect.* Journal of Physical Chemistry C, 2008, **112** (29): p. 10637-10640.

16. Ferrari, A. C., Meyer, J. C., Scardaci, V., Casiraghi, C., Lazzeri, M., Mauri, F., Piscanec, S., Jiang, D., Novoselov, K. S., Roth, S. and Geim, A. K., *Raman spectrum of graphene and graphene layers.* Physical Review Letters, 2006, **97** (18).
17. Ferrari, A. C., *Raman spectroscopy of graphene and graphite: Disorder, electron-phonon coupling, doping and nonadiabatic effects.* Solid State Communications, 2007, **143** (1-2): p. 47-57.
18. Costa, S. D., Righi, A., Fantini, C., Hao, Y., Magnuson, C., Colombo, L., Ruoff, R. S. and Pimenta, M. A., *Resonant Raman spectroscopy of graphene grown on copper substrates.* Solid State Communications, 2012, **152** (15): p. 1317-1320.
19. Nemanich, R. J. and Solin, S. A., *First- and second-order Raman scattering from finite-size crystals of graphite.* Physical Review B, 1979, **20** (2): p. 392-401.

Chapter 5: Quality control of graphene deposited over polycrystalline nickel.

Resumen

En el presente capítulo se muestran los resultados obtenidos en el estudio de optimización del tipo de grafeno depositado sobre níquel policristalino usando el método de Deposición Química en fase Vapor a presión atmosférica. Se usaron CH_4 e H_2 como gases precursores. Las principales técnicas de caracterización empleadas para la caracterización del grafeno obtenido fueron la Microscopía Óptica y la espectroscopía Raman. La calidad del grafeno se cuantificó usando la aplicación Excel-VBA diseñada específicamente para tal fin. Dicha aplicación asigna un valor de calidad entre 1 y 1000 y permite conocer el porcentaje de cada tipo de grafeno depositado sobre la lámina de níquel (multicapa, pocas capas, bicapa o monocapa).

Se estudió en detalle la influencia de la temperatura de reacción, la relación entre los caudales de CH_4/H_2 y el caudal total de gases (CH_4+H_2) durante la etapa de reacción para diferentes tiempos de reacción. Las imágenes de Microscopía Óptica mostraron que las muestras no eran homogéneas, estando las láminas metálicas recubiertas por grafeno multicapa, pocas capas, bicapa y monocapa. Las variables de síntesis se optimizaron de acuerdo con el valor del parámetro de calidad del grafeno sintetizado. Se obtuvo un valor de calidad máxima (810 sobre 1000) para la muestra sintetizada a 980ºC con una relación entre caudales CH_4/H_2 de 0,07 v/v y un caudal total de gases de 80 Nml/min para un tiempo reacción de 60 segundos. Para estas condiciones de reacción, aproximadamente el 80% de la lámina de níquel estaba recubierta por grafeno monocapa.

Abstract

The optimization of the graphene growth over polycrystalline nickel foils using an atmospheric pressure Chemical Vapor Deposition set up is report. CH_4 and H_2 were used as precursor gases. Optical Microscopy and Raman spectroscopy were used as for graphene characterization. The quality of the sample, related with the number of graphene layers in the synthesized graphene, was quantified using an Excel-VBA application, which assigned a quality value between 1 and 1000 and allowed to know the percentage of each type of graphene (multilayer, few-layer, bilayer and monolayer), deposited over the Ni foil.

The influence of the reaction temperature, CH_4/H_2 flow rate ratio and the total flow of gases (CH_4+H_2) during the reaction step for different reaction times was studied in detail. Optical Microscopy showed that samples were not homogeneous, being covered with multilayer, few-layer, bilayer and monolayer graphene. Synthesis variables were optimized according to the quality value. It was observed a maximum quality value (810) for a temperature, a CH_4/H_2 flow rate ratio and a total flow of gases of 980ºC, 0.07 v/v and 80 Nml/min for 60 second of reaction time, respectively. At these conditions, about 80% of the nickel foil was covered with monolayer graphene.

5.1. Introduction

In previous chapters, the synthesis of CVD-graphene using copper as catalyst has been reported. Other remarkable metal used to synthesized graphene is nickel. As was explained, in CVD method, a metal substrate is put into a furnace and heated to high temperatures. The heat anneals the metal, increasing its domain size [1]. Methane and hydrogen gases are flowed through the furnace. Hydrogen catalyzes the reaction between methane and the metal substrate, resulting carbon atoms, which are deposited onto the metal surface. After the reaction, the furnace is cooled to avoid the aggregation of the deposited carbon atoms, which crystallizes into a continuous graphene layer on the metal surface [2].

As was commented, nickel and copper are commonly used in the CVD method as the metal substrate material for graphene synthesis [3]. Due to the high solubility of carbon in nickel, the precipitation of extra-carbon occurs at the metal surfaces during cooling [4]. Since the segregation is a non-equilibrium process, this makes thickness control of graphene a challenge [4]. When nickel is used as the catalyst, graphene growth occurs after methane gas decomposition, causing the diffusion of carbon atoms through the metal surface forming a solid solution. After that, carbon atoms segregate from inside of the metal to the metal surface and then precipitate, forming graphene layers. It has been reported that carbon segregation on nickel is non-uniform at low-temperature [4]. However, the high decomposition temperature of methane, favored a constant carbon coverage over the nickel surface [4]. Furthermore, high melting point of nickel enables high-temperature annealing, which results in larger domains, thus making it favorable for large-area low-defects growth [5]. Monocrystalline nickel favors crystal formation on its surface obtaining more uniform monolayer and bilayer graphene with smooth surface and with practically no defects. Simultaneously, it prevents the formation of multiple layers on the grain boundaries. Conversely, polycrystalline Ni has a rougher surface,

where the presence of grain boundaries facilitates the formation of multilayer graphene. However, monocrystalline metals are more expensive than polycrystalline ones. From a large-scale production point of view, the use of polycrystalline Ni is more profitable, being the researches focused on improving the conditions of the main variables that influence over the reproducible synthesis of high quality graphene at large scale [6]. Several studies have demonstrated a close correlation between the CVD growth parameters, the number of graphene layers and the quality of the synthesized graphene, which enables the formation of monolayer, bilayer, few-layers and multilayer graphene on Ni substrates. Lavin-Lopez et al. (2014) found that the growth temperature significantly influenced over the graphene quality [7]. The thermodynamically driven precipitation can be kinetically controlled to some extent. For example, low temperature and low hydrocarbon exposures have been employed successfully to control carbon diffusion to the surface and thus, leading to the monolayer, bilayer, few-layer or multilayer graphene formation [8]. The high carbon solubility in nickel implies that the conditions for monolayer growth require low precursor pressures and temperatures [8].

The aim of this work was to optimize the graphene growth over polycrystalline nickel foils using a homemade atmospheric pressure Chemical Vapor Deposition setup. CH_4 was used as the precursor gas whereas H_2 and N_2 were used as carrier gases. Thus, different growth operation conditions, presumably affecting the CVD-grown graphene characteristics, e.g. reaction temperature, CH_4/H_2 flow rate ratio in the feed and reaction time, were studied in detail.

The resulting materials were characterized by Raman spectroscopy in order to evaluate both the number of graphene layers and the defects present in them [9]. Furthermore, a homemade Excel-VBA application allowed to analyze the quality of the graphene samples and thus

evaluate the percentage of each type of graphene covering the polycrystalline nickel sheet [7].

5.2. Experimental

5.2.1. Materials

25 μm thick polycrystalline nickel sheets with a high purity grade (99.99%) were purchased from GOODFELLOW. Hydrogen and nitrogen with high purity grade (99.999%) and methane (99.5 %,) were supplied by Praxair.

5.2.2. Methods

Graphene samples were grown at atmospheric pressure on 25 μm thick polycrystalline nickel foils in a 40-inch quartz tube heated by a furnace (Figure 5.1.) using the CVD method [10].

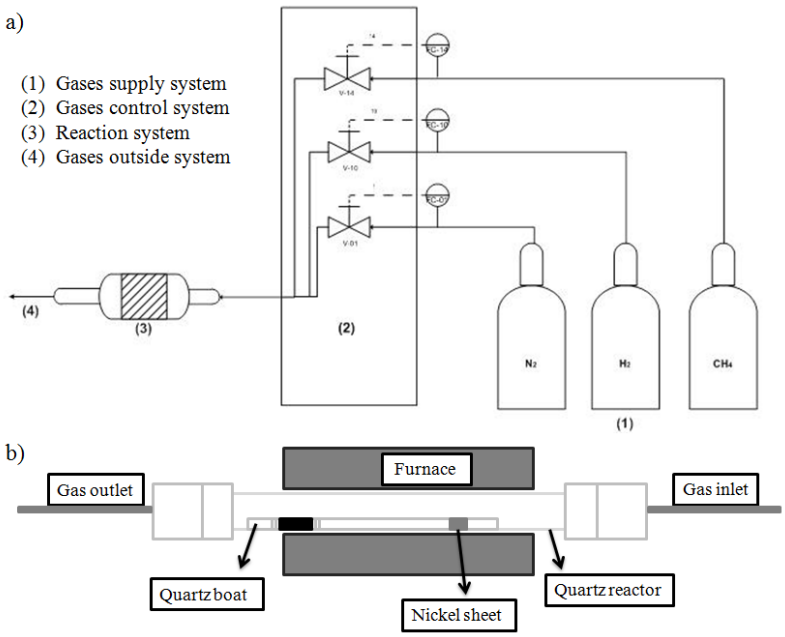

Figure 5.1. Set-up used for the CVD synthesis of graphene on polycrystalline nickel.

The furnace was heated to 900˚C by passing through it a flow of N_2 (400 sccm) and H_2 (100 sccm) to prevent nickel oxidation. The furnace was maintained at 900˚C for 45 minutes to allow the annealing of the polycrystalline nickel foil. Then, its temperature set point was set at a value ranging from 900 and 1050˚C, depending on the selected reaction temperature. Next, 30 sccm of a mixture of methane and hydrogen (CH_4/H_2 flow rate ratio in the range 0.4-0.07 v/v) was introduced during a time ranging from 30 second to 900 seconds. Finally, the system was cooled (10˚C min^{-1}) by flowing 400 sccm of nitrogen. The synthesis process is summarized in Figure 5.2. Repetitiveness studies were performed demonstrating that as-synthesized samples characteristics were reproducible.

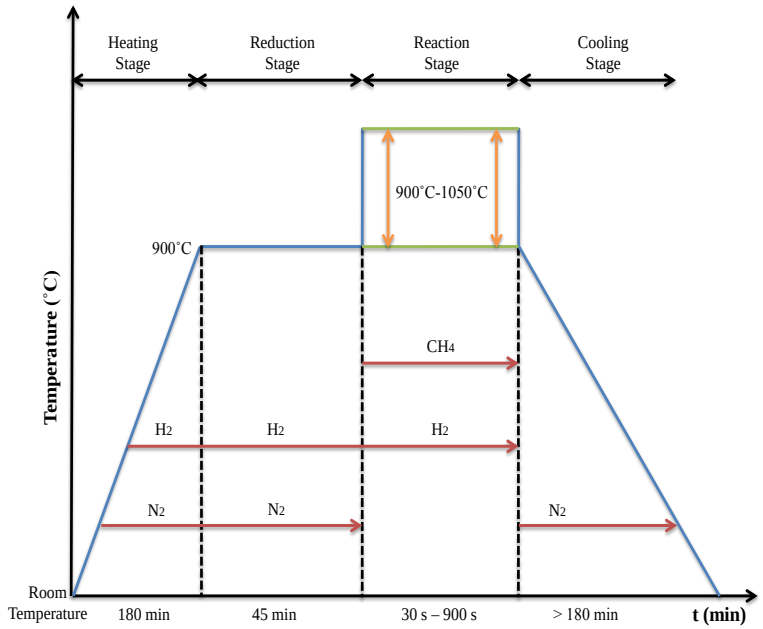

Figure 5.2. Summary of the stages times, temperatures and gases used during graphene synthesis.

5.2.3. Characterization methods

Raman spectroscopy

A SENTERRA Raman spectrometer with 600 lines per mm grating and 532 nm laser wavelength at a very low laser power level (<1mW) to avoid any heating effect was used to characterize the different graphene samples. Raman spectroscopy is considered as a reliable and quick method to characterize graphene [11-14]. D peak, visible at ~ 1350 cm^{-1}, is related to the presence of defects (edges, dislocations, cracks or vacancies) in graphitic materials [14]. Two more peaks named G and 2D bands are visible at around 1580-1620 cm^{-1} and ~2700 cm^{-1}, respectively. G peak denotes the symmetry-allowed graphite band and, is a way of checking the vibration on the same plane of sp^2 hybridized carbon atoms, which compose graphene sheets [14]. 2D peak, originated from second order double resonant Raman scattering from zone boundary, is the hallmarks of different numbers of graphene layers [15, 16].

The amount of defects present in graphene samples can be quantified by measuring the intensity ratio of D and G bands (I_D/I_G). On the other hand, the number of graphene layers is directly related to the ratio of G and 2D bands (I_{2D}/I_G). These parameters are characteristics of CVD-grown of graphene [17]. Other remarkable parameters in the characterization of graphene are the following ones: **FWHM** (Full Width at Half Maximum) and **2D and G peak position** (Raman Shift, cm^{-1}). FWHM is related to the life-time of the excited states (life-time for the Raman scattering process), which is the time delay between the absorption of the incident photon and the emission of the outgoing one [18], which is calculated as the Raman Shift difference to the half average height of 2D band. On the other hand, G peak position in graphene Raman spectrum is located around 1560 cm^{-1}. A variation in the position of this peak may be attributed to electronic doping between the graphene and the substrate [9]. Finally 2D peak position in graphene Raman spectrum (around 2700 cm^{-1}) should be displaced to lower

Raman shift values if compared to that in graphite Raman spectrum (ranging from 2710 to 2720 cm^{-1}) [11].

It is important to note that 2D Raman band shape and position are good fingerprints that indicate the presence of monolayer, bilayer, few-layer and multilayer graphene samples. Thus, the 2D mode in bulk graphite, few-layer and multilayer graphene has been reported to be decomposed in two components [19]. Monolayer graphene has a single component. Nevertheless, the 2D Raman band in bilayer graphene is fitted to four components. Finally, although the Raman spectrum of graphene grown on metals shows fluorescence [20], this one has been treated using the SENTERRA Raman spectrometer software, thus allowing to clearly identify the different peaks appearing in the Raman spectrum.

Optical Microscopy

A SENTERRA X50 microscope equipped with the software OPUS was used to analyze the graphene samples. About 50 Optical Microscope images (132.4 μm*98.53 μm) were analyzed (although only six of them were considered as representative to be showed). In each image, four different colours were detected. It was checked that, dark orange colour would correspond with multilayer graphene, light orange colour was associated to few-layers graphene, yellow colour would correspond to bilayer graphene whereas white areas were associated to monolayer graphene.

5.2.4. Determination of the graphene quality value

A homemade Excel-VBA software application was designed with the aim of control the graphene quality. This software allow to evaluate the percentage of the different types of graphene existing over a polycrystalline nickel foil by checking the different colours present in a digitalized Optical Microscope image. It was clearly demonstrated that, the different colours appearing in the Optical Microscope images were

related to different types of graphene by using Raman spectroscopy (Figure 5.3.).

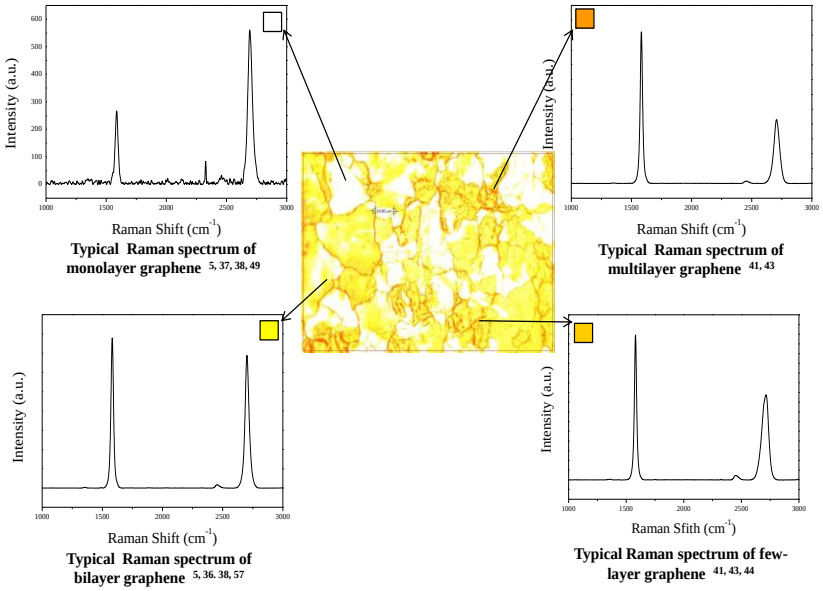

Figure 5.3. Relation between the different colours present in an Optical Microscopy image and the type of graphene present in the sample by Raman spectroscopy.

The Excel-VBA software application allowed to evaluate the percentage of each type of graphene (multilayer, few-layer, bilayer and monolayer graphene) attending to its corresponding colour in the optical micrographs. For this purpose, a logarithmic scale (similar to that used for representing the pH in liquids) was considered. Thus, values 1, 10, 100 and 1000 were assigned to multilayer, few-layer, bilayer and monolayer graphene, respectively. The quality value of the sheet was calculated as an average of the percentage obtained for each type of graphene [7].

5.3. Results and discussion

5.3.1. Influence of the reaction temperature

In order to analyze the influence of the reaction temperature over the main characteristics of the synthesized graphene, different experiments were carried out by varying it between 900 and 1050 ºC. As it is well known, methane is a hydrocarbon with strong C-H bonds [21, 22]. Thus, the reaction temperature is considered a critical factor to be controlled during graphene synthesis then, high energy is needed to achieve methane dissociation. This dissociation is easier in Ni grain boundaries than in single crystal nickel surface since, in the former, higher chemical activation energy is required [23].

Figure 5.4. shows a diagram that represents the mechanism of graphene formation onto polycrystalline nickel, which involves two different steps. The first one is related to the absorption of C atoms into the bulk nickel or the incorporation of C atoms into the Ni substrate. The second one consists of the out-diffusion and/or adsorption of C atoms to the Ni surface[24]. As observed in Figure 4, the smooth parts of the polycrystalline Ni favors the growth of monolayer or bilayer graphene, while the rough surface with large amount of grain boundaries promotes the growth of multilayer graphene onto the nickel surface[6].

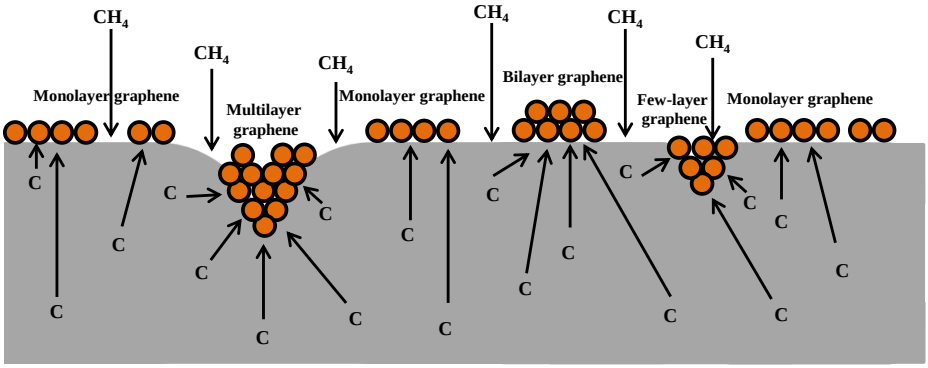

Figure 5.4. Mechanism graphene growth on polycrystalline nickel.

Figure 5.5. shows representative Optical Microscopy images of each sample obtained at different reaction temperatures. As observed, the orange color was more intense at both low (900-950 ºC) and high temperatures (1025-1050 ºC), indicating that multilayer graphene was mostly covering the sample. At intermediate temperatures, the color intensity decreased appearing lighter orange zones (few-layers graphene), yellow areas (bilayer graphene) and white areas (monolayer graphene), which was indicative of the deposition of thinner graphene.

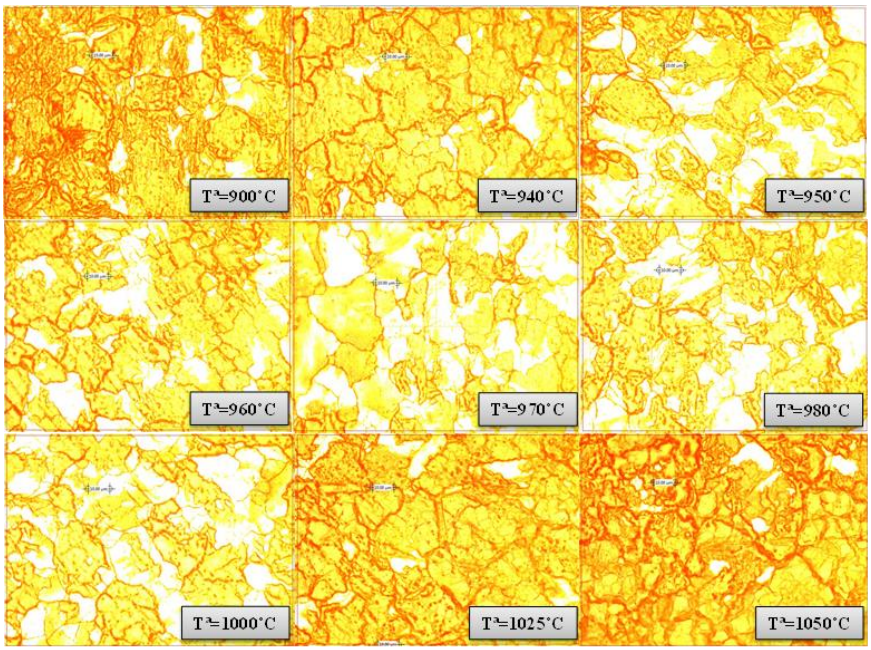

Figure 5.5. Influence of the reaction temperature. Optical Microscopy images. *(Synthesis conditions: 900-1050ºC, 600 s reaction time, CH_4/H_2 = 0.30 v/v, 130 Nml (CH_4+H_2)/min).*

In order to obtain a representative analysis of each synthesized sample, numerous pictures corresponding to different areas of the same graphene sample were analyzed by the EXCEL-VBA application previously described. As above mentioned, darker orange zones, including grain boundaries (characteristics of polycrystalline Ni), were associated to multilayer graphene. Lighter orange areas were assigned to few-layers graphene. Yellow areas were associated to bilayer

graphene. Finally, white areas were assigned to monolayer graphene. As an example of how to operate with all the synthesized samples, Figure 5.6. shows six representative Optical Microscope pictures and Table 5.1. the obtained results derived of them (percentages of each type of graphene and quality value) for sample synthesized at 980 ºC.

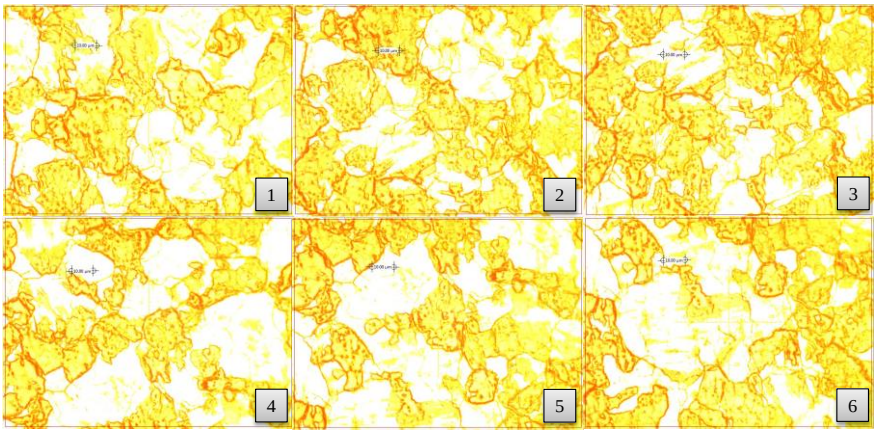

Figure 5.6. Influence of the reaction temperature. Optical Microscopy images corresponding to the sample synthesized at 980 ºC.
(Synthesis conditions: 980ºC, 600 s reaction time, CH_4/H_2 = 0.3 v/v, 130 Nml (CH_4+H_2)/min).

Table 5.1. Influence of the reaction temperature. Percentage of each type of graphene and quality values corresponding to the sample synthesized at 980 ºC.

(Synthesis conditions: 980 ºC, 600 s reaction time, CH_4/H_2 = 0.3 v/v, 130 Nml (CH_4+H_2)/min).

Picture	Multilayer graphene (%)	Few-layers graphene (%)	Bilayer graphene (%)	Monolayer graphene (%)	Quality value
1	0.57	36.56	20.05	42.82	451
2	1.10	44.33	24.44	30.12	330
3	0.68	49.57	26.88	22.86	260
4	0.75	32.43	17.04	49.78	518
5	1.06	37.10	19.33	42.51	448
6	1.02	41.23	23.06	34.69	374
Average	0.87	40.20	21.80	37.13	397

Figure 5.7. summarizes the effect of the reaction temperature on the quality value of the graphene deposited on Ni foils as well as the standard errors of each measurement. A maximum quality value (397) was observed at 980 ºC, which was taken as a reference (optimum sample) in the following studies. As observed, Ni foil was covered with few-layer, bilayer and monolayer graphene obtaining a quality value of 397.

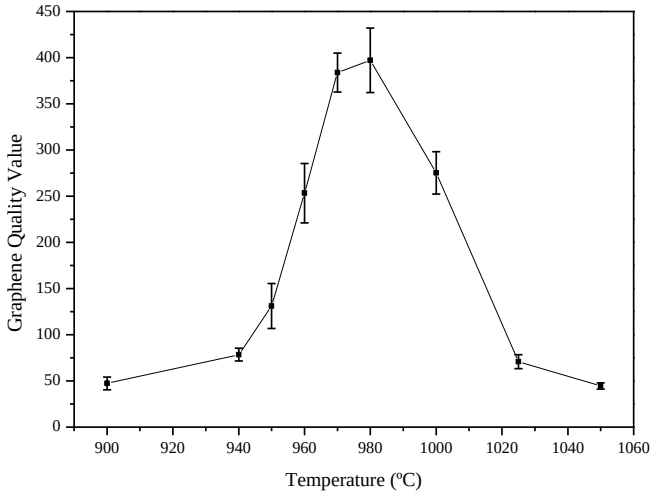

Figure 5.7. Influence of the reaction temperature. Graphene quality value vs temperature. Standard errors values have been also included.
(Synthesis conditions: 900-1050ºC, 600 s reaction time, CH_4/H_2 = 0.3 v/v, 130 Nml (CH_4+H_2)/min).

Table 5.2. shows the main characteristic Raman parameters and the percentage of each type of graphene corresponding to graphene samples synthesized at three different reaction temperatures (900ºC, 980ºC (optimum Tª) and 1050ºC). These Raman parameters have been reported in the literature for each type of graphene [10, 16, 25-30].
As observed, I_D/I_G ratio values were very low, indicating the absence of defects in the sample. On the other hand, I_{2D}/I_G ratio values were increased from the multilayer graphene to the monolayer one [31].

The contrary effect was observed when the parameter FWHM was analyzed. On the other hand, G and 2D peak positions were maintained constant in values around 1581 cm^{-1} and 2700 cm^{-1}, respectively [31], [9]. Furthermore, it can be observed that the best percentage of monolayer graphene was obtained at 980ºC, decreasing this percentage considerably at higher and lower temperatures. In the cases that the percentage of monolayer graphene was low, the one of few-layer and multilayer graphene increased, maintaining the percentage of bilayer graphene practically constant for all the temperatures.

Table 5.2. Influence of the reaction temperature. Raman spectroscopy parameters and percentage of each type of graphene.
(Synthesis conditions: 900-1050 ºC, 600 s reaction time, CH_4/H_2 = 0.3 v/v, 130 Nml (CH_4+H_2)/min).

INFLUENCE OF THE REACTION TEMPERATURE (time = 600 s; CH_4/H_2=0.3 v/v; Q_T=130 Nml/min)							
T^a (ºC)	Type of graphene	%	I_D/I_G	I_{2D}/I_G	FWHM	2D Raman Shift (cm^{-1})	G Raman Shift (cm^{-1})
900	Monolayer	1.5	0.061	2.520	53	2703	1580
	Bilayer	25.8	0.013	0.976	69	2699	1580
	Few-layer	62.9	0.013	0.599	74	2707	1580
	Multilayer	9.8	0.016	0.533	79	2703	1580
980	Monolayer	37.1	0.184	2.542	37	2705	1584
	Bilayer	21.8	0.006	1.007	42	2704	1584
	Few-layer	40.2	0.001	0.346	74	2713	1584
	Multilayer	0.9	0.027	0.329	79	2708	1584
1050	Monolayer	1.5	0.007	2.230	58	3699	1580
	Bilayer	23.5	0.014	0.952	58	2707	1580
	Few-layer	57.7	0.160	0.610	69	2703	1580
	Multilayer	17.3	0.015	0.410	74	2708	1580

5.3.2. Influence of the CH_4/H_2 flow rate ratio

In order to analyze the influence of the CH_4/H_2 flow rate ratio over the main characteristics of the synthesized graphene, different experiments were carried out by varying it between 0.4 and 0.07 v/v.

As mentioned, the amount of carbon precursor (CH_4) during the reaction, greatly determines the quality of the synthesized graphene [22]. Ni acts as active catalyst dissolving a large quantity of carbon atoms. Thus, CH_4/H_2 flow rate ratio can successfully be used to control the carbon diffusion to the Ni surface, thus favoring monolayer or bilayer graphene formation [22, 32].

Figure 5.8. shows representative Optical Microscopy images of each sample obtained at different CH_4/H_2 flow rate ratios. As observed, orange color was more intense at higher CH_4/H_2 flow rate ratio values indicating that, samples were mainly covered by multilayer graphene. As the CH_4/H_2 flow rate ratios decrease, the color intensity decreased, appearing lighter orange zones (few-layer graphene), yellow areas (bilayer graphene) and white zones (monolayer graphene), highlighting the deposition of thinner graphene over the Ni foil.

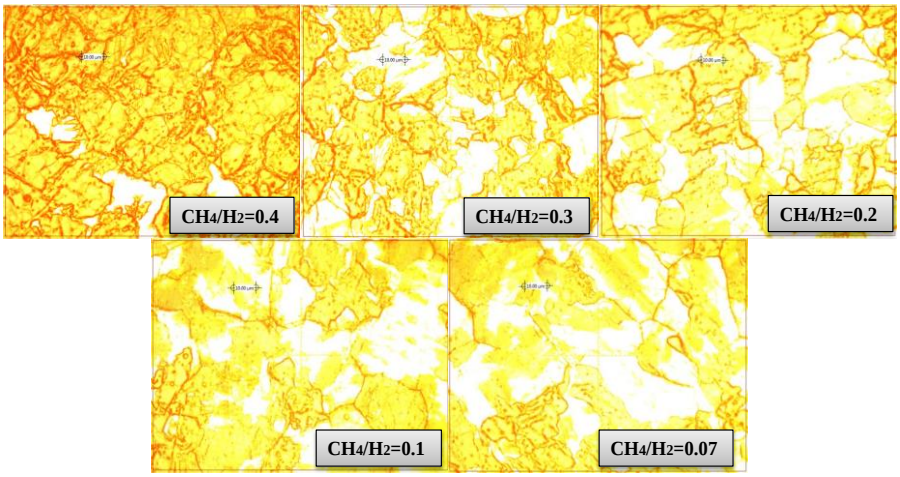

Figure 5.8. Influence of the CH_4/H_2 flow rate ratio. Optical Microscopy images. *(Synthesis conditions: 980ºC, 600 s reaction time, CH_4/H_2 = 0.07-0.4 v/v, 130 Nml (CH_4+H_2)/min).*

Figure 5.9. summarizes the effect of the CH_4/H_2 flow rate ratio on the quality value of the graphene deposited over Ni foils as well as the standard errors of each measurement. A maximum quality value (536) was obtained for graphene synthesized using 0.07 v/v CH_4/H_2 flow rate ratio which was taken as a reference in the following studies.

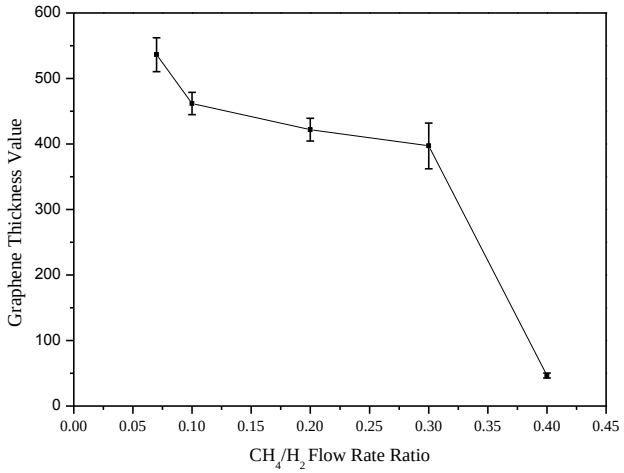

Figure 5.9. Influence of the CH_4/H_2 flow rate ratio. Graphene quality value vs CH_4/H_2 flow rate ratio. Standard errors values have been also included. *(Synthesis conditions: 980ºC, 600 s reaction time, CH_4/H_2 = 0.07-0.4 v/v, 130 Nml (CH_4+H_2)/min).*

Figure 5.10. shows six representative Optical Microscopy pictures and Table 5.3. the obtained results derived of them (percentages of each type of graphene) for sample synthesized using a CH_4/H_2 flow rate ratio value of 0.07 v/v. As observed, as the CH_4/H_2 flow rate ratio decrease, the percentage of few-layer graphene decreased and, the one corresponding to monolayer graphene increased. By its part, the percentage of bilayer graphene was kept practically constant. Consequently, the quality value increased from 397 (sample synthesized by using a CH_4/H_2 flow rate ratio value of 0.3 v/v) to 536 (sample synthesized by using a CH_4/H_2 flow rate ratio value of 0.07 v/v).

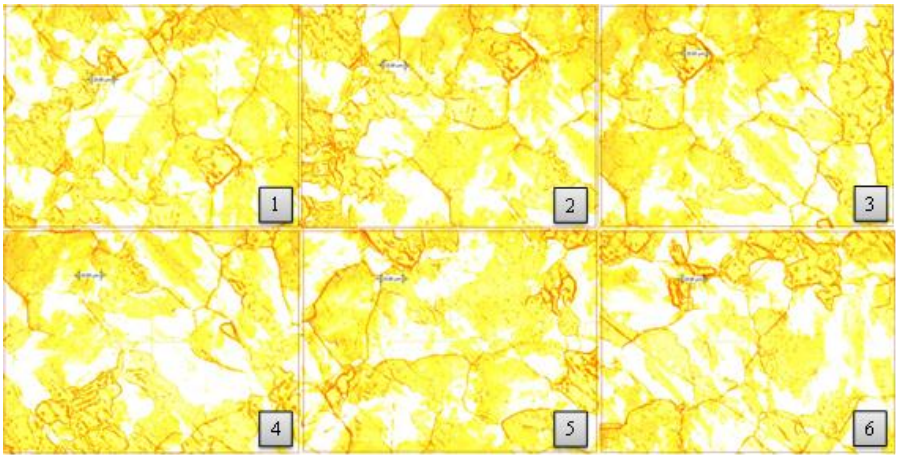

Figure 5.10. Influence of the CH_4/H_2 flow rate ratio. Optical Microscopy images corresponding to the sample synthesized using a CH_4/H_2 flow rate ratio value of 0.07 v/v.

(Synthesis conditions: 980ºC, 600 s reaction time, CH_4/H_2 = 0.07 v/v, 130 Nml (CH_4+H_2)/min).

Table 5.3. Influence of the CH_4/H_2 flow rate ratio. Percentage of each type of graphene and quality values corresponding to the sample synthesized using a CH_4/H_2 flow rate ratio value of 0.07 v/v.
(Synthesis conditions: 980ºC, 600 s reaction time, CH_4/H_2 = 0.07 v/v, 130 Nml (CH_4+H_2)/min).

Picture	Multilayer graphene (%)	Few-layers graphene (%)	Bilayer graphene (%)	Monolayer graphene (%)	Quality Value
1	0.25	23.65	21.50	54.60	569
2	0.52	29.32	22.10	48.05	505
3	0.45	33.46	25.09	41.00	438
4	0.17	21.37	17.80	60.66	606
5	0.83	32.07	20.56	46.54	489
6	0.52	23.03	15.32	61.13	608
Average	0.46	27.15	20.40	52.00	536

Table 5.4. shows the main characteristic Raman parameters and the percentage of each type of graphene corresponding to graphene samples synthesized at three different values of the CH_4/H_2 flow rate ratios (0.4 v/v, 0.2 v/v and 0.07 v/v).

As observed, I_D/I_G ratio values were, in all cases, very low indicating the absence of defects in the sample. On the other hand, I_{2D}/I_G ratio values increased and FWHM values decreased from the multilayer graphene to the monolayer one [31]. Finally, G and 2D peaks were located around 1581 cm^{-1} and 2700 cm^{-1}, respectively [31], [9]. Additionally, it can be observed that the highest percentage of monolayer graphene was obtained by using a CH_4/H_2 flow rate ratio of 0.07 v/v.

Table 5.4. Influence of the CH_4/H_2 flow rate ratio. Raman spectroscopy parameters and percentage of each type of graphene.
(Synthesis conditions: 980ºC, 600 s reaction time, CH_4/H_2 = 0.07-0.4 v/v, 130 Nml) (CH_4+H_2)/min).

INFLUENCE OF THE CH_4/H_2 FLOW RATE RATIO (T^a=980ºC; time = 600 s; Q_T=130 Nml/min)							
CH_4/H_2 (v/v)	Type of graphene	%	I_D/I_G	I_{2D}/I_G	FWHM (cm^{-1})	2D Raman Shift (cm^{-1})	G Raman Shift (cm^{-1})
0.4	Monolayer	1.5	0.058	1.960	53	2707	1584
	Bilayer	25.1	0.045	0.941	58	2695	1584
	Few-layer	61.3	0.004	0.415	74	2713	1584
	Multilayer	12.1	0.004	0.405	79	2708	1584
0.2	Monolayer	34.7	0.034	2.021	42	2695	1581
	Bilayer	20.8	0.043	1.296	47	2707	1581
	Few-layer	38.3	0.010	0.473	63	2713	1581
	Multilayer	6.2	0.001	0.415	63	2713	1581
0.07	Monolayer	51.9	0.142	2.159	40	2707	1581
	Bilayer	20.4	0.027	1.136	53	2700	1581
	Few-layer	27.1	0.006	0.435	69	2709	1581
	Multilayer	0.6	0.062	0.429	74	2704	1581

5.3.3. Influence of the total flow of gases (CH_4+H_2) during the reaction step at different reaction times

In order to analyze the influence that the total gas flow (CH_4+H_2) during the reaction step at different reaction times (15 min–30 s) has on the main characteristics of the synthesized graphene, different experiments were carried out by varying the flow between 130 Nml/min and 80 Nml/min. The other operational parameters, such as reaction temperature and CH_4/H_2 flow rate ratio, were optimized in previous studies and were kept constant when assessing the influence of total gas flow during reaction step at different reaction times. The synthesis conditions were as follows: reaction temperature: 980ºC,reaction time:

15 min-30 s, CH_4/H_2 flow rate ratio: 0.07 v/v, total gas flow (CH_4+H_2): 80-130 Nml (CH_4+H_2)/min [33]. According to previous studies and the experimental result obtained, two different steps could be distinguish in the CVD-graphene growth mechanism over polycrystalline nickel. The first one was associated to the absorption of carbon atoms into the nickel substrate. The second one comprise the out diffusion and adsorption of these carbon atoms to the nickel surface [24, 33].

The images obtained by optical microscopy for a total gas flow (CH_4+H_2) of 130 Nml/min (a), 100 Nml/min (b) and 80 Nml/min (c) for different reaction times are shown in Figure 5.11. It can be seen that four different colors can be distinguished over the sample. For all the total gas (CH_4+H_2) flows applied during the reaction step, darker orange colors were mainly observed at higher reaction times. In this way, multilayer and few-layer graphene, which correspond to the darker and paler orange colors respectively, covered the samples synthesized with longer reaction times (>5min) due to the longer exposure of the nickel foil to the carbonaceous source. In contrast, optical microscopy images corresponding to nickel sheets exposed for shorter times to the carbonaceous gas were lighter in color. In this way, samples synthesized at lower reaction time (<3 min) were mostly covered with yellow and white areas, which correspond with bilayer and monolayer graphene, respectively.

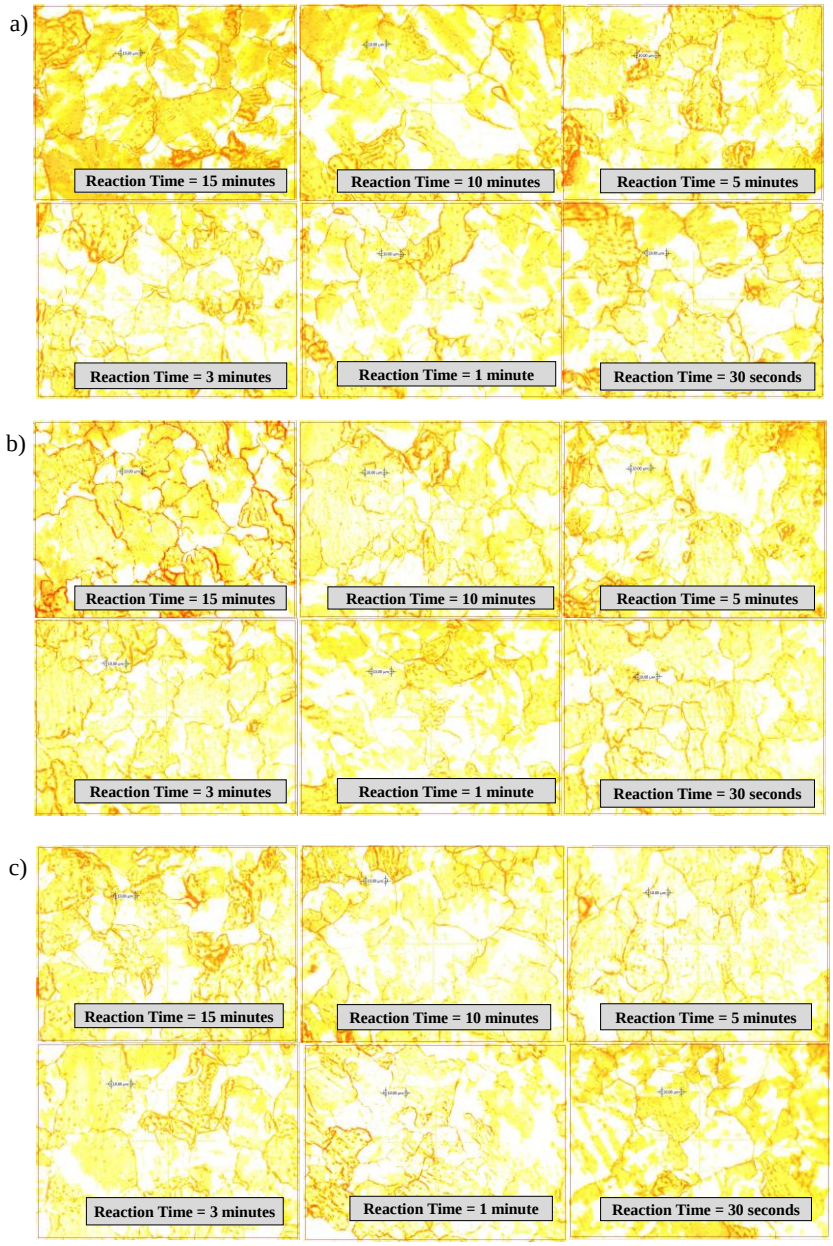

Figure 5.11. Influence of the total flow of gases (CH_4+H_2) during the reaction step at different reaction times. Optical microscopy images: total gas flow during reaction step of: (a) 130 Nml/min, (b) 100 Nml/min, (c) 80 Nml/min.
(Synthesis conditions: 980ºC, 15 min–30 s reaction time, CH_4/H_2 = 0.07 v/v, 130–80Nml (CH_4+H_2)/min).

The effect that the total gas flow (at different reaction times) had on the quality value of graphene deposited on the polycrystalline nickel foil are summarized in Figure 5.12. A maximum quality value was obtained for each total gas flow (CH_4+H_2) studied. In all cases, a reaction time of 1 minute gave the highest quality value and this was therefore considered to be the optimum reaction time. Lower quality values were obtained with higher reaction times because the longer exposure to the carbonaceous source led to the formation of higher numbers of graphene layers and, consequently, to a lower quality value [33]. On employing a reaction time of 30 seconds, the quality value decreased because there was insufficient time to allow homogeneous graphene growth over the entire sample. This led to the presence of zones without graphene on the polycrystalline metal.

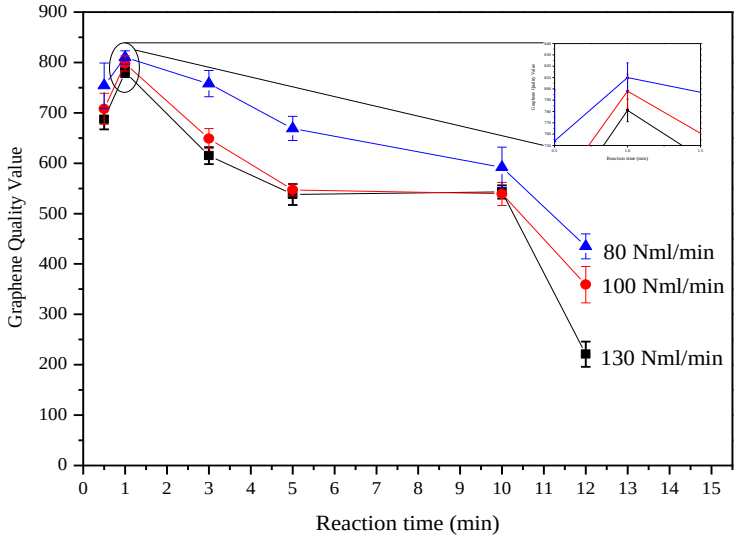

Figure 5.12. Influence of the total flow of gases (CH_4+H_2) during the reaction step at different reaction times. Graphene quality value vs. time.
(Synthesis conditions: 980ºC, 15 min–30 s reaction time, CH_4/H_2 = 0.07 v/v, 80–130 Nml (CH_4+H_2)/min).

Furthermore, an increase in the quality value on decreasing the total gas flow (CH_4+H_2) applied during the reaction step can be observed. In this

way, the lowest quality value (781) was obtained for a total gas flow of 130 Nml/min. This quality value increased to 798 on using a total gas flow of 100 Nml/min. Finally, the highest quality value was 810 and this corresponds to a total gas flow of 80 Nml/min. Therefore, a low total gas flow (CH_4+H_2), i.e., 80 Nml/min, was considered to be optimum.

Six representative optical microscopy images for the optimum total gas flow (CH_4+H_2) applied during reaction step (80 Nml/min) for the optimum total time (1 minute) are shown in Figure 5.13. The results obtained for these samples are given in Table 5.5. Most of the samples (around 80%) were covered with monolayer graphene, which corresponds to white areas in the photomicrographs. Multilayer graphene on the polycrystalline nickel foil was present at less than 1%. The rest of the sample was covered with few-layer and bilayer graphene, with the percentage of these graphene varying in the range from 18 to 5%.

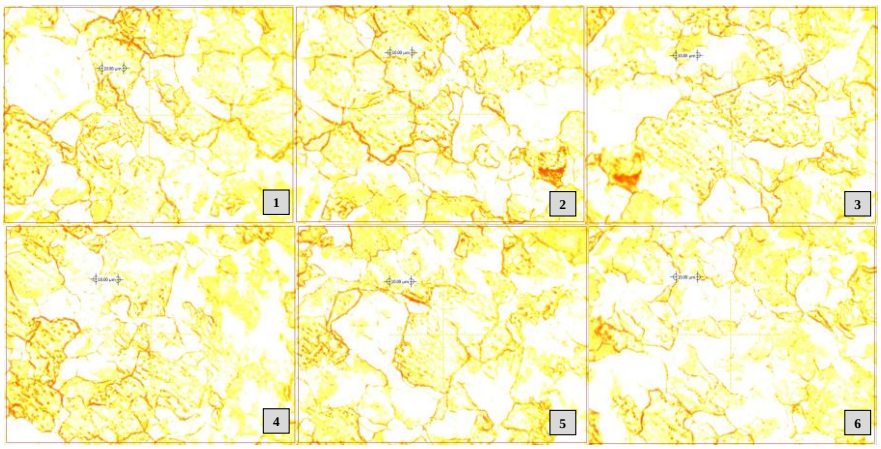

Figure 5.13. Influence of the total flow of gases (CH_4+H_2) during the reaction step at different reaction times. Optical microscopy images corresponding to the optimized graphene sample.
(Synthesis conditions: 980ºC, 1 min reaction time, CH_4/H_2 = 0.07 v/v, 80 Nml (CH_4+H_2)/min).

Table 5.5. Influence of the total flow of gases (CH_4+H_2) during the reaction step at different reaction times. Percentage of each type of graphene and quality values corresponding to the optimized graphene sample.
(Synthesis conditions: 980ºC, 1 min reaction time, CH_4/H_2 = 0.07 v/v, 80 Nml (CH_4+H_2)/min).

Picture	Multilayer graphene (%)	Few-layers graphene (%)	Bilayer graphene (%)	Monolayer graphene (%)	Quality Value
1	0.21	12.62	9.04	78.13	792
2	0.97	18.08	11.22	69.73	710
3	0.36	8.40	7.46	83.88	847
4	0.28	13.76	9.75	76.21	773
5	0.11	8.93	7.59	83.36	842
6	0.05	5.15	5.42	89.38	899
Average	0.33	11.16	8.41	80.11	810

In an effort to corroborate the optimum results obtained, Raman spectroscopy was used to characterize the graphene samples synthesized; this technique is considered to be a reliable and quick method to characterize graphene [11-14]. The main characteristic Raman parameters are listed in Table 5.6. for samples synthesized under 1 minute reaction time with different total gas flow (CH_4+H_2) applied during the reaction step.

In general, I_D/I_G ratio values were very low for all of the samples synthesized with different total gas flows, this means that the synthesized samples had low amount of defects. As one would expect, the I_{2D}/I_G ratios increased from the multilayer graphene to the monolayer graphene [31]. According to Havener et al. [34] the variation in I_{2D}/I_G values for the different types of graphene obtained for each total flow studied could be due to the coupling effect of the graphene layer. Smaller values of this relationship derivate in a stronger coupling of the graphene sheets. For the synthesized sample, the opposite effect that the one occurred for I_{2D}/I_G rate was observed for the FWHM parameter,

which decreased from the multilayer graphene to the monolayer graphene [31]. All of these parameters are characteristic of the CVD-growth of graphene [17]. Furthermore, 2D and G position are located in the typical values of CVD-graphene [11].

Table 5.6. Influence of the total flow of gases (CH_4+H_2) during the reaction step at different reaction times. Raman spectroscopy parameters and percentage of each type of graphene.
(Synthesis conditions: 980ºC, 1 min reaction time, CH_4/H_2 = 0.07 v/v, 80-130 Nml (CH_4+H_2)/min).

INFLUENCE OF THE TOTAL FLOW OF GASES (time = 60 s; CH_4/H_2=0.07 v/v; Q_T=130-80 Nml/min)							
Total gas flow (NmL/min)	Type of graphene	%	I_D/I_G	I_{2D}/I_G	FWHM (cm^{-1})	G Raman Shift (cm^{-1})	2D Raman Shift (cm^{-1})
130	Monolayer	76.9	0.015	2.5	32	1580	2703
	Bilayer	11.4	0.016	1.4	47	1580	2699
	Few-layer	11.6	0.006	0.6	63	1580	2707
	Multilayer	0.1	0.007	0.5	74	1581	2708
100	Monolayer	78.5	0.032	1.5	56	1581	2699
	Bilayer	11.4	0.002	1.0	58	1580	2703
	Few-layer	9.9	0.002	0.5	69	1581	2711
	Multilayer	0.2	0.006	0.5	79	1580	2708
80	Monolayer	80.2	0.075	3.7	42	1580	2699
	Bilayer	8.4	0.019	2.1	47	1580	2714
	Few-layer	11.1	0.005	0.5	71	1580	2713
	Multilayer	0.3	0.006	0.4	74	1580	2711

A combination of Raman spectroscopy data and Excel-VBA results verified that the best results were obtained for the sample synthesized with a reaction time of 1 minute and a total flow of 80 Nml/min; this sample was considered the optimum material. Four characteristic Raman spectra of the optimum sample are shown in Figure 5.14. along

with the corresponding 2D peak deconvolution for each type of graphene. The 2D peak deconvolutions of multilayer (a) and few-layer (b) graphene were fitted with two different peaks, which were similar to those corresponding to graphite. Bilayer graphene (c) was deconvoluted to four different contributions, whereas monolayer graphene (d) presented one single symmetrical peak [20].

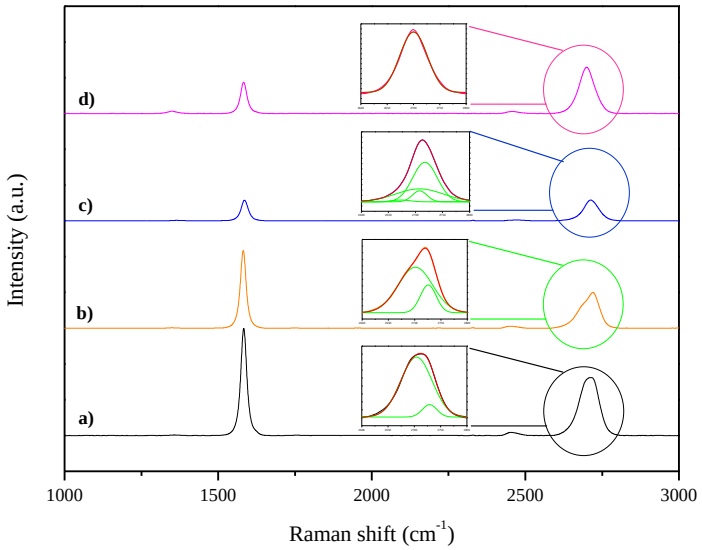

Figure 5.14. Influence of the total flow of gases (CH_4+H_2) during the reaction step at different reaction times. Raman spectra and 2D peak deconvolution corresponding to the optimized graphene sample a) multilayer graphene, b) few-layer graphene, c) bilayer graphene and d) monolayer graphene. *(Synthesis conditions: 980ºC, 1 min reaction time, CH_4/H_2 = 0.07 v/v, 80 Nml (CH_4+H_2)/min).*

5.4. Conclusions

The aim of this work was to optimize the graphene growth over polycrystalline nickel foils using a homemade atmospheric pressure Chemical Vapor Deposition setup. A cheaper alternative to synthesize high quality graphene is considered by using polycrystalline Ni foils instead of single crystal. CH_4 was used as the precursor gas whereas H_2 and N_2 were used as carrier gases. Three different growth parameters

affecting the CVD-grown graphene characteristics, e.g. reaction temperature, CH_4/H_2 flow rate ratio and reaction time, were studied in detail.

It was observed that synthesized graphene was not homogeneously grow over the entire Ni foil and four different types of graphene (e.g. monolayer, bilayer, few-layer and multilayer) were deposited, as indicated the different colors in the Optical Microscope images. It was observed a maximum of the quality value (810) for a temperature, a CH_4/H_2 flow rate ratio and a total flow of gases (CH_4+H_2) during the reaction step of 980 ºC, 0.07 v/v and 80 Nml/min at 60 seconds of reaction time, respectively. At these conditions, about 80% of the Ni foil was covered with monolayer graphene.

5.5. References

1. Bae, S., Kim, H., Lee, Y., Xu, X., Park, J. S., Zheng, Y., Balakrishnan, J., Lei, T., Ri Kim, H., Song, Y. I., Kim, Y. J., Kim, K. S., Özyilmaz, B., Ahn, J. H., Hong, B. H. and Iijima, S., *Roll-to-roll production of 30-inch graphene films for transparent electrodes.* Nature nanotechnology, 2010, **5** (8): p. 574-578.
2. Kim, K. S., Zhao, Y., Jang, H., Lee, S. Y., Kim, J. M., Ahn, J. H., Kim, P., Choi, J. Y. and Hong, B. H., *Large-scale pattern growth of graphene films for stretchable transparent electrodes.* Nature, 2009, **457** (7230): p. 706-710.
3. López, G. A. and Mittemeijer, E. J., *The solubility of C in solid Cu.* Scripta Materialia, 2004, **51** (1): p. 1-5.
4. Umair, A. and Raza, H., *Controlled synthesis of bilayer graphene on nickel.* Nanoscale Research Letters, 2012, **7**.
5. Rümmeli, M. H., Rocha, C. G., Ortmann, F., Ibrahim, I., Sevincli, H., Börrnert, F., Kunstmann, J., Bachmatiuk, A., Pötschke, M., Shiraishi, M., Meyyappan, M., Büchner, B., Roche, S. and

Cuniberti, G., *Graphene: Piecing it together.* Advanced Materials, 2011, **23** (39): p. 4471-4490.

6. Zhang, Y., Gomez, L., Ishikawa, F. N., Madaria, A., Ryu, K., Wang, C., Badmaev, A. and Zhou, C., *Comparison of graphene growth on single-crystalline and polycrystalline Ni by chemical vapor deposition.* Journal of Physical Chemistry Letters, 2010, **1** (20): p. 3101-3107.
7. Lavin-Lopez, M. P., Valverde, J. L., Cuevas, M. C., Garrido, A., Sanchez-Silva, L., Martinez, P. and Romero-Izquierdo, A., *Synthesis and characterization of graphene: Influence of synthesis variables.* Physical Chemistry Chemical Physics, 2014, **16** (7): p. 2962-2970.
8. Dahal, A. and Batzill, M., *Graphene-nickel interfaces: A review.* Nanoscale, 2014, **6** (5): p. 2548-2562.
9. Ferrari, A. C., Meyer, J. C., Scardaci, V., Casiraghi, C., Lazzeri, M., Mauri, F., Piscanec, S., Jiang, D., Novoselov, K. S., Roth, S. and Geim, A. K., *Raman spectrum of graphene and graphene layers.* Physical Review Letters, 2006, **97** (18).
10. Li, X., Cai, W., An, J., Kim, S., Nah, J., Yang, D., Piner, R., Velamakanni, A., Jung, I., Tutuc, E., Banerjee, S. K., Colombo, L. and Ruoff, R. S., *Large-area synthesis of high-quality and uniform graphene films on copper foils.* Science, 2009, **324** (5932): p. 1312-1314.
11. Calizo, I., Teweldebrhan, D., Bao, W., Miao, F., Lau, C. N. and Balandin, A. A., *Spectroscopic Raman nanometrology of graphene and graphene multilayers on arbitrary substrates.* Journal of Physics: Conference Series, 2008, **109** (1): p. 5.
12. Das, A., Chakraborty, B. and Sood, A. K., *Raman spectroscopy of graphene on different substrates and influence of defects.* Bulletin of Materials Science, 2008, **31** (3): p. 579-584.

13. Rao, C. N. R., Maitra, U. and Matte, H. S. S. R., *Synthesis, Characterization, and Selected Properties of Graphene*. 2012, Wiley-VCH. p. 1-47.
14. Wall, M., *Raman spectroscopy optimizes graphene characterization.* Advanced Materials and Processes, 2012, **170** (4): p. 35-38.
15. Suk, J. W., Kitt, A., Magnuson, C. W., Hao, Y., Ahmed, S., An, J., Swan, A. K., Goldberg, B. B. and Ruoff, R. S., *Transfer of CVD-grown monolayer graphene onto arbitrary substrates.* ACS Nano, 2011, **5** (9): p. 6916-6924.
16. Reina, A., Jia, X., Ho, J., Nezich, D., Son, H., Bulovic, V., Dresselhaus, M. S. and Jing, K., *Large area, few-layer graphene films on arbitrary substrates by chemical vapor deposition.* Nano Letters, 2009, **9** (1): p. 30-35.
17. Gong, Y., Zhang, X., Liu, G., Wu, L., Geng, X., Long, M., Cao, X., Guo, Y., Li, W., Xu, J., Sun, M., Lu, L. and Liu, L., *Layer-controlled and wafer-scale synthesis of uniform and high-quality graphene films on a polycrystalline nickel catalyst.* Advanced Functional Materials, 2012, **22** (15): p. 3153-3159.
18. Wang, Y. Y., Ni, Z. H., Yu, T., Shen, Z. X., Wang, H. M., Wu, Y. H., Chen, W. and Wee, A. T. S., *Raman studies of monolayer graphene: The substrate effect.* Journal of Physical Chemistry C, 2008, **112** (29): p. 10637-10640.
19. Ferrari, A. C., *Raman spectroscopy of graphene and graphite: Disorder, electron-phonon coupling, doping and nonadiabatic effects.* Solid State Communications, 2007, **143** (1-2): p. 47-57.
20. Costa, S. D., Righi, A., Fantini, C., Hao, Y., Magnuson, C., Colombo, L., Ruoff, R. S. and Pimenta, M. A., *Resonant Raman spectroscopy of graphene grown on copper substrates.* Solid State Communications, 2012, **152** (15): p. 1317-1320.
21. Chen, Z., Ren, W., Liu, B., Gao, L., Pei, S., Wu, Z. S., Zhao, J. and Cheng, H. M., *Bulk growth of mono- to few-layer graphene on nickel*

particles by chemical vapor deposition from methane. Carbon, 2010, **48** (12): p. 3543-3550.

22. C. Miao, C. Z., O. Liang and Y. H. Xie *Chemical Vapor Deposition of Graphene, Physics and Applications of Graphene - Experiments*, ed. Mikhailov, D. S. 2011.
23. C. Miao, C. Z., O. Liang and Y. H. Xie, *Chemical Vapor Deposition of Graphene, Physics and Applications of Graphene - Experiments* 2011.
24. Losurdo, M., Giangregorio, M. M., Capezzuto, P. and Bruno, G., *Graphene CVD growth on copper and nickel: Role of hydrogen in kinetics and structure.* Physical Chemistry Chemical Physics, 2011, **13** (46): p. 20836-20843.
25. Hwang, J. Y., Kuo, C. C., Chen, L. C. and Chen, K. H., *Correlating defect density with carrier mobility in large-scaled graphene films: Raman spectral signatures for the estimation of defect density.* Nanotechnology, 2010, **21** (46).
26. Mattevi, C., Kim, H. and Chhowalla, M., *A review of chemical vapour deposition of graphene on copper.* Journal of Materials Chemistry, 2011, **21** (10): p. 3324-3334.
27. Ruan, G., Sun, Z., Peng, Z. and Tour, J. M., *Growth of graphene from food, insects, and waste.* ACS Nano, 2011, **5** (9): p. 7601-7607.
28. Chen, S., Cai, W., Piner, R. D., Suk, J. W., Wu, Y., Ren, Y., Kang, J. and Ruoff, R. S., *Synthesis and characterization of large-area graphene and graphite films on commercial Cu-Ni alloy foils.* Nano Letters, 2011, **11** (9): p. 3519-3525.
29. Lee, S., Lee, K. and Zhong, Z., *Wafer scale homogeneous bilayer graphene films by chemical vapor deposition.* Nano Letters, 2010, **10** (11): p. 4702-4707.
30. Lee, D., Lee, K., Jeong, S., Lee, J., Choi, B. and Kim, O., *Process optimization for synthesis of high-quality graphene films by low-pressure chemical vapor deposition.* Japanese Journal of Applied Physics, 2012, **51** (6 PART 2).

31. Nemanich, R. J. and Solin, S. A., *First- and second-order Raman scattering from finite-size crystals of graphite.* Physical Review B, 1979, **20** (2): p. 392-401.
32. Weatherup, R. S., Dlubak, B. and Hofmann, S., *Kinetic control of catalytic CVD for high-quality graphene at low temperatures.* ACS Nano, 2012, **6** (11): p. 9996-10003.
33. Lavin-Lopez, M. P., Valverde, J. L., Ruiz-Enrique, M. I., Sanchez-Silva, L. and Romero, A., *Thickness control of graphene deposited over polycrystalline nickel.* New Journal of Chemistry, 2015, **39** (6): p. 4414-4423.
34. Havener, R. W., Zhuang, H., Brown, L., Hennig, R. G. and Park, J., *Angle-resolved raman imaging of interlayer rotations and interactions in twisted bilayer graphene.* Nano Letters, 2012, **12** (6): p. 3162-3167.

Chapter 6: Improving the continuous growth of monolayer CVD-graphene over polycrystalline iron sheets.

Resumen

La finalidad de este capítulo fue la de optimizar las condiciones de operación que permitieran sintetizar grafeno de alta calidad, (grafeno monocapa), usando hierro polycristalino como catalizador. El grafeno se sintetizó mediante el método de Deposición Química en fase Vapor usando metano como fuente carbonosa. Se investigó el efecto de la temperatura de reacción, la relación CH_4/H_2 y el caudal total de gases (CH_4+H_2) durante la etapa de reacción a diferentes tiempos de reacción sobre el crecimiento del grafeno. Las láminas de grafeno se caracterizaron mediante microscopía óptica y espectroscopía Raman. Además, se usó la aplicación Excel-VBA, con el fin de determinar el porcentaje de cada uno de los tipos de grafeno (monocapa, bicapa, pocas capas y multicapa) depositados sobre el metal.

La lámina de grafeno sintetizada en las condiciones óptimas de operación mostró un elevado porcentaje de grafeno monocapa (62.4%), un alto valor de la relación I_{2D}/I_G (~2.9), valores reducidos de la relación I_D/I_G (~0.026) y del parámetro FWHM (~22 cm^{-1}) y un desplazamiento de la señal Raman del pico 2D a valores más bajo de frecuencia. Las condiciones óptimas de síntesis fueron las siguientes: 1025 ºC, CH_4/H_2=0.25 v/v, caudal total de gases (CH_4+H_2) = 80 Nml/min y un tiempo de reacción=7 min).

Abstract

A high quality graphene film, mostly composed by monolayer graphene, on polycrystalline iron foil ,was successfully grown by the CVD process using methane as the carbonaceous source. The effect of the reaction temperature, the CH_4/H_2 flow rate ratio and the total flow of gases (CH_4/H_2) on the formation of graphene during the reaction step at different reaction times was investigated. Optical microscopy and Raman spectroscopy were used as characterization techniques. A homemade Excel-VBA application was designed in order to determine the percentage of the different types of graphene (monolayer, bilayer, few-layer and multilayer) deposited on the metal foil, thus a quantitative quality value was computed.

Graphene film deposited at the optimal experimental conditions showed a high percentage of monolayer graphene (62.4% in the sample), a high I_{2D}/I_G ratio (~2.9), a low I_D/I_G ratio (~0.026) and a narrow FWHM of 2D peak (~22 cm^{-1}). It was found that the optimal synthesis conditions were: 1025 ºC, CH_4/H_2=0.25 v/v, total flow (CH_4+H_2) = 80 Nml/min and reaction time=7 min).

6.1. Introduction

As it has been commented in previous chapters, CVD-graphene growth involves the thermal decomposition of a hydrocarbon source (methane, ethylene, acetylene, benzene, etc.) over a heated substrate [1]. It is important to denote that, in a CVD process, the metallic substrates not only act as the catalyst but also determine the growth mechanism. Two different graphene growth mechanism can be distinguish depending on the carbon solubility. In the case of low carbon solubility metals, such as copper, carbon atoms experiment a nucleation and expansion around the nucleus forming graphene domains through hydrocarbon decomposition, catalyzed by the high temperature substrate. Growth process finishes when the substrate is fully covered by graphene layers. This growth mechanism is normally called *self-limited* surface deposition [2, 3]. On the other hand, the growth process when high carbon solubility metals, such as nickel or iron, are used involves the diffusion of carbon atoms into the metal substrate. As the substrate is cooled down, the dissolved carbon segregates to the metal surface forming graphene sheets [2, 4, 5]. The high quality synthesis of CVD-graphene depends not only on the metallic catalyst but also on the different synthesis conditions [6]. Among all the transition metals, iron has not attracted attention in graphene synthesis in spite of its binary phase diagram is one of the most well-known and has been used as catalyst in other CVD synthesis processes, such as that of carbon nanotubes [7]. Iron is cheaper, easier to purchase and easier to etch than other transition metals, which are significant advantages for graphene synthesis. However, few researchers have considered this metal for the synthesis of this carbon material. For example, *An et col.* [8] obtained single to few-layers graphene sheets by partially covering the iron at short exposure times by using acetylene as the carbonaceous source. To

achieve continuous graphene layers, large exposure times (15-30 min) are required. *Xue et al.* [9] obtained large area, few-layer high quality graphene over Fe using methane as the carbonaceous source. Some authors [4, 10] have reported the relevance of specific variables that can affect the quality of graphene produced. Temperature can be considered as a key factor during CVD-graphene synthesis. Other parameters such as gas flow or exposure time may affect the graphene deposition over the metal substrate [6]. *Lavin-Lopez et al.* [4, 10, 11] reported that the control of the exposure to hydrocarbon sources (total flow of gases during the reaction step and the hydrocarbon flow rate ratio), the exposure time and the reaction temperature led to the formation of high quality graphene layers deposited on polycrystalline copper and nickel.

The aim of this work was to optimize the atmospheric pressure CVD-graphene synthesis over polycrystalline iron foils. Polycrystalline iron is a cheap material. Thus, the synthesis cost could be considerably reduced in comparison to that of other transition metals commonly used (Ni or Cu). Nitrogen and hydrogen were used as carrier gases and methane was chosen as the carbonaceous source. The main variables that might affect the graphene growth (reaction temperature, CH_4/H_2 flow rate ratio and total flow during the reaction step at different reaction times) were studied in detail in order to increase the percentage of monolayer graphene deposited over the iron substrate.

6.2 Experimental

6.2.1. Material

Methane (99.5%), Hydrogen (99.999%) and Nitrogen (99.999%) were purchased from Praxair. 25 μm thick polycrystalline iron foil with a purity of 99.99% were purchased from GOODFELLOW.

6.2.2. Method

Graphene samples were growth in an atmospheric pressure CVD system composed of a 40-inch quartz tube encase into a furnace (Figure 6.1.a.). Graphene were deposited over 25 μm thick polycrystalline iron sheets, which were used as catalysts. The furnace was heated to the reduction temperature (900ºC) under 400 sccm flow of N_2 and 100 sccm flow of H_2. The furnace was maintained at this temperature for 45 minutes to complete the reduction step and allow the annealing of the metal sheet. After that, the selected reaction temperature (900-1050ºC) was reached and 30 sccm of CH_4 flow was introduced into the furnace while N_2 flow was turned off during the reaction time (5-15 min). Finally, the system was cooled down by flowing 400 sccm of N_2 (Figure 6.1.b.).

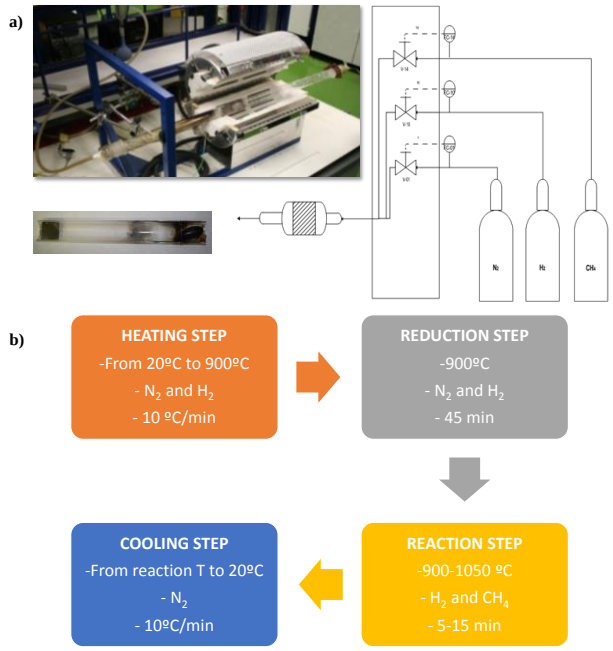

Figure 6.1. a) CVD-graphene synthesis experimental installation and b) Synthesis procedure for CVD-graphene synthesis.

6.2.3. Characterization

Raman spectroscopy

A SENTERRA Raman spectrometer, with 600 lines per mm grating and 532 nm laser wavelength at a very low laser power level (<1mW) to avoid any heating effect, was used to characterize the graphene obtained over the polycrystalline iron.

Optical Microscopy

A SENTERRA X50 microscope equipped with the OPUS software was used to analyze the graphene synthesized. Around fifty optical microscope images were analyzed per sample but only six were considered as representative ones. In each optical microscope image, four different colors could be observed, corresponding each one with one type of graphene (monolayer, bilayer, few-layer and multilayer). By using Raman Spectroscopy, it was checked that lighter colors correspond to less number of graphene layers (white areas corresponds to monolayer graphene and yellow areas to bilayer graphene) whereas darker colors correspond to more number of graphene layers (dark orange corresponds to multilayer graphene and the lighter one to few-layer graphene).

6.2.4. Excel-VBA application: determination of a quality value

A homemade Excel-VBA application was programmed to determine a graphene quality value, which is closely related with the thickness of the number of graphene layers. The smaller the graphene thickness, the lower the number of graphene covering the iron foil and, thus, the higher the quality value obtaining for the graphene sample were.

First of all, Excel-VBA application analyze the optical microscope graphene images by checking the different colors presented on it, which are related with the different types of graphene (multilayer, few-layer,

bilayer or monolayer) as corroborated by Raman spectroscopy. In addition, the application calculates the percentage of each type of graphene covering the sample attending to the corresponding colors presenting in the optical microscope images. Thus, quality values of 1, 10, 100 and 1000 were assigned to the 100% of the iron foil covered with multilayer, few-layer, bilayer and monolayer graphene, respectively. The quality value of the graphene sample was calculated as an average of the percentage obtained for each type of graphene [4, 10, 11] (Figure 6.2.).

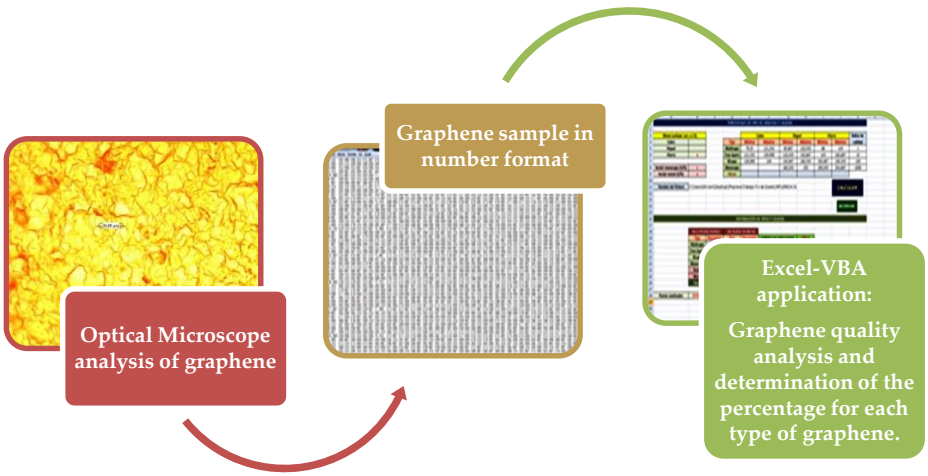

Figure 6.2. Excel-VBA application to determine the percentage of each type of graphene and the graphene quality value.

6.3. Results and discussion

6.3.1. Influence of the reaction temperature

In order to analyze the influence of the reaction temperature on the number of graphene layers in the products (through the determination of a quality value), different experiments were performed between 900 and 1050ºC. It has been demonstrated that the reaction temperature

plays an important role on the graphene characteristics [4, 10, 12]. *Xu et al.* [9] reported that a suitable temperature influenced over the graphene crystallinity and, consequently, over its thickness.

A maximum quality value of 354.2 was obtained for the sample synthesized at 1025 ºC. At this temperature, the 30.77% of the iron foil was covered with monolayer graphene and the 44.8% with bilayer graphene. Only the 7.2% of the iron sheet presented multilayer graphene over it.

Around fifty optical microscope images taken in different areas of each product obtained at each temperature were taken to obtain a representative analysis. Four different colors could be distinguished in these optical microscope images. Raman spectroscopy demonstrated that each color corresponded to one type of graphene (see Figure 6.3. where it is possible to observe the Raman spectrum of a parent iron foil and that of a random graphene sample). Thus, darker orange colors, mostly visible at the grain boundaries, correspond to multilayer graphene; lighter orange colors are assigned to few-layer graphene; yellow areas correspond to bilayer graphene and, finally, white and lighter areas are assigned to monolayer graphene [4, 10]. Optical microscope images generated by the Raman spectrometer were analyzed by using a homemade Excel-VBA application, thus, the corresponding quality value and the percentage of each type of graphene was evaluated for all the samples prepared at different temperatures.

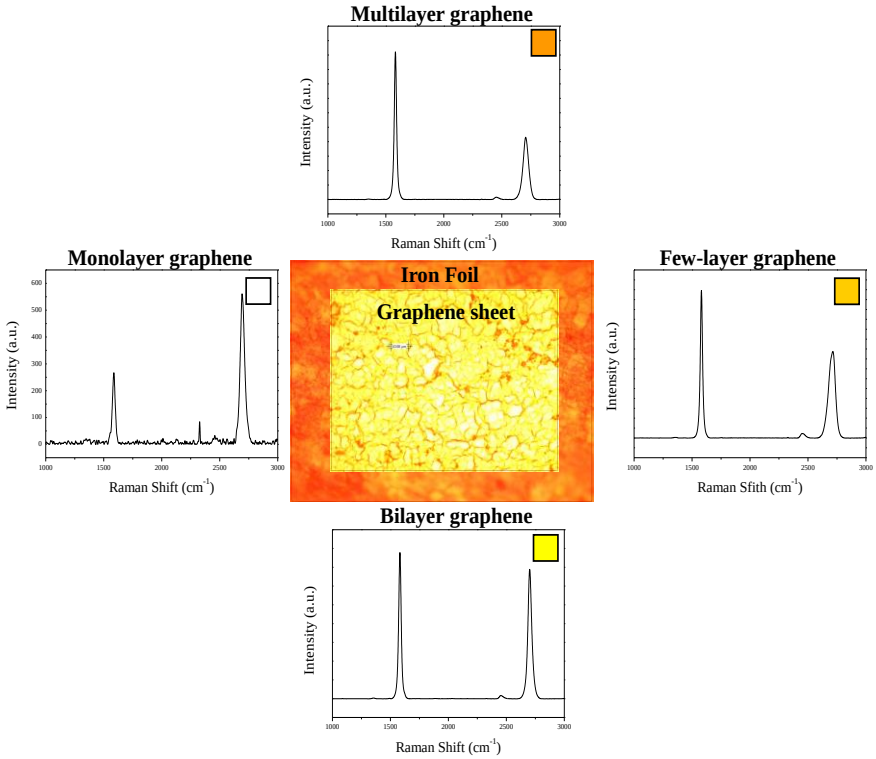

Figure 6.3. Raman spectra corresponding to the different zones observed in optical microscope images.

Figure 6.4. shows an optical microscope image for the sample obtained at the different reaction temperatures. As observed, orange colors were more intense for lower reaction temperatures (925-950ºC). Conversely, the higher the reaction temperature, the lower the intensity of the colors was. Below 925 ºC, it was not possible to observe a continuous graphene growth over the polycrystalline iron foil.

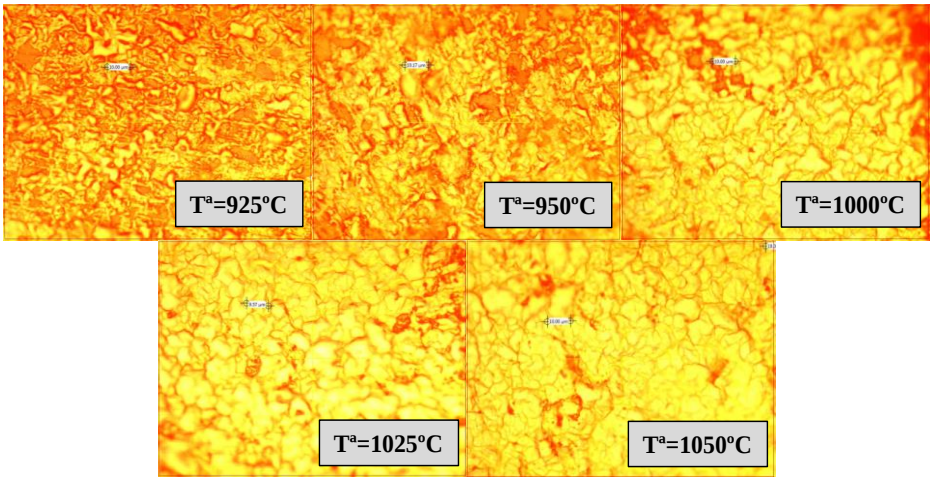

Figure 6.4. Influence of the reaction temperature. Optical microscope images at different reaction temperatures.
(Synthesis conditions: 925-1050 ºC, CH_4/H_2=0.30 v/v, 130 Nml/min, 10 minutes of reaction time)

The analysis of the images generated by the optical microscope of the Raman spectrometer by the Excel-VBA application allowed to determine the percentage of each type of graphene deposited over the iron foil at different temperatures (Table 6.1.). As observed, the percentage of monolayer and bilayer graphene increased with the reaction temperature until 1025ºC was reached.

Table 6.1. Influence of the reaction temperature. Average values of each type of graphene obtained from the representative optical microscope images.
(Synthesis conditions: 925-1050 ºC, CH_4/H_2=0.30 v/v, 130 Nml/min, 10 minutes of reaction time)

T (ºC)	Monolayer graphene (%)	Bilayer graphene (%)	Few-layer graphene (%)	Multilayer graphene (%)
925	2.6	23.2	31.3	43
950	3.8	28.2	32.9	35.1
1000	14.1	42.3	26.0	17.6
1025	31.5	44.1	17.1	7.4
1050	21.8	50.3	20	7.9

Figure 6.5. shows the variation of the quality value as a function of the reaction temperature. Polycrystalline metals have irregular surfaces with high amount of grain boundaries, which facilitate the formation of more layered graphene because impurities present in these metals, have a tendency to segregate at these positions [13]. Thus, at low reaction temperatures (925-1000ºC), most of the dissolved carbon atoms were deposited over these grain boundaries, favoring the formation of more layered graphene and, consequently, decreasing the quality value. However, at high temperatures, the dissolution of grain boundaries of the metal sheet on iron foils and the high solubility of carbon oil promote the formation of less layered graphene [14, 15], leading to an increase of the graphene quality. However, an excessively high temperature (1050ºC) could cause an excessive solubility of the carbon atoms, leading to the formation of graphite flakes and, consequently, decreasing the quality value of the samples. Hence, the growth of monolayer graphene is less favored [8]. The optimal reaction temperature was considered 1025 ºC for which a balance between the synthesis of high quality graphene, a proper carbon dissolution and a low amount of grain boundaries occurs. As it will be shown below, at this temperature the quality was maximum (354.2).

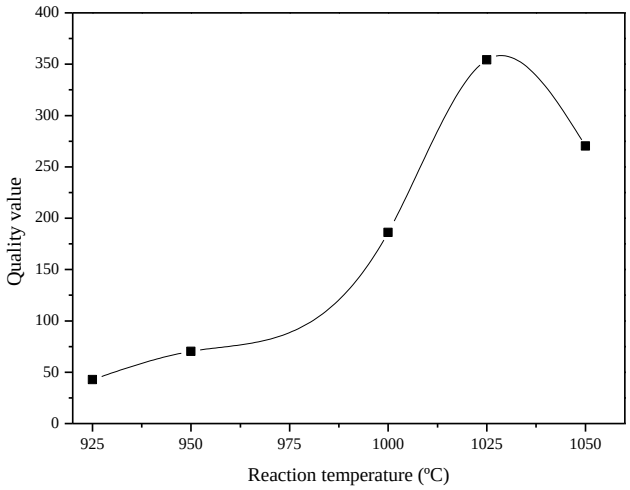

Figure 6.5. Influence of the reaction temperature. Quality value vs. reaction temperature.

Figure 6.6. shows the optical microscope images selected (among more than 50 images) for the sample synthesized at 1025ºC (optimum reaction temperature) whereas Table 6.2. lists the corresponding quality value and the percentage of each type of graphene obtained. At this temperature, 30.8 % of the sample was covered with monolayer graphene and the 44.8 % with bilayer graphene.

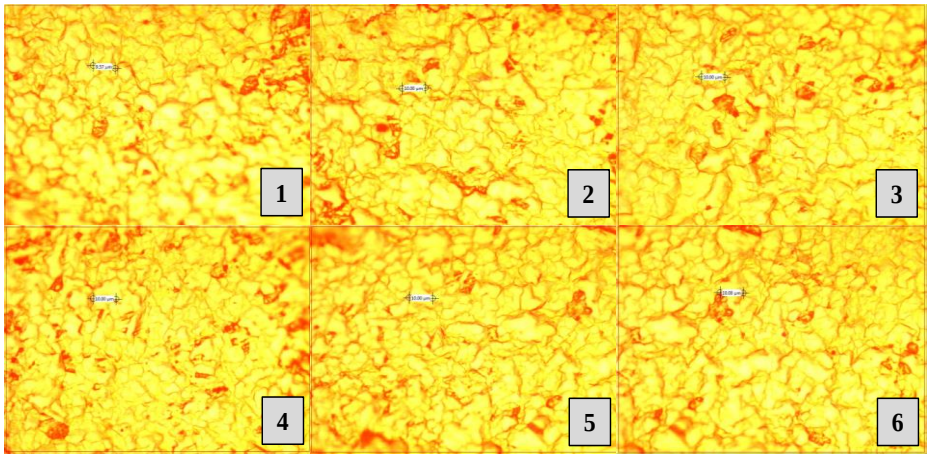

Figure 6.6. Influence of the reaction temperature. Optical microscope images taken in different areas of the sample prepared at the optimum reaction temperature.
(Synthesis conditions: 1025 ºC, CH_4/H_2=0.30 v/v, 130 Nml/min, 10 minutes of reaction time)

Table 6.2. Influence of the reaction temperature. Quality and percentage of each type of graphene deposited over the sample prepared at the optimum reaction temperature. *(Synthesis conditions: 1025 ºC, CH_4/H_2=0.30 v/v, 130 Nml/min, 10 minutes of reaction time)*

Optical microscopy images	Monolayer graphene (%)	Bilayer graphene (%)	Few-layer graphene (%)	Multilayer graphene (%)	Quality value
1	28.34	46.94	18.29	6.43	332.3
2	31.45	43.41	16.49	8.65	359.7
3	30.04	47.57	16.83	5.56	349.7
4	29.99	44.22	16.36	9.43	345.8
5	30.89	43.04	18.68	7.38	353.9
6	33.89	43.30	16.94	5.87	384.0
Average	**30.77**	**44.75**	**17.27**	**7.21**	**354.2**

6.3.2. Influence of the CH_4/H_2 flow rate ratio

The influence of the CH_4/H_2 flow rate ratio was ranged between 0.4 and 0.1 v/v, keeping constant the other synthesis parameters (1025 ºC of reaction temperature, 130 Nml/min of total flow rate ratio and 10 minutes of reaction time). Methane flow has been revealed as an important factor during graphene growth [4, 10, 11]. *Xue et col.* [9] reported that a decreasing of the methane flow from 300 to 180 sccm allowed to obtain bilayer graphene instead of multilayer one. This fact was due to the smaller amount of carbon that was dissolved and segregated into and from the catalyst, respectively.

Figure 6.7. shows a representative optical microscope image for the samples obtained at each of the CH_4/H_2 flow rate ratio studied.

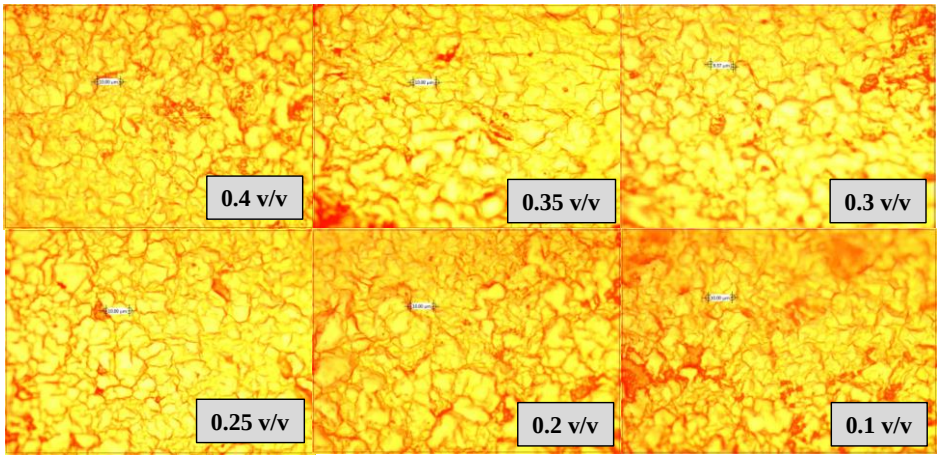

Figure 6.7. Influence of the CH_4/H_2 flow rate ratio. Optical microscope images obtained at different CH_4/H_2 flow rate ratios.
(Synthesis conditions: 1025 ºC, CH_4/H_2=0.1-0.4 v/v, 130 Nml/min, 10 minutes of reaction time)

Again, around fifty optical microscope images taken in different areas of each product obtained at each CH_4/H_2 flow rate ratio were taken to obtain a representative value of the quality and the percentage of each type of graphene deposited over the polycrystalline iron foils (Table 6.3.). Note that as CH_4/H_2 flow rate ratio decreased up to a value of 0.25 v/v, the percentage of monolayer graphene on the iron foil grew up.

Table 6.3. Influence of the CH_4/H_2 flow rate ratio. Average values of each type of graphene obtained from the representative optical microscope images.
(Synthesis conditions: 925-1050 ºC, CH_4/H_2=0.30 v/v, 130 Nml/min, 10 minutes of reaction time)

CH_4/H_2 Flow rate ratio (v/v)	Monolayer graphene (%)	Bilayer graphene (%)	Few-layer graphene (%)	Multilayer graphene (%)
0.4	11.05	46.06	29.53	13.35
0.35	23.77	45.14	20.66	10.44
0.3	29.55	45.58	17.72	7.15
0.25	30.77	44.75	17.27	7.21
0.2	8.09	46.19	31.20	14.51
0.1	5.44	40.37	34.58	19.60

Figure 6.8. shows the variation of the quality value as a function of the CH_4/H_2 flow rate ratio.

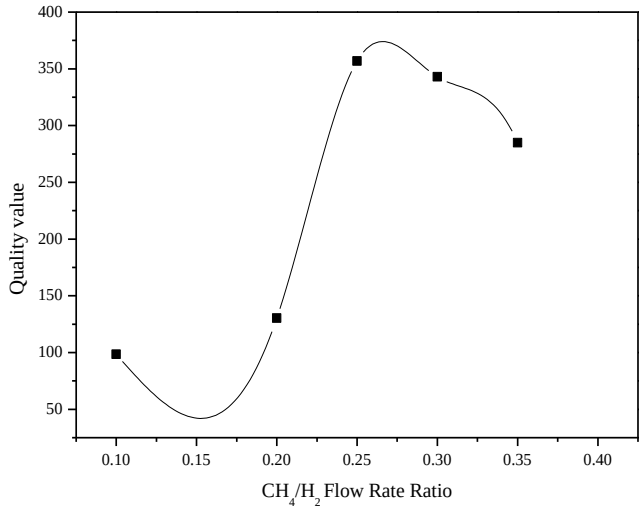

Figure 6.8. Influence of the CH_4/H_2 flow rate ratio. Quality value vs CH_4/H_2 flow rate ratio.

The higher the CH_4/H_2 flow rate ratio, the higher the amount of CH_4 flowed into the system and, thus, the more the carbon atoms dissolved that would be deposited over the metal foil. Some researchers have reported that with iron foils and low methane flow rates, the formation of few layered graphene is favored probably due to the smaller amount of carbon atoms dissolved and segregated from the metal foil [6, 9]. For the highest CH_4/H_2 flow rate ratio (0.4 v/v), an excess of carbon atoms would be deposited over the iron sheet leading to the formation of more layered graphene, thus obtaining a quality value of 159.6. This quality value increased by decreasing the CH_4/H_2 flow rate ratio until a maximum quality value (356.9) was reached for a CH_4/H_2 flow rate ratio of 0.25 v/v. The quality value drastically decreased when the CH_4/H_2 flow rate ratio was also decreased, thus leading to the production of non-homogeneous graphene.

Figure 6.9. shows the optical microscope images (among more than 50 images) corresponding to the sample synthesized using a CH_4/H_2 flow rate ratio of 0.25 v/v, which was considered as the optimum value. The corresponding percentage of each type of graphene and its quality value is listed in Table 6.4.

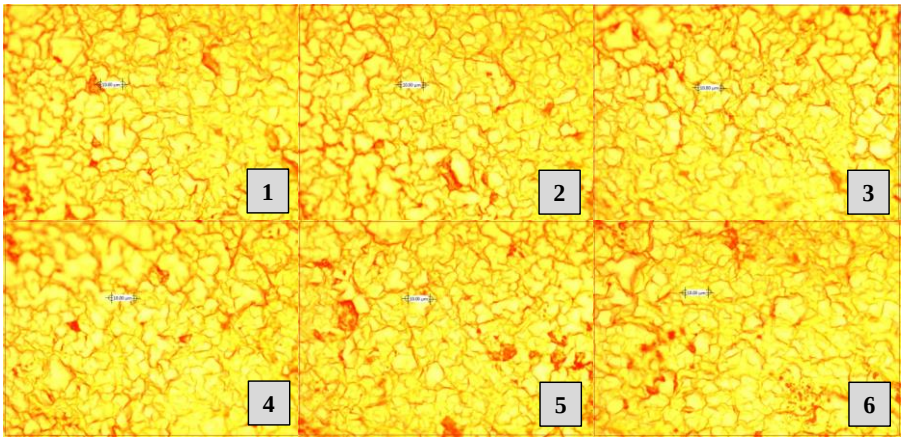

Figure 6.9. Influence of the CH_4/H_2 flow rate ratio. Optical microscope images.
(Synthesis conditions: 1025 ºC, CH_4/H_2=0.25 v/v, 130 Nml/min, 10 minutes of reaction time)

Table 6.4. Influence of the CH_4/H_2 flow rate ratio. Quality and percentage of each type of graphene deposited over the sample synthetized at the optimum CH_4/H_2 flow rate ratio.
(Synthesis conditions: 1025 ºC, CH_4/H_2=0.25 v/v, 130 Nml/min, 10 minutes of reaction time)

Optical microscopy images	Monolayer graphene (%)	Bilayer graphene (%)	Few-layer graphene (%)	Multilayer graphene (%)	Quality value
1	33.46	41.80	17.30	7.45	378.2
2	34.28	41.46	17.38	6.88	386.1
3	31.13	41.84	17.57	9.46	355.0
4	28.95	43.90	18.62	8.52	335.4
5	30.27	43.38	18.50	7.84	348.0
6	29.34	43.17	18.98	8.51	338.5
Average	**31.24**	**42.60**	**18.05**	**8.11**	**356.9**

As observed, the CH_4/H_2 flow rate ratio has an influence on the percentage of monolayer graphene deposited over the polycrystalline iron foil.

6.3.3. Influence of the total flow of gases (CH_4+H_2) during the reaction step at different reaction times

The optimization of the value of the total flow of gases during the reaction step, at different reaction times (15 min-5 min), has been performed in the range from 130 and 60 Nml/min. It has been reported that the influence of the total flow during the reaction step is closely related to that of the reaction time. Longer exposure times to the reaction gases are required for low total flow of them, because the amount of carbonaceous source flowing during the reaction step is low and, consequently, longer times are also required to obtain an homogeneous graphene layer [8, 11, 16].

Figure 6.10. shows the representative optical microscope images corresponding to each sample synthesized using different total flows (130-60 Nml/min) and exposure times (5-15 minutes). The corresponding percentages of each type of graphene deposited over the iron foil, determined by the homemade Excel-VBA application, are listed in Table 6.5.

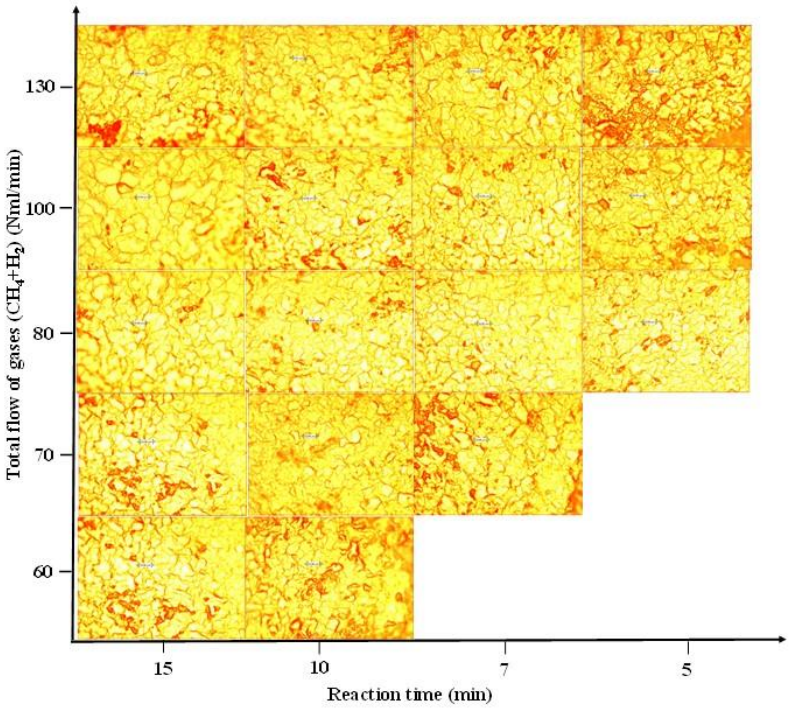

Figure 6.10. Influence of the total flow of gases (CH_4+H_2) during the reaction step at different reaction times. Optical microscope images.
(Synthesis conditions: 1025 ºC, CH_4/H_2=0.25 v/v, 130-60 Nml/min, 15-5 minutes of reaction time)

Different authors have reported that a balance between the value of reaction time and that of the total flow of gases are needed to promote the growth of monolayer graphene over metal foils since excessively high reaction times can result in the formation of more layered graphene [16, 17]. As expected, the lower the total flow of gases, the longer the reaction times are required to obtain less layered structures (corresponding to optical microscope images where light colors in a uniform way predominate). At low total flow of gases (60-70 Nml/min) and times lesser than 10 min, the graphene growth was not favored as a result of not having carbon atoms enough flowing through the reaction system to achieve a uniform deposition of graphene over the polycrystalline iron foil. Moreover, at low total flows (60 and 70

Nml/min), zones presenting free-graphene islands were observed. On the other hand, the higher the total flow (130 and 100 Nml/min) was, the darker the colors presented in optical microscope images were observed, thus observing orange (in different color tonalities) zones that correspond to multilayer graphene. For the intermediate value of the total flow (80 Nml/min), clearer colors were observed in the microscopy images (lower thickness value) (Table 6.5.).

Table 6.5. Influence of the total flow of gases (CH_4+H_2) during the reaction step at different reaction times. Average values of each type of graphene obtained from the representative optical microscope images.

(Synthesis conditions: 1025 ºC, CH_4/H_2=0.25 v/v, 130-60 Nml/min, 15-5 minutes of reaction time)

INFLUENCE OF THE TOTAL FLOW OF GASES (CH_4+H_2) DURING THE REACTION STEP (time = 15-5 min; CH_4/H_2=0.07 v/v; Q_T=80-130 Nml/min)					
2D Raman Shift (cm^{-1})	Reaction time (min)	Monolayer graphene (%)	Bilayer graphene (%)	Few-layer graphene (%)	Multilayer graphene (%)
130	15	31.41	37.51	18.71	12.38
	10	31.24	45.59	18.05	8.11
	7	34.81	38.49	17.30	9.40
	5	17.56	32.78	23.59	26.07
100	15	36.78	44.91	13.26	5.04
	10	42.40	33.76	14.28	9.55
	7	51.39	29.88	11.70	7.02
	5	31.02	34.91	19.37	14.71
80	15	51.78	31.38	11.59	5.24
	10	54.56	28.13	11.17	6.14
	7	62.4	24.57	8.75	4.29
	5	57.97	26.31	9.91	5.81
70	15	51.71	27.58	10.39	8.54
	10	34.78	39.49	17.18	8.53
	7	31.97	30.50	18.00	19.52
60	15	42.26	32.59	12.25	5.89
	10	31.86	32.33	19.18	16.63

Figure 6.11. shows the quality value versus the total flow of gases (CH_4+H_2) at different reaction times.

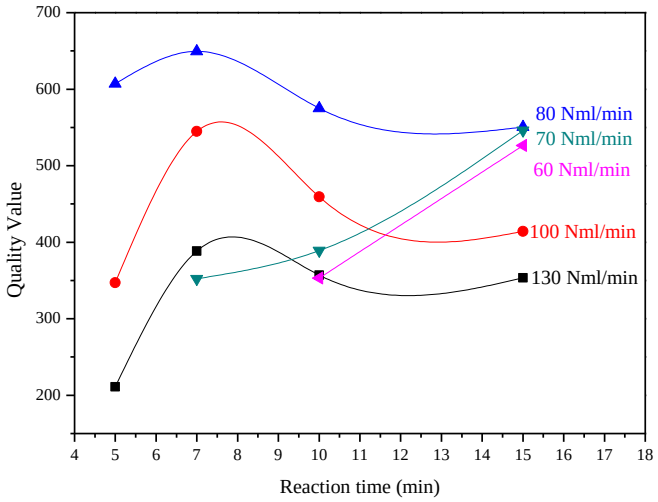

Figure 6.11. Influence of the total flow of gases (CH_4+H_2) during the reaction step at different reaction times. Quality value vs reaction time at the different total flow of gases (CH_4+H_2).

A maximum of quality value was obtained for the sample synthesized using a total flow of 80 Nml/min and 7 minutes of reaction time. Figure 6.12. shows the more representative optical microscope images corresponding to this optimal sample whereas Table 6 lists the quality and the percentage of each type graphene deposited on it (Table 6.6.). As observed, this optimal sample presented a value of the percentage of monolayer graphene deposited over the metal foil close to 62.5%.

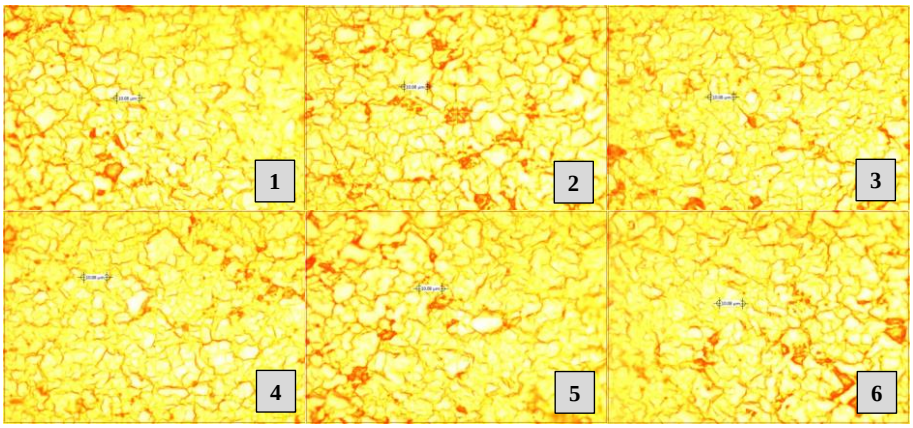

Figure 6.12. Influence of the total flow of gases (CH_4+H_2) during the reaction step at different reaction times. Optical microscope images corresponding to the sample showing the maximum quality value.
(Synthesis conditions: 1025 ºC, CH_4/H_2=0.25 v/v, 80 Nml/min, 7 minutes of reaction time)

Table 6.6. Influence of the total flow of gases (CH_4+H_2) during the reaction step at different reaction times. Quality and percentage of each type of graphene obtained from the sample showing the maximum quality value using the home made Excel-VBA application.
(Synthesis conditions: 1025 ºC, CH_4/H_2=0.25 v/v, 80 Nml/min, 7 minutes of reaction time)

Optical microscopy images	Monolayer graphene (%)	Bilayer graphene (%)	Few-layer graphene (%)	Multilayer graphene (%)	Quality value
1	62.45	25.26	8.71	3.58	650.7
2	61.86	22.31	9.94	5.89	642.0
3	61.48	25.95	8.30	4.27	641.6
4	63.40	25.58	7.88	3.14	660.4
5	61.90	24.14	9.50	4.47	644.1
6	63.31	24.16	8.15	4.37	658.1
Average	**62.4**	**24.57**	**8.75**	**4.29**	**649.5**

As observed, the growth of the monolayer graphene over the polycrystalline iron foil clearly depends on the total flow of gases passing through it and the exposure time to such gases.

Finally, Figure 6.13. shows the Raman spectroscopy results and the 2D peak deconvolution corresponding to the different graphene types presented in the optimum sample. Raman spectroscopy parameters (I_D/I_G, I_{2D}/I_G, FWHM and 2D peak position) agree with those reported in literature [18-25].

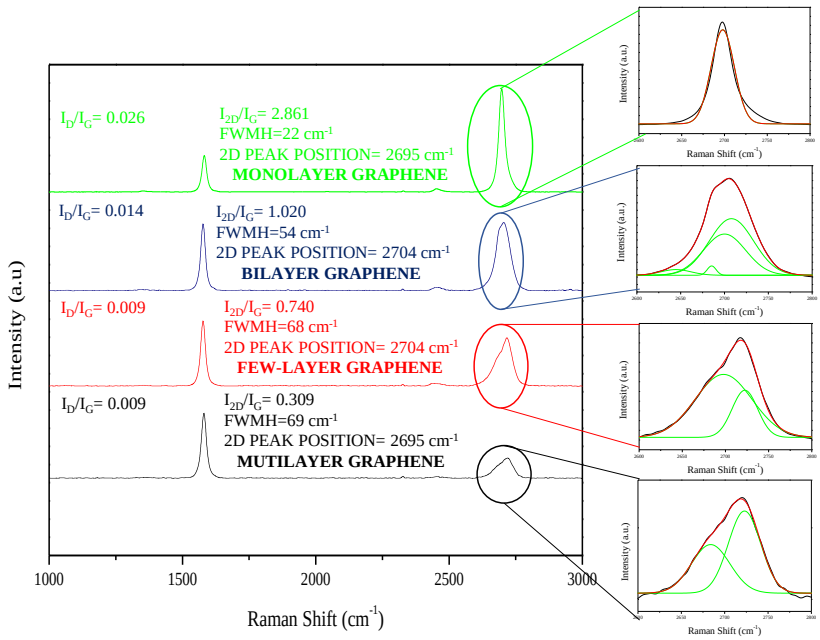

Figure 6.13. Influence of the total flow (CH_4+H_2) during the reaction stage at different reaction times. Raman spectroscopy results corresponding to the optimum sample.

(Synthesis conditions: 1025 ºC, CH_4/H_2=0.25 v/v, 80 Nml/min, 7 minutes of reaction time)

All types of graphene showed insignificant I_D/I_G ratio values indicating that it is a free-defects graphene. I_{2D}/I_G ratio increased when the number of graphene layers decreased, achieving for monolayer graphene the

highest value (2.86). The opposite effect was observed for the FWHM parameters. They decreased with decreasing graphene layers, obtaining for monolayer graphene the lowest value (22 cm^{-1}). 2D peak position was located around 2700 cm^{-1} for all graphene types, which is a characteristic value of this material [4, 10, 11, 26].

Finally, 2D peak deconvolution confirmed the typology of the graphene present in the sample [27]. According to the literature, 2D peak was deconvoluted in a single Lorentzian peak for monolayer graphene; this peak was split into four different peaks in bilayer graphene [28]. Finally, 2D peaks corresponding to few-layer and multilayer graphene were deconvoluted in two peaks [4].

6.4. Conclusions

In the present work, it has been demonstrated that a high quality graphene film, mostly covered by monolayer graphene, can be successfully growth on polycrystalline iron foil by an atmospheric pressure CVD process using methane as the carbonaceous source. The thickness of the graphene sample (number of layers) can be controlled by tuning the reaction temperature, the CH_4/H_2 flow rate ratio and the total flow of gases (CH_4+H_2) during the reaction step at different reaction times. By means of a process of parameter optimization, a high quality graphene film was achieved, showing a high percentage of monolayer graphene (62.4 %), a high I_{2D}/I_G (~2.9), a low I_D/I_G ratio (~0.026) and a narrow FWHM of 2D peak (~22 cm^{-1}).

The quality of graphene films could be enhanced by increasing the growth temperature and the CH_4/H_2 flow rate ratio up to 1025ºC and 0.25 v/v, respectively. In addition, low values of the total flow (CH_4+H_2) of gases (80 Nml/min) and short exposure times (7 minutes) were found to be required for obtaining high quality graphene.

These findings could help to manufacture high-quality graphene on iron foils for different applications, mainly electronic ones.

6.5. References

1. Bhuyan, M. S. A., Uddin, M. N., Islam, M. M., Bipasha, F. A. and Hossain, S. S., *Synthesis of graphene.* International Nano Letters, 2016, **6** (2): p. 65-83.
2. Chen, X., Zhang, L. and Chen, S., *Large area CVD growth of graphene.* Synthetic Metals, 2015, **210, Part A**: p. 95-108.
3. Huang, L., Chang, Q. H., Guo, G. L., Liu, Y., Xie, Y. Q., Wang, T., Ling, B. and Yang, H. F., *Synthesis of high-quality graphene films on nickel foils by rapid thermal chemical vapor deposition.* Carbon, 2012, **50** (2): p. 551-556.
4. Lavin-Lopez, M. P., Valverde, J. L., Ruiz-Enrique, M. I., Sanchez-Silva, L. and Romero, A., *Thickness control of graphene deposited over polycrystalline nickel.* New Journal of Chemistry, 2015, **39** (6): p. 4414-4423.
5. Yu, Q., Lian, J., Siriponglert, S., Li, H., Chen, Y. P. and Pei, S. S., *Graphene segregated on Ni surfaces and transferred to insulators.* Applied Physics Letters, 2008, **93** (11).
6. Muñoz, R. and Gómez-Aleixandre, C., *Review of CVD synthesis of graphene.* Chemical Vapor Deposition, 2013, **19** (10-12): p. 297-322.
7. Shah, K. A. and Tali, B. A., *Synthesis of carbon nanotubes by catalytic chemical vapour deposition: A review on carbon sources, catalysts and substrates.* Materials Science in Semiconductor Processing, 2016, **41**: p. 67-82.
8. An, H., Lee, W. J. and Jung, J., *Graphene synthesis on Fe foil using thermal CVD.* Current Applied Physics, 2011, **11** (4 SUPPL.): p. S81-S85.

9. Xue, Y., Wu, B., Guo, Y., Huang, L., Jiang, L., Chen, J., Geng, D., Liu, Y., Hu, W. and Yu, G., *Synthesis of large-area, few-layer graphene on iron foil by chemical vapor deposition.* Nano Research, 2011, **4** (12): p. 1208-1214.
10. Lavin-Lopez, M. P., Valverde, J. L., Cuevas, M. C., Garrido, A., Sanchez-Silva, L., Martinez, P. and Romero-Izquierdo, A., *Synthesis and characterization of graphene: Influence of synthesis variables.* Physical Chemistry Chemical Physics, 2014, **16** (7): p. 2962-2970.
11. Lavin-Lopez, M. P., Valverde, J. L., Sanchez-Silva, L. and Romero, A., *Influence of the Total Gas Flow at Different Reaction Times for CVD-Graphene Synthesis on Polycrystalline Nickel.* Journal of Nanomaterials, 2016, **2016**: p. 9.
12. Shen, Y. and Lua, A. C., *A facile method for the large-scale continuous synthesis of graphene sheets using a novel catalyst.* Scientific Reports, 2013, **3**.
13. Wang, Y. M., Cheng, S., Wei, Q. M., Ma, E., Nieh, T. G. and Hamza, A., *Effects of annealing and impurities on tensile properties of electrodeposited nanocrystalline Ni.* Scripta Materialia, 2004, **51** (11): p. 1023-1028.
14. Van Bommel, A. J., Crombeen, J. E. and Van Tooren, A., *LEED and Auger electron observations of the SiC(0001) surface.* Surface Science, 1975, **48** (2): p. 463-472.
15. Verguts, K., Vermeulen, B., Vrancken, N., Schouteden, K., Van Haesendonck, C., Huyghebaert, C., Heyns, M., De Gendt, S. and Brems, S., *Epitaxial Al2O3(0001)/Cu(111) Template Development for CVD Graphene Growth.* Journal of Physical Chemistry C, 2016, **120** (1): p. 297-304.
16. Yang, H., Shen, C.-M., Tian, Y., Wang, G.-Q., Lin, S.-X., Zhang, Y., Gu, C.-Z., Li, J.-J. and Gao, H.-J., *Influence of reaction parameters on synthesis of high-quality single-layer graphene on Cu using*

chemical vapor deposition. Chinese Physics B, 2014, **23** (9): p. 096803.

17. Dathbun, A. and Chaisitsak, S. *Effects of three parameters on graphene synthesis by chemical vapor deposition*. in *Nano/Micro Engineered and Molecular Systems (NEMS), 2013 8th IEEE International Conference on*. 2013.
18. Reina, A., Jia, X., Ho, J., Nezich, D., Son, H., Bulovic, V., Dresselhaus, M. S. and Jing, K., *Large area, few-layer graphene films on arbitrary substrates by chemical vapor deposition.* Nano Letters, 2009, **9** (1): p. 30-35.
19. Li, X., Cai, W., An, J., Kim, S., Nah, J., Yang, D., Piner, R., Velamakanni, A., Jung, I., Tutuc, E., Banerjee, S. K., Colombo, L. and Ruoff, R. S., *Large-area synthesis of high-quality and uniform graphene films on copper foils.* Science, 2009, **324** (5932): p. 1312-1314.
20. Hwang, J. Y., Kuo, C. C., Chen, L. C. and Chen, K. H., *Correlating defect density with carrier mobility in large-scaled graphene films: Raman spectral signatures for the estimation of defect density.* Nanotechnology, 2010, **21** (46).
21. Mattevi, C., Kim, H. and Chhowalla, M., *A review of chemical vapour deposition of graphene on copper.* Journal of Materials Chemistry, 2011, **21** (10): p. 3324-3334.
22. Ruan, G., Sun, Z., Peng, Z. and Tour, J. M., *Growth of graphene from food, insects, and waste.* ACS Nano, 2011, **5** (9): p. 7601-7607.
23. Chen, S., Cai, W., Piner, R. D., Suk, J. W., Wu, Y., Ren, Y., Kang, J. and Ruoff, R. S., *Synthesis and characterization of large-area graphene and graphite films on commercial Cu-Ni alloy foils.* Nano Letters, 2011, **11** (9): p. 3519-3525.
24. Lee, S., Lee, K. and Zhong, Z., *Wafer scale homogeneous bilayer graphene films by chemical vapor deposition.* Nano Letters, 2010, **10** (11): p. 4702-4707.

25. Lee, D., Lee, K., Jeong, S., Lee, J., Choi, B. and Kim, O., *Process optimization for synthesis of high-quality graphene films by low-pressure chemical vapor deposition.* Japanese Journal of Applied Physics, 2012, **51** (6 PART 2).
26. Nemanich, R. J. and Solin, S. A., *First- and second-order Raman scattering from finite-size crystals of graphite.* Physical Review B, 1979, **20** (2): p. 392-401.
27. Ferrari, A. C., Meyer, J. C., Scardaci, V., Casiraghi, C., Lazzeri, M., Mauri, F., Piscanec, S., Jiang, D., Novoselov, K. S., Roth, S. and Geim, A. K., *Raman spectrum of graphene and graphene layers.* Physical Review Letters, 2006, **97** (18).
28. Ryan, B., Luiz Gustavo, C. and Lukas, N., *Raman characterization of defects and dopants in graphene.* Journal of Physics: Condensed Matter, 2015, **27** (8): p. 083002.

Chapter 7: Influence of different Improved Hummers Method modifications on the characteristics of graphite oxide.

Resumen

En este capítulo, se prepararon diferentes muestras de óxido de grafito (GrO) usando el *Método de Hummers Mejorado* al cual se van introduciendo diversas modificaciones de forma paulatina con el fin de disminuir los elevados costes de producción asociados al proceso. Para ello, se partió de grafito como material de partida y $KMnO_4$ como agente oxidante. La caracterización de las muestras de GrO se llevó a cabo mediante espectroscopía Raman, SEM, TEM, análisis elemental, Difracción de Rayos X, adsorción-desorción de N_2 y análisis termogravimétrico. Los resultados mostraron que, una vez modificado el método de partida, el tiempo de oxidación se redujo de 12 a 3 horas, se eliminó la etapa de coagulación, las etapas de lavado se redujeron a la mitad, y se demostró que el uso de H_3PO_4 durante la etapa de oxidación no era necesario. Finalmente, la producción de GrO se logró incrementar hasta cinco veces consiguiéndose de este modo, disminuir los costes de producción del óxido de grafito si estos se comparan con los reportados para el *Método de Hummers Mejorado*.

Abstract

Different samples of graphite oxide (GrO) were prepared by the optimization of the *Improved Hummers Method* reported in literature. Graphite was used as the raw material and $KMnO_4$ and H_2SO_4 were used as the chemical reagents. GrO samples were analyzed by Raman spectroscopy, SEM, TEM, elemental analysis, XRD, N_2 adsorption-desorption and thermogravimetric analysis. The results indicate that, after optimize the synthesis method, the oxidation time was reduced from 12 to 3 hours, the coagulation step was removed, the wash step was halved, and the use of H_3PO_4 during the oxidation step was no longer necessary. This way, the production of graphite oxide per batch was increased by increasing five times the amount of graphite. Therefore, synthesis costs were significantly lower than those reported for the *Improved Hummers Method*.

7.1. Introduction

Great emphasis is currently focused on the development of large-scale production methods for graphene-based products synthesis. In this respect, graphite oxide (GrO) and graphene oxide have been identified as the most important graphene derivatives. The main properties of graphite oxide are as follows: it is an insulator material but its conductivity varies depending on its chemical and structural properties [1]; it is an amphiphilic material, which allows the dispersion of GrO in both aqueous and organic solvents [2, 3]; and it has antibacterial properties [4]. All of these properties make graphite oxide a suitable material for numerous applications such as supercapacitors [5], the removal of radioactive waste from water [6], the fabrication of transparent conductors [7] and in biomedical applications [8], for example to inhibit tumour formation in multiple cell lines [9].

Graphite oxide can be defined as a set of functionalized graphene sheets that are mainly composed of carbon, oxygen and hydrogen atoms. This material can be used as a precursor of graphene itself. The structure of graphite oxide is similar to that of graphite as they differ only in the oxygenated groups present in GrO, which give rise to an increase of the distance between the graphene layers [1]. This material consists of a hexagonal network of sp^2- and sp^3-hybridized carbon atoms that bear hydroxyl and epoxide functional groups on the 'basal' plane and carboxyl and carbonyl groups at the edges [10].

Graphite oxide can be synthesized by either the Brodie [11], Staudenmaier [12] or Hummers [13] methods or by a variation of the latter one, namely *Modified Hummers Method* or *Improved Hummers Method* [14]. The main differences between the above mentioned methods are summarized in Table 7.1., with particular emphasis on the nature of the oxidant, the toxicity and the main advantages or

disadvantages of each approach. It can be observed that *Improved Hummers Method* is characterized by lower toxicity and several advantages in terms of the synthesized product.

The main objective of the present work was to optimize the synthesis of graphite oxide by the *Improved Hummers Method* with the ultimate goal of reducing the reaction time and the quantities of chemical reagents required in the synthesis. As a result of this optimization, a considerably decrease of the production costs associated with the synthesis was observed. In addition, an economic assessment of the industrial scale of the process was study in order to know the viability of the graphite oxide synthesis.

Table 7.1. Synthesis Methods for Graphite Oxide [11-17].

Brodie Method [12, 25]

- **Oxidants:** $KClO_3$, HNO_3
- **Toxicity:** Yes
- **Disadvantages:**
  - Weak acidity.
  - Soft dispersability in basic solutions.
  - Small size, limiting thickness and providing an imperfect structure.

Staudenmaier Method [13, 26]

- **Oxidants:** $KClO_3$ ($NaClO_3$), HNO_3, H_2SO_4
- **Toxicity:** Yes
- **Disadvantages:**
  - Time-consuming and dangerous method.
  - Addition of $KClO_3$ generally takes longer than a week and CO_2 is evolved, thus making necessary to remove an inert gas.
  - The risk of explosions is a constant danger.

Hummers Method [27, 14]

- **Oxidants:** $KMnO_4$, H_2SO_4, $NaNO_3$
- **Toxicity:** No (NOx is released)
- **Advantages:**
  - Higher oxidation degree than that obtained in Brodie or Staudenmaier Methods.
- **Disadvantages:**
  - It is still considered that the oxidation is incomplete.
  - Separation and purification processes are tedious process.
  - Highly time-consuming process.

Table 7.1. Continuation. Synthesis Methods for Graphite Oxide [11-17].

Modified Hummers Method [27, 28]

- **Oxidants:** $KMnO_4$, H_2SO_4, $NaNO_3$, $KMnO_4$, H_2SO_4
- **Toxicity:** No (NO_x is released)
- **Advantages:**
  - Improved level of oxidation and, therefore, product performance.
- **Disadvantages:**
  - Separation and purification processes are tedious process.
  - Highly time-consuming process.

Improved Hummers Method [27]

- **Oxidants:** $KMnO_4$, H_2SO_4, H_3PO_4
- **Toxicity:** No
- **Advantages:**
  - Defects in the basal plane are reduced.
  - Larger amount of oxidized graphite is provided.
  - The degree of reduction provides an equivalent level of conductivity when compared to other methods.
  - Best process yield compared to Brodie, Staudenmaier and Hummers method.
  - Environmentally friendly, toxic gases are not generated during the preparation.
  - The product has a more organized structure compared to graphite oxide obtained by Brodie and Staudenmaier methods.
- **Disadvantages:**
  - Separation and purification processes are tedious process.
  - Highly time-consuming process.

7.2. Experimental

7.2.1 Materials

Graphite powder with a particle size <20 μm was supplied by Sigma Aldrich. $KMnO_4$ (purity of 99%), H_2SO_4 (purity of 96%), H_3PO_4 (purity of 50%), H_2O_2 (purity of 33%), HCl (5N), ethanol (purity of 99.5%) and dry diethyl ether (purity of 99.75%) were supplied by Panreac.

7.2.2. Method

7.2.2.1. Graphite oxide synthesis procedure

Graphite oxide was synthesized by the *Improved Hummers Method*. The first step consists on the oxidation of graphite using $KMnO_4$ as the oxidizing agent. For this purpose, 360 mL of H_2SO_4 and 40 mL of H_3PO_4 were introduced into an Erlenmeyer flask with constant and vigorous

shaking. 9 g $KMnO_4$ and 3 g of graphite (3:1) was slowly added to the H_2SO_4/H_3PO_4 mixture. The reaction mixture was maintained at 50 ºC for 12 hours. After the oxidation step, the resulting mixture was added to a beaker containing 400 g of flake ice and 3 mL of H_2O_2 in order to quench the reaction. The mixture was filtered under vacuum through a 10–20 μm filter. The resulting compact cake was washed twice (by vacuum filtration) with deionized water (200 mL), HCl (200 mL) and ethanol (200 mL) to clean the oxidized graphite. Finally, the compact cake was slurred with dry diethyl ether (200 mL), filtered off and dried at 100 ºC overnight.

7.2.3. Characterization

Raman spectroscopy

A SENTERRA Raman spectrometer with a grating of 600 lines per mm and a laser wavelength of 532 nm at a very low laser power level (<1 mW), to avoid any heating effect, was used to characterize the different graphite oxide samples. Raman spectroscopy is considered a reliable and quick method to characterize graphene-based materials [18, 19]. The D peak, which is visible at ~1350 cm^{-1}, is related to the presence of defects (edges, dislocations, cracks or vacancies) in graphitic materials. Note that Raman spectroscopy is a surface sensitive method so, it is possible that some information from inside graphite oxide cannot be reflected. On other words, information in the defects density of the planes inside GrO particles could be missing.

The G peak, which is visible at 1580–1620 cm^{-1}, denotes the symmetry-allowed graphite band and is a way of checking the vibrations in the same plane as the sp^2 hybridized carbon atoms that form the graphene sheets. Finally 2D peak, which only appear on graphene at around 2700 cm^{-1}, is the hall mark of the number of graphene layers [20, 21]. One of the most commonly used characterization parameters for samples that deviate relatively little from graphitic order is the intensity of the D

band relative to the G band, expressed as the ratio of their intensities (I_D/I_G). The intensity ratio increases with structural disorder in the graphite network and is inversely proportional to the average size of the sp^2 clusters [22]. This relationship for graphite oxide is usually in the range 0.7–1.0 [23-26]. The distance between defects points (L_D) of the samples was calculated from the intensities of the D and G bands in the RAMAN spectra using the formula $L_D = \sqrt{C(\lambda)/(I_D/I_G)}$ [27].

Scanning Electron Microscopy (SEM)

A Hitachi S-4800 Scanning Electron Microscope with a field emission gun with a resolution of 1.4 Nm to 1 KV was used to analyze the surface morphology of the samples. The equipment incorporated a Bruker backscatter detector for microanalysis and five motorized axes.

Elemental analysis

Analyses were performed according to the standard UNE-EN 15104:2011. The elemental analyser (model LECO CHNS-932) was capable of detecting C, H, N, O and S contents of a sample by different mechanisms. Results were provided as a mass percentage of each element on a dry basis.

X-Ray diffraction

XRD analyses were conducted on a Philips X´Pert instrument using nickel-filtered Cu-Kα radiation. The samples were scanned at a rate of $0.02º\ step^{-1}$ over the range $5º \leq 2\theta \leq 90º$ (scan time = $2s\ step^{-1}$) and the diffractograms were compared with the PDF-ICDD references. The in-plane crystallite size (L_a), c-axis crystallite size (L_c) and the interlaminar distances of sheets were obtained from the (002) reflection of the XRD patterns ([001] reflection in the case of GrO) using the Scherrer equation.

BET

Surface area/porosity measurements were made using a QUANTRA QUADRASORB SI apparatus with N_2 as the sorbate at 77 -196ºC. The samples were out gassed at 453 K under vacuum (1×10^{-2} Torr) for 12 hours prior to analysis. The total specific surface areas were determined by multipoint BET methods, while the specific total pore volume was evaluated from N_2 uptake at a relative pressure of $P/P_0 = 0.99$.

Thermogravimetric analysis (TGA)

The TG curve represents the evolution of the mass as a function of the temperature. The combustion of the graphite oxide was carried out in a TGA apparatus (TGA-DSC 1, METTLER TOLEDO). The sample was heated from 30 to 1000 ºC at 10 ºC/min under a reactive atmosphere of 21% of oxygen and 79% of nitrogen. The sample weight was 8 mg and the flow rate was 100 NmL/min.

Fourier Transform Infrared Spectroscopy (FTIR)

FTIR analysis was took place in a "Spectrum Two Spectrometer" (Perkin Elmer, Inc.) with a universal refracting and diamond as accessories. Detection range carried from 350 to 8300 cm^{-1} for KBr method and from 550 to 6000 cm^{-1} for ZnSe method. During sample measures, small amount of the material was place on the diamond under pressure until the transmittance stays constant.

7.3. Results and discussion

Optimization of *Improved Hummers Method* was focused on obtaining a less time-consuming method and lower production costs in an effort to identify a more easily scalable procedure to synthesize high quality graphite oxide. The quantities of reagents and the synthesis conditions for the *Improved Hummers Method,* as reported in the literature, are represented in Figure 7.1. [14].

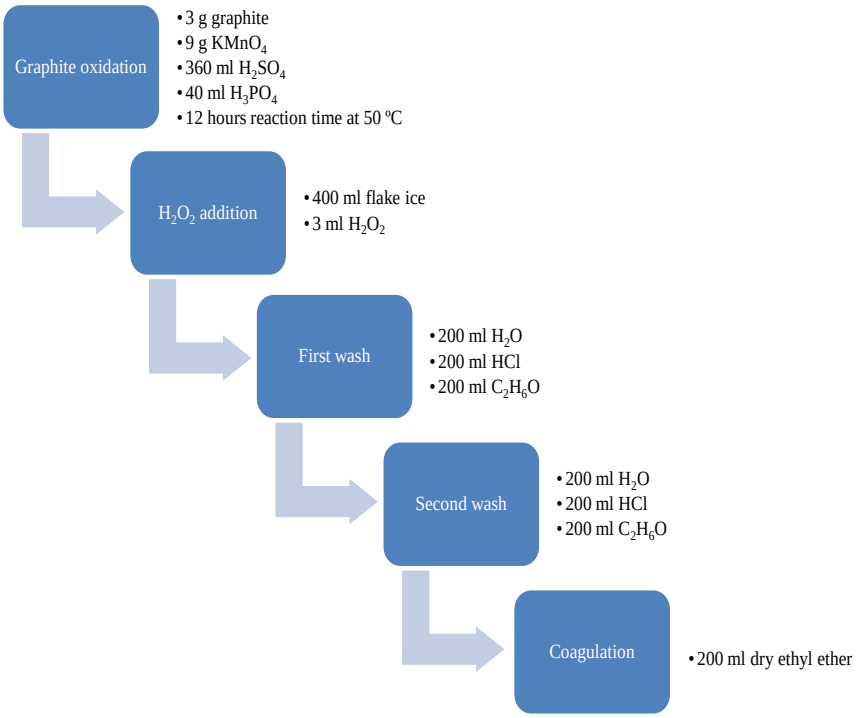

Figure 7.1. *Improved Hummers Method:* GrO synthesis conditions and reagent quantities [14, 28-30].

Raman spectrum corresponding to GrO synthesized using the *Improved Hummers Method* is shown in Figure 7.2.a. It can be observed the two characteristic GrO peaks (D and G). The D peak, which appears at around 1348 cm^{-1}, indicates the presence of imperfections in the graphitic structure of carbon atoms at the layer edges. The G peak, which is related to the movement of pairs of carbon atoms linked by sp^2, is located at 1586 cm^{-1}. This peak is commonly related to the graphitic order [31]. Thus, the broad G band and the more prominent D band associated with GrO (when compared to graphite) indicate a reduction in the size of the sp^2 domains due to oxidation. The relationship between the intensities of the two peaks (I_D/I_G), which had a value of 0.726 for the GrO synthesized using the *Improved Hummers Method*, will be used to compare the way in which the structural disorder grows in the graphitic

network. Both the locations of both the D and G bands and the ratio between their intensities are consistent with these characteristic values reported in the bibliography [23-26].

The first stage of the optimization concerned the reaction time for the oxidation step. With this aim in mind, the reaction time was reduced from 12 to 3 hours while keeping all other conditions constant. The Raman spectrum of the sample synthesized using an oxidation time of 3 hours is shown in Figure 7.2.b. Once again, the two characteristic peaks of graphite oxide can be observed, with the D band intensity being slightly stronger (I_D/I_G ratio value of 0.845). This indicates a slightly higher level of structural disorder and a greater number of defects in the graphene layers because of the oxidation process [23-26]. However, the decrease in the reaction time did not seem to have an influence on the oxidation of the raw material (as discussed later). In other words, the introduction of functional groups, both in the basal plane and at the edges, was achieved appropriately with reaction times of 12 and 3 hours. A significant reduction in the reaction time will have a positive effect on both the process time and the energy costs.

In order to assess whether the coagulation step has a significant influence on the final characteristics of the synthesized material, the GrO synthesis was carried out without carrying out this stage. The Raman spectrum of the resulting material is shown in Figure 7.2.c. It can be observed that the D and G peaks were located at 1343 and 1586 cm^{-1}, respectively, and the I_D/I_G ratio was 0.847, i.e., similar to the results obtained previously [23-26]. These results highlight the fact that the function of the dry diethyl ether is not decisive during the GrO synthesis because the final characteristics of the synthesized GrO were unchanged. This aspect will be discussed in more detail below.

Following the optimization of the as-published *Improved Hummers Method*, it was decided to combine in a single stage the initial two-stage washing process while maintaining the same reagent wash used in the

initial method. Thus, the function of deionized water is to neutralize the pH, HCl is used to remove remaining metal ions from the final product and ethanol is used to achieve faster drying of the graphite oxide cake. The Raman spectrum of the sample synthesized using a single washing stage is shown in Figure 7.2.d. Once again, the D and G bands were characteristic of this type of carbon material, with an I_D/I_G ratio value of 0.895 [23-26].

An interesting and novel aspect in the optimization of the *Improved Hummers Method* concerns the removal of any of the chemical reagents (H_2SO_4, H_3PO_4 and $KMnO_4$) used during the oxidation stage. The main reagent responsible for the oxidation of the graphite is manganese oxide (VII) (Mn_2O_7), which is formed in a reaction between $KMnO_4$ and H_2SO_4 [32]. The role of H_3PO_4 is only related to the formation of a more intact ring structure [14, 33] and it was decided not to use this reagent during the oxidation step. In the Raman spectrum of the resulting product (Figure 7.2.e) the D/G band intensity ratio for the GrO sample synthesized without H_3PO_4 (0.925) is higher than those obtained previously it. Despite the observed change, the I_D/I_G ratio value is consistent with those reported previously for most GrO samples [23-26].

Finally, the amount of H_2SO_4 was optimized maintaining constant *graphite: $KMnO_4$* ratio (1:3) in order to achieve the same oxidation degree as in the *Improved Hummers Method*. The quantities of both reagents were progressively increased and obtaining an optimum amount of graphite and $KMnO_4$ of 15 and 45 grams, respectively. In the Raman spectrum of the resulting product (see Figure 7.2.f) the characteristic D and G peaks were observed and the D/G intensity ratio was 0.946 [23-26].

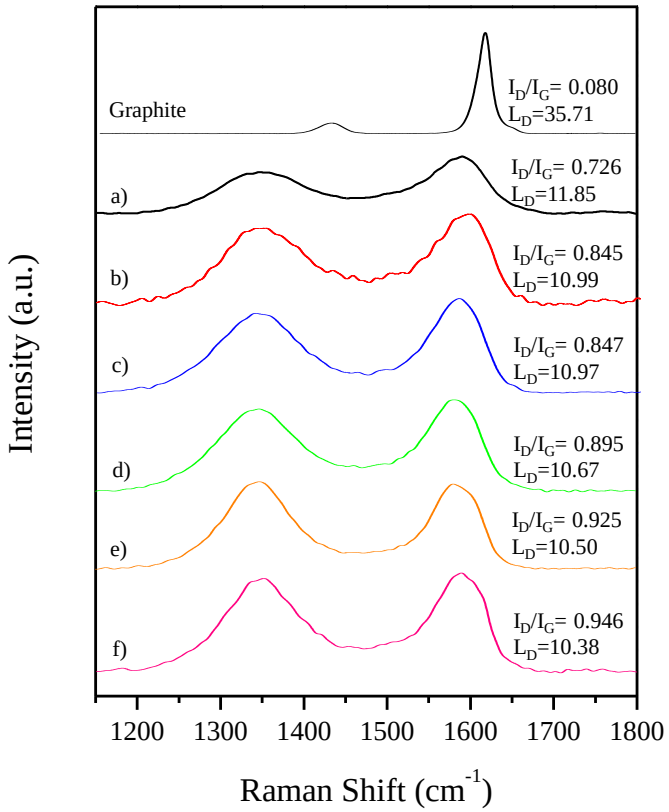

Figure 7.2. Raman spectra of GrO samples synthesized: **a)** following the as-published *Improved Hummers Method* **b)** after optimization of the oxidation time **c)** after removal of the coagulation step **d)** after optimization of the washing step **e)** after H_3PO_4 removal (oxidation step) and f) after optimization of the amounts of graphite and $KMnO_4$ (oxidation step). Inset: graphite RAMAN spectrum.

Summarizing, obtained results have shown that the structural disorder of the GrO samples progressively increased as the synthesis parameters have been changed respect to the *Improved Hummers Method*. The I_D/I_G value increase is due to the fact that in nanocrystalline graphite and graphene-based materials, the higher defects density creates more elastic scattering [27]. The disorder evolution in graphene-based materials can be also quantified by the distance between defects (L_D) according to the equation $L_D = \sqrt{C(\lambda)/(I_D/I_G)}$, where C ($\lambda$) has a value of 102 nm^2. As expected, L_D values were considerably lower in GrO

samples (compared to graphite) and, were gradually decreased as the synthesis parameters were changing.

The final conditions and amounts of reagents for the starting method (*Improved Hummers Method)* and the optimized one are represented in Figure 7.3. It is worth highlighting the considerable savings in reagents and experimental time needed to obtain the final product in a higher yield, which make the process considerably cheaper. At laboratory scale and using the Optimized Improved Hummers Method, 34 grams of graphite oxide was obtained per batch.

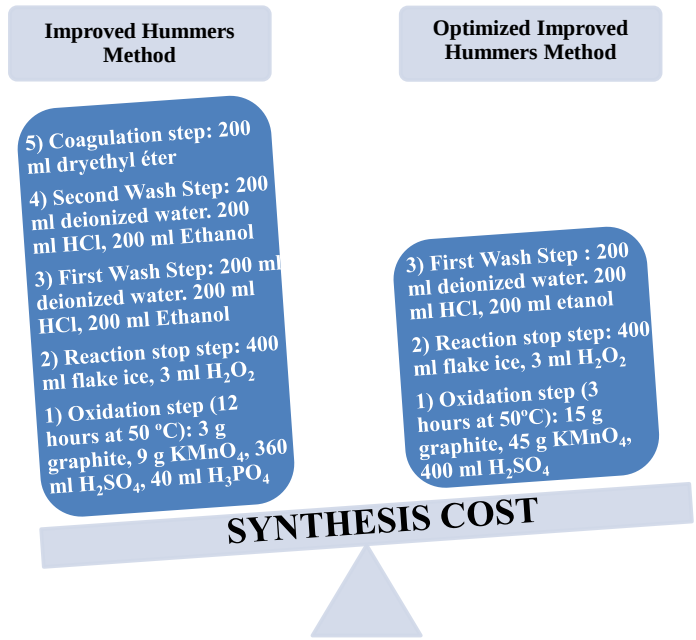

Figure 7.3. Comparison between the *Improved Hummers Method* and the optimized approach.

In order to check that GrO samples maintained the same morphology, SEM analysis were performed. Representative images of graphite and the synthesized GrO samples are shown in Figure 7.4. SEM image of graphite showed a crystalline structure composed of several layers. GrO

synthesized for both methods, showed a similar structure composed of an agglomerated powder that had several microns in size. GrO morphology resembled a fluffy appearance decreasing the number of layers in comparison with graphite due to the oxidation process.

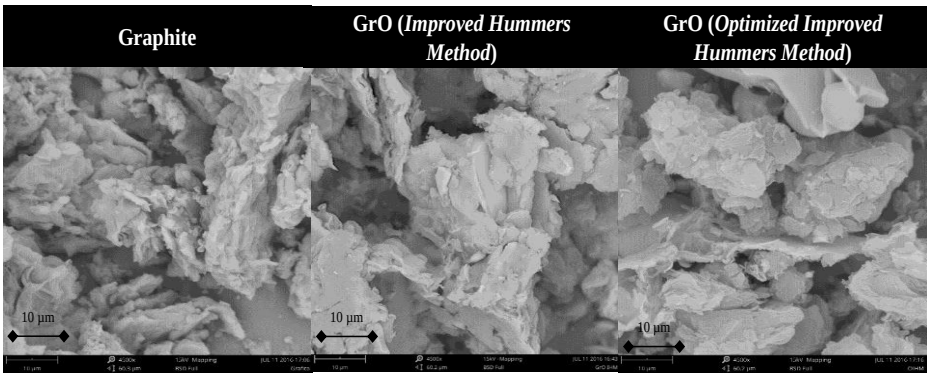

Figure 7.4. Representative SEM images corresponding graphite, GrO synthetized by the *Improved Hummers Method* and GrO synthesized by the optimized *Improved Hummers Method.*

Elemental analysis results (expressed as wt. %) corresponding to graphite and GrO samples are shown in Table 7.2. Graphite is composed of 98 wt. % carbon. The amount of carbon present in GrO samples was considerably lower (compared to graphite) due to the carbon replacements by oxygenated groups after the oxidation process. It has been demonstrated that oxygen is mostly present as hydroxyl, epoxy and carboxyl groups, which are located at the edges of the sheets and in the interior of the aromatic domains [34]. The elemental analysis of GrO synthetized by the optimized method presented a slightly lower oxygen content and more sulphur and nitrogen in its structure. This last fact was related to the cleaning step, which was reduced from two to one washes, increasing the amount of residual elements in the sample.

Table 7.2. Elemental composition (wt.%) of GrO samples.

SAMPLE (wt. %)	C	H	N	S	O	O/C ratio
Graphite	97.91	0.09	0	0.04	1.96	0.02
GrO (Improved Hummers Method)	32.78	1.52	0	1.13	64.57	1.97
GrO (Optimized Improved Hummers Method)	39.11	2.19	0.15	5.71	52.83	1.35

In order to assess the thermal stability of the graphite and the different GrO samples, TGA measurements were carried out. TGA results are represented in Figure 7.5. It can be seen that graphite and GrO samples differed in their thermal behaviour. TGA results for graphite showed the stability of this material. Its degradation started at 645ºC and the complete decomposition of graphite ended at 970ºC, losing a 91% of weight mass and leaving a residue of around 10% [35].

By its part, GrO samples showed a similar thermal behaviour. Three decomposition steps for both GrO could be observed. As was reported [36, 37], GrO started to lose mass upon heating even below 100 ºC, so the first decomposition step (I) started at 50ºC and finished at temperatures close to 200ºC. It was due to the elimination of loosely bound or adsorbed water and gas molecules. In this first decomposition step, the main differences between both GrO were observed. In the case of GrO synthesized by the *Improved Hummers Method,* the weight loss was 14% whereas in the case of the optimized one, this weight of mass was around 18%, demonstrating that the presence of labile groups (-OH, COOH) in the optimized GrO was higher than in the case of GrO synthesized by the *Improved Hummers Method*. A second decomposition step (II) occurred between 200 ºC and 475 ºC representing a weight loss of around 25% for the GrO synthesized by the Improved Hummers

Method and 31% for the optimized one. This step had been related to the decomposition of more stable oxygen groups to yield CO, CO_2 and steam and to a gas release, resulting in a rapid thermal expansion of the material, which is evident by a large mass loss [36] in the case of GrO synthesized by the *Improved Hummers Method*. This thermal expansion of the material was observed at lower temperatures (~200ºC) for the optimized GrO, due to the predominance of more labile oxygen groups easier to decompose. Finally, the third decomposition step (III) common for both GrO samples, occurred up to 475ºC and corresponded to a weight loss of around 45% (48% for GrO synthesized by the Improved Hummers Method and 44% for the optimized one) and was attributed to the removal of more stable oxygen groups (phenol, carbonyl) [15] and the combustion of the carbon skeleton. The TGA results indicated the excellent thermal stability of GrO sheets for both GrO samples [38].

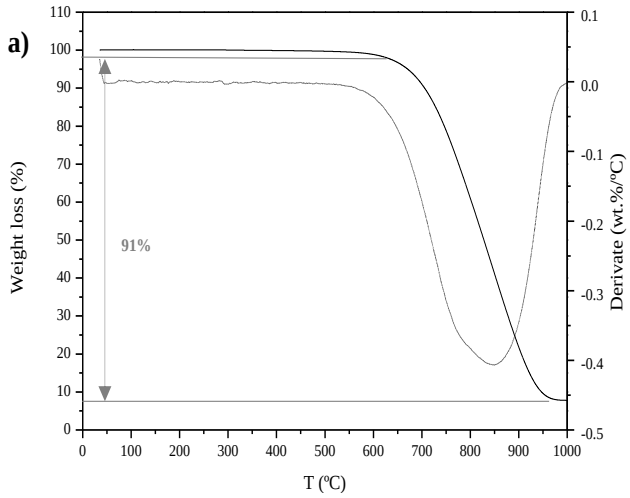

Figure 7.5. TGA and DTG analysis: a) Graphite

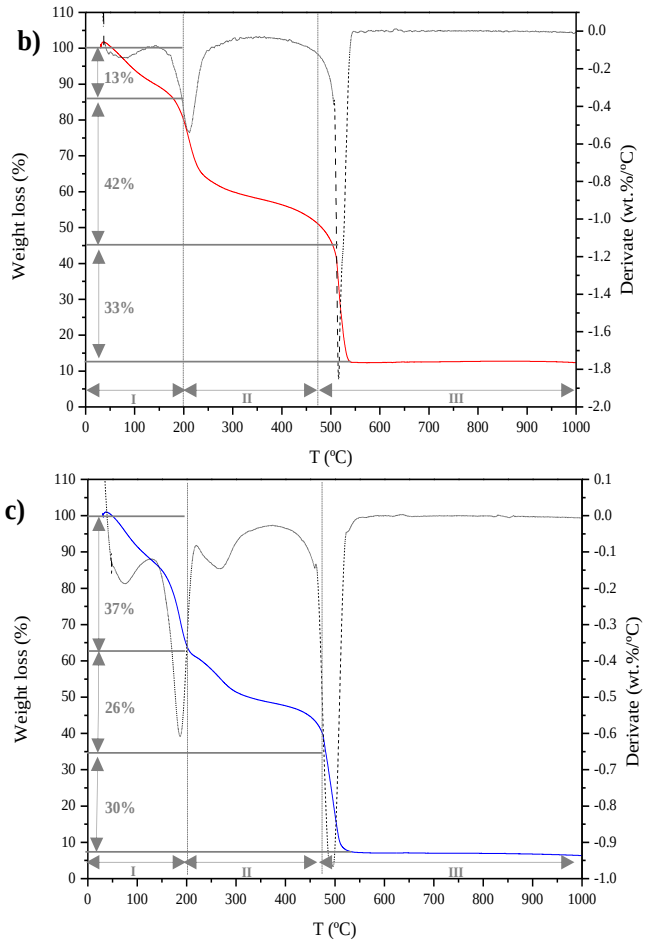

Figure 7.5. Continuation. TGA and DTG analysis: *b) GrO Improved Hummers Method and c) GrO Optimized Improved Hummers Method.*

Fourier Transform Infrared Spectroscopy (FTIR) spectra for graphite and both GrO samples is showed in Figure 7.6. FTIR is considered a suitable tool to determinate the functional groups presented in graphite oxide. FTIR spectrum of graphite showed a mostly carbon composition (~98%), as was reported in the elemental analysis (Table 7.2.), and almost no oxygen bonds were observed. GrO FTIR spectrum showed that oxygen functional groups were introduced in the structure after graphite oxidation. Both GrO show the characteristics peaks shown in

bibliography [39, 40]. In this way, the stretching of hydroxyl group can be observed 1410 cm^{-1} and from 2375 to 3677 cm^{-1}, stretching band of C=O at 1770 cm^{-1}, aromatic C=C from unoxidized sp^2 bonds at 1650 cm^{-1}, anhydride group CO-O-CO at 1050 cm^{-1}, C-H group at 755 cm^{-1} and, finally, C-O group at 1225 cm^{-1}. As observed, GrO synthesized by the optimized method showed more presence of C-OH, OH, CO-O-CO, C=O and epoxy groups. In other words, FTIR confirms the presence of higher amount of labile oxygen groups in GrO synthesized by the optimized method.

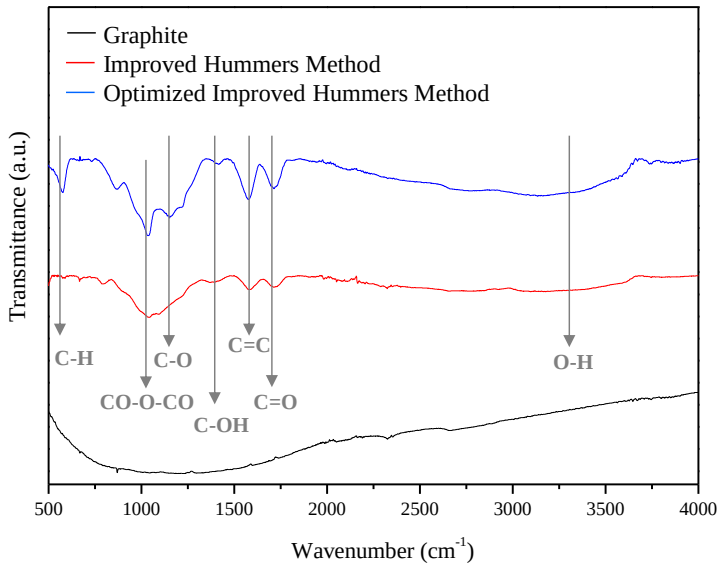

Figure 7.6. FTIR to graphite and GrO samples synthesized using both the *Improved Hummers Method* and the optimized method.

BET surface areas, which were obtained from the nitrogen adsorption-desorption isotherms, are shown in Figure 7.7. and the main textural characterization parameters corresponding to graphite and GrO samples are listed in Table 7.3. BET-surface area measured values were around 25 m^2/g for graphite oxides. It is evident from the results that graphite has a very low BET surface area of 1.7 m^2/g, because most of the atoms in graphite are not at the surface, being the interplanar space too small to allow gas molecules to enter [41]. By comparison, a

significant increase in the surface area was observed after the oxidation process and this was due to the expansion of the graphene layers [42]. Likewise, graphite oxide developed a more mesoporous structure, with both GrO samples retaining a similar surface area, average pore size and total pore volume, which again confirm the fact that the characteristics of the graphite oxide did not alter significantly after optimization of the synthesis method.

Table 7.3. Textural characterization parameters.

	Graphite	**Improved Hummers Method**	**Optimized Improved Hummers Method**
Surface area (m^2/g)	1.7	22.2	28.1
Total Pore Volume (cm^3/g)	0.038	0.113	0.129

Figure 7.7. Adsorption-desorption isotherms corresponding to graphite and GrO samples synthesized using both the *Improved Hummers Method* and the optimized method.

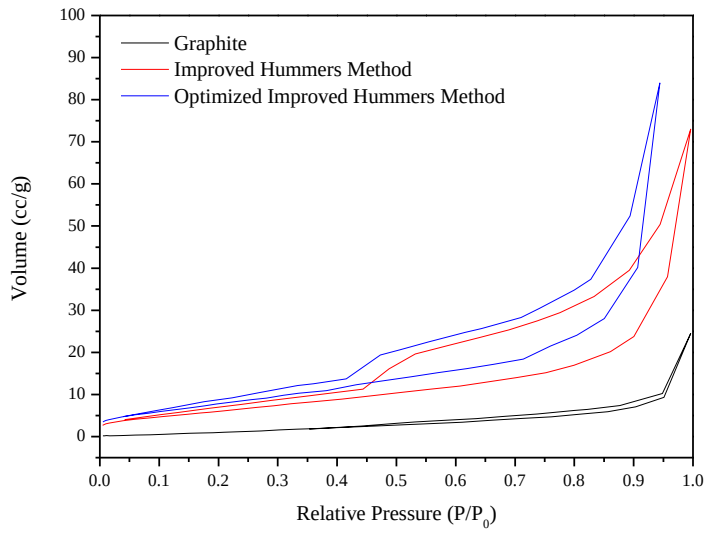

Graphite oxidation degree was studied by X-Ray Diffraction, obtaining information about the interlaminar distance, the structure and the oxidation state of the bulk materials. XRD spectra corresponding to graphite and GrO samples synthesized by both the *Improved Hummers Method* and the optimized one are shown in Figure 7.8. Graphite showed a characteristic [002] peak at 26.6º corresponding to the highly organized layer structure. This fact indicates a separation between the layers (d_{002}) of 0.33 nm. XRD patterns changed after the oxidation process. The sharp reflection of graphite had disappeared and a new diffraction [001] peak appeared at around 2θ = ~10º, which is characteristic of graphite oxide [43]. Thus, graphite oxide synthesized using the *Improved Hummers Method* showed a characteristic [001] peak at 10.9º, which indicates a separation between the layers of 0.81 nm. On the other hand, graphite oxide synthesized by the optimized method showed a characteristic XRD peak at 9.96º, which is consistent with a separation between layers of 0.89 nm. This increase in the interlaminar distance between graphite and GrO might be attributed to the perturbation of the oxygen groups bound to the graphite sheet [40].The measured d_{002} values were similar to those reported in the literature, which are in the range from 0.56 nm [44] to 0.95 nm [14]. The increase in the interlayer spacing observed after oxidation has been attributed to the expansion caused by the presence of oxygen functional groups and water molecules held in the interlayer galleries of hydrophilic GrO [45, 46]. Although more oxygenated groups were observed for GrO synthetized by the *Improved Hummers Method* and, therefore it could be expected that d_{002} will be higher in this case. However, the opposite effect was observed, obtaining higher value of d_{002} for the GrO obtained by the optimized method which may be due to the higher surface area presented for this GrO (28.1 m^2/g). This increase in the interlaminar distance value could be due to the higher presence of more labile oxygenated groups, which increased the separation between layers in the basal plane of GrO synthesized by the optimized method.

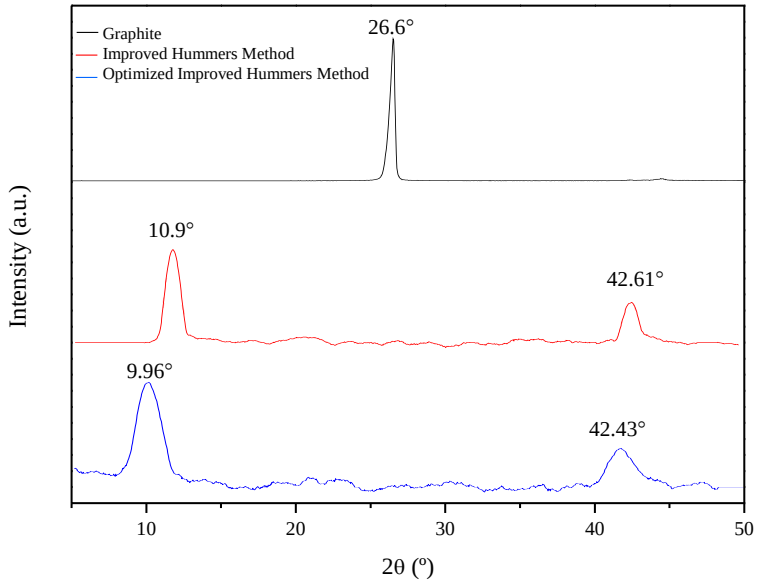

Figure 7.8. XRD spectrum corresponding to graphite and GrO synthesized using *Improved Hummers Method* and optimized *Improved Hummers Method*.

The in-plane crystallite size (L_a), calculated with [100] peak, and the crystal stack height or crystalline size along the x-axis (L_c), calculated with [002] peak, were estimated by XRD spectrum and the corresponding formula. The values obtained are summarized in Table 7.4. As observed, crystallite domains (both L_a and L_c) had reduced in size after the incorporation of functional groups into the graph sheets, which again indicates that an increase in structural disorder occurs after oxidation [47]. Similar values were obtained for both GrO, indicating that the oxidation method did not influence the crystalline domains of the material. The number of layers in the stacking structure ($N_c = L_c/d_{002}$) decreased markedly indicating the graphite oxidation.

Table 7.4. Crystal dimensions described by layer size L_a, stack height L_c and the number of layers in the stacking structure (N_c).

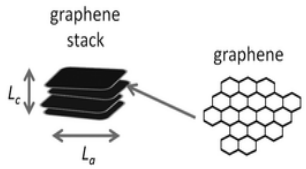	**L_a (nm) XRD**	**L_c (nm) XRD**	**d_{002} (nm) XRD**	**N_c**
Graphite	39.7	19.43	0.33	58.05
Improved Hummers Method	11.17	4.78	0.81	5.89
Optimized *Improved Hummers Method*	11.03	4.43	0.89	4.99

Graphite oxide exfoliation to graphene oxide was performed in order to study the differences between them. Figure 7.9. summarized the most important characterization parameters of both materials. As can be observed, almost all characterization techniques showed similar results because the exfoliation process was performed using sonication, which involved a physical process not a chemical one, obtaining a similar structure for both material, only differentiated for the distance between layers.

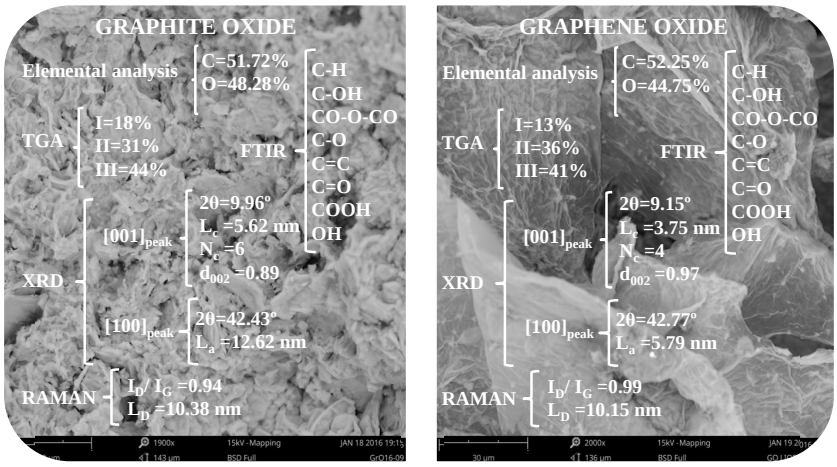

Figure 7.9. Graphite oxide vs graphene oxide.

According to the obtained results, it can be affirmed that the exfoliation capabilities of GrO obtained after the optimization of the *Improved Hummers Method* was not affected so this oxidation process was took place correctly.

The yield of the exfoliation of GrO to GO was around 80% (starting with 34 grams of GrO, 27 grams of GO was obtained when exfoliation process finished).

7.4. Conclusions

Different samples of graphite oxide were prepared by modification of the *Improved Hummers Method* reported in literature [14]. Graphite was used as the raw material and $KMnO_4$ and H_2SO_4 were used as chemical reagents to produce manganese oxide, which is mainly responsible for the oxidation of graphite. After the synthesis method had been optimized, the oxidation time was reduced from 12 to 3 hours, the coagulation step was removed, the washing step was halved, the use of H_3PO_4 during the oxidation step was removed and the graphite oxide production per batch was increased by increasing the amount of graphite that could be treated from 3 to 15 grams (while keeping the graphite/$KMnO_4$ ratio constant). The results obtained clearly show a significant reduction in the synthesis costs.

7.5. References

1. Pei, S. and Cheng, H. M., *The reduction of graphene oxide.* Carbon, 2012, **50** (9): p. 3210-3228.
2. Pan, S. and Aksay, I. A., *Factors controlling the size of graphene oxide sheets produced via the graphite oxide route.* ACS Nano, 2011, **5** (5): p. 4073-4083.

3. Parades, J. I., Villar-Rodil, S., Martínez-Alonso, A. and Tascón, J. M. D., *Graphene oxide dispersions in organic solvents.* Langmuir, 2008, **24** (19): p. 10560-10564.
4. Hu, W., Peng, C., Luo, W., Lv, M., Li, X., Li, D., Huang, Q. and Fan, C., *Graphene-based antibacterial paper.* ACS Nano, 2010, **4** (7): p. 4317-4323.
5. Wang, H., Hao, Q., Yang, X., Lu, L. and Wang, X., *Graphene oxide doped polyaniline for supercapacitors.* Electrochemistry Communications, 2009, **11** (6): p. 1158-1161.
6. Romanchuk, A. Y., Slesarev, A. S., Kalmykov, S. N., Kosynkin, D. V. and Tour, J. M., *Graphene oxide for effective radionuclide removal.* Physical Chemistry Chemical Physics, 2013, **15** (7): p. 2321-2327.
7. Becerril, H. A., Mao, J., Liu, Z., Stoltenberg, R. M., Bao, Z. and Chen, Y., *Evaluation of solution-processed reduced graphene oxide films as transparent conductors.* ACS Nano, 2008, **2** (3): p. 463-470.
8. Yang, K., Feng, L., Hong, H., Cai, W. and Liu, Z., *Preparation and functionalization of graphene nanocomposites for biomedical applications.* Nature Protocols, 2013, **8** (12): p. 2392-2403.
9. Fiorillo, M., Verre, A. F., Iliut, M., Peiris-Pagés, M., Ozsvari, B., Gandara, R., Cappello, A. R., Sotgia, F., Vijayaraghavan, A. and Lisanti, M. P., *Graphene oxide selectively targets cancer stem cells, across multiple tumor types: Implications for non-toxic cancer treatment, via "differentiation-based nano-therapy".* Oncotarget, 2015, **6** (6): p. 3553-3562.
10. Suk, J. W., Piner, R. D., An, J. and Ruoff, R. S., *Mechanical properties of monolayer graphene oxide.* ACS Nano, 2010, **4** (11): p. 6557-6564.
11. Brodie, B. C., *XXIII. - Researches on the atomic weight of graphite.* Quarterly Journal of the Chemical Society of London, 1860, **12** (1): p. 261-268.

12. Staudenmaier, L., *Verfahren zur darstellung der graphitsäure.* Berichte der Deutschen Chemischen Gesellschaft 1898, **31**: p. 1481-1487.
13. Hummers Jr, W. S. and Offeman, R. E., *Preparation of graphitic oxide.* Journal of the American Chemical Society, 1958, **80** (6): p. 1339.
14. Marcano, D. C., Kosynkin, D. V., Berlin, J. M., Sinitskii, A., Sun, Z., Slesarev, A., Alemany, L. B., Lu, W. and Tour, J. M., *Improved synthesis of graphene oxide.* ACS Nano, 2010, **4** (8): p. 4806-4814.
15. Szabó, T., Berkesi, O., Forgó, P., Josepovits, K., Sanakis, Y., Petridis, D. and Dékány, I., *Evolution of surface functional groups in a series of progressively oxidized graphite oxides.* Chemistry of Materials, 2006, **18** (11): p. 2740-2749.
16. Chua, C. K., Sofer, Z. and Pumera, M., *Graphite oxides: Effects of permanganate and chlorate oxidants on the oxygen composition.* Chemistry - A European Journal, 2012, **18** (42): p. 13453-13459.
17. Park, S., An, J., Piner, R. D., Jung, I., Yang, D., Velamakanni, A., Nguyen, S. T. and Ruoff, R. S., *Aqueous Suspension and Characterization of Chemically Modified Graphene Sheets.* Chemistry of Materials, 2008, **20** (21): p. 6592-6594.
18. Kudin, K. N., Ozbas, B., Schniepp, H. C., Prud'homme, R. K., Aksay, I. A. and Car, R., *Raman spectra of graphite oxide and functionalized graphene sheets.* Nano Letters, 2008, **8** (1): p. 36-41.
19. Kaniyoor, A. and Ramaprabhu, S., *A Raman spectroscopic investigation of graphite oxide derived graphene.* AIP Advances, 2012, **2** (3).
20. Suk, J. W., Kitt, A., Magnuson, C. W., Hao, Y., Ahmed, S., An, J., Swan, A. K., Goldberg, B. B. and Ruoff, R. S., *Transfer of CVD-grown monolayer graphene onto arbitrary substrates.* ACS Nano, 2011, **5** (9): p. 6916-6924.

21. Reina, A., Jia, X., Ho, J., Nezich, D., Son, H., Bulovic, V., Dresselhaus, M. S. and Jing, K., *Large area, few-layer graphene films on arbitrary substrates by chemical vapor deposition.* Nano Letters, 2009, **9** (1): p. 30-35.
22. Akhavan, O. and Ghaderi, E., *Escherichia coli bacteria reduce graphene oxide to bactericidal graphene in a self-limiting manner.* Carbon, 2012, **50** (5): p. 1853-1860.
23. Willemse, C. M., Tlhomelang, K., Jahed, N., Baker, P. G. and Iwuoha, E. I., *Metallo-Graphene nanocomposite electrocatalytic platform for the determination of toxic metal ions.* Sensors, 2011, **11** (4): p. 3970-3987.
24. Gao, E., Wang, W., Shang, M. and Xu, J., *Synthesis and enhanced photocatalytic performance of graphene-Bi 2WO6 composite.* Physical Chemistry Chemical Physics, 2011, **13** (7): p. 2887-2893.
25. Huan, T. N., Van Khai, T., Kang, Y., Shim, K. B. and Chung, H., *Enhancement of quaternary nitrogen doping of graphene oxide via chemical reduction prior to thermal annealing and an investigation of its electrochemical properties.* Journal of Materials Chemistry, 2012, **22** (29): p. 14756-14762.
26. Peng, H., Mo, Z., Liao, S., Liang, H., Yang, L., Luo, F., Song, H., Zhong, Y. and Zhang, B., *High performance Fe- and N- Doped carbon catalyst with graphene structure for oxygen reduction.* Scientific Reports, 2013, **3**.
27. Lucchese, M. M., Stavale, F., Ferreira, E. H. M., Vilani, C., Moutinho, M. V. O., Capaz, R. B., Achete, C. A. and Jorio, A., *Quantifying ion-induced defects and Raman relaxation length in graphene.* Carbon, 2010, **48** (5): p. 1592-1597.
28. Zhang, F. F., Zhang, X. B., Dong, Y. H. and Wang, L. M., *Facile and effective synthesis of reduced graphene oxide encapsulated sulfur via oil/water system for high performance lithium sulfur cells.* Journal of Materials Chemistry, 2012, **22** (23): p. 11452-11454.

29. Shi, C., Chen, L., Xu, Z., Jiao, Y., Li, Y., Wang, C., Shan, M., Wang, Z. and Guo, Q., *Monitoring influence of chemical preparation procedure on the structure of graphene nanosheets.* Physica E: Low-Dimensional Systems and Nanostructures, 2012, **44** (7-8): p. 1420-1424.
30. Bansal, P., Panwar, A.S. and Bahadur, D., *Effect of Reaction Temperature on Structural and Optical Properties of Reduced Graphene Oxide.* International Journal of Materials, Mechanics and Manufacturing, 2014, **2** (1): p. 18-20.
31. Ferrari, A. C. and Robertson, J., *Interpretation of Raman spectra of disordered and amorphous carbon.* Physical Review B - Condensed Matter and Materials Physics, 2000, **61** (20): p. 14095-14107.
32. Koch, K. R., *Oxidation by Mn207: An impressive demonstration of the powerful oxidizing property of dimanganeseheptoxide.* Journal of Chemical Education, 1982, **59** (11): p. 973.
33. Higginbotham, A. L., Kosynkin, D. V., Sinitskii, A., Sun, Z. and Tour, J. M., *Lower-defect graphene oxide nanoribbons from multiwalled carbon nanotubes.* ACS Nano, 2010, **4** (4): p. 2059-2069.
34. Botas, C., Álvarez, P., Blanco, C., Santamaría, R., Granda, M., Gutiérrez, M. D., Rodríguez-Reinoso, F. and Menéndez, R., *Critical temperatures in the synthesis of graphene-like materials by thermal exfoliation-reduction of graphite oxide.* Carbon, 2013, **52**: p. 476-485.
35. Crumpton, D. M., Laitinen, R. A., Smieja, J. and Cleary, D. A., *Thermal analysis of carbon allotropes: An experiment for advanced undergraduates.* Journal of Chemical Education, 1996, **73** (6): p. 590-591.
36. Stankovich, S., Dikin, D. A., Piner, R. D., Kohlhaas, K. A., Kleinhammes, A., Jia, Y., Wu, Y., Nguyen, S. T. and Ruoff, R. S., *Synthesis of graphene-based nanosheets via chemical reduction of exfoliated graphite oxide.* Carbon, 2007, **45** (7): p. 1558-1565.

37. Fang, M., Wang, K., Lu, H., Yang, Y. and Nutt, S., Journal of Materials Chemistry, 2009, **19**: p. 7098.
38. Song, J., Wang, X. and Chang, C. T., *Preparation and characterization of graphene oxide.* Journal of Nanomaterials, 2014, **2014**.
39. Chen, W. and Yan, L., *Preparation of graphene by a low-temperature thermal reduction at atmosphere pressure.* Nanoscale, 2010, **2** (4): p. 559-563.
40. Peng, S., Fan, X., Li, S. and Zhang, J., *Green synthesis and characterization of graphite oxide by orthogonal experiment.* Journal of the Chilean Chemical Society, 2013, **58** (4): p. 2213-2217.
41. Wang, H. and Hu, Y. H., *Effect of oxygen content on structures of graphite oxides.* Industrial and Engineering Chemistry Research, 2011, **50** (10): p. 6132-6137.
42. Zhao, W., Kido, G., Hara, K. and Noguchi, H., *Characterization of neutralized graphite oxide and its use in electric double layer capacitors.* Journal of Electroanalytical Chemistry, 2014, **712**: p. 185-193.
43. Ramesh, P., Bhagyalakshmi, S. and Sampath, S., *Preparation and physicochemical and electrochemical characterization of exfoliated graphite oxide.* Journal of Colloid and Interface Science, 2004, **274** (1): p. 95-102.
44. Casabianca, L. B., Shaibat, M. A., Cai, W. W., Park, S., Piner, R., Ruoff, R. S. and Ishii, Y., *NMR-based structural modeling of graphite oxide using multidimensional 13C solid-state NMR and ab initio chemical shift calculations.* Journal of the American Chemical Society, 2010, **132** (16): p. 5672-5676.
45. Buchsteiner, A., Lerf, A. and Pieper, J., *Water dynamics in graphite oxide investigated with neutron scattering.* Journal of Physical Chemistry B, 2006, **110** (45): p. 22328-22338.

46. Park, S., An, J., Potts, J. R., Velamakanni, A., Murali, S. and Ruoff, R. S., *Hydrazine-reduction of graphite- and graphene oxide.* Carbon, 2011, **49** (9): p. 3019-3023.
47. Guerrero-Contreras, J. and Caballero-Briones, F., *Graphene oxide powders with different oxidation degree, prepared by synthesis variations of the Hummers method.* Materials Chemistry and Physics, 2015, **153**: p. 209-220.

Chapter 8: Synthesis and characterization of Reduced Graphene Oxide: Influence of the reduction strategy.

8.5. References

Resumen

En el presente capítulo se estudiaron y compararon diferentes estrategias para reducir óxido de grafeno y sintetizar óxido de grafeno reducido. Para comenzar, se sintetizó óxido de grafito mediante una optimización del *Método de Hummers Mejorado* (Capítulo 7). A continuación, se sintetizó óxido de grafeno reducido mediante diferentes estrategias: química (usando hidracina y ácido ascórbico como agentes reductores), térmica y múltiples fases. Las muestras obtenidas fueron analizadas con espectroscopía Raman, SEM, FTIR, análisis elemental, difracción de Rayos X y TGA. Se comprobó que el método de reducción múltiples fases, basado en la combinación de más de un método de reducción concretamente, reducción térmica seguida de reducción química, mostró los mejores resultados. Un tratamiento térmico suave seguido de una reducción química usando ácido ascórbico como agente reductor, permitió una reducción de los grupos funcionales oxigenados del 47%. En este trabajo se demuestra que la estructura del óxido de grafeno reducido depende en gran medida de la estrategia de reducción usada lo cual, indudablemente, repercutirá sobre su utilización o no en algunas de las aplicaciones propuestas en bibliografía para este material.

Abstract

Different graphene oxide reduction strategies to produce reduced graphene oxide are compared and discussed. Firstly, the optimization of the most popular oxidation route reported in literature (*Improved Hummers Method*) to obtain graphite oxide was carried oud. Subsequently, different sets of reduced graphene oxide powders were synthesized through three different reduction routes: chemical (by using hydrazine and ascorbic acid), thermal and multiphase methods. Samples were analyzed by Raman spectroscopy, SEM, FTIR, elemental analysis, X-ray diffraction and TGA. It was shown that multiphase reduction method, e.g. combination of more than one reduction route, specifically, thermal and chemical ones, allowed to enhance the effectiveness for the functional oxygen groups' removal. A mild thermal treatment followed by a chemical reduction of graphene oxide using ascorbic acid as the reducing agent, showed a functional groups reduction of 47%. This work demonstrates that the reduced graphene oxide structure is highly dependent on the reduction strategy followed, which could affect its performance in some of the different potential applications proposed in bibliography for this kind of material.

8.1. Introduction

As it was commented in previous chapters, *Bottom-Up* approach consists of the synthesis of graphene starting with carbon atoms or molecules and build up to graphene deposited over a substrate. On the other hand, in the *Top Down* approach, a pattern generated on a large scale (graphite) is reduced to graphene [1].

Graphite is the most popular raw material used in the *Top Down* approach to synthesize reduced graphene oxide or powder graphene. Graphite oxide is obtained by treating graphite with strong oxidizing agents [2]. This material can be defined as a set of functionalized sheets of graphene formed by epoxides, hydroxides and carboxyl groups. This oxygen group's incorporation into graphite makes its structure more hydrophobic, making possible the separation of its layers in aqueous solution by sonication [3, 4] to obtain graphene oxide. Several methods to synthesize graphite oxide have been reported in the literature: Brodie [5], Staudenmaier [6] and Hummers Method [2] and its variations (Modified and Improved Hummers method) [7]. This material is considered to be an intermediate for the manufacture of reduced graphene oxide, which can be obtained by removing the oxygen functional groups by either the action of chemical reducing agents or the temperature. Reduced graphene oxide can be defined as a homogeneous material with structural defects, resulting from the elimination of a large portion of functional oxygen groups from the graphene oxide structure [8]. In general, reduced graphene oxide structure is similar to that of graphite oxide but it is not completely homogenous like graphene due to the occurrence of remaining functional groups [9]. The principal aim of the reduction techniques is to remove, as much as possible, the oxygen functional groups to obtain graphene powder [10]. Different strategies can be followed to remove these oxygen functional groups: thermal reduction [11, 12], photo

reduction [13], electrochemical reduction [14], microwave reduction [15], solvothermal reduction [16], chemical reduction [17-19] by using a wide variety of reducing agents (hydroiodic acid, ascorbic acid, hydrazine, $NaBH_4$ or some metal hydrides [10]) and, finally, multiphase reduction [20-22]. Figure 1 summarizes the advantages and disadvantages of the most important reduction techniques listed above.

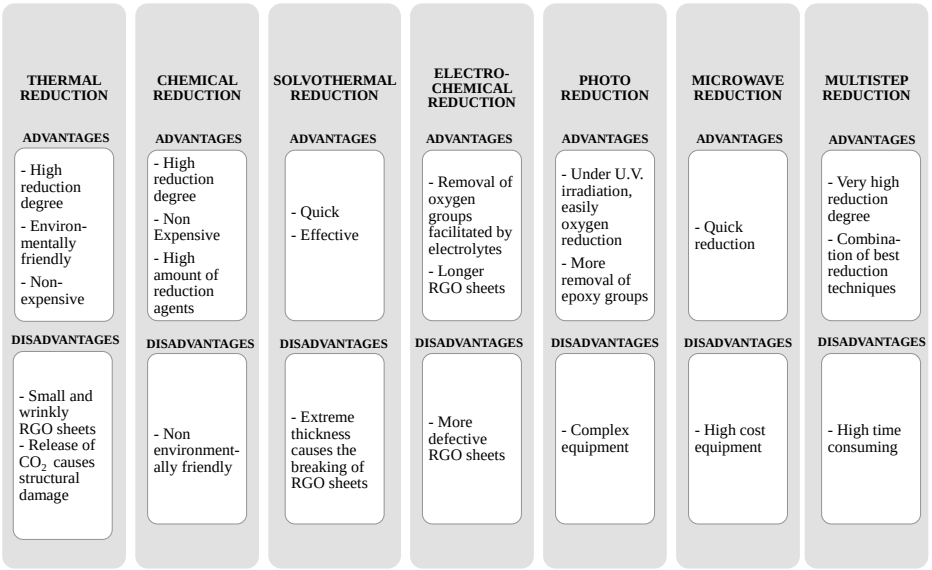

Figure 1. Advantages and disadvantages of reduction strategies used in the production of reduced graphene oxide.

In this work, the structure and chemistry of different reduced graphene oxide samples prepared through different graphene–reduction strategies: chemical, thermal and multiphase techniques were compared. Graphene oxide can be chemically reduced by using several reducing agents. In this work, hydrazine and ascorbic acid have been selected as the reducing agents. Hydrazine (N_2H_4) is a colourless flammable liquid with an ammonia-like odor, highly toxic and dangerously unstable unless handled in a solution [23] but it is a powerful and a convenient reductant because the by-products yielded in the reduction process are typically nitrogen gas and water. On the other hand, ascorbic acid is a natural organic compound with

antioxidant properties that owns both innocuous nature and environmentally friendly characteristics. It is a white solid that dissolves well in water to give mildly acidic solutions [24]. Ascorbic acid has been proposed recently as a potential agent to be used for graphene oxide reduction [25, 26]. Anyway, chemical reduction technique involves the use of a liquid media which can difficult the industrial production of reduced graphene oxide. In this sense, other reduction procedures do not required liquid media such as the thermal reduction of graphene oxide are also used to remove the oxygen functional groups from this material. However, this procedure presents the disadvantage that a violent expansion of the material occurs, which could damage the structure of the resulting material. Finally, a combination of both chemical and thermal reduction techniques was performed and the resulting products were compared to those separately obtained with each of these techniques.

8.2. Experimental

8.2.1. Materials

Graphite powder (< 20 μm) was supplied by ALDRICH CHEMISTRY. Potassium permanganate ($KMnO_4$), sulfuric acid (H_2SO_4), chlorhydric acid (HCl), hydrogen peroxide (H_2O_2) and ethanol (CH_3CH_2OH) with a purity grade of 99%, 96%, 37%, 99.5% and 99.5%, respectively, were supplied by PANREAC. Monohydrate hydrazine with a purity grade of 98% was supplied by SIGMA-ALDRICH, and ascorbic acid with a purity grade of 99% was supplied by VWR.

8.2.2. Methods

8.2.2.1. Synthesis of Graphite Oxide (GrO)

Graphite oxide was synthesized following the *Improved Hummers Method* slightly modified [2]. A mixture of 15 grams of graphite and 45 grams of $KMnO_4$ (oxidizer agent) was slowly added to 400 ml of H_2SO_4

under constant agitation. The mixture was maintained at 50ºC for 3 hours. Then, the mixture was added to a beaker containing a mixture of 400 g of flake ice and 3 ml of H_2O_2 to stop the oxidation reaction. The mixture was filtered under vacuum; then, it was washed with 200 ml of deionized water, HCl and CH_3CH_2OH. Finally, the compact cake was dried at 100ºC overnight.

8.2.2.2. Synthesis of Graphene oxide (GO)

Graphene oxide synthesis was carried out by graphite oxide exfoliation. Thus, a mixture of 800 mg of graphite oxide and 800 ml of deionized water was introduced in a cooling jacketed reactor to maintain the solution at room temperature. The mixture was sonicated (50% amplitude and a complete cycle) for 2 hours in order to separate the graphene sheets of graphite oxide to obtain graphene oxide [27]. The final mixture was centrifuged to precipitate the graphene oxide and the obtained solid was dried overnight at 80ºC.

8.2.2.3. Synthesis of Reduced Graphene oxide: Reduction strategies

- **Chemical reduction**

Chemical reduction of graphene oxide was carried out using two different oxidizing agents: hydrazine and ascorbic acid. As commented above, hydrazine was selected because of its powerful reduction capacity but it is a very toxic product, which is also detrimental for the environment. For this reason, an alternative reducer agent, ascorbic acid, was proposed. This agent is innocuous and environmentally friendly.

The chemical reduction with hydrazine was carried out by mixing 800 ml of graphene oxide solution with hydrazine monohydrate in a relation 1:1. The mixture was maintained under constant agitation at 90ºC for 3 hours [19]. After reduction, the dissolution was centrifuged to precipitate the ***H****ydrazine* ***R****educed* ***G****raphene* ***O****xide* (H-RGO). The product was filtered and washed until pH=7 with deionized water to

eliminate the remaining hydrazine. Finally, the obtained solid was dried at 80ºC overnight.

The chemical reduction with ascorbic acid was carried out by mixing 800 ml of graphene oxide solution and 800 mg of ascorbic acid. The reduction was maintained under constant agitation for 48 hours at room temperature [25]. After the reduction, the dissolution was centrifuged to precipitate the ***A**scorbic acid **R**educed **G**raphene **O**xide* (A-RGO). The product was filtered and washed several times with deionized water (until pH=7) to remove the remaining acid. Finally, the obtained solid was dried overnight at 80ºC.

- **Thermal reduction**

Thermal reduction process was carried out by introducing graphite oxide in a laboratory drying oven at low temperatures (<300ºC). The material expansion took place after a certain time, separating the graphene layers and, removing some oxygen functional groups from the structure. The obtained product was named as **T**hermally **R**educed **Gr**aphite **O**xide (T-RGrO).

After thermal reduction, T-RGrO was sonicated (30% amplitude) for 2 hours to complete its exfoliation obtaining **T**hermally **R**educed **G**raphene **O**xide (T-RGO).

- **Multiphase reduction**

Multiphase reduction was carried out by combining the two previously commented reduction strategies (thermal reduction followed by the chemical one, using both hydrazine and ascorbic acid as reducing agents). The product obtained by thermal reduction followed by hydrazine chemical reduction was named as **H**ydrazine **M**ulti**P**hase **R**educed **G**raphene **O**xide (HMP-RGO) whereas the product obtained by thermal reduction followed by ascorbic acid chemical reduction was

named as **A**scorbic acid **M**ulti**P**hase **R**educed **G**raphene **O**xide (AMP-RGO).

8.2.3. Characterization techniques

The Fourier transform infrared (FTIR) spectra analysis was carried out on a *SPECTRUM TWO* spectrometer (Perkin Elmer, Inc). Raman spectra were obtained with a *SENTERRA* spectrometer using an excitation wavelength of 532 nm. Thermogravimetric analysis (TGA) data were recorded on a *METTLER TOLEDO TGA/DSC1* instrument at a heating rate of 10 °C min^{-1} using air atmosphere. The morphology of the samples was observed with scanning electron microscopy (SEM) (*Phenom ProX*). Elemental analysis was carried out using the EDX software of SEM equipment. The powder X-ray diffraction (XRD) analysis was performed on a diffractometer (*PHILIPS, PW-1711*) with CuKα radiation (λ = 1.5404 Å). Characteristic crystallographic parameters (interlaminar space (d_{002}); crystal stack height (L_c); in-plane crystallite size (L_a) and, number of graphene layers in the crystal (N_c)) were determined as follows [28, 29]:

$$d_{002} = \frac{\lambda}{2 \cdot sen\theta_1}; \quad L_c = \frac{k_1 \cdot \lambda}{FWHM \cdot cos\theta_1}; \; La(nm) = \frac{k_2 \cdot \lambda}{FWHM \cdot cos\theta_2}; \; N_c = \frac{L_c}{d_{002}}$$

where:

- λ, radiation wavelength (λ =0,15404 nm)
- θ_1, [002] and [001] diffraction peak position (º)
- θ_2, [100] diffraction peak position (º)
- k_1, form factor (k=0,9)
- k_2, Warren Form Factor constant (k=1,84)
- $FWHM$, width at half height of the corresponding diffraction peak (rad)

8.3. Results and discussion

Different reduction methods (e.g. chemical, thermal and multistep techniques) have been used to maximize the removing of oxygen functional groups in graphite oxide.

Figure 2 shows the oxygen and carbon atoms content (wt. %) of the different graphene-based materials prepared in this study. Graphite, the non-oxidized raw material, is composed by 100% of carbon atoms. After the oxidation process to obtain graphite oxide (GrO), the content of oxygen as part of a functional group was increased to up 51.7%. Graphene oxide (GO), obtained after GrO exfoliation by means of sonication, showed an oxygen content like that of GrO (52%) which seems logical due to sonication is a physical process and not a chemical one.

It was confirmed that hydrazine was more effective than ascorbic acid as the reducing agent, because oxygen functional groups were reduced from 52% (graphene oxide) to 33.3 % in H-RGO and 40.5% in A-RGO, respectively. Thus, only 22% of the oxygen groups were removed using ascorbic acid whereas about 36% of them were removed using hydrazine.

Removal of oxygenated functional groups by thermal reduction is mainly due to CO and CO_2 evolution, which involves the generation of atomic vacancies and voids into the structure. Although the elimination of an isolated functional group in graphene (e.g., an epoxy group removed as CO) is energy costly, the process is enhanced both thermodynamic and kinetically in presence of more oxygen functional groups located ones next to other. In other words, the functional oxygen group energy stabilizes both the final structure and the transition states [30]. The high oxygen density in graphite oxide allows to eliminate much of the oxygen present therein at unusually low temperatures (150-300 °C). The remaining oxygen functional groups in the structure are

most likely in the form of isolated groups, thus requiring much higher temperatures for their removal. Recent studies have shown that high temperatures (1050 ºC) are necessary to completely remove oxygen groups of graphene oxide [34]. Finally, temperatures higher than 2000 ºC allows to remove structural defects remaining in this material.

After the thermal reduction process, the percentage of oxygen was decreased from 51.7% (GrO) to 37% (T-RGrO), removing around 28% of functional oxygen groups. Again, the T-RGrO exfoliation by sonication to obtain T-RGO did not affect the oxygen percentage, which is kept practically constant (37%).

Finally, elemental analysis of the reduced graphene samples prepared by the multistep method (HMP-RGO and AMP-RGO, when hydrazine and ascorbic acid were used as the reducing agents, respectively) demonstrated the effectiveness of this oxygen removing technique. Thus, around 30% and 27% of the carbon atoms remained in the HMP-RGO and AMP-RGO structures after the reduction. Consequently, AMP-RGO is the material for which higher degree of reduction was attained.

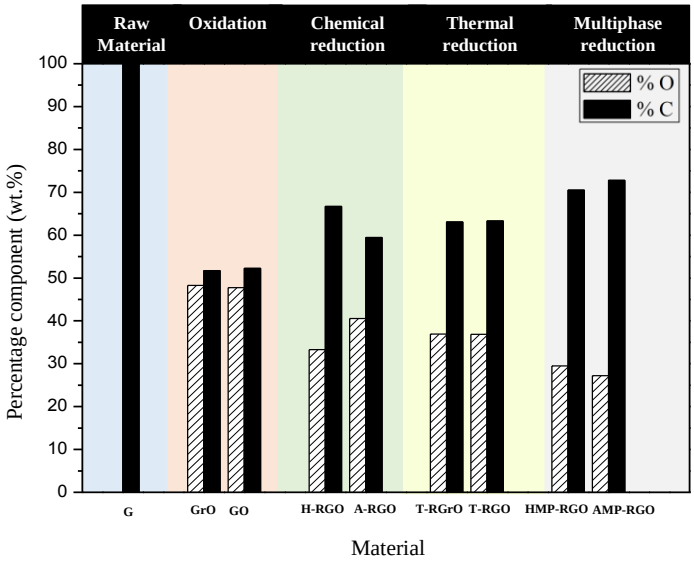

Figure 2. Elemental analysis of graphite (G), graphite oxide (GrO), graphene oxide (GO) and reduced graphene oxide samples.

Figure 3 shows the TGA and DTG profiles corresponding to graphite (G), graphite oxide (GrO) and graphene oxide (GO). Regarding graphite, the corresponding TGA curve confirmed its high thermal stability, which did not start its decomposition until 650°C, losing around 92% of its mass at 900ºC [31]. Graphite oxide and graphene oxide showed similar TGA curves. In both cases, three different weight loss steps could be differentiated. The first one (I), appearing between 0 and 200°C, was mainly due to the elimination of both water solvent molecules and the decomposition of the more labile oxygen functional groups [32]. Regarding GO, the weight loss corresponding in this first step (21%) was lower than that observed for GrO (37%), indicating that sonication and subsequent drying of graphite oxide considerably reduced the amount of water molecules in the resulted material. The second weight loss step (II), occurring between 200 and 475°C, was due to the removal of the more stable oxygen groups. Similar weight loss was observed for both GrO and GO (27% and 28%, respectively), indicating that both materials had the same stable oxygen functional

groups. Finally, a third step (III) for temperatures above 475°C was observed, which was a consequence of the material thermal degradation (unstable carbon remaining in the structure yields CO and CO_2 [33]), losing around 30% of the remaining mass.

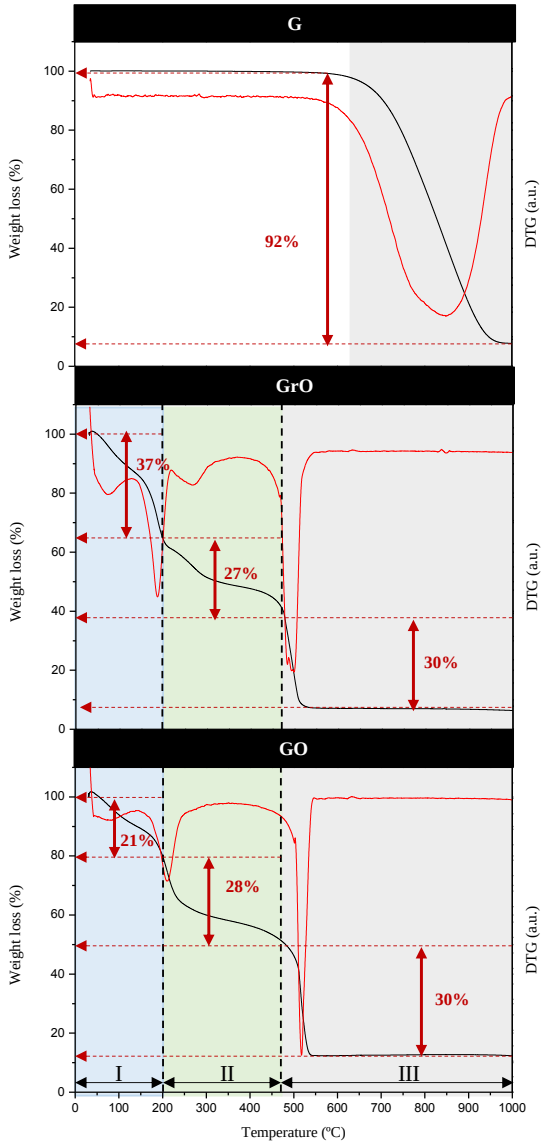

Figure 3. TGA and DTG curves of graphite (G), graphite oxide (GrO) and graphene oxide (GO).

Thermogravimetric analyses results were corroborated by FTIR (Figure 4). FTIR spectrum of graphite showed the absence of bonds different from those expected in its structure. After the oxidation process, several functional groups were incorporated into the structure (Table 1) [33, 34].

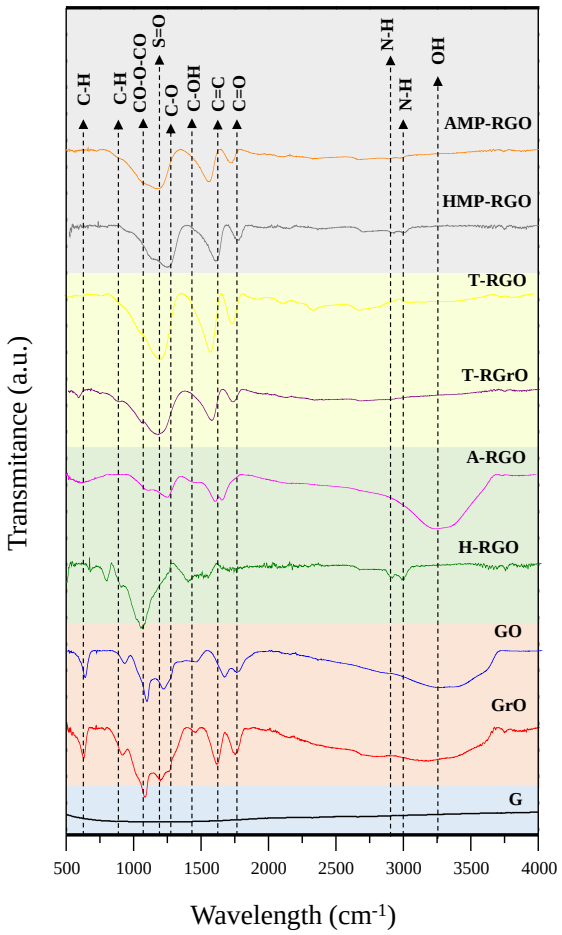

Figure 4. FTIR analyses of graphite (G), graphite oxide (GrO), graphene oxide (GO) and reduced graphene oxide samples.

Table 1. Functional groups present in graphite (G), graphite oxide (GrO), graphene oxide (GO) and reduced graphene oxide samples [35].

Functional groups	Wavelength (cm^{-1})
C-H (CH group)	755-900
CO-O-CO (Anhidride group)	1050
C-O (Ether group)	1275
C=C (Alkene group)	1650
C=O (Ester, aldehyde and carboxilic acid groups)	1720-1780
n-h (Amine group)	2800-3000
C-OH (Hydroxil group)	1420, 3700

Figure 5 shows TGA and DTG curves corresponding to the reduced graphene oxide samples obtained through different reduction strategies. Three different weight loss steps was also observed, confirming that the superior reduction power of hydrazine if is compared to that of the ascorbic acid. Thus, H-RGO sample showed a minimum weight loss in step (I) (≈ 2%), which was linked to the elimination of the most labile oxygen groups after the reduction process. Nevertheless, sample A-RGO showed a step (I) weight loss of 25%, demonstrating that the more labile oxygen groups were not completely removed from graphene oxide structure after the reduction process. On the other hand, the weight loss corresponding to step (II) was quite similar for both chemically reduced samples, being the weight loss associated to step (III) higher in sample H-RGO (66%) than in A-RGO (45%) due to its higher amount of unstable carbon (see elemental analysis results). These results were also corroborated by FTIR analysis (Figure 4). Thus, in sample H-RGO the broad band corresponding to hydroxyl groups (around 3700 cm^{-1}) disappeared due to hydrazine attacks to the OH groups by nucleophilic substitution [36] causing different hydrogen bond rearrangements [33]. On the other hand, two new small bands appearing at 2899 cm^{-1} and 3000 cm^{-1} were appreciated due to the tendency of the oxygen functional groups to form complex structures with nitrogen (azide complex). These results are in good agreement with those reported by *Chua et al.* [37], whom demonstrated

through a computational study that hydrazine reduction removed favourably OH groups present in the graphene oxide basal plane.

For its part, A-RGO spectrum showed that the hydroxyl groups were not completely removed after the reduction process. Other oxygen functional groups that were partially removed after hydrazine/ascorbic acid reduction were C=O groups (1770cm^{-1}) associated to esters, aldehydes and carboxylic acids, and C=C groups (1650 cm^{-1}), corresponding to phenolic rings, which is a consequence of their interaction with the reducing agent causing bond deformations [33].

TGA curves corresponding to thermally reduced samples (T-RGrO and T-RGO) did not shown any weight loss during step (I) confirming the elimination of almost all the labile functional groups and water molecules. Weight loss corresponding to step (II) was quite similar in samples T-RGrO and T-RGO (around 20-23%), indicating that most of the more stable oxygen groups remained in the structure after thermal reduction. Finally, material thermal degradation started at temperatures above 500-550ºC, showing a step (III) weight loss of around 70% [12].

FTIR analysis of samples T-RGrO and T-RGO showed that hydroxyl groups were practically removed after the thermal reduction, disappearing completely the broadband occurring at around 3700 cm^{-1} [33, 34]. Furthermore, bands corresponding to C-O (1275 cm^{-1}) and C=O groups (1770 cm^{-1}) were partially removed after the violent thermal expansion happened.

TGA curves corresponding to multiphase reduced samples (HMP-RGO and AMP-RGO) were similar to those of the thermally reduced ones; e.g. TGA curves did not show any weight loss in step (I) confirming the elimination of almost all the labile functional groups and water molecules. Around 20% of the mass was lost in step (II) due to the partial removal of the more stable oxygen groups. Finally, total thermal

decomposition of the reduced graphene oxide samples took place around 550ºC. Again, these results were confirmed by FTIR analyses, where no band associated to –OH groups was observed. In addition, C-O or C=O groups were also partially removed after multiphase reduction. Bands associated to complexes structures with nitrogen (complex azide) appeared in sample HMP-RGO due to the action of the hydrazine [37]. Regardless of the reduction technique, C-H groups (755-900 cm^{-1}) were almost completely removed.

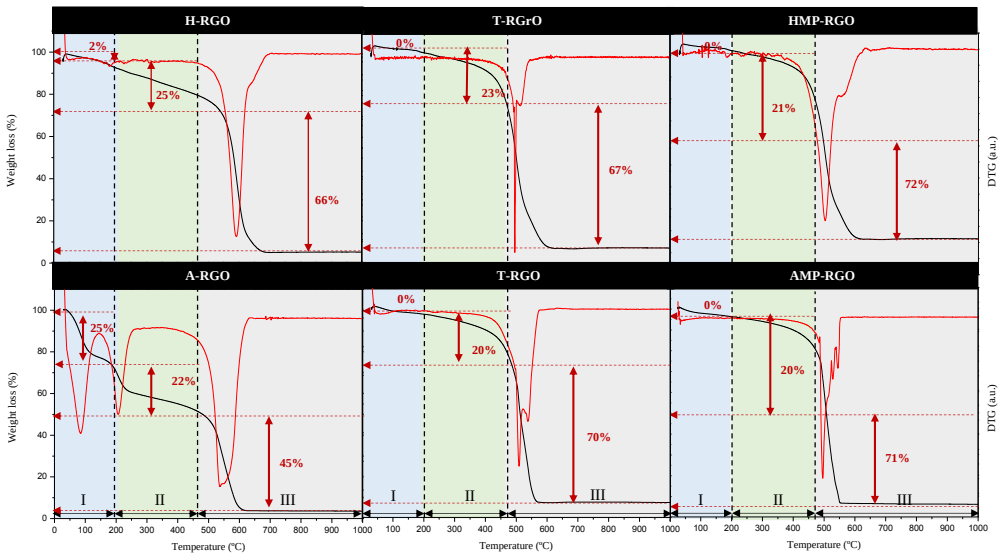

Figure 5. TGA and DTG curves of reduced graphene oxide samples.

Raman spectroscopy is considered a very interesting tool in the study of carbon nanomaterials due to its quickness and trustworthiness [38]. Raman spectrum and the most characteristics Raman parameters corresponding to both GrO and GO are shown in Figure 6 and Table 2, respectively. The two characteristic peaks (D and G) could be easily differentiated. D peak, which appears around 1348 cm^{-1}, indicates the presence of imperfections in the graphitic structure of carbon atoms at the layer edges [39]. G peak is related to the movement of pairs of carbon atoms linked by sp^2 bonds and this is located at 1586 cm^{-1}. This peak is

commonly related to the graphitic order [40]. Thus, the broad G band and the more prominent D one associated with GrO and GO (when compared to graphite) indicate a reduction in the size of the sp^2 domains due to oxidation. The relationship between the intensities of the two peaks (I_D/I_G) will be used to compare the way in which the structural disorder grows in the graphitic network. The locations of both D and G bands and the ratio between their intensities are consistent with the characteristic values reported elsewhere [36].

When pristine graphite was oxidized to GrO, the I_D/I_G ratio of the resulting material significantly increased indicating a higher level of structural disorder and a larger number of defects in the graphene layers due to the oxidation process. After sonication to obtain GO, I_D/I_G relationship in the resulting material lightly increased, indicating that exfoliation process also incorporated further defects in the structure. Logically, the distance between defects (determined as $L_D=\sqrt{C\ (\lambda)/(ID/IG)}$, being $C(\lambda)=102$ nm² [41], decreased from graphite to both GrO and GO [34].

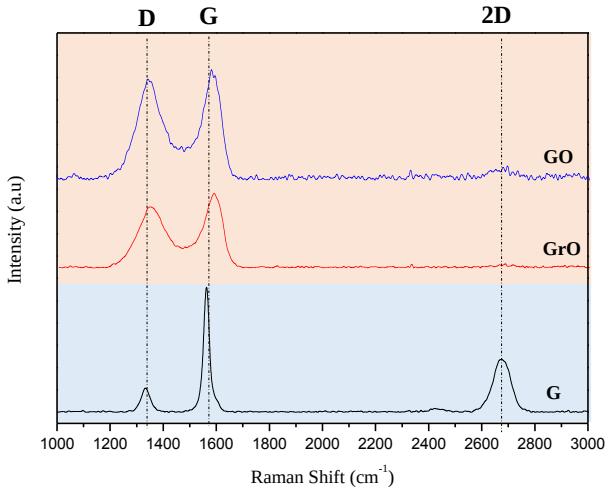

Figure 6. Raman spectra of graphite (G), graphite oxide (GrO) and graphene oxide (GO).

Table 2. Raman and XRD characteristic parameters of graphite (G), graphite oxide (GrO) and graphene oxide (GO) and reduced graphene oxide samples.

	XRD						RAMAN	
Sample	2θ(º) [002] or $[001]_{peak}$	L_c (nm)	d_{002} (nm)	N_c	2θ(º) $[100]_{peak}$	L_a (nm)	I_D/I_G	L_D (nm)
G	26.58	37.10	0.34	111	-	-	0.19	23.2
GrO	9.96	4.43	0.89	5	42.43	11.03	0.94	10.4
GO	9.15	3.75	0.97	4	42.77	5.79	0.99	10.2
H-RGO	24.19	1.06	0.37	3	43.11	2.63	1.25	9
A-RGO	23.56	1.38	0.38	4	43.51	4.55	1.16	9.4
T-RGrO	23.7	1.61	0.37	4	43.33	4.50	0.96	10.3
T-RGO	23.02	0.92	0.39	3	43.68	3.59	0.97	10.3
HMP-RGO	21.4	0.96	0.40	2	43.57	5.17	1.18	9.3
AMP-RGO	22.09	0.97	0.41	2	43.24	6.28	1.15	9.4

Results derived from Raman spectra were corroborated by XRD analysis. Figure 7 shows X-Ray diffraction patterns whereas Table 2 lists the characteristic XRD parameters corresponding to graphite, GrO and GO. Graphite showed a [002] peak at a 2θ value of around 26.6°, which is consistent with a separation between layers (d_{002}) of 0.34 nm. After oxidation, [002] peak disappeared, appearing two new peaks: [001] at 2θ≈ 9.9º, and [100] at 2θ≈ 42.5º. As consequence, the interlayer distance (d_{002}) clearly increased while the crystal domains (both the crystal stack height, L_c and the in-plane crystallite size, L_a) decreased after the oxidation process. The d_{002} increase was attributed to the expansion caused by the presence of oxygen functional groups and water molecules located in the interlayer galleries of the hydrophilic GrO and GO samples. For its part, crystallite domains reduction indicated that an increase in the structural disorder occurred after the oxidation process (GrO) and subsequent exfoliation to yield GO. Finally, the number of layers in the stacking structure (N_c) decreased markedly after graphite

oxidation and subsequent sonication, which was related not only to the graphene layer separation but also to the crystallinity loss in the ultimate material.

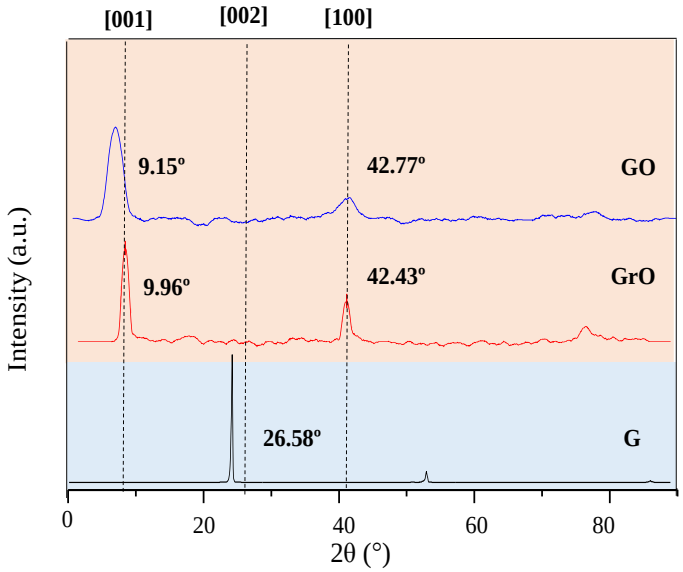

Figure 7. XRD spectra of graphite (G), graphite oxide (GrO) and graphene oxide (GO).

Raman spectra and characteristics Raman parameters corresponding to the reduced graphene samples are shown in Figure 8 and Table 2, respectively. As observed, I_D/I_G ratio increased after chemical reduction indicating that not only the oxidation but also the chemical reduction process contributed to an increase of the structural disorder, which was much higher in sample H-RGO than in sample A-RGO. As above mentioned, hydrazine removed oxygen functional groups more efficiently than ascorbic acid, as corroborated by elemental and FTIR analyses.

Both chemically reduced products showed characteristics values of I_D/I_G, which ranged from 1.14 to 1.28 [34]. As expected, distance between defects (L_D) was higher for sample A-RGO due to it presented a lower number of defects.

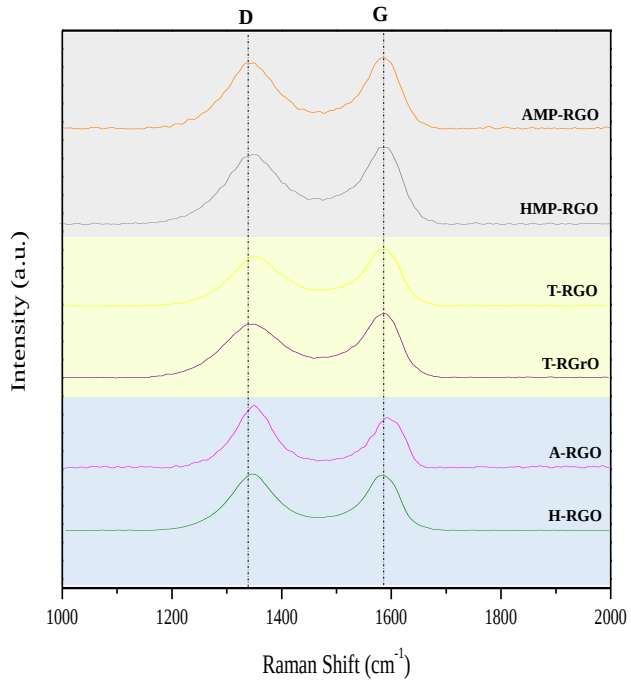

Figure 8. Raman spectra of reduced graphene oxide samples.

XRD analysis (Figure 9) showed that when GO was chemically reduced peak [001] was widener and shifted to higher 2θ values, due to the tendency of the reduced material to recover the original graphite structure although the crystallinity of the resulting material is reduced. As observed, d_{002} and crystal domains (Lc and La) decreased after chemical reduction due to the structural disorder increase, obtaining a higher reduction in the case of sample H-RGO due to the above mentioned high reduction power of hydrazine.

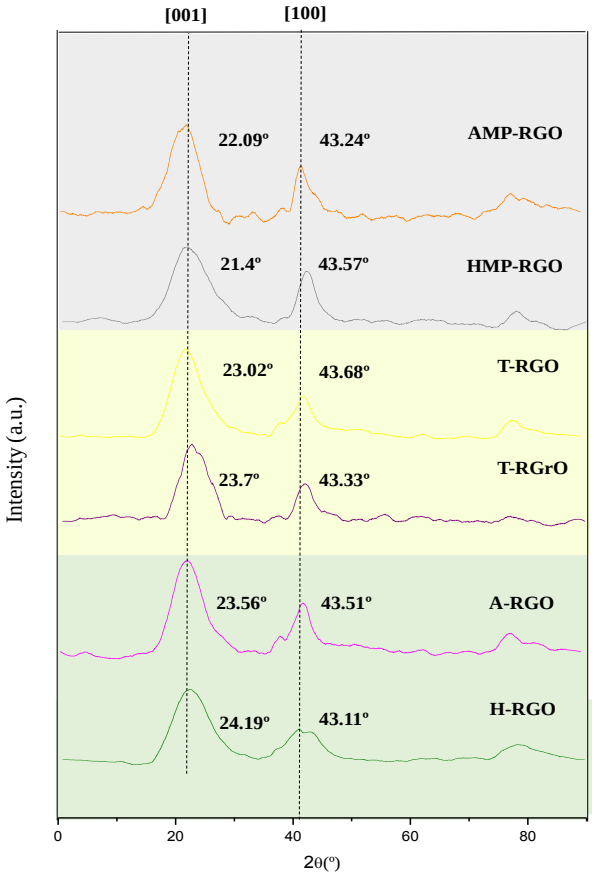

Figure 9. XRD spectra of reduced graphene oxide samples.

On the other hand, after thermal reduction both I_D/I_G ratio and distance between defects (L_D) presented a similar tendency as the non-reduced material (GrO). In other words, thermal expansion, which removed mainly the more labile oxygen functional groups (mostly located out of the basal plane [18]), did not practically contributed to add further structural defects in the resulting reduced material. Similar Raman results were obtained for samples T-RGrO and T-RGO, which agree well with thermal and elemental analysis results.

XRD patterns of samples T-RGrO and T-RGO were quite similar. Again, d_{002} and crystal domains decreased after the reduction process. Note that

L_a and L_c values considerably decreased after the exfoliation indicating that the T-RGrO sonication to obtain T-RGO caused not only the exfoliation of the structure but also the breakage of the crystal structure.

Finally, Raman spectra of multiphase reduced samples showed that when hydrazine was used as the reducing agent the number of defects in the final material (HMP-RGO) were slightly higher than that evaluated when ascorbic acid was used (AMP-RGO), due to hydrazine attacks more intensely the structure increasing the number of defects. This fact was also evidenced by XRD measurements where crystal domains were slightly higher in sample AMP-RGO than in sample HMP-RGO.

Morphological properties of the different materials here used, evaluated by Scanning Electron Microscopy (SEM), are shown in Figure 10. Graphite structure showed a crystalline platelet-like structure with well-defined sheets. After the oxidation process, sample GrO presented a damaged structure. GO showed a single flakes structure with relatively large surface, resembling a thin curtain, which indicates that a very good exfoliation took place after the oxidation process [33]. SEM images corresponding to reduced samples showed structures with a more developed surface, resembling cluttered products with poor crystallinity, as demonstrated by the XRD analysis.

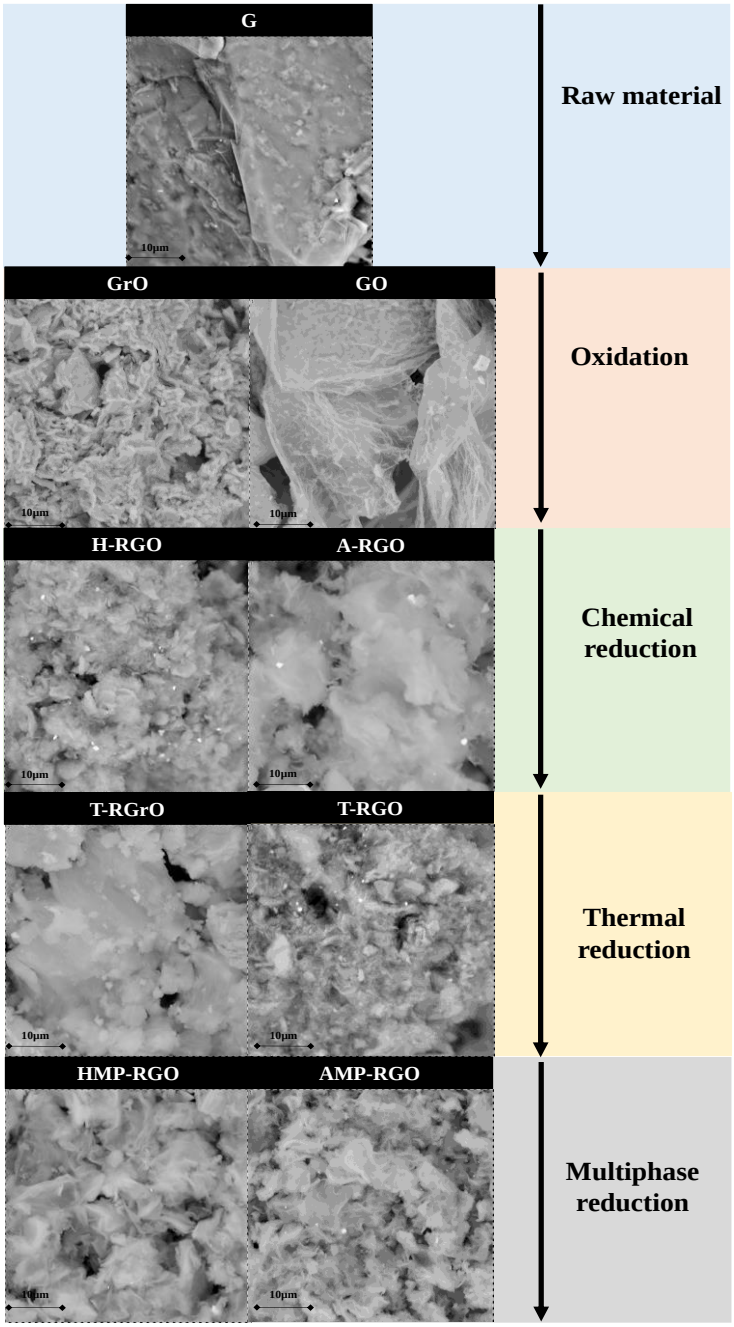

Figure 7. SEM images of graphite (G), graphite oxide (GrO), graphene oxide (GO) and reduced graphene oxide samples

8.4. Conclusions

In this work, different graphene–reduction strategies were used to synthesize reduced graphene oxide. An optimization of the most popular oxidation route reported in the literature (*Improved Hummers Method*) was used to obtain graphite oxide. Subsequently, different sets of reduced graphene oxide powders were synthesized employing three different reduction routes: chemical (hydrazine/ascorbic acid), thermal and a multiphase method, yielding eight separate final products.

Obtained results showed that the multiphase reduction method, resulting from the combination of more than one reduction route, specifically, thermal and chemical ones, led to an effective removal of functional oxygen groups. Thus, a mild thermal treatment followed by the chemical reduction of graphene oxide using ascorbic acid, as the reducing agent, showed a functional groups reduction of 47%. A detailed characterization of these material confirmed the removal of the most labile functional oxygen groups and some of the other one more stable, without appreciating an increase in the number of structural defects and limiting the extension of lattice reconstruction after reduction. This work has showed that the reduced graphene oxide structure is highly dependent on the reduction strategy followed.

8.5. References

1. Tour, J. M., *Top-Down versus Bottom-Up Fabrication of Graphene-Based Electronics.* Chemistry of Materials, 2014, **26** (1): p. 163-171.
2. Hummers Jr, W. S. and Offeman, R. E., *Preparation of graphitic oxide.* Journal of the American Chemical Society, 1958, **80** (6): p. 1339.
3. Park, S. and Ruoff, R. S., Nature Nanotechnol., 2009, **4**: p. 217.
4. Shao, G., Lu, Y., Wu, F., Yang, C., Zeng, F. and Wu, Q., *Graphene oxide: The mechanisms of oxidation and exfoliation.* Journal of Materials Science, 2012, **47** (10): p. 4400-4409.

5. Abel, L. L., Levy, B. B., Brodie, B. B. and Kendall, F. E., *A simplified method for the estimation of total cholesterol in serum and demonstration of its specificity.* The Journal of biological chemistry, 1952, **195** (1): p. 357-366.
6. Staudenmaier, L., *Verfahren zur darstellung der graphitsäure.* Berichte der Deutschen Chemischen Gesellschaft 1898, **31**: p. 1481-1487.
7. Marcano, D. C., Kosynkin, D. V., Berlin, J. M., Sinitskii, A., Sun, Z., Slesarev, A., Alemany, L. B., Lu, W. and Tour, J. M., *Improved synthesis of graphene oxide.* ACS Nano, 2010, **4** (8): p. 4806-4814.
8. Erickson, K., Erni, R., Lee, Z., Alem, N., Gannett, W. and Zettl, A., *Determination of the local chemical structure of graphene oxide and reduced graphene oxide.* Advanced Materials, 2010, **22** (40): p. 4467-4472.
9. Bagri, A., Mattevi, C., Acik, M., Chabal, Y. J., Chhowalla, M. and Shenoy, V. B., *Structural evolution during the reduction of chemically derived graphene oxide.* Nat Chem, 2010, **2** (7): p. 581-587.
10. Pei, S. and Cheng, H. M., *The reduction of graphene oxide.* Carbon, 2012, **50** (9): p. 3210-3228.
11. Huh, S. H., *Thermal Reduction of Graphene Oxide, Physics and Applications of Graphene - Experiments,*, Mikhailov, D. S., Editor. 2011, InTech.
12. McAllister, M. J., Li, J. L., Adamson, D. H., Schniepp, H. C., Abdala, A. A., Liu, J., Herrera-Alonso, M., Milius, D. L., Car, R., Prud'homme, R. K. and Aksay, I. A., *Single sheet functionalized graphene by oxidation and thermal expansion of graphite.* Chemistry of Materials, 2007, **19** (18): p. 4396-4404.
13. Zhang, Y., Guo, L., Wei, S., He, Y., Xia, H., Chen, Q., Sun, H. B. and Xiao, F. S., *Direct imprinting of microcircuits on graphene oxides film by femtosecond laser reduction.* Nano Today, 2010, **5** (1): p. 15-20.

14. Ramesha, G. K. and Sampath, N. S., *Electrochemical reduction of oriented Graphene oxide films: An in situ Raman spectroelectrochemical study.* Journal of Physical Chemistry C, 2009, **113** (19): p. 7985-7989.
15. Zhu, Y., Murali, S., Stoller, M. D., Velamakanni, A., Piner, R. D. and Ruoff, R. S., *Microwave assisted exfoliation and reduction of graphite oxide for ultracapacitors.* Carbon, 2010, **48** (7): p. 2118-2122.
16. Wang, H., Robinson, J. T., Li, X. and Dai, H., *Solvothermal reduction of chemically exfoliated graphene sheets.* Journal of the American Chemical Society, 2009, **131** (29): p. 9910-9911.
17. Stankovich, S., Dikin, D. A., Piner, R. D., Kohlhaas, K. A., Kleinhammes, A., Jia, Y., Wu, Y., Nguyen, S. T. and Ruoff, R. S., *Synthesis of graphene-based nanosheets via chemical reduction of exfoliated graphite oxide.* Carbon, 2007, **45** (7): p. 1558-1565.
18. Chua, C. K. and Pumera, M., *Chemical reduction of graphene oxide: a synthetic chemistry viewpoint.* Chemical Society Reviews, 2014, **43** (1): p. 291-312.
19. Park, S., An, J., Potts, J. R., Velamakanni, A., Murali, S. and Ruoff, R. S., *Hydrazine-reduction of graphite- and graphene oxide.* Carbon, 2011, **49** (9): p. 3019-3023.
20. Gao, W., Alemany, L. B., Ci, L. and Ajayan, P. M., Nature Chem., 2009, **1**: p. 403.
21. Si, Y. and Samulski, E. T., Nano Letters, 2008, **8**: p. 1679.
22. Nethravathi, C. and Rajamathi, M., Carbon, 2008, **46**: p. 1994.
23. Schirmann, J.-P. and Bourdauducq, P., *Hydrazine*, in *Ullmann's Encyclopedia of Industrial Chemistry*. 2000, Wiley-VCH Verlag GmbH & Co. KGaA.
24. Lachapelle, M. Y. and Drouin, G., *Inactivation dates of the human and guinea pig vitamin C genes.* Genetica, 2010, **139** (2): p. 199-207.
25. Zhang, J., Yang, H., Shen, G., Cheng, P. and Guo, S., *Reduction of graphene oxide vial-ascorbic acid.* Chemical Communications, 2010, **46** (7): p. 1112-1114.

26. Ding, H., Zhang, S., Chen, J. T., Hu, X. P., Du, Z. F., Qiu, Y. X. and Zhao, D. L., *Reduction of graphene oxide at room temperature with vitamin C for RGO-TiO<inf>2</inf> photoanodes in dye-sensitized solar cell.* Thin Solid Films, 2015, **584**: p. 29-36.
27. Choucair, M., Thordarson, P. and Stride, J. A., *Gram-scale production of graphene based on solvothermal synthesis and sonication.* Nature nanotechnology, 2009, **4** (1): p. 30-33.
28. Stobinski, L., Lesiak, B., Malolepszy, A., Mazurkiewicz, M., Mierzwa, B., Zemek, J., Jiricek, P. and Bieloshapka, I., *Graphene oxide and reduced graphene oxide studied by the XRD, TEM and electron spectroscopy methods.* Journal of Electron Spectroscopy and Related Phenomena, 2014, **195**: p. 145-154.
29. Warren, B. E., *X-Ray Diffraction in Random Layer Lattices.* Physical Review, 1941, **59** (9): p. 693-698.
30. Sun, T., Fabris, S. and Baroni, S., *Surface precursors and reaction mechanisms for the thermal reduction of graphene basal surfaces oxidized by atomic oxygen.* Journal of Physical Chemistry C, 2011, **115** (11): p. 4730-4737.
31. Crumpton, D. M., Laitinen, R. A., Smieja, J. and Cleary, D. A., *Thermal analysis of carbon allotropes: An experiment for advanced undergraduates.* Journal of Chemical Education, 1996, **73** (6): p. 590-591.
32. Fernández-Merino, M. J., Guardia, L., Paredes, J. I., Villar-Rodil, S., Solís-Fernández, P., Martínez-Alonso, A. and Tascón, J. M. D., *Vitamin C is an ideal substitute for hydrazine in the reduction of graphene oxide suspensions.* Journal of Physical Chemistry C, 2010, **114** (14): p. 6426-6432.
33. Loryuenyong, V., Totepvimarn, K., Eimburanapravat, P., Boonchompoo, W. and Buasri, A., *Preparation and Characterization of Reduced Graphene Oxide Sheets via Water-Based*

Exfoliation and Reduction Methods. Advances in Materials Science and Engineering, 2013, **2013**: p. 5.

34. Eigler, S., Dotzer, C. and Hirsch, A., *Visualization of defect densities in reduced graphene oxide.* Carbon, 2012, **50** (10): p. 3666-3673.
35. Chemistry. *Infrared Spectroscopy Absorption Table*. 2014 [cited 2016 06-10-2012]; Available from: http://chem.libretexts.org/.
36. Gao, J., Liu, F., Liu, Y., Ma, N., Wang, Z. and Zhang, X., *Environment-friendly method to produce graphene that employs vitamin C and amino acid.* Chemistry of Materials, 2010, **22** (7): p. 2213-2218.
37. Chua, C. K. and Pumera, M., *The reduction of graphene oxide with hydrazine: elucidating its reductive capability based on a reaction-model approach.* Chemical Communications, 2016, **52** (1): p. 72-75.
38. Kudin, K. N., Ozbas, B., Schniepp, H. C., Prud'homme, R. K., Aksay, I. A. and Car, R., Nano Letters, 2008, **8**: p. 36.
39. Fernández, P. S., *Modificación superficial de materiales de carbono: grafito y grafeno.* Departamento de Ciencia de los Materiales e Ingeniería Metalúrgica. Universidad de Oviedo, 2011.
40. Ferrari, A. C. and Robertson, J., *Interpretation of Raman spectra of disordered and amorphous carbon.* Physical Review B - Condensed Matter and Materials Physics, 2000, **61** (20): p. 14095-14107.
41. Lucchese, M. M., Stavale, F., Ferreira, E. H. M., Vilani, C., Moutinho, M. V. O., Capaz, R. B., Achete, C. A. and Jorio, A., *Quantifying ion-induced defects and Raman relaxation length in graphene.* Carbon, 2010, **48** (5): p. 1592-1597.

Conclusiones

De los resultados obtenidos en la presente tesis doctoral se pueden derivar las siguientes conclusiones:

- El método de Deposición Química en fase Vapor a presión atmosférica usando nitrógeno (N_2) como gas inerte, hidrógeno (H_2) como gas reductor y metano (CH_4) como fuente carbonosa, es una técnica viable para sintetizar grafeno sobre diferentes substratos metálicos.

- Se pueden diferenciar dos mecanismos de crecimiento de grafeno en función de la solubilidad hacia el carbón que presente el catalizador metálico empleado: *Bottom-Up* y *Top Down*.

- El uso de cobre policristalino como catalizador permite la síntesis de grafeno bicapa, pocas capas y multicapa en las condiciones de operación estudiadas.

- Las condiciones óptimas de síntesis usando cobre policristalino como catalizador son: 1050ºC, 10 minutos de reacción, relación CH_4/H_2 de 0,07 y caudal total de gases (CH_4+H_2) durante la etapa de reacción de 60 Nml/min.

- La transferencia de grafeno sintetizado por el método CVD usando cobre policristalino como catalizador sobre substratos arbitrarios (obleas de PET y placas de microscopio óptico) se puede llevar a cabo empleando diferentes agentes químicos tales como: $FeCl_3$ (usando normalmente en bibliografía), $HF:2Na_2CO_3{\cdot}3H_2O_2$ (4:1) y H_2O_2 (30%p./v.):agua regia ($1HNO_3$:3HCl):H_2O (1:1:2).

- El uso de hierro y níquel policristalino como catalizadores, permiten la síntesis de grafeno monocapa, bicapa, pocas capas y multicapa en las condiciones de operación estudiadas.

- Las condiciones óptimas de síntesis usando níquel policristalino como catalizador son: 980ºC, 1 minuto de reacción, relación

CH_4/H_2 de 0,07 y caudal total de gases (CH_4+H_2) durante la etapa de reacción de 80 Nml/min.

- Las condiciones óptimas de síntesis usando hierro policristalino como catalizador son: 1025ºC, 7 minutos de reacción, relación CH_4/H_2 de 0,07 y caudal total de gases (CH_4+H_2) durante la etapa de reacción de 80 Nml/min.

- Es posible introducir determinadas modificaciones al tradicional *método de Hummers Mejorado* que optimizan significativamente los costes de producción, sin alterar las propiedades y características del producto final obtenido: óxido de grafito. Dichos cambios suponen reducir el tiempo de oxidación, eliminar el H_3PO_4 como reactivo del proceso, eliminar la etapa de coagulación, reducir a la mitad las etapas de lavado y aumentar hasta cinco veces la cantidad obtenida de producto final.

- Es posible sintetizar óxido de grafeno reducido usando diferentes estrategias de reducción (reducción química, térmica y una combinación de las anteriores, conocida como de múltiples fases).

- Es posible sintetizar óxido de grafeno reducido de alta calidad usando pasa ello una estrategia de reducción basada en la combinación de una reducción térmica y química usando como agente reductor ácido ascórbico, que es inocuo y respetuoso con el medioambiente.

Recomendaciones

Con la finalidad de completar en un futuro los resultados obtenidos en la presente tesis doctoral, se recomienda:

- Estudiar nuevos catalizadores para la síntesis de grafeno por el método de Deposición Química en fase Vapor: tungsteno, aluminio, rutenio, etc.
- Investigar la influencia del gas inerte en la etapa de reacción, así como la influencia de otros gases inertes durante la síntesis de grafeno por el método CVD.
- Probar nuevas fuentes carbonosas, tales como gas natural o residuos orgánicos, en la síntesis de grafeno por el método de Deposición Química en fase Vapor.
- Considerar otros agentes oxidantes en la síntesis de óxido de grafito con la finalidad de mejorar el grado de oxidación del producto.
- Probar nuevas técnicas de reducción para mejorar la calidad de la de reducción del óxido de grafeno reducido y ensayar otros agentes reductores químicos respetuosos con el medioambiente.
- Realizar un análisis de viabilidad económica de los diferentes métodos de síntesis de grafeno estudiados.

Producción científica

De la presente tesis doctoral han derivado las siguientes publicaciones:

Artículos en revisión:

- *Improving the continuous growth of monolayer CVD-graphene over polycrystalline iron sheets.* M.P. Lavin-Lopez, M. Fernandez-Diaz, L. Sanchez-Silva, J.L. Valverde, A. Romero. Submited to: Chemical Engineering Journal.
- *Synthesis and characterization of reduced graphene oxide: influence of the reduction strategy.* M.P. Lavin-Lopez, A. Paton-Carrero, L. Sanchez-Silva, J.L. Valverde, A. Romero. Submited to: Carbon.

Artículos publicados:

- *Synthesis and characterization of graphene: Influence of synthesis variables.* M.P. Lavin-Lopez, J.L. Valverde, M.C. Cuevas, A. Garrido, L. Sanchez-Silva, P. Martinez, A. Romero-Izquierdo. ***Physical Chemistry Chemical Physic***, 2014,**16**, 2962-2970
- *Novel etchings to transfer CVD-grown graphene from copper to arbitrary substrates.* M.P. Lavin-Lopez, J.L. Valverde, A. Garrido, L. Sanchez-Silva, P. Martinez, A. Romero-Izquierdo. ***Chemical Physic Letter***, 2014, **614**, 89-94.
- *Thickness control of graphene deposited over polycrystalline nickel.* M.P. Lavin-Lopez, J.L Valverde, M.I. Ruiz-Enrique, L. Sanchez-Silva, A. Romero. ***New Journal of Chemistry***, 2015, **39**, 4414-4423.
- *Influence of the total gas flow at different reaction times for CVD-graphene synthesis on polycrystalline nickel.* M.P. Lavin-Lopez, J.L Valverde, L. Sanchez-Silva, A. Romero. ***Journal of Nanomaterials***, 2016, **2016**, Número de artículo 7083284.

- *Lavin-Lopez, M. d. P., Romero, A., Garrido, J., Sanchez-Silva, L. and Valverde, J. L., Influence of Different Improved Hummers Method Modifications on the Characteristics of Graphite Oxide in Order to Make a More Easily Scalable Method.* ***Industrial & Engineering Chemistry Research****, 2016, DOI: 10.1021/acs.iecr.6b03533.*

Otras publicaciones relacionadas:

- *Solvent-based exfoliation via sonication of graphitic materials for graphene manufacture.* M.P. Lavin-Lopez, J.L Valverde, L. Sanchez-Silva, A. Romero. ***Industrials&Engineering Chemistry Research***, 2016, **55**, 845-855.

Comunicaciones a congresos:

- *Synthesis study of CNF-reinforced organic aerogel: CNF content and solvents.* L. Sanchez-Silva, S. Victor-Roman, M.P. Lavin-Lopez, A. Romero, J.L. Valverde. **NanoSmat Conference 2014**. Dublín (Irlanda). Septiembre, 2014.

- *CVD-graphene synthesis using different transition metals as catalyst.* M.P. Lavin-Lopez, J.L. Valverde, L- Sanchez-Silva, A. Romero. **Graphene&2D Materials International Conference and Exhibition 2015**. Montreal (Canada). Octubre, 2015.

- *Mejora de la calidad del grafeno depositado sobre Ni por el método de CVD.* M.P. Lavin-Lopez, J.L. Valverde, A- Romero-Izquierdo. **I Encuentro de Jóvenes Investigadores de la SECAT (JJ.II. SECAT 2014)**. Málaga. Junio, 2014.

- *Síntesis de grafeno mediante deposición química en fase vapor usando diferentes metales como catalizadores.* M.P. Lavin-Lopez, J.L. Valverde, L. Sánchez-Silva, A- Romero. **IX**

Simposio de Ciencia Joven. Facultad de Ciencias y Tecnologías Químicas de Ciudad Real. Ciudad Real. Mayo, 2015.

- *Grafeno: Síntesis y aplicaciones.* M.P. Lavin-Lopez, J.L. Valverde, L. Sánchez-Silva, A- Romero. **IV Jornadas Doctorales del Grupo 9 de Universidades (G-9).** Pamplona. Marzo, 2016.

- *Síntesis de grafeno mediante el método CVD usando hierro como catalizador.* M.P. Lavin-Lopez, J.L.Valverde, M. Fernandez-Diaz, A. Paton-Carrero, L. Sánchez-Silva, A- Romero. **II Encuentro de jóvenes investigadores de la SECAT: Catálisis como herramienta en procesos sostenibles.** Ciudad Real. Junio, 2016.

- *Synthesis and characterization of CVD-grown bilayer graphene on copper: Influence of the synthesis conditions.* M.P. Lavin-Lopez, A- Romero-Izquierdo, J.L. Valverde. **Trends in Nanotechnology (TNT2013)**. Sevilla (España). Septiembre, 2013.

- *Improving the quality of graphene synthesized by CVD over Ni substrates.* M.P. Lavin-Lopez, A- Romero-Izquierdo, J.L. Valverde. **VIII Edición de la Reunión Bienal del Grupo Especializado de Física del Estado Sólido de la Real Sociedad Española de Física (GEFES 2014).** Ciudad Real (España). Enero 2014.

- *Improving the quality of graphene synthesized by CVD over Ni substrates.* M.P. Lavin-Lopez, A. Romero-Izquierdo, L. Sanchez-Silva, J.L. Valverde. **NanoSmat Conference 2014**. Dublín (Irlanda). Septiembre, 2014.

- *Graphene obtained via sonication for the manufacture of daily products.* M.P. Lavin-Lopez,, J.L. Valverde, A. Romero. **EuroNanoForum 2015.** Riga (Letonia). Junio 2015.
- *Improving the synthesis of monolayer CVD-graphene over polycrystalline iron foils.* J.L. Valverde, A. Romero, L-Sanchez-Silva, M.P. Lavin-Lopez. **Graphene&2D Materials International Conference and Exhibition 2016**. Montreal (Canada). Octubre, 2016.
- *Síntesis y caracterización de grafeno depositado sobre cobre: Influencia de las variables de síntesis.* M.P. Lavin-Lopez, A-Romero-Izquierdo, J.L. Valverde. **I Workshop en Ingeniería Química (Organizado por FEIQ).** Ciudad Real. Noviembre, 2013.
- *Mejora de la calidad del grafeno sintetizado por el método CVD usando Ni como substrato catalítico.* M.P. Lavin-Lopez, J.L. Valverde, L. Sanchez-Silva, A. Romero-Izquierdo. **IV Jornadas Doctorales de la Universidad de Castilla-La Mancha.** Cuenca. Octubre, 2014.
- *Síntesis de grafeno mediante el método CVD usando diferentes metales de transición como catalizadores.* M.P. Lavin-Lopez, J.L. Valverde, L. Sanchez-Silva, A. Romero. **SECAT 2015.** Barcelona. Julio, 2015.
- *Grafeno, síntesis y aplicaciones*. M.P. Lavin.Lopez, J.L. Valverde, L. Sanchez-Silva, A. Romero. **V Jornadas Doctorales de la Universidad de Castilla-La Mancha.** Ciudad Real. Octubre, 2015.
- *Grafeno, síntesis y aplicaciones*. M.P. Lavin.Lopez, J.L. Valverde, L. Sanchez-Silva, A. Romero. **IV Jornadas Doctorales del G-9.** Pamplona. Marzo, 2016.

- *Síntesis de grafeno mediante el método CVD usando hierro como catalizador*. M.P. Lavin-Lopez, J.L.Valverde, M. Fernandez-Diaz, A. Paton-Carrero, L. Sánchez-Silva, A- Romero. **II Encuentro de jóvenes investigadores de la SECAT: Catálisis como herramienta en procesos sostenibles.** Ciudad Real. Junio, 2016.

- *Recetas para sintetizar grafeno*. M.P. Lavin.Lopez, J.L. Valverde, L. Sanchez-Silva, A. Romero. **VI Jornadas Doctorales de la Universidad de Castilla-La Mancha.** Toledo. Octubre, 2016.

Capítulos de libros:

- *Optimization of the synthesis procedures of graphene and graphite oxide*. **M.P. Lavin-Lopez, J.L. Valverde, L. Sanchez-Silva, A. Romero**. Recent advances in graphene research (Editor: Pramoda Kumar Nayak). Página 113. Intech (2016), South Korea. ISBN: 978-953-51-2639-3.